Leveraging Nanomaterial Design for Next Generation Antimicrobials

by

Lisa M. Stabryla

B.S. Engineering Science, University of Pittsburgh, 2015

M.S. Civil Engineering, University of Pittsburgh, 2017

Submitted to the Graduate Faculty of the

Swanson School of Engineering in partial fulfillment

of the requirements for the degree of

Doctor of Philosophy

University of Pittsburgh

2021

UNIVERSITY OF PITTSBURGH

SWANSON SCHOOL OF ENGINEERING

This dissertation was presented

by

Lisa M. Stabryla

It was defended on

May 27, 2021

and approved by

Leanne M. Gilbertson, Ph.D. Assistant Professor, Department of Civil and Environmental Engineering, Department of Chemical and Petroleum Engineering

Sarah-Jane Haig, Ph.D., Assistant Professor, Department of Civil and Environmental Engineering, Department of Environmental and Occupational Health

Jill E. Millstone, Ph.D., Associate Professor, Department of Chemistry, Department of Chemical and Petroleum Engineering, Department of Mechanical Engineering and Materials Science

Janet E. Stout, Ph.D., Associate Professor, Department of Civil and Environmental Engineering

Dissertation Director: Leanne M. Gilbertson, Ph.D. Assistant Professor, Department of Civil and Environmental Engineering, Department of Chemical and Petroleum Engineering

Copyright © by Lisa M. Stabryla

2021

Leveraging Nanomaterial Design for Next Generation Antimicrobials

Lisa M. Stabryla, Ph.D.

University of Pittsburgh, 2021

Silver nanoparticles (AgNPs) are promising alternatives to conventional antimicrobials due to their efficacy against a wide spectrum of bacteria. However, the mechanism of the particle contributions (distinct from their released Ag(I) ions) to microbial inactivation is not fully resolved and is needed to enable *a priori* design for maximizing antimicrobial activity. This dissertation demonstrates an ability to rationally design AgNPs by manipulating their morphology and establishing relationships that correlate material properties to their biological response and underlying mechanisms imparting antimicrobial activity.

A systematic literature review that critically analyzes conclusions about ion and NP contributions is conducted as an initial step to evaluate the potential impact of the particle in AgNP design. Results indicate that NP-specific effects exist and act in concert with and/or independently from solubilized Ag(I) ions, suggesting that more efficacious antimicrobials can be obtained through NP design. Next, the unintended consequence of resistance in *E. coli* repeatedly exposed to sublethal AgNPs concentrations is explored using an experimental evolution approach. Resistance evolves in response to AgNPs but not to Ag(I) ions alone, indicating a specific resistance to AgNPs. Selective emergence of AgNP resistance based on bacterial motility is also found, suggesting that the mechanism of resistance may be mediated by flagella. The results are promising for considering motility as a predictor of AgNP resistance and could inform design of nano-enabled antimicrobials that target non-motile bacteria. Finally, the influence of AgNP shape on antimicrobial activity is further explored as no consensus has been reached regarding the

differential influence of shape on antimicrobial activity and further, the mechanism(s) underlying the differential impact. To avoid material and experimental variables confounding the resolution of shape, antimicrobial activity is evaluated with a systematically prepared and comprehensively characterized material suite of AgNP shapes with well-controlled physicochemical properties, including pseudo-spheres, cubes, and discs. Differential antimicrobial activity arises from the AgNP shapes, which is hypothesized to arise from differences in NP characteristics (e.g., surface reactivity, crystal facet).

Collectively, the research in this dissertation enables progress beyond the current disparate findings in the literature and supports the use of nanoparticle design to control antimicrobial activity and resistance outcomes.

Table of Contents

1.0 Dissertation Introduction 18

1.1 Motivation 18

1.1.1 Antimicrobial Usage 18

1.1.2 Antimicrobial Resistance (AMR) as a Global Public Health Challenge 20

1.1.3 History of Silver as Antimicrobial Agents 23

1.1.4 Bacterial Inactivation Mechanisms of Silver (Ion versus Nanoparticle Effects) 24

1.1.4.1 Silver Ion Effects 24

1.1.4.2 AgNP Effects 25

1.1.5 Mechanisms of Antimicrobial Resistance 29

1.1.5.1 Resistance to Antibiotics and Conventional Chemical Antimicrobials 29

1.1.5.2 Ag and AgNP Resistance 30

1.1.5.3 General Notes about Evolution of Resistance 32

1.1.6 Nanoparticle Shape as a Design Handle 33

1.2 Dissertation Objectives and Scope 41

1.3 Dissertation Organization 42

2.0 It's Not All About the Ion: Support for Particle-Specific Contributions to Silver Nanoparticle Antimicrobial Activity 45

2.1 Introduction 46

2.2 State of the Art: Factors Influencing Ion Release and Current Practices of Scaling Ion Controls 50

2.2.1 Factors that Influence the Extent of AgNP Oxidation and Ion Release Can Guide Ion Control Selection 50

2.2.2 Equating the Concentration of the Ion Control to the Total Ag Concentration in the AgNP System 54

2.2.3 Quantifying Ion Release in Bulk Solution to Inform an Ion Control.....55

2.2.4 Quantifying Intracellular Ion Release to Inform an Ion Control.....56

2.2.5 Suggested Best-Practice for Scaling Ion Controls.....57

2.3 Experimental..... 57

2.3.1 Literature Review.....57

2.3.2 Scaled Ion Control Calculations 59

2.3.3 Using Pivot Tables to Identify AgNP Properties and Experimental Variables that Discriminate Ion-Only, Particle-Only, and Combined Ion-Particle Contributions to Observed Antimicrobial Activity.....65

2.4 Results and Discussion 66

2.4.1 Identification and Evaluation of Studies Implementing Scaled Ion Controls 66

2.4.2 Support for Ion-Only, Particle-Only, and Combined Ion-Particle Contributions to AgNP Antimicrobial Activity 67

2.4.2.1 Size-Dependent Mechanisms of AgNP Antimicrobial Activity 71

2.4.2.2 Surface Chemistry-Dependent Mechanisms of Antimicrobial Activity 74

2.4.2.3 Effect of Aggregation on Ion-Only, Particle-Only, and Combined Ion-Particle Contributions to Antimicrobial Activity 79

2.4.3 Experimental Methods Used to Distinguish Ion-Only, Particle-Only, and Combined Ion-Particle Mechanisms Influences the Conclusions Drawn 81

2.4.3.1 Quantifying Ag(I) Ion Released in AgNP Exposure Conditions Provide Support for Particle-Only and Combined Ion-Particle Contributions to Antimicrobial Activity 83

2.4.3.2 Methodological Approaches that Create Particle-Only Exposures Support an Ion-Only Mechanism of AgNP Antimicrobial Activity.. 86

2.4.3.2.1 Anaerobic Conditions..... 88

2.4.3.2.2 Sequestering Ag(I) Ions..... 90

2.4.3.3 Methods Used to Elucidate Specific Mechanisms of AgNP-Bacteria Interactions Support Ion-Only, Particle-Only, and Combined Ion-Particle Contributions to Antimicrobial Activity 90

2.5 Conclusions and Future Outlook 94

3.0 Role of Bacterial Motility in Differential Resistance Mechanisms of Silver Nanoparticles and Silver Ions..... 99

3.1 Introduction 100

3.2 Methods 102

3.2.1 Chemicals.....102

3.2.2 Bacterial Strains and Cultivation 103

3.2.3 Synthesis and Ligand Exchange of AgNPs 103

3.2.4 AgNP Characterization 105

3.2.5 Quantifying Resistance in Response to Ag(I) Ions and AgNPs.....106

3.2.6 Genomic Analysis.....109

3.2.7 Monitoring AgNP Aggregation.....109

3.2.8 Statistics 110

3.3 Results and Discussion 111

3.3.1 *E. coli* Develops Resistance to AgNPs but Not to Ag(I) Ions.....111

3.3.2 AgNP Resistance in Hyper-motile *E. coli* is Permanent and Conferred by *CusS* Mutation 116

3.3.3 Evolution of AgNP Resistance May be Shaped by Bacterial Motility 120

3.4 Conclusions 127

4.0 The Influence of Nanoparticle Shape on *E. coli* Antimicrobial Activity 130

4.1 Introduction 130

4.2 Materials and Methods 136

4.2.1 Chemicals.....136

4.2.2 Synthesis and Ligand Exchange to PVP-Capped Pseudospherical-AgNPs136

4.2.3 Synthesis of PVP-Capped Cube-AgNPs.....138

4.2.4 Synthesis of PVP-Capped Disc-AgNPs 139

4.2.5 AgNP Characterization 139

4.2.6 Bacterial Strains and Cultivation 140

4.2.7 Antimicrobial Activity of AgNPs 140

4.2.8 Effective Concentration Calculation 141

4.3 Results and Discussion 142

4.3.1 Characterization of AgNP Suite 142

4.3.2 Antimicrobial Activity of AgNPs Related to Their Shape.....145

5.0 Summary and Conclusions 149

5.1 Major Findings 149

5.2 Implications..... 150

5.3 Future Research..... 151

5.3.1 Immediate Next Steps 151

5.3.2 Probing the Mechanism(s) Underlying AgNP Shape-Dependent Antimicrobial Activity.....153

5.3.3 Designing Evolutionary Traps: Using Different Resistances That Work Against Each Other 154

5.3.4 Designing AgNPs For Use Against Biofilms 157

Appendix A Chapter 2 – Supplemental Information 160

Appendix A.1 Discussion 1 – Total Ag atoms calculations 160

Appendix A.2 Discussion 2 – Surface Ag atoms calculations 161

Appendix B Chapter 3 – Supplemental Information 189

Appendix B.1 Discussion 1 – Microbial Growth Kinetics Corroborate AgNP Resistance 193

Appendix B.2 Discussion 2 – Controlling for Total Ag and Ag(I) Content: Rationale Supporting Particle Specific Contributions to Resistance from the MIC Assay. 201

Appendix B.3 Discussion 3 – Other Mutations Explained..... 202

Appendix C Additional Contributions to the Field 207

Bibliography 209

List of Tables

Table 1.1 Summary of existing antimicrobial agents. 23

Table 1.2 Literature of silver nanoparticle toxicity and driving contributions. 26

Table 1.3 Summary of the AgNP shape literature showing conflicting conclusions and experimental design. 36

Table 2.1. Summary of ion-only, particle-only, and combined ion-particle hypotheses for AgNP antimicrobial activity as influenced by NP parameters. 68

Table 2.2. Critical characterization parameters for future studies aiming to distinguish ion and particle contributions. 96

Table 3.1. Statistical analysis of initial and final minimum inhibitory concentrations (MIC, µg/mL). 114

Table 3.2. Summary of observed mutations in the ancestor, control, and treatment populations of hyper-motile *E. coli* K-12 MG1655. 119

Table 3.3. Aggregation as measured through changes in hydrodynamic diameter (Dh) and full width at half maximum, (FWHM). 125

Table 4.1. Summary of the geometries, volumes, and surface areas of the AgNP shapes. Estimated volume and specific surface area as well as mean values for particle radii, edge lengths, and thickness for the different shapes, approximated using ideal geometries and average edge lengths. 144

Table 4.2. Comparison of shape on an atom basis. 144

Table 4.3. Surface area comparison on a concentration basis, using the average EC_{50}. 148

Appendix Table A.1. Compilation of qualitative and empirical data reported in the final subset of studies used for the pivot table analysis. 165

Appendix Table A.2. Analysis of bulk ion release reported and theoretically calculated, determination of a scaled ion control, and the resulting conclusion from each study in the final subset. 175

Appendix Table B.1. Information about bacteria strains used in the study. 189

Appendix Table B.2. Explained percentage (%) variation of MIC by treatment group, passage number, and the interaction between the two variables under varying experimental conditions 193

Appendix Table B.3. Statistical analysis of initial and final duration of the lag phase (λ, h) and maximum specific growth rate (μ, h^{-1}) corresponding to repeated AgNP (50 μg/mL) exposure (i.e., experimental group) in the hyper-motile *E. coli* (+IS*1*) strain, and after the AgNP pressure is removed and reintroduced, ... 200

Appendix Table B.4. Explained percentage (%) variation of duration of the lag phase by treatment group, passage number, and the interaction between the two variables 200

Appendix Table B.5. Explained percentage (%) variation of maximum specific growth rate by treatment group, passage number, and the interaction between the two variables 201

List of Figures

Figure 1.1 Global antiseptics and disinfectants by type 20

Figure 1.2. Factors exacerbating antimicrobial resistance. 21

Figure 1.3. Silver nanoparticles market by application. UNAVAILABLE DUE TO COPYRIGHT. 24

Figure 1.4. Antibiotic targets and resistance mechanisms related to cell physiology. 30

Figure 1.5. Global AgNP market by shape. UNAVAILABLE DUE TO COPYRIGHT. 33

Figure 1.6. Summary of the four levels of shape effects from the AgNP shape literature... 35

Figure 2.1. Potential Ag(I) ion release pathways, binding, and partitioning events within the AgNP exposure condition. 54

Figure 2.2. Theoretical dissolution of a given AgNP monolayer. 63

Figure 2.3. Scheme of the literature review process. 70

Figure 2.4. Ion-only, particle-only, and combined ion-particle conclusions drawn from studies that include AgNPs only within certain size ranges. 73

Figure 2.5. Ion-only, particle-only, and combined ion-particle conclusions drawn from studies that include AgNPs with certain surface chemistries. 76

Figure 2.6. Ion-only, particle-only, and combined ion-particle conclusions drawn from studies that monitor particle aggregation. 80

Figure 2.7. Ion-only, particle-only, and combined ion-particle conclusions drawn from studies that used three main methods. 83

Figure 2.8. Ion-only, particle-only, and combined ion-particle conclusions drawn from studies that measured ionization. 84

Figure 3.1. Resistance profiles of hyper-motile (+IS*1*) *E. coli*..... 113

Figure 3.2. Resistance profiles of non-motile (Δ*flhD::kan*) *E. coli*. 122

Figure 3.3. AgNP aggregation by UV-vis and DLS..... 124

Figure 4.1. UV-vis and TEM characterization of AgNP shapes. 143

Figure 4.2. Antimicrobial activity of AgNPs to *E. coli*. 146

Figure 4.3. EC_{50} values of AgNPs of different shapes for *E. coli* (3 h assay)..... 146

Figure 5.1. Assessing the efficacy of an antimicrobial polymer-nanocomposite film against biofilms to simulate real-world applications. 158

Appendix Figure A.1. Schematic demonstrating the difference between an appropriate and inappropriate ion control. 183

Appendix Figure A.2. Comparison of the reported dissolution values in studies that measured dissolution to our theoretical calculations of dissolution..... 184

Appendix Figure A.3. Ion-only, particle-only, and combined ion-particle conclusions drawn from studies that expose bacteria to different concentrations..... 185

Appendix Figure A.4. Ion-only, particle-only, and combined ion-particle conclusions drawn from studies based on AgNP purification..... 185

Appendix Figure A.5. Ion-only, particle-only, and combined ion-particle conclusions drawn from studies that monitor dissolution 186

Appendix Figure A.6. Ion versus particle conclusions drawn from studies that measure ion release..... 187

Appendix Figure A.7. Ion-only, particle-only, and combined ion-particle conclusions drawn from studies that expose AgNPs and Ag(I) ions to various bacteria..... 188

Appendix Figure B.1. Particle size of pseudospherical PEGSH-AgNPs..... 189

Appendix Figure B.2. Long-term stability of PEGSH-AgNPs..... 190

Appendix Figure B.3. Resistance profiles of raw MIC data. 191

Appendix Figure B.4. Replicate lineage data. 192

Appendix Figure B.5. Lag phase analysis of all conditions..... 198

Appendix Figure B.6. Growth rate analysis of all conditions..... 199

Appendix Figure B.7. 3D Structure of the CusS protein..... 204

Appendix Figure B.8. Amino acid sequence of CusS..... 205

Appendix Figure B.9. Filtration causes some AgNP loss. 206

Appendix Figure B.10. Filtration removes bacteria. 206

Preface

This dissertation was written at my parent's home in the lovely neighborhood of Mt. Oliver in the south hills of Pittsburgh, Pennsylvania in the middle of the COVID-19 pandemic. This is one of my many and biggest dreams that is coming into fruition and is at the hands of my village of family and unforgettable friends that have been there throughout the time I embarked on this scientific journey, some who have come and gone, some who have gone and come back, and some that will remain with me as life-long friends. It was a fun and joyful start, a long middle, and a quick sprint to the finish, albeit bittersweet.

First and foremost, I thank the best roommates I could ask for, who double as my parents, Darla and Robert Stabryla, for everything they have sacrificed to make me the person I am today and help chase my dreams as if they were their own. I would also like to thank my other roommate, my sister Dana, for all of the fun (including the creation of many TikTok videos and exchange of endless movie quotes) she has distracted me with along the way to make this a bearable 5-year journey (10 years including undergrad at Pitt). I thank them all for sitting in on countless practice presentations throughout my tenure as PhD student, putting up with my first of many conference trips across the country, the many long days that turned into nights, and the melancholic feelings associated with being their first bird to leave the nest away from Pittsburgh. I also would like to thank my brother Robert and my nieces Tori and Ally for their unconditional love and support.

Secondly, I thank my friends who have roamed Benedum Hall with me, stayed late with me in the 712 lab, my 341 officemates (when going into the office was a thing), the OG crew (you know who you are!), and my friends and lab mates in the Millstone Lab (especially Katie for mentoring me and Bo for teaching me so much about science and about life), all of which who at

some point or another pulled me aside from my work for trips to Hemingway's, walks to Fuku Tea for bubble tea and Asian Alley for hot pot, ski trips, beach trips, white-water rafting trips, many departmental gatherings at the Porch, friends' backyards for BBQ's and parties, and those fun nights dancing at Cavo and Tequila Cowboy. These memories and the people and their incredible kindness will live on in me forever. I would also especially like to thank my life-long friends, Yan and Nathalia, for being my support system from Day 1, through the pandemic, and staying connected with daily sanity checks despite the distance. And of course, I would also like to thank Matt for his love, support, and patience with me and whose laptop was lent to me to finish my PhD.

I would also like to acknowledge the generous support from the US Department of Defense through a National Defense Science and Engineering Graduate Fellowship I received in 2017, the Department of Civil and Environmental Engineering, and the Swanson School of Engineering at the University of Pittsburgh.

Lastly, I would like to thank my advisor, Dr. Leanne Gilbertson, for culturing me in many things (NO PUN INTENDED) and taking me under her wing. She has helped me in so many ways along this journey, giving me opportunities to grow as a researcher, as a teacher, and as a confident leader in my field and offering me sound advice as I embark on the next journey.

I Dedicate This Dissertation

To My Parents (Darla and Bob) and My Sister (Dana),

For Being My World.

1.0 Dissertation Introduction

1.1 Motivation

1.1.1 Antimicrobial Usage

Antimicrobial agents are ubiquitous in many high value industries, including healthcare (e.g., medical device coatings, disinfectants), food and agriculture (e.g., food preparation surfaces), and drinking water treatment and distribution (e.g., chlorination, copper-silver ionization) with the aim of pathogen inactivation, infection prevention, and biofilm control.[1-3] Antimicrobial coatings in particular comprise a billion-dollar industry, with the global market having reached $3.3 billion in 2020 and projecting to grow to $5.6 billion by 2025.[4] Silver-based antimicrobial coatings specifically are projected to lead this market, particularly due to their high efficacy, low toxicity to humans, long-lasting performance, and high thermal stability as compared to copper, titanium dioxide, and zinc-based formulations.[4] The increase in demand for antimicrobial coatings can be attributed to the growing desire for infectious disease control, particularly from the medical and healthcare sector and government initiatives to prevent the spread of hospital-acquired infections.[4] At healthcare facilities, hospital-acquired infections are the leading cause of mortality and morbidity, affecting 1.7 million patients and causing 100,000 deaths in the US each year.[4] These infections often arise from the use of medical devices during treatment procedures as they are a breeding ground for bacteria and are difficult to disinfect with conventional antimicrobials.[4] Increased awareness about safety and hygiene, more stringent regulations for infection-control procedures and practices in the workplace, and their increasing

adoption in other industrial applications have also been driving factors, along with the COVID-19 pandemic, the rise of antibiotic resistant bacteria, and the growing population.[4]

A recent BCC market report [5] provides insight into another similar industry. Antiseptics (applied to the body) and disinfectants (applied to non-living surfaces such as countertops and handrails) also comprise a billion-dollar industry, with the global market having reached $7.1 billion in 2017 and projected to increase to $9.1 billion in 2022.[5] Revenue in North America alone was nearly $3 billion in 2017.[5] Of this, healthcare was the largest sector of spending, with $1.2 billion spent on antiseptics and disinfectants, while another $1.0 billion was directed to industrial and commercial use, in settings such as food services and food-processing units, restaurants, restrooms, and several others.[5] Phenolic antiseptics and disinfectants consume the largest global market share at $1.5 billion in revenue (**Figure 1.1**), followed by quaternary ammonium ($1.4 billion), oxidizing agents ($1.3 billion), and alcohol ($1.1 billion).[5] However, with the recent FDA ban on phenolic compounds from consumer products (e.g., triclosan), their market in North America is declining as manufacturers are withdrawing or reformulating their products.[5] In comparison, the silver-based antiseptics and disinfectants market was $63 million in 2017 and is projected to surpass $112 million in 2022.[5] This is the highest growth rate due to expanded use in wide ranging fields, including textiles, medical-devices, and personal-care products, as well as the launch of several innovative silver-based technologies: (i) Microban International's SilverShield technology that inhibits microbial growth on product surfaces, (ii) Rudolf GmbH's Silverplus technology that controls odor-causing bacteria in textiles, and (iii) PPG Industries' PPG SILVERSAN antibacterial powder coating, to name a few.[4, 5] Silver-based disinfectants are increasing rapidly in the food industry too. For example, Chipotle Mexican Grill adopted PURE Bioscience Inc's Silver Dihydrogen Citrate (SDC) antimicrobial technology as a

food-contact surface sanitizer and disinfectant to prevent food-borne illness outbreaks caused by *Salmonella*, *E. coli*, and *Listeria*.[5] Silver-based antimicrobial additives are incorporated into products during the manufacturing stage and can exist as various forms such as salts, zeolites, and nanoparticles. They can be incorporated into a wide range of product types, including medical equipment (e.g., urinary and intravenous catheters, wound dressings, bandages), food-contact surfaces, textiles, and others.

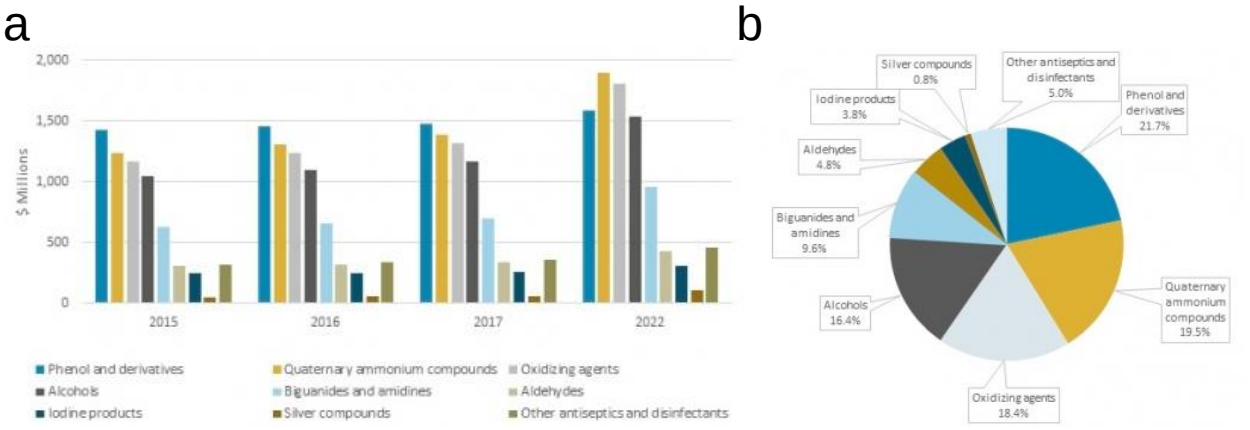

Figure 1.1 Global antiseptics and disinfectants by type, in a) USD and b) %. Reprinted from BCC Research with permission.[5]

1.1.2 Antimicrobial Resistance (AMR) as a Global Public Health Challenge

A major challenge associated with the use of antimicrobial coatings, antiseptics, and disinfectants is the development of resistance in the target microorganism, i.e., the ability to withstand the toxic effects of chemicals, thereby decreasing the antimicrobial's efficacy over time and leading to the emergence of bacteria called 'superbugs'. Antimicrobial resistance (AMR) poses a serious threat to global public health[6] as the number of resistant bacteria strains increase and challenges our ability to adequately treat diseases (**Figure 1.2A**).[7, 8] Six nosocomial pathogens in particular have been identified as priority pathogens by the World Health

Organization (WHO) as they exhibit multidrug resistance and virulence and are referred to as the ESKAPE pathogens (*Enterococcus faecium*, *Staphylococcus aureus*, *Klebsiella pneumoniae*, *Acinetobacter baumannii*, *Pseudomonas aeruginosa*, and *Enterobacter* species).[9] The Center for Disease Control and Prevention (CDC) estimate that, in the United States alone, at least 2.8 million illnesses and 35,000 deaths are attributed to AMR infections annually, with $20-35 billion in healthcare expenses and productivity losses.[8] This problem is exacerbated by the fact that there is a diminishing number of antimicrobial agents being approved by the FDA (**Figure 1.2B**).[7, 10] Drug development has not kept pace with the development of antibiotic resistance,[11, 12] which is in part due to the significant investment (i.e., $800 million-$1.7 billion) required to bring a drug to market.[7]

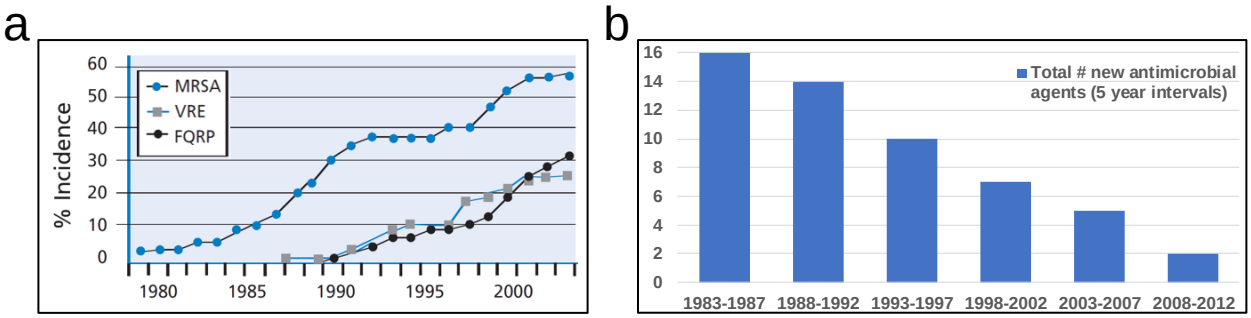

Figure 1.2. Factors exacerbating antimicrobial resistance. a) Increase in resistance rates for three bacteria identified as serious public health threats. MRSA = methicillin-resistant Staphylococcus aureus. VRE = vancomycin-resistant enterococci. FQRP = fluoroquinolone-resistant Pseudomonas aeruginosa. Source: IDSA and CDC.[7, 8] b) Historic trend of FDA approved antimicrobial agents. Source: IDSA and CDC.[7, 8]

Furthermore, antimicrobials are increasingly being regulated due to toxicity concerns (arising from both the parent compound and potentially more toxic by-products), receiving requests for more data collection (e.g., benzethonium chloride), or have been banned altogether from some personal care products (e.g., triclosan) (**Table 1.1**).[13-20] Similar concerns for

resistance arise in drinking water, where chlorine is often used as a disinfectant and a number of microorganisms such as *Sphingomonas, Giardia, Cryptosporidium*, and *Legionella pneumophila* have been reported to possess resistance to chlorine.[21-24]

Silver nanoparticles (AgNPs) and other ionizing engineered nanomaterials (ENMs) are increasingly being developed and proposed as promising alternatives to conventional antimicrobials due to their high efficacy in a wide spectrum of multi-drug resistant bacteria,[25, 26] multiple modes of bacterial inactivation,[27] and ability to manipulate nanoparticle parameters, namely size, shape, and surface chemistry, to influence the magnitude and mechanisms of antimicrobial activity.[27] Since AgNPs deliver multiple mechanisms of inactivation to the cell, it is thought that it will be difficult for microorganisms to evolve resistance towards them and thus they are being projected as a solution to the growing AMR crisis.[27]

Table 1.1 Summary of existing antimicrobial agents. [13-20]

Antimicrobial Agent	Chemical Structure	Mechanism of Inactivation	Advantages	Disadvantages
Triclosan	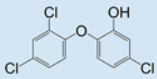	➢ Multiple mechanisms ➢ Disrupts cell wall functions	➢ Broad spectrum activity ➢ Was active against Gram-positive and some Gram-negative bacteria	➢ Toxic to humans, linked to hormone disruption ➢ Banned by FDA in antimicrobial soaps ➢ Resistance acquired through multiple mechanisms ➢ Contributes to resistance of other medically relevant antimicrobial agents
β-lactam antibiotics (methicillin)	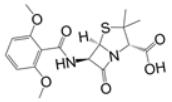	➢ Inhibits cell wall formation	➢ Displayed broad spectrum activity	➢ Decreased effectiveness against *Staphylococcus* aureus ➢ Not effective in Gram-negative bacteria
Floroquinolones (ciprofloxacin)	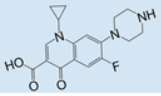	➢ Inhibits production of nucleic acids	➢ Displayed broad spectrum activity	➢ Central nervous system side effects ➢ Prohibited in some countries ➢ Decreased effectiveness against *E. coli, Shigella*, and *Salmonella*
Benzethonium chloride	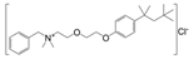	➢ Multiple mechanisms	➢ Highly effective against AMR bacteria	➢ Long-term exposure linked to cancer, allergies, and organ toxicity ➢ Banned in Canada and Japan for use in cosmetic products and soaps
Oxazolidinones (linezolid)	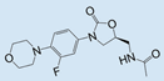	➢ Uniquely inhibits initiation step of protein synthesis	➢ Relatively safe ➢ Effective against AMR bacteria ➢ Can switch quickly from IV to oral use	➢ Long-term exposure could cause nerve damage and bone marrow suppression
Silver nanoparticles (AgNPs)		➢ DNA damage ➢ Membrane destruction ➢ Oxidative stress	➢ Smaller size, higher surface area ➢ Effective against AMR bacteria ➢ Multiple modes of inactivation ➢ Chance of being "resistance-free"	➢ Toxicity to humans and environment is unresolved ➢ Same wide-spread usage of sub-lethal amounts could result in resistance

1.1.3 History of Silver as Antimicrobial Agents

Bulk silver, and arguably nanoparticulate silver (AgNPs), are among the oldest antimicrobial agents.[1, 28, 29] In ancient times, roughly 7,000 years ago, silver was used to line vessels and silver coins were added to containers of water or milk were used to preserve rations during military conflicts.[1, 30, 31] Silver was also instrumental during this time to treat ulcers and aid in wound healing.[25, 30, 31] Today, AgNPs comprise a billion-dollar industry, which includes more than just antimicrobial applications (**Figure 1.3**), with the global market being valued at $1.8 billion in 2019.[32] It is projected to reach $4.1 billion by 2027 particularly due to the rise in

demand for antimicrobial applications, disinfectants, and pharmaceuticals and decline in traditional antimicrobials due to toxicity and resistance concerns.[32] They are employed in numerous industries including healthcare, textiles, electronics, food and beverages, pharmaceuticals, cosmetics and personal care, water treatment, and others due to their antimicrobial properties. Additionally, around 360–450 tons of AgNPs are produced globally per year.[33]

a IMAGE UNAVAILABLE DUE TO COPYRIGHT

b IMAGE UNAVAILABLE DUE TO COPYRIGHT

Figure 1.3. Silver nanoparticles market by application. UNAVAILABLE DUE TO COPYRIGHT.a) globally (%) in 2014 and b) projected in North America (USD million) in 2012-2022.[34]

Bacterial Inactivation Mechanisms of Silver (Ion versus Nanoparticle Effects)

1.1.4.1 Silver Ion Effects

The antimicrobial mechanisms of bulk silver are attributed to the release of Ag(I) ions and their interactions with various aspects of the microbe.[19, 27, 35] For example, Ag(I) ions can interact with sulfhydryl groups on the cell surface, where the subsequent formation of thiol-silver bonds block respiration and electron transfer, leading to the collapse of the proton motive force, the de-energizing of the membrane, and eventually cell death.[1] The ionic radius of a Ag(I) ion is also sufficiently small (0.115 nm) to travel through transmembrane proteins such as porins (30–50 kDa; pore size, 1–3 nm).[27, 36, 37] Once inside the cell, Ag(I) ions may react with thiol functional groups in proteins and nucleic acids, interfering with DNA replication and deactivating many enzymatic functions.[1] Ag(I) ions also increase the level of reactive oxygen species (ROS) inside

the cell because thiol-containing anti-oxidative enzymes are deactivated by silver, thus exacerbating the damage done to proteins, lipids, and nucleic acids.[1]

1.1.4.2 AgNP Effects

The mechanisms of antimicrobial activity for AgNPs have been widely studied, and many researchers largely attribute this activity to the release of Ag(I) ions via oxidation and dissolution of the AgNP surface atoms.[27, 30, 35] Compared to their macroscale counterparts, AgNPs exhibit enhanced ion release per unit mass mainly due to an increased surface area to volume ratio. However, it has also been established that Ag ion exposure alone does not elicit the same bacterial response as exposure to AgNPs,[19, 38] which suggests that the observed antimicrobial activity is induced not only by solubilized ions but also by the ENM itself. Thus, the contribution of the particle and ion remains an open question in AgNP systems as there is no general consensus in the AgNP toxicity literature (**Table 1.2**). Several studies only compare endpoint toxicity between the two silver forms (**Table 1.2**) rather than attempting to isolate the major contributor of toxicity in the AgNP system, which is challenging due to multiple inactivation modes (e.g., physical mechanisms such as membrane disruption and chemical mechanisms such as ROS generation) that are likely occurring simultaneously. Furthermore, the use of different microorganisms, exposure media, and particle parameters across studies unintentionally creates different AgNP systems and thus leads to varying conclusions (**Table 1.2**). Additionally, many studies do not make appropriate comparisons between the two silver forms, i.e., Ag(I) ion controls are often not scaled to the quantities of bioavailable Ag released from the AgNPs (**Table 1.2**).

Table 1.2 Literature of silver nanoparticle toxicity and driving contributions.

NP size	NP ligand	NP shape	Biological model	Exposure media	Appropriate comparison between silver forms	Identified effects and/or relative toxicity between silver forms	Refs
Various	Various	Spherical	*E. coli*	Hard water	In some cases yes	Ion > NP, Particle effects	[39]
83-100 nm	--	Wires, spherical	*E. coli*	Water	Yes	Ion > NP, Ion effects	[40]
15 nm	PVA	Spherical	Nitrifying bacteria	Inorganic medium	No	NP > Ion	[41]
15-21 nm	PVA	Spherical	*E. coli*	Nutrient broth	Yes	Ion > NP	[42]
2 nm	--	Spherical	*E. coli*	Luria-Bertani	No	Ion > NP	[43]
8 nm, 29 nm	PVP	Spherical	Several gram+ and gram-	Mueller-Hinton, Luria-Bertani	In some cases yes	Ion > NP, Particle effects	[44]
25-50 nm	--	Cubic	Several gram+ and gram-	Mueller-Hinton	No	Particle effects	[26]
25 nm	Various	Spherical	*Candida* spp	Mueller-Hinton	No	Ion ≈ NP	[45]
11 nm	Citrate	Spherical	*Shewanella oneidensis*	Ferric citrate	Yes	Ion effects	[46]
52 nm	--	Mainly spherical	*E. coli*	Luria-Bertani, DI water	Yes	Ion effects	[47]
35 nm	Carbon	Spherical	Activated sludge	Mixed liquor suspended solids	Yes	NP > Ion, Particle effects	[48]
20 nm	Citrate	--	*Nitrosomonas europaea*	DFR media	No	Ion > NP, Ion effects	[49]
21-27 nm	Citrate, gum Arabic, PVP	Spherical	*Nitrosomonas europaea*	AOB medium	In some cases yes	Ion effects	[50]
20 nm, 80 nm	Phosphate monolayer	Spherical	*Nitrosomonas europaea*	HEPES buffer	Yes	Ion effects	[51]
7 nm	Cysteine and glutathione	Spherical	*S. aureus, E. coli*	ISB, Dulbecco's PBS	Yes	Ion ≈ NP *E. coli* Ion > NP *S. aureus*, Particle effects	[52]
35 nm	Various	Spherical	*Pseudomonas putida*	Various	Yes	Ion > NP, Particle effects	[53]
9 nm	Various	Spherical	*E. coli*	Various	No	NP > Ion	[54]
Various	PVP	Cubes, wires, spheres	Several gram+ and gram-	Luria-Bertani	No	Ion > NP, Ion effects	[55]

Table 1.2 (continued)

<10 nm	--	--	*Pseudomonas putida*	Mineral salt media	Yes	Ion effects	[56]
50-100 nm	--	Spherical	*Pseudomonas putida*	Phosphate buffer	In most cases yes	Particle effects	[57]
16-20 nm, 50-30 nm	PVP	Spherical	Human lung carcinoma epithelial-like cell line	DMEM	No	Particle effects	[58]
40 nm	--	Spherical	*Pseudomonas aeruginosa*	GLYM9	No	Particle effects	[59]
Various	Various	Spherical	*C. elegans*	EPA water, K+ medium	No	Particle effects	[60]
Various	Phosphate monolayer	Spherical	*E. coli*	PBS	Yes	Ion > NP, Ion effects	[61]
6 nm	--	Spherical	Natural community of aquatic microorganisms	Pond water	No	Ion effects	[62]
5-10 nm	--	--	*S. aureus* (MSSA, MRSA)	Mueller-Hinton, Luria-Bertani	No	Inconclusive	[63]
Various	Various	Spherical	*E. coli*	Luria-Bertani	In most cases yes	Particle effects	[38]
35 nm	Amorphous carbon	Spherical	*E. coli*	Sodium bicarbonate buffer	Yes	Ion effects	[64]
Various	PEG, PVP	Spherical	*E. coli*	Sodium bicarbonate buffer	Yes	Ion effects	[35]
Various	--	Spherical	*Vibrio fisheri*	2% NaCl	Yes	Particle effects	[65]
24 nm	PEGSH	Spherical	*E. coli*	Mueller-Hinton, Luria-Bertani	Yes	Particle effects	[66]
6 nm	Various	Spherical	*E. coli, S. aureus*	Luria-Bertani, Tryptic soy agar	Yes	Ion effects	[67]
45 nm	Citrate	Mainly spherical	*B. subtilis, E. coli*	Luria-Bertani	Yes	Particle effects	[68]
7 nm	Starch	Spherical	Nitrifying sludge	Synthetic wastewater	Yes	Ion effects	[69]
70 nm	PVP	Spherical	*E. coli, S. aureus*	Luria-Bertani, Roswell park Memorial Institute medium	Yes	Ion effects	[70]

Nanoparticle parameters, namely size, shape, and surface chemistry, define the nanoparticle and can control particle and ion effects by inducing various physical and chemical mechanisms of inactivation, although these remain to be precisely elucidated. Nanoparticle size has been shown to influence antimicrobial activity, with smaller particles (i.e., particles having a diameter <10 nm) inducing greater antimicrobial activity.[27, 71-73] This is often related to the increase in ion release occurring with decreasing nanoparticle size.[27, 71-73] Nanoparticle shape most notably changes the crystal facets present on the particle, which can influence both the physical interaction with the cell as well as ion release through differential reactivity between the exposed surface facets and oxygen.[1, 73, 74] Finally, surface chemistry can influence dissolution via capping ligands (i.e., molecules providing stability to the AgNPs) and insoluble passivation layers.[39, 50, 75-79] The capping ligand is known to influence AgNP antimicrobial activity through regulation of ion release,[79, 80] with the potential for some ligands to chelate released ions and drive more dissolution (i.e., Le Chatelier's principle), while other ligands can enhance or reduce ion release by exposing more or less nanoparticle surface and making it available for interaction with oxygen.[79, 80] In addition to influencing chemical behavior, surface chemistry has also been shown to impact physical behavior (e.g., aggregation, affinity for the bacterial cell),[79, 81] which can further influence AgNP antimicrobial activity.[38, 75] For example, there is large agreement around positively charged nanoparticles inducing greater antimicrobial activity as they have high affinity for the negatively-charged bacterial cell.[38, 39, 75] The surrounding media chemistry can also influence ion release and particle behavior.[66] The above examples for all three nanoparticle parameters suggest that while differential microbial responses can be a result of varying ionization among different nanoparticle formulations, antimicrobial activity attributed to the physical mechanisms associated with the nanoparticle parameters remains unknown. Thus,

the precise mechanisms of AgNP action remain unresolved, particularly the dynamic contributions of the nanoparticle and ion.[27]

1.1.5 Mechanisms of Antimicrobial Resistance

1.1.5.1 Resistance to Antibiotics and Conventional Chemical Antimicrobials

The mechanism of action for antibiotics and conventional chemical antimicrobials typically involves targeting one specific aspect of bacterial physiology and biochemistry during the growth process of a cell (e.g., the bacterial cell wall, the cell membrane, lipid synthesis, protein synthesis, DNA and RNA synthesis, and folic acid metabolism) (**Figure 1.4**).[82] Resistance in a cell builds in response to that one specific target. It can arise specifically from efflux and changes in membrane permeability (eliminating the antimicrobial agent via protein pumps), enzymatic inactivation or degradation (modification of the antimicrobial agent by enzymes to eliminate the functional characteristics that enable them to interact with their targets), target modification (alteration and mutation of the targets themselves or production of enzymes that modify the targets), and immunity (the act of binding proteins to the antimicrobial or its target to prevent the binding of the antimicrobial to its target) (**Figure 1.4**).[82] Some defenses, such as the cell membrane and efflux pumps, are inherent to particular organisms and is referred to as intrinsic resistance.[83] Other times, these defenses are acquired from other bacteria via the integration of released, free-floating genetic material (e.g., horizontal gene transfer, plasmids, transposons), which permits intraspecies and even interspecies transfer to occur even without exposure to the antimicrobial.[83] Finally, adaptive resistance, a third category of defenses, is developed under pressure of an antimicrobial, involves alterations in gene and/or protein expression, and is being

repeatedly correlated with multidrug resistance, i.e., repeated exposure to one drug elicits resistance to another drug.[83] This type of resistance can only be passed on to progeny.[84]

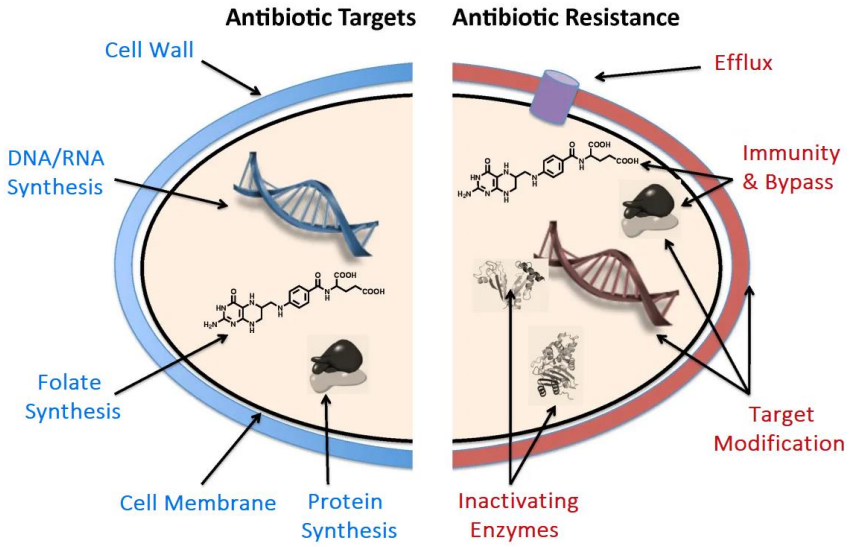

Figure 1.4. Antibiotic targets and resistance mechanisms related to cell physiology.Modified from Wright 2010 under the Creative Commons CC BY 2.0 attribution license.[82]

1.1.5.2 Ag and AgNP Resistance

There are numerous reports on bacterial resistance to ionic silver, several of which have isolated silver-resistant strains of *Acinetobacter baumanni*, *Escherichia coli*, *Klebsiella pneumoniae*, *Pseudomonas aeruginosa*, *Pseudomonas stutzeri*, and multiple *Salmonella* species from silver-rich clinical (e.g., hospital burn wards) and environmental (e.g., silver mines) settings.[1, 31, 85-99] These resistant strains detoxify Ag(I) ions through reduction to a less toxic oxidative state (e.g., Ag(I) to Ag(0)) or by eliminating the threat of Ag(I) ions altogether through active efflux of Ag(I) ions from the cell by efflux pumps.[87-89, 91, 100-103] In some strains such as *P. stutzeri*, silver resistance is conferred via a plasmid.[1, 27, 87, 88] However, silver resistance genes are not commonly found on enterobacterial (e.g., *E. coli*) plasmids, but rather are acquired

through a de novo mutation in the chromosome.[88] Silver ion resistance is specifically associated with the *sil* operon,[1, 87] and contains two periplasmic metal-binding chaperone proteins SilE and SilF as well as two efflux pumps - a P-type ATPase SilP and antiporter SilCBA.[87] Since silver is not an essential metal, bacteria likely do not have an innate mechanism to eliminate Ag(I) ions.[31, 84, 104] Therefore, this system of resistance genes may have stemmed from an established copper resistance system (involving multicopper oxidase cueO and transport ATPase copA).[104-106] An additional proposed mechanism emerged from studying silver-resistant *E. coli* mutants, which were found to have cell membranes deficient in outer membrane porins, thereby decreasing silver uptake.[89, 101]

Unlike the established resistance mechanisms for Ag(I) ions, the potential for bacteria to develop resistance to AgNPs emerged in the past 10 years,[100, 107-111] with the potential to be exacerbated because of widespread AgNP use in many commercially available products.[29, 82, 108] Unlike intrinsic or acquired resistance commonly seen with antibiotics, adaptive resistance that is developed under an antimicrobial pressure may be most relevant to AgNPs, as their widespread use can facilitate prolonged microorganism exposure to sublethal concentrations of bioavailable silver. The studies that show emergence of bacterial resistance to AgNPs conclude an ion elimination mechanism.[107, 109] One study specifically found that *Bacillus subtilis* has a natural ability to adapt to cellular oxidative stress induced by the release of Ag(I) ions upon prolonged exposure to AgNPs.[109] Another study found a plasmidic silver resistance determinant (i.e., SilB) upon exposure to AgNPs in *S. senftenberg*, similar to what has been found for Ag(I) ions.[100] Genomic or chromosomal mutations have also been suggested.[100, 107, 109] For example, Graves et al. identified small mutations in four genes: *cusS* related to intracellular copper ion concentrations, *purL* related to nucleotide synthesis, *rpoB* related to RNA polymerase, and

ompR related to the production of an outer membrane protein that plays a role in regulating responses to Ag(I) ion resistance.[107] However, Panacek et al. proposed an alternate resistance mechanism that does not involve a genetic mutation.[111] Rather, they show bacterial resistance towards AgNPs emerges from particle aggregation induced by the cell's secretion of flagellin (the principal protein component of bacterial flagella).[111] The flagellin is postulated to reduce AgNP colloidal stability, causing aggregation and decreasing the particle surface area, which subsequently reduces AgNP bioavailability and likely suppresses the surface reactions that cause antimicrobial effects.[111] Despite these advancements in understanding AgNP resistance mechanisms, it is still a nascent area and there remains substantial opportunity and need to identify the precise, underlying resistance mechanisms that develop in response to ion- and particle-driven effects (whether chemical or physical), particularly as we strive to use these materials to combat, rather than contribute, to the AMR crisis. The current lack of mechanistic resolution around AgNP resistance could become a barrier to the success of their use, i.e., they will not be used in a way that does not spur resistance.

1.1.5.3 General Notes about Evolution of Resistance

Both the level of resistance and the mechanisms that occur are dependent on the duration and concentration of the antimicrobial exposure.[83, 112] Fast, transient mechanisms occur over short timescales and involve rapid, small phenotypic and epigenetic changes (e.g., DNA methylation, elevated rates of point mutations), which are less stable.[83] On the other hand, slow, more stable mechanisms occur over longer timescales and are imparted by a series of genetic or chromosomal mutations to confer a permanent form of resistance.[83] The standard timeframe for observing resistance development is 20 serial passages of repeated antimicrobial exposure,[83,

111, 113-115] which is considered a long evolutionary path that can lead to the appearance of recurrent and sequential mutations promoting a permanent resistance response.[83]

1.1.6 Nanoparticle Shape as a Design Handle

There is a growing demand for the development of design criteria to maximize the functional performance of AgNP-enabled products and thus current research is aimed at understanding the role that nanoparticle parameters (i.e., size, shape, and surface chemistry) play in the magnitude and mechanisms of antimicrobial activity. Since nanoparticle shape can be manipulated and the particle interacts directly with the microorganism, it is a key design handle for maximizing antimicrobial activity in a way that avoids the risk of resistance. The influence of nanoparticle shape on the bacteria response, however, is not well understood, particularly the link between the material properties imposed by shape and the underlying mechanisms of action imparted to the bacteria cell. With the potential to enhance the physical and chemical mechanisms of antimicrobial activity, manipulations of AgNP shape can be utilized as a route toward rational design. Spherical particles are currently the most studied shape in the literature and in the global AgNP market, but the utilization of other shapes in AgNP-enabled products has been increasing (**Figure 1.5**).[32]

IMAGE UNAVAILABLE

DUE TO COPYRIGHT

Figure 1.5. Global AgNP market by shape. UNAVAILABLE DUE TO COPYRIGHT.[32]

As highlighted in **Table 1.3** and **Figure 1.6A**, no consensus has been reached regarding which shape imparts the greatest antimicrobial activity, and further, which material properties

govern the bacterial response to shape. For example, some studies show that shape does not influence bacterial response,[55, 116] while others conclude faceted shapes (e.g., prisms) display greater biocidal activity due to more ion release, increased interaction with the cell, and enhanced membrane disruption.[74] Opposingly, shapes with soft edges (e.g., elongated nanospheres) have also been identified as enhancing membrane association and increasing antimicrobial activity.[117] These varying conclusions likely arise from the different particle systems and different model organisms used across studies as well as inappropriate shape comparisons made within studies as other particle parameters are often changed simultaneously along with shape (**Table 1.3**). Still, the crystal facets present on the particle and the surface area available for interaction with the cell have been proposed by several studies as the material properties governing shape-driven antimicrobial activity (**Table 1.3**, **Figure 1.6B**). There is also the potential for different contributions from the released Ag(I) ions and the particles themselves to influence shape-driven bacterial responses. As stated earlier, nanoparticle shape can influence both ion and particle behavior and induce various physical and chemical mechanisms of inactivation. For example, nanoparticle shape notably changes the crystal facets present on the particle, which can influence both the physical interaction of the nanoparticle with the cell as well as ion release through differential reactivity between the exposed surface facets and dissolved oxygen.[1, 73, 74] However, studies that investigate nanoparticle shape do not reach consensus on whether ion-driven[40, 116] or particle-specific[72, 118-122] effects exist, and few studies monitor dissolution kinetics necessary to inform mechanistic distinction[116] (**Table 1.3**, **Figure 1.6C**). Finally, mechanistic resolution at the cellular level has not been achieved, although a few studies propose membrane damage as directly underlying the shape-driven bacterial responses[74, 119] (**Table 1.3**, **Figure 1.6D**).

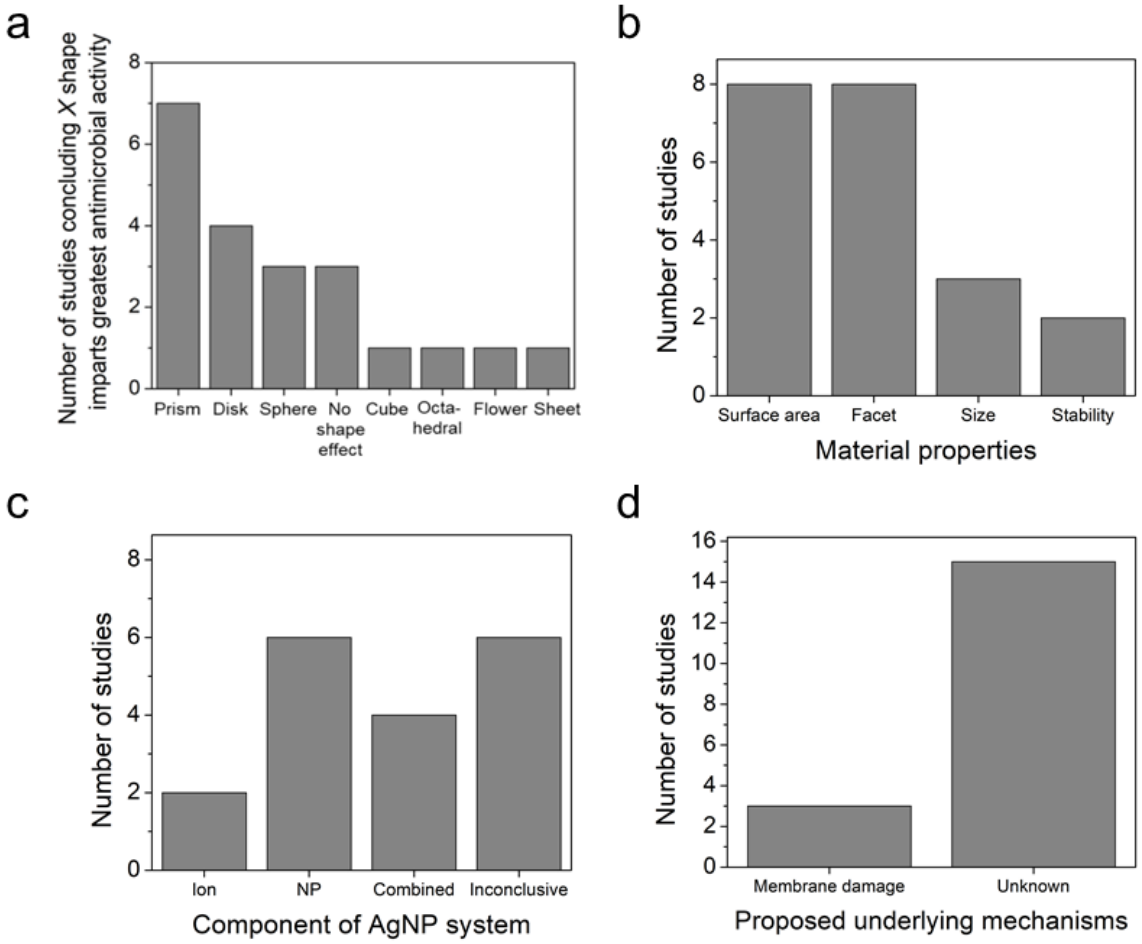

Figure 1.6. Summary of the four levels of shape effects from the AgNP shape literature. Studies identifying a) shapes imparting greatest antimcirobial activity, b) material properties governing shape-driven effects, c) ion and particle effects, and d) underlying physical and chemical mechanisms imparted by those components upon interaction with the cell.[40, 55, 73, 74, 116, 118-130]

Table 1.3 Summary of the AgNP shape literature showing conflicting conclusions and experimental design.

Relative anti-microbial activity between shapes	Bacteria strains	Biological endpoints	NP charact-erization	Size (surface area)**	Ligand	Ion release	Identified ion and particle effects	Identified governing material properties	Identified mechanism of shape-based inactivation	Ref
Hierarch-ical / prism / polygonal > sphere/ disk	*E. coli* > *S. aureus*	% viability	UV-vis, SEM, TEM, BET, FTIR, ICP	32-64 nm vs 50 nm vs 10-100 nm vs 20-110 nm (30.1, 18.2, 17.6, 14.8, 12.0 m^2/g)	Citrate-methyl cellulose-SDS	Eluted Ag(I) ions after washing of cotton samples are similar for all shapes, but loading efficiency is different	Ion, particle?	Surface area	--	[127]
Disk > sphere > rod > cube	*S. aureus*	MBC, % viability	SEM, AFM, DCS, DLS	20-60 nm vs 40-70 and 120-180 nm vs 50-100 nm x 1,000-20,000 nm vs 140-180 nm	all PVP (zeta potential varied)	In water: Disk (68%) > sphere (42-54%) > rod (37%) > cube (30%)	Ion	Surface area	--	[116]

Table 1.3 (continued)

Sphere > cube > wire > prism Prism > sphere > wire > cube	*E. coli*, *B. subtilis* *S. aureus*	% viability	XRD, EM, UV-vis, DLS	17 nm vs 450 nm vs 92 nm vs 50 nm	all PVP except prisms	--	--		--	[124]
Prism > sphere > rod	*E. coli*	Growth curve, killing kinetics, % viability	TEM, ICP, UV-vis	40 nm vs 39 nm vs 16 nm x 100-200 nm	CTAB-citrate	--	Combined ion and particle?	Facet (111), surface area?	Membrane damage	[74]
Cube > sphere > wire	*E. coli*	Growth curve, MIC, % viability	TEM, XRD, UV-vis	55 nm vs 60 nm vs 2,000-4,000 nm	All PVP?	--	Particle	Surface area, facet (100)	Membrane damage	[119]

Table 1.3 (continued)

Prism > sphere > cube	*E. coli* = *P. aeruginosa* > *S. aureus*	MIC, colori-metric change, IC_{50}	TEM, DLS	30 nm vs 50 nm vs 80 nm	all PVP (zeta potential varied)	Water: Prism (39%) > sphere (23%) > cube (4%) BSA: Prism (0.2%) = sphere (0.2%) > cube (0.04%) MHB: spheres (4.2%) > prism (0.4%) > cubes (0.2%)	--nothing or combined ?	Aggreg-ation, facet (111)?	--	[126]
Prism > sphere > cube across same size Small sphere > prism	Recombinant GFP expressing *E. coli* BL21	Growth curve, fluoresc-ence, zone of inhibition	TEM, UV-vis	all shapes at 70 nm and additional 10 nm and 20 nm spheres	Unknown	--	Particle?	Size, surface area, facet (111)	--	[128]

Table 1.3 (continued)

Hexagon > sphere > prism	*E. coli*	NP-cell interaction, growth curve, zone of inhibition	SEM, TEM, UV-vis	All average size 40 nm	PEG-citrate-PVP	--	Particle		--	[118]
Plate > rod > hexagon	*S. aureus* > *E. coli*	Zone of inhibition, MIC, % viability, growth curve	BET, SEM	Unknown (121, 40, 17 m^2/g)	all PVP	--	--	Surface area, stability	Membrane damage	[129]
Prism > sphere	*E. coli*, *S. enterica*, *P. aeruginosa*	MBC, inactivation curve, % viability	UV-vis, TEM, EDX, DLS, ICP-OES	22.5 nm vs 18.92 nm (citrate), 24.5 nm vs 23.56 nm (PVP), 114 nm vs 90.75 nm (poly-Arg-PVP)	Citrate (-29 vs -38mV), PVP (-26 vs -30 mV), poly-Arg-PVP (+29 vs +34 mV)	--	--	Sharp vertexes and edges	--	[130]
Sphere > prism	*E. coli*, *S. aureus*, *P. aeruginosa*	Zone of inhibition, MIC, MBC	XRD, TEM, UV-vis, FTIR	40-60 nm	PVP	--	--	Surface area	--	[125]
Small sphere > prism > large sphere	*P. aeruginosa* > *E. coli*	Zone of inhibition	SEM, UV-vis, XRD	15-90 nm vs 150 nm	PVP-citrate-none	--	Combined particle and ion?	Size, surface area, facet (111)	--	[73]
Cube > octahedral	*E. coli*	% viability	TEM, SEM, XRD	40-80 nm, 500-800 nm		--	Particle	Facet (100)	--	[122]

Table 1.3 (continued)

Prism mixture > sphere	*E. coli*	MIC, growth rate, lag phase	SEM, XRD, HR-TEM	10-50 nm vs 5 nm	all citrate	--	Combined particle and ion	Facet (111), number of interaction /binding sites	--	[120]
Prism > small spheres > large spheres	*E. coli*	Zone of inhibition	TEM, UV-vis, XRD, EDX	25-400 nm vs 4-40 nm	Citrate-Borohydride-PVP	--	Particle	Facet (111), geometry – sharp vertex and edge, size	--	[121]
Sphere = wire (no shape-based effects)	Recombinant bio-luminescent and Ag(I)-induced *E. coli* MC1061	EC_{50}, growth curve, % inhibition of bacterial bioluminescence, % viability	GF-AAS, SEM-FIB-EDX, ELS/DLS	50-100 nm vs 70-150 nm by 3,000-8,000 nm	Citrate, unknown (-36 and -46 mV)	Wire (2.4%) = sphere (2.2%)	Ion*		--	[40]
Cube = sphere = wire (no shape-based effects)	*E. coli* > *B. cereus* > *P. aeruginosa*	Growth curve	TEM, XRD, UV-vis	36 nm vs 44 nm vs 82 nm (15, 13, 5 cm^2/mL)	all PVP	--	--	--	--	[55]
Prism = cube = sphere (no shape-based effects)	*S. aureus*, *methicillin-resistant S. aureus*	Growth curve, % viability	SEM, DLS, UV-vis	20 nm vs 30 nm 15 nm	all PVP (zeta potential varied)	--	--		--	[123]

1.2 Dissertation Objectives and Scope

As discussed above, the identified research gaps and inconsistent findings in nanoparticle-driven antimicrobial activity as well as the need for a next-generation antimicrobial to combat the AMR crisis motivates the work of this dissertation. The overall objective of this dissertation is to inform rational design of antimicrobial silver nanoparticles (AgNPs) by elucidating underlying mechanisms of bacterial inactivation and resistance development in response to nanoparticle-specific properties. The central hypothesis is that tuning nanoparticle-specific properties is an effective approach to maximize antimicrobial activity and avoid the risk of bacterial resistance as an unintended consequence of its widespread use. Ideally, if we are able to uncover mechanistically what causes bacteria inactivation and what causes resistance to emerge, then (depending on what those mechanisms are) there is the potential to manipulate particle properties to maximize one and minimize the other. (Note: a possible outcome is that we cannot decouple the two – that the particle properties that lead to one are also linked to the other).

The following specific aims have been pursued to attain the overall objective:

i) Resolve the role of the nanoparticle on antimicrobial activity. This involves identifying studies that make appropriate comparisons between ion and nano-particulate forms of silver in their experimental design, critically analyzing their conclusions about ion and particle contributions to the observed biological response, and identifying trends between nanoparticle parameters and mechanisms of antimicrobial activity.

ii) Uncover the mechanism(s) of bacterial resistance towards AgNPs. This objective employs an experimental evolution approach, whole-population genome sequencing, comprehensive characterization of particle aggregation, and bacteria strains of varying motility to study the development of bacterial resistance towards ion and nano-particulate forms of silver.

iii) Elucidate the influence of nanoparticle shape on *E. coli* antimicrobial activity. This objective is attained through preparation of a suite of nanoparticle shapes with controlled physicochemical properties, comprehensive characterization of their material properties, evaluation of their antimicrobial activity in *E. coli*, a detailed look at the effect of NP surface area, and speculation of underlying mechanisms of action imposed on the cells.

1.3 Dissertation Organization

Tuning nanoparticle-specific behavior to obtain unique, nanoparticle-driven antimicrobial activities is an under-utilized feature and current missed opportunity of using ionizing ENMs for antimicrobial applications. However, employing nanoparticle-specific behavior necessitates a mechanistic understanding of interactions between microorganisms and the nanoparticles, which is currently lacking. When this resolution is achieved, there is the opportunity to potentially optimize particle design to achieve high antimicrobial activity and low antimicrobial resistance using the identified nanoparticle features to tune their respective governing mechanisms. This

strategic design of nano-enabled antimicrobials has the potential to positively impact global public health, especially in this upcoming post-antibiotic era.

In Chapter 2, the role of the nanoparticle on antimicrobial activity is investigated. A systematic literature review was conducted to identify studies that make appropriate comparisons between the two forms of silver and draw valid conclusions of ion and particle contributions to antimicrobial activity. This included only studies that scaled Ag ion controls to the concentration of Ag ions released from the AgNPs. Conclusions from these studies were analyzed and trends between nanoparticle parameters and particle-specific mechanisms of antimicrobial activity were identified. The results of this analysis indicate that the antimicrobial effects of AgNPs are not governed by ion release alone or in all cases, but that nanoparticle-specific activity is present, and at times, acts in concert with or independently from the Ag ions. This suggests an opportunity to elucidate both underlying ion-independent antimicrobial mechanisms and mechanisms that act in concert with Ag ions, as well as whether nanoparticle-specific parameters can be manipulated to influence these mechanisms. Nanoparticle size and surface chemistry are identified as two critical factors that have been suggested to elicit particle-specific effects. Interestingly, the identified subset of literature reveals nanoparticle shape as being understudied using appropriate ion and particle comparisons.

As an unintended consequence of widespread AgNP use, the development of bacterial resistance towards AgNPs is explored in Chapter 3. Here, an experimental evolution approach was used to select for and measure *E. coli* resistance to both ion and nano-particulate forms of silver. Results show that *E. coli* emerges resistance to AgNPs but not to Ag ions, indicating a specific resistance to AgNPs. Stability of the resistant phenotype was also explored by removing and re-introducing the AgNP pressure, after which whole-population genome sequencing was carried out

to identify any mutations associated with the heritable resistance. A *cusS* mutation was identified and likely imparts resistance by increasing silver ion efflux. Lastly, this chapter examines whether AgNP resistance emerges because of particle aggregation or from bacteria-interactions with the particle, particularly interactions centered around the flagella. For this, particle aggregation was monitored and the emergence of AgNP resistance was evaluated in hyper- and non-motile *E. coli* strains. Upon comparing AgNP resistance profiles, selective emergence of AgNP resistance based on bacterial motility is found with no difference in particle aggregation, suggesting that the mechanism may be mediated by flagellum-based motility. This bodes well for using motility as a predictor of AgNP resistance and could inform design of nano-enabled antimicrobials that target specific bacteria.

Given the lack of mechanistic understanding of nanoparticle shape identified in Chapter 2, the influence of nanoparticle shape on *E. coli* antimicrobial activity is further explored in Chapter 4. First, a suite of AgNP shapes including pseudo-spheres, cubes, and discs were prepared with controlled surface areas and surface chemistries and comprehensively characterized. Antimicrobial activity, as half-maximum effective concentration EC_{50}, was then evaluated in *E. coli* and compared amongst the shapes. Results indicate that discs impart the greatest antimicrobial activity, followed by cubes and then spheres, which remains the same trend when antimicrobial activity is normalized to NP surface area, suggesting that surface area likely does not play a major role in shape-based antimicrobial activity.

Finally, Chapter 5 summarizes the key findings of the dissertation research, underscores the significance of the work and discusses its implications, and suggests areas for future research.

2.0 It's Not All About the Ion: Support for Particle-Specific Contributions to Silver Nanoparticle Antimicrobial Activity

This chapter has been published as:

Stabryla, L.M.; Johnston, K.A.; Millstone, J.E.; Gilbertson, L.M. Emerging investigator series: it's not all about the ion: support for particle-specific contributions to silver nanoparticle antimicrobial activity. *Environmental Science: Nano*, **2018**, 5(9): 2047-2068. DOI: 10.1039/c8en00429c. **(reprinted with permission from the Royal Society of Chemistry)**

Silver nanoparticles (AgNPs) and other ionizing engineered nanomaterials (ENMs) are candidates for the development of antimicrobial agents due to their efficacy, multiple modes of bacterial inactivation, and tunability with respect to both the magnitude and mechanisms of antimicrobial activity. Exploiting this versatility requires elucidating the bacterial inactivation pathway(s) of the ENM, and in particular, the link between material properties and the desired biological endpoint. The mechanisms of antimicrobial activity for macrosilver, silver salts, and AgNPs have been widely studied, and largely attribute this activity to the release of Ag ions via oxidation and dissolution of the surface Ag atoms. However, it has also been established that Ag ion exposure alone does not elicit the same bacterial response as exposure to AgNPs, which suggests that the observed antimicrobial activity is induced not only by solubilized ions but also by the ENM itself. Resolving the role of the AgNP is critical to informing design of nano-enabled antimicrobials *a priori*. Herein, we present a systematic review of the AgNP antimicrobial activity literature, and specifically focus on studies that scale Ag ion controls to the likely quantities of bioavailable Ag released from AgNPs. This literature selection criterion reveals the critical role of

scaled ion controls in distinguishing ion and particle contributions to the observed antimicrobial activity. Overall, our analysis of this literature indicates that in most cases of bacteria exposure to AgNPs, particle-specific activity is observed and acts in concert with and/or independently from solubilized Ag ions alone. These results are exciting and suggest that more efficacious Ag- and ENM-enabled antimicrobials can be obtained through ENM design.

2.1 Introduction

Antimicrobial agents are crucial and ubiquitous in many industries, including health care,[1-3, 25, 31, 131-134] food and agriculture,[2, 3, 135-137] water treatment,[1-3, 131, 138] and drinking water distribution.[1-3, 131, 138] An increasingly critical challenge associated with antimicrobial use is that the target microbe can build resistance over time.[1, 2, 27, 31, 86, 107, 132, 133, 139, 140] Silver nanoparticles (AgNPs) and other ionizing engineered nanomaterials (ENMs) are candidates for the development of superior antimicrobial agents due to their efficacy, multiple modes of organism inactivation, and tunability with respect to both the magnitude and mechanisms of antimicrobial activity. Exploiting the enhanced functionality of ENMs as well as ensuring that they combat rather than contribute to the global antimicrobial resistance challenge requires resolving their mechanisms of organism inactivation, particularly the link between material properties and the desired biological endpoint.

Silver and AgNPs are among the oldest and most widely used antimicrobial agents,[28, 29, 138] and their antimicrobial properties have been studied extensively.[27, 139] For example, dating back to 7,000 years ago, silver-lined vessels and silver coins in containers of water or milk were used to preserve rations during military conflicts.[30, 31] Silver has also been used to treat

ulcers and aid in wound healing.[27, 30] The antimicrobial mechanism(s) of silver at the macroscale are attributed to the release of Ag(I) ions and their interactions with various aspects of the microbe.[27, 30, 139] For example, Ag(I) ions can interact with sulfhydryl groups on the cell surface, where the subsequent formation of the Ag-S bonds blocks respiration and electron transfer, leading to the collapse of the proton motive force, the de-energizing of the membrane, and eventually cell death.[1] The ionic radius of a Ag(I) ion is also sufficiently small (0.115 nm)[37] to travel through transmembrane proteins such as porins (30-50 kDa; pore size, 1- 3 nm).[36] Once inside the cell, Ag(I) ions may react with thiol functional groups in proteins and nucleic acids, interfering with DNA replication and deactivating many enzymatic functions.[1] In general, Ag(I) ions also increase the level of ROS inside the cell because thiol-containing anti-oxidative enzymes are deactivated by silver, thus exacerbating the damage done to proteins, lipids, and nucleic acids.[1]

Compared to their macroscale counterparts, AgNPs exhibit enhanced ion release per unit mass mainly due to an increased surface area to volume ratio. Yet, the precise mechanism(s) of AgNP action remain unresolved, particularly the dynamic contributions of the NP and Ag(I) ion.[27, 139] There are three overarching possibilities for mechanisms of AgNP antimicrobial activity. The first is that AgNPs are simply a passive Ag(I) ion reservoir, and (as in the case of macroscopic silver) released Ag(I) ions are responsible for any antimicrobial activity.[19, 27, 35, 38, 60, 64, 141, 142] The second possibility is that antimicrobial activity of AgNPs is a result of particle-only effects (e.g., physical disruption or alteration of the phospholipid cell membrane, production of ROS at the cell surface, or surface proteins that can bind to the NP but do not bind Ag(I) ions), putting into question the necessity of Ag(I) ions and their claim as the main agent of cellular impact.[27, 38, 75, 143] The third possibility is some combination of the first two

mechanisms, and/or some degree of synergistic effects between the released Ag(I) ions and the particle action. For example, there may be unique passive transport pathways in the bacterial cell (e.g., outer membrane porins, altered membrane permeability) accessible to particles at the nanoscale that facilitate the delivery of intracellular Ag(I) ions, a phenomenon known as the Trojan horse mechanism.[27, 64, 72, 144-146] Overall, the current literature contains support for all three possibilities. This ambiguity in the mechanisms of AgNP antimicrobial activity limits our ability to rationally design nanoparticle-enabled antimicrobials, and further, to leverage the material tunability of these ENMs.

While some of the existing mechanistic ambiguity is surely due to the complexity of the systems themselves, a non-trivial component arises from inconsistences in experimental designs across studies. Critical components of the experimental design include control of AgNP morphology (i.e. size, shape, surface chemistry), NP synthesis and washing steps, composition of the bacterial growth medium, bacterial strain used, measured toxicity endpoint and the methodology used to assess it,[66] and the treatment of the pure Ag(I) ion control.

Of all of these parameters, the most critical for distinguishing particle-specific antimicrobial activity is arguably the measurement and experimental controls for Ag(I) ion release. Ion controls are used in experiments analyzing the antimicrobial activity of ionizing ENMs in order to identify the biological effects that arise solely due to the ion portion of the ENM system and then compare to the effects of the ENM. Ion controls may be delivered to the experimental system as a silver salt (e.g., $AgNO_3$, $AgC_2H_3O_2$, Ag_2SO_4) or as the isolated ions in the supernatant of a AgNP suspension. There are two key components to a pure Ag(I) ion control: the concentration of ions introduced to the bacteria and the kinetics of that introduction. The total concentration of Ag(I) ion used as a control should reflect, as closely as possible, the concentration of ions released

from the NPs used in the study. Matching these concentrations requires the ability to measure released Ag(I) ions, which can be challenging (*vide infra*).

In order to accurately dose the bacteria with the established concentration of ions, ideally, the rate of Ag(I) ion release would also be known. Many studies deliver a single or pulse dose of Ag(I) ions that is equivalent to the total silver concentration in the AgNP system, which mimics the complete and instantaneous dissolution of the AgNP rather than the release of Ag(I) ion from the AgNP over time. In addition to not capturing the kinetics of Ag(I) ion release, this approach to ion controls does not accurately represent the AgNP system, since only a fraction of the AgNP forms Ag(I) ions at any given time.[147-149] As such, the resulting conclusions regarding ion-only, particle-specific, and combined ion-particle effects are confounded by the inaccurate representation of the Ag(I) ion component of the AgNP system.

Here, we review more than 300 publications on the cytotoxicity of AgNPs, 59 of which specifically aimed to distinguish ion-only, particle-only, and combined ion-particle contributions to the observed antimicrobial activity using methodologies that included an ion control. In other words, we focus on studies that specifically draw conclusions about the *contribution* that the ion and particle play in the *mechanism* of antimicrobial activity and not studies that only evaluated the potency of AgNPs. We then critically analyze the conclusions from 30 of these 59 studies (51%), focusing on those studies that implemented scaled ion controls (*vide infra*), to identify trends in particle parameters and other experimental factors that indicate ion-only, particle-specific, and combined ion-particle mechanisms of antimicrobial activity. Interestingly, while the results of this analysis suggest an important role of Ag(I) ions, they also clearly highlight that the impact of the particle alone cannot be ignored. Further, the analysis reveals a critical opportunity to elucidate

these particle-specific antimicrobial mechanisms as well as whether particle-specific parameters can be manipulated to influence these mechanisms.

2.2 State of the Art: Factors Influencing Ion Release and Current Practices of Scaling Ion Controls

It is critical to systematically quantify released Ag(I) ions from the AgNPs to inform conclusions regarding the ion and particle contributions on antimicrobial activity. In this section, we discuss the state of the art in measuring the quantity and kinetics of Ag(I) ion release from AgNPs to inform ion controls.

2.2.1 Factors that Influence the Extent of AgNP Oxidation and Ion Release Can Guide Ion Control Selection

For AgNPs in aqueous systems, Ag(I) ion release typically begins with oxidation of the NP surface. Oxidation of the AgNP surface and release of Ag(I) ions involves several processes that occur simultaneously and are dependent on both particle (e.g., size, shape, and surface chemistry) and experimental factors (e.g., dissolved oxygen, time, and broth chemistry).[35, 64, 66, 75-77, 149-153] Modulating these pathways can control both the quantity and kinetics of ion release.

In general, Ag(I) ion release is initiated by the adsorption of oxygen onto the particle surface followed by subsequent electron transfer.[153] Then, AgNPs evolve a surface bound silver oxide (Ag_2O) layer.[149, 154] The process of ion release begins as this layer is stripped and a new layer forms. However, once the initial silver oxide surface layers are removed by dissolution, Ag(I)

ion release is minimized.[149] The amount and strength of oxidizers (e.g., H_2O_2 versus O_2) present in solution influence the extent of oxidation.[81, 148] The stronger the oxidizer (i.e., having greater redox potential), the faster the oxidation rate, where the process follows Arrhenius behavior.[81, 152] Protons are then required for the dissolution of the silver oxide layer and thus, Ag(I) ion release is strongly pH dependent.[149, 152, 154] In addition, suppression of oxidation can occur with the addition of organic matter and stabilizing ligands, a reduction in temperature, or an increase in pH.[152] Given these differences in kinetics, the relevant extent of Ag(I) ion release also depends on the exposure time between AgNPs and the bacteria system of interest.[152] This time-dependent ion release suggests the importance of monitoring ion release continuously in the AgNP system and using it to inform both the concentration of the ion control and the rate at which it should be delivered to the system in order to mimic the AgNP system as accurately as possible.

The particle alone can influence the oxidation and dissolution process and so the ion control needed for each particle type will be different. Generally, smaller particles have a greater radius of curvature and therefore oxidize at a faster rate, a phenomenon described by the Ostwald-Freundlich equation.[76, 155, 156] Different surface-exposed facets also have different reactivity towards oxygen,[72, 74, 157-159] highlighting the effect of parameters such as particle shape on the oxidation process. Finally, surface chemistry also influences dissolution via capping ligands[79] and insoluble passivation layers, which influence the dissolution behavior (total concentration and location).[76, 77, 150, 151, 160] Silver oxide surface layers can be removed to varying degrees when AgNPs are washed post-synthesis (to remove residual impurities), synthesized anaerobically, or synthesized aerobically and reduced by hydrogen to zero-valent AgNPs before exposure to bacteria, which can all significantly reduce Ag(I) release.[149] Biologically synthesized NPs from plant extracts can also induce different surface chemistries

(number and packing distribution of ligands and biomolecules) as compared to chemically synthesized NPs.[65, 141, 161] Thus, the AgNP synthesis and purification approach may affect the surface structure and as a result, Ag(I) ion release. These studies highlight the importance of performing and reporting the AgNP method of synthesis and purification procedures.[75, 149] Overall, particle-type specific dissolution is a determining factor guiding the selection of an appropriately scaled ion control for specific particle types.

It is critical that ion release is monitored in the exposure media/environment of the AgNP system because the type of environment can influence dissolution, and in turn, the ion control that should be used for that specific system. For example, there are multiple types of growth media used to provide vital nutrients that enable bacterial growth (e.g., buffers, sodium chloride, water, and commonly used broths such as Mueller Hinton, MH, and Luria-Bertani, LB). Due to differences in pH and media constituents (e.g., dissolved ionic species, proteins, peptides, carbohydrates), the specific media used can impact dissolution, the magnitude of AgNP antimicrobial activity, and the dominant mechanism through which that activity occurs (i.e., the Ag(I) ion, the AgNP, or a dynamic synergism between the particle and its released Ag(I) ions). In one case, we have compared AgNP antibacterial activity in two commonly used bacterial growth media (LB and MH broth).[66] Using controlled exposures to AgNPs and Ag(I) ion, we measured a differential impact (measured as a difference in the bacterial growth delay and maximum achieved bacterial growth in relation to the untreated bacteria) – in the two media.[66] This difference suggests that there is a complex interplay between the particle and the surrounding environment, which can result in enhancement or inhibition of Ag(I) release from the AgNP surface[76, 77, 150-152, 162] as well as changes in surface charge and particle stability that could eliminate particle-specific effects.[76, 77, 81, 150, 151, 163, 164] For example, dissolution can be

influenced by the concentration of chloride present in the growth medium; low chloride concentrations form a AgCl(s) passivation layer on the AgNP surface that inhibits dissolution whereas high concentrations of chloride result in the formation of soluble AgCl complexes and promote dissolution.[162] Overall, the confounding influence of media on AgNP behavior not only cautions comparison of antimicrobial activity across studies, but also underlines the importance of determining interactions of media constituents with themselves, the NP surface, and the released ions.

The presence of bacteria and their metabolic state additionally affect dissolution, and thus will affect the concentration of the ion control needed to accurately model the AgNP system. Bacteria (i) play a role in altering the dissolved oxygen concentration and pH of the experimental system and (ii) introduce extracellular polymeric substances (EPS) that can non-specifically adsorb to AgNPs.[35] For example, EPS (and other components of the growth media) can form a protein corona around the NP surface and either prevent dissolution or increase the dissolution gradient by binding the released Ag(I) ions upon direct association with the cell (via Le Chatelier's principle).[35] In this regard, bulk dissolution should be monitored in the presence of bacteria and be used to inform accurate concentrations and kinetics needed for appropriately scaled ion controls.

Upon release to the experiential system, there are numerous binding and partitioning events that Ag(I) ions can experience. Ag(I) ions can resorb onto the AgNP surface, remain free in solution, complex with media components, bind to the cell surface, or enter the cell where they can bind to intracellular components or be reduced by them to form new AgNPs.[76, 152] However, more work is needed to accurately capture the dynamics of the AgNP oxidation process by considering the complex interplay of all factors discussed.[152] This complexity suggests the

need to monitor intracellular ion release in addition to bulk ion release. Also, techniques should be used to resolve Ag bound to macromolecules in suspension. Combined, such experiments can inform the delivery of ion controls that accurately mimic the AgNP system and allow us to decouple true ion and particle contributions to antimicrobial activity. **Figure 2.1** presents a visual summary of all potential Ag(I) ion release pathways, binding, and partitioning events.

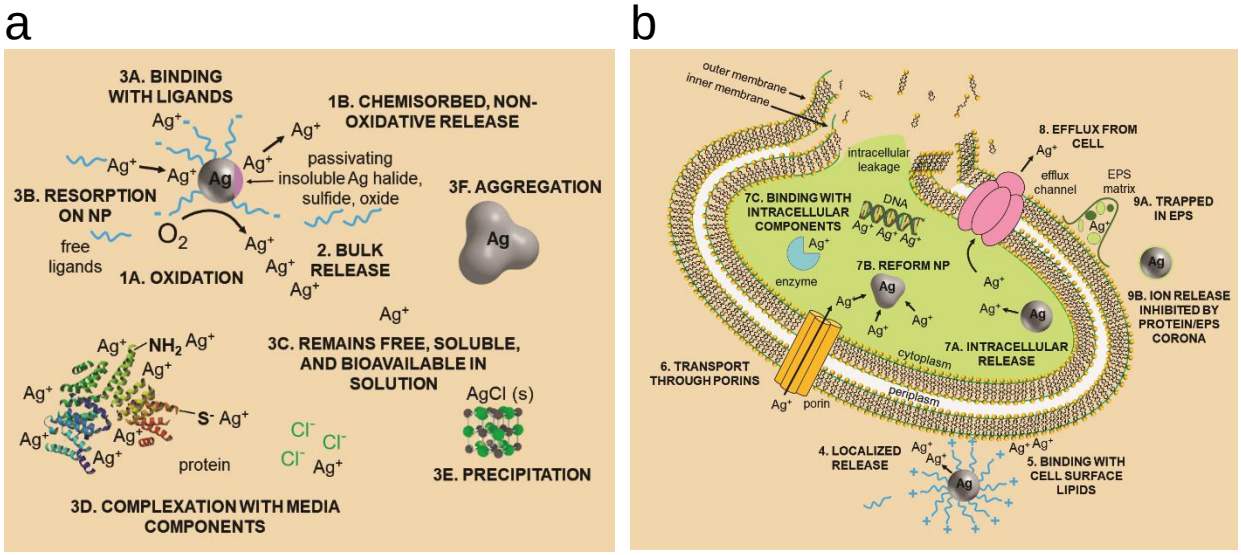

Figure 2.1. Potential Ag(I) ion release pathways, binding, and partitioning events within the AgNP exposure condition.a) State of Ag in the media, external to the bacterial cell. b) Interaction of silver with the cell and state of Ag inside the cell. Note: figure is not to scale as the particle is enlarged to demonstrate effect.

2.2.2 Equating the Concentration of the Ion Control to the Total Ag Concentration in the AgNP System

The challenge with many ion controls used in AgNP antimicrobial activity studies is that they are equivalent to the total silver concentration in the AgNP system and therefore, do not accurately represent the portion of Ag(I) ion present in the test system. There are different forms

and concentrations of silver present in the AgNP system (i.e., the Ag(0) form of the nanoparticle and the dissolved Ag(I) form, **Appendix Figure A.1A**), which influences the bioavailability of the silver and the resulting biological impacts. The amount of Ag(I) present depends on the extent to which the AgNP oxidizes to release Ag(I) ions as well as the tendency for those ions to complex with components of the exposure media (e.g., chloride to form AgCl(s) or soluble AgCl complexes). Typically, only a portion of the AgNP oxidizes to form Ag(I) ions and as a result, the proportion of silver present as Ag(I) is small relative to Ag(0). Therefore, using an ion control at the same mass concentration as the total silver content of the AgNPs (hereafter referred to as an overestimated ion control) makes for an unequal comparison of the resulting biological activity and calls into question the mechanistic conclusions drawn from such studies (**Appendix Figure A.1B and 1C**).

2.2.3 Quantifying Ion Release in Bulk Solution to Inform an Ion Control

An improved approach to selecting the concentration of the ion control involves the quantification of Ag(I) ion release in the AgNP system, which is commonly pursued using either a Ag(I) ion-selective electrode or ultraviolet-visible (UV-vis) spectroscopy, or by first separating the Ag(I) ions from the AgNPs by centrifugation or dialysis and then analyzing with inductively coupled-plasma mass or atomic emission spectroscopy (ICP-MS or AES) or graphite furnace atomic absorption spectroscopy (GF-AAS).[35, 38, 39, 46, 48, 50, 51, 56, 64-66, 69, 79, 119, 165, 166] It is important to note that when dialysis membranes are used to separate ions from particles,[52, 167, 168] the osmotic pressure difference does not allow for complete isolation of Ag(I) ions, limiting the utility of this approach. Furthermore, Ag(I) ion concentration in the bulk suspension is most often measured at a single time point (typically at the culmination of the

experiment),[35, 38-40, 50, 52, 56, 64, 79, 119] which excludes the kinetics of ion release. An alternative approach that aims to capture the dynamics of ion release will quantify Ag(I) ion concentration at multiple time points over the duration of the experiment.[19, 46, 65, 66, 68, 69, 165, 167] When this approach is used, Ag(I) ion controls can be employed in a way that closely mimics the AgNP exposure system. Finally, these techniques measure the free Ag(I) ions present in the bulk solution but do not capture the Ag(I) ions that are removed from solution via subsequent interactions with the surrounding environment (e.g., inside the cell or bound to macromolecules in the suspension). As a result of this limitation, the concentration of Ag(I) ions dosed in as a silver salt control may be inconsistent with the "real" concentration released by the AgNP (both intracellularly and extracellularly).

2.2.4 Quantifying Intracellular Ion Release to Inform an Ion Control

In an effort to circumvent the abovementioned confounding interactions, researchers measure intracellular Ag using a bioluminescent *E. coli* Ag-biosensor[36, 38, 40, 165, 169] or the Ag content of the membrane and cytoplasm fractions of the cell,[79] rationalizing that these fractions of silver are impacting the bacteria. Yet similar to the methods above, intracellular ion release is monitored at a single time point.[38, 40, 165, 169] While intracellular Ag monitoring quantifies the concentration of Ag to which the cell is directly exposed, it has not typically been used to inform the concentrations and dosing of silver salt ion controls. Doing so would allow for accurate modeling of the AgNP system, particularly if used in combination with bulk dissolution monitoring.

2.2.5 Suggested Best-Practice for Scaling Ion Controls

The complexity of the system and challenges faced when quantifying the presence of released ions in solution and in the microorganism suggest that a new approach to ion controls is necessary to obtain comprehensive ion release profiles within the AgNP exposure condition. The desired approach will account for the kinetics of Ag(I) ion release and model an accurate representation of the AgNP system. To ascertain and then implement these controls, there are three key experimental components: (i) continuous monitoring of ion release from AgNPs in the exposure media and in the presence of bacteria as well as intracellularly over the duration of the experiment,[19, 46, 65, 66, 68, 69, 165, 167] (ii) deliver these measured ion concentrations as a series of continuous doses that mirror their release from the ENM, and (iii) subsequently monitor the bacterial endpoint of interest. This preferred comprehensive best practice approach to achieve an appropriately scaled ion control, although labor intensive, is necessary to robustly decouple the contributions of the particle and the ion.

2.3 Experimental

2.3.1 Literature Review

A comprehensive literature survey to identify studies on the cytotoxicity of AgNPs resulted in more than 300 publications. Google Scholar, Scopus, Compendex, and Web of Science databases were queried using all combinations of the following search terms: “silver nanoparticle”, “silver ion”, “antimicrobial”, “(cyto)toxicity”, and “mechanism”. The SciFinder database was also

queried using “silver nanoparticle and toxicity and mechanism” as the initial search term and then further refined to include “ion” and “bacteria”. The sheer size of this set of studies and the heterogeneity of experimental designs did not allow for meaningful discernment of the contributions of the AgNP and Ag(I) ions. Given the extensive use of AgNPs as antimicrobials in a wide range of products, we decided to limit the scope of our literature review to studies that use bacteria as their model organism. With the goal of resolving the ion and particle debate, we further narrowed the scope to those publications that specifically aim to distinguish ion-only, particle-only, and combined ion-particle contributions to the observed antimicrobial activity. In other words, we focus on studies that specifically draw conclusions about the *contribution* that the ion and particle play in the *mechanism* of antimicrobial activity and not studies that only evaluated the *potency* of AgNPs (often culminating in the conclusion that the Ag(I) ions are *more toxic* than the AgNPs). This selective literature set included 59 studies. The literature was further refined to attain a final subset of studies that (i) included comprehensive characterization of AgNP size (by transmission electron microscopy, TEM, at a minimum) and shape, (ii) defined the AgNP dose(s) delivered under the exposure condition using ICP-MS, UV-vis, or GF-AAS, and (iii) included a scaled ion control (as determined through calculation, described in detail below, using results from criteria i and ii) that was delivered under the same exposure conditions as the AgNP (i.e., in the same growth medium and bacteria). This final subset of literature contained 30 studies and was used in our analysis. Given that we used scaled ion controls as a metric for determining inclusion and exclusion of studies (i.e., pre-specified eligibility criteria), we refer to our analysis as a systematic review.[170] A descriptive summary of each study is compiled in **Appendix Table A.1.**

A scaled ion control is defined here as having an equivalent concentration of silver atoms to the bioavailable silver that is released from the AgNPs as Ag(I) and is delivered to the experimental system as a silver salt (e.g., $AgNO_3$, $AgC_2H_3O_2$, Ag_2SO_4) or as the isolated ions from the AgNP. This factor is a distinguishing criterion because scaled ion controls are crucial for valid comparison of ion-only, particle-only, and combined ion-particle contributions to AgNP antimicrobial activity. The calculations we use to determine a scaled ion control consider the extent to which a AgNP of a given particle size and shape can dissolve to its bioavailable Ag(I) form based on the surface atoms available for oxidation and will be discussed in detail below.

2.3.2 Scaled Ion Control Calculations

The following calculations outline our approach to determine scaled ion controls in each experimental AgNP system. Briefly, the percent of AgNP oxidation and subsequent ion release necessary to obtain Ag(I) ion concentrations equivalent to the ion controls used in a given study (i.e., the expected bioavailable silver) was calculated by comparing the total concentration of silver atoms (on a mol/mL basis) present in the reported ion control and in the delivered particle dose(s). The theoretical percentage of AgNP surface atoms available for oxidation was calculated by considering the size and shape of the AgNP studied (*vide infra*), which is why inclusion of particle characterization by TEM is critical and serves as the basis for defining a scaled ion control.

Due to ambiguity in the concentrations of the ion controls and AgNPs reported in the literature, we carried out the calculations under two feasible assumptions: (i) the reported concentration indicates the concentration of the total silver salt or AgNP, and (ii) the reported concentration indicates the total silver atom concentration of the silver salt or AgNP. The difference in results for these two assumptions was insignificant for the silver salt, but significant

for the AgNP. The assumption that the reported concentrations of AgNPs were as amount of AgNPs per unit volume resulted in unrealistic values of necessary AgNP oxidation (e.g., 10^{29}%) and rejection of every study for having an overestimated ion control. Therefore, the calculations proceeded assuming the reported concentration was of the total silver atom concentration unless otherwise specified in the study. This assumption is further rationalized by the fact that those studies including details on how they determined AgNP concentrations used characterization techniques (e.g., ICP-MS or AES, UV-vis, or GF-AAS) that measure total silver atom concentrations.

The following example calculation demonstrates the approach used to determine the concentration of Ag(I) ions in the silver salt control in units of moles per mL:

$$\frac{\mu g}{mL}\ Ag(I)\ as\ silver\ salt * \frac{1\ g}{10^6 \mu g} * \frac{1\ mol\ Ag(I)}{107.87\ g} = \frac{mol\ Ag(I)}{mL}\ as\ silver\ salt \qquad \textbf{Eq. 2-1}$$

which for a reported concentration of 0.4 $\frac{\mu g}{mL}$ Ag(I) (delivered as $AgNO_3$) equates to 3.71x10^9 $\frac{mol\ Ag(I)}{mL}$ (delivered as $AgNO_3$). The same approach was used to determine the equivalent concentration for AgNPs (shown here as an example for a reported concentration of 0.4 $\frac{\mu g}{mL}$ AgNP):

$$0.4\frac{\mu g}{mL}\ Ag(I)\ as\ AgNP * \frac{1\ g}{10^6 \mu g} * \frac{1\ mol\ Ag(I)}{107.87\ g} = 3.71\ x\ 10^{-9}\frac{mol\ Ag(I)}{mL}\ as\ AgNP \qquad \textbf{Eq. 2-2}$$

Since the silver salt ion control is at the same mass concentration as the AgNP (0.4 $\frac{\mu g}{mL}$), the values are the same, which is expected given the assumption that the concentration represents the total silver atoms. This ion control assumes that the AgNPs completely dissolve, and thus delivers an ion concentration that exceeds the amount of Ag(I) ions that is realistically released from the

AgNPs (*vide infra*). Example calculations using the alternative assumption are outlined in Appendix A. The percent of AgNP oxidation necessary to release Ag(I) ion concentrations equivalent to the ion controls used in the respective study was calculated as follows:

$$\%\ AgNP\ oxidation = \frac{\frac{mol}{mL}\ Ag(I)\ as\ AgNO_3}{\frac{mol}{mL}\ Ag(I)\ as\ AgNP} * 100 \qquad \textbf{Eq. 2-3}$$

To determine whether the necessary extent of oxidation is reasonable, the theoretical extent of oxidation was calculated under the assumption that only a single monolayer of the NP is available for oxidation. This assumption is empirically supported. For example, Sotiriou et al. found that the equilibrium Ag(I) ion concentration released from the particle into solution corresponds with the dissolution of one to two monolayers and is dependent on the particle size.[149] For particles greater than 8 nm, the mass fraction of released Ag(I) ions is equivalent to the mass of a single silver oxide monolayer, whereas dissolution of particles less than 5 nm in diameter corresponds to oxidization of two silver oxide surface layers.[149] An intermediate extent of oxidation, i.e., in between one to two silver oxide surface layers, appears for particles sizes between 5-8 nm. We proceeded with the assumption that theoretical dissolution was equivalent to the oxidation of the outermost surface monolayer because 95.5% (64/67) of the AgNPs in the identified literature are greater than 5 nm (the three studies that include AgNPs less than 5 nm also included AgNPs with diameters greater than 5 nm). To estimate this monolayer, the percentage of surface atoms on a given AgNP was calculated as follows:

$$\%\ surface\ atoms = \%\ ionization = \frac{surface\ atoms}{total\ atoms} * 100 \qquad \textbf{Eq. 2-4}$$

The method used to calculate the volume (needed for determination of the total number of atoms) and surface area (necessary for determination of the total number of surface atoms) takes into account the size and shape of the AgNP used in a given study (equations in SI). For the

determination of surface atoms, the percentages of different surface facets present on AgNPs of different shapes were also considered, as this factor can influence the number and packing of the atoms on the surface, as well as influence surface reactivity and the propensity to oxidize. Pseudo-spherical particles were the predominant particle shape studied in the identified literature subset and were approximated as cuboctahedrons, having eight (111) faces and six (100) faces, containing 63.4% and 36.6% of the surface atoms, respectively.[171] The monotonic relationship between nanoparticle size and the total number and percent of surface atoms is well established; the total number of surface atoms increases with increasing particle size and the percentage of surface atoms increases with decreasing particle size (see Figure 2 and Table 2 in reference [172]).[172] Forty percent oxidation was determined as a conservative threshold for a scaled ion control based on (i) the available percent surface atoms (0.6-26% based on calculation) determined from the AgNP size and shape, and (ii) the potential for additional ionization due to known influences of experimental conditions (*vide supra*), which cannot uniformly or robustly be considered in these calculations. As a result, ion controls that require > 40% of the AgNP to oxidize were considered overestimated. Following the example calculation above, the 1:1 ratio of Ag(I) ions as silver salt and AgNP would result in 100% of the AgNP needing to oxidize. This systematic review focuses solely on the results and conclusions presented in the subset of studies that included at least one scaled ion control. A schematic illustrating the approach to scaled ion control determination is presented in **Figure 2.2.**

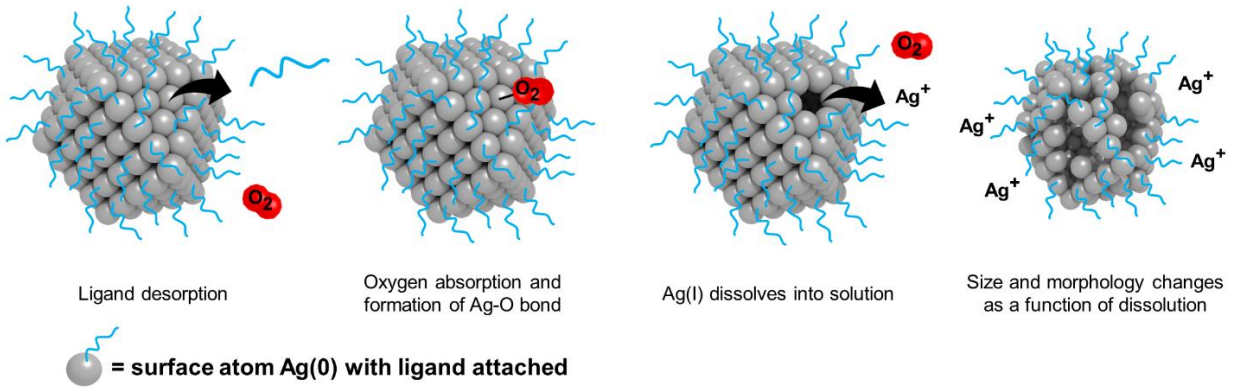

Figure 2.2. Theoretical dissolution of a given AgNP monolayer. The depicted process serves as the underlying assumption for establishing the threshold for a scaled ion control. The atom-by-atom surface dissolution of AgNPs initiated by (i) ligand desorption, (ii) oxygen sorption and formation of the Ag-O complex that begins oxidation of Ag(0) to Ag(I), (iii) Ag(I) dissolves into the continuous phase, and (iv) size and morphology of the particle changes as a function of dissolution.

These calculations enabled isolation of those studies that incorporated a scaled ion control that is representative of the total possible Ag(I) ion released from the AgNP studied. This narrowed the focus to conclusions drawn from these isolated studies with the goal of gaining clarity in the ion versus particle antimicrobial activity debate. Still, the calculations are not without limitations. First, the solvent environment (e.g., growth media),[64, 66, 77, 150, 151] the presence of bacteria,[35, 46] and surface chemistry (e.g., ligand identity, silver oxide formation), [38, 39, 50, 65-67, 75, 76, 78, 79, 160, 166, 173] among other factors, have all been shown to influence AgNP ionization (vide supra). Yet, the mechanisms remain unresolved and thus limit our ability to predict the influence of experimental conditions on Ag(I) ion release in the studies reviewed herein. Second, the calculations determine how much silver can theoretically ionize from the AgNPs indicating the bulk concentration of Ag(I) ion in solution, not the concentration of Ag(I) ion

internalized by the bacteria (intracellular silver), which Ivask et al. reports as being a better indicator and comparison of antimicrobial activity.[38]

Once Ag(I) ion enters the bulk solution, there are many possible interactions that occur depending on the environment, including diverse binding events and equilibria that can inhibit or drive ion release (*vide supra*). These interactions influence the fate of Ag(I) ions in a given experimental system and as a result, it is impossible to predict how many Ag(I) ions can and will enter the cell. Third, the calculations do not consider kinetics of ion release (i.e., the result represents the total possible dose of Ag(I) ion released from the AgNP). This omission is not to say that the studies reviewed do not consider kinetics, but rather that the kinetics of ion release are not included to determine whether a study incorporated a scaled ion control. Finally, these calculations are applicable to only particle diameters greater than 5 nm because the shapes are well-defined with easily calculable volume and surface area, have face-centered cubic (FCC) packing, and allow us to include a correction for the surface facets. As the particle diameter decreases to below 5 nm, the number of competing structural factors increases and the propensity for it to be referred to as a 'nanocluster' emerges. Different atom packing densities and arrangements become competitive and influence the shape and geometry of nanoclusters (e.g., the cuboctahedral geometry becomes icosahedral) so that they can no longer be easily approximated as spheres.[81, 174, 175] (Note: Only 3 studies included particles with diameters < 5 nm and those studies also included particles > 5 nm, so the calculations for the 5 nm NPs will not significantly influence the conclusions drawn in this study.)

2.3.3 Using Pivot Tables to Identify AgNP Properties and Experimental Variables that Discriminate Ion-Only, Particle-Only, and Combined Ion-Particle Contributions to Observed Antimicrobial Activity

The pivot table feature in Microsoft Excel (Ver. 2016, Microsoft Corporation, Redmond, WA) was used to identify discriminating factors influencing ion-only, particle-only, and combined ion-particle contributions to AgNP antimicrobial activity. Pivot tables are particularly useful for summarizing and making sense of large, detailed data sets. Qualitative data (e.g., experimental method parameters, conclusion drawn from the study) and empirical data (e.g., particle size, zeta potential) was compiled for each study and organized into an Excel spreadsheet (**Appendix Table A.1**), from which several analyses using pivot tables were conducted.

Conclusions from the identified subset of studies were categorized based on the study conclusions and accompanying data in support of an ion-only, particle-only, or combined ion-particle mechanism. Studies that attribute antimicrobial activity solely to Ag(I) ion release and concluded negligible particle-specific effects were categorized as 'ion-only'. Studies that identified and demonstrated the particle influence on antimicrobial activity – independent or in concert with Ag(I) ion release – were categorized as having a 'particle-only' or 'combined ion-particle' effect. For example, enhanced localized dissolution at the NP-cell interface or intracellular dissolution is enabled by the NP (as in the case of appending cationic capping ligands to guide targeted delivery[38]), yet the increased concentration of ions released in close proximity to the bacteria is often claimed to be responsible for the inactivation. The resulting enhanced bioavailability increases the antimicrobial impact over the equivalent concentration of bulk dissolved silver. The particle does not work independently from the ion, but the particle parameters can influence the magnitude of impact. In this paper, this mechanism is classified as 'combined

ion-particle' since the ion and particle are both necessary to achieve this enhanced antimicrobial activity. However, because ion release occurs concurrently with particle-only effects, it is difficult to decouple 'particle-only effects' and 'combined ion-particle' effects, especially when multiple particle types and support for multiple mechanisms appear in one study. Some studies include support for multiple conclusions as a result of particle manipulations and different methodology used to assess antimicrobial activity and so were categorized under multiple mechanisms.[38, 64] For example, in one study, there is evidence for 'combined ion-particle' effects when using one particle type, but 'particle-only' effects are supported when using another particle type.[38] The unknown mechanism through which the particle induces specific effects or enhances localized and/or intracellular dissolution adds to the complexity of decoupling these contributions, but further suggests the importance of the particle and the ability to shift mechanisms by manipulating particle parameters.

2.4 Results and Discussion

2.4.1 Identification and Evaluation of Studies Implementing Scaled Ion Controls

From the 59 studies identified as investigating ion-only, particle-only, and combined ion-particle contributions to bacterial cytotoxicity or antimicrobial activity, 30 studies (51%) included a scaled ion control as determined by the calculations presented above. Results of these calculations are compiled in **Appendix Table A.2.** From these 30 studies, 22 studies (73%) measured Ag(I) ion release from the AgNP in the experimental system. The reported dissolution in these 22 studies strongly agreed with our calculated theoretical dissolution, which serves as

further validation of the calculation method (see **Appendix Table A.2** and **Appendix Figure A.2** for demonstrated agreement of values). Additionally, this validation establishes the calculation method as a robust approach that can be used to inform scaled Ag(I) ion controls, especially if coupled with an empirical kinetic law of oxidation to estimate the kinetics of ion release, similar to those developed by Liu and Hurt for low AgNP concentrations[152] and Molleman and Hiemstra for pH-dependent and size-dependent ion release.[154] Of those 22 studies, the majority (74%) did not monitor the kinetics of Ag(I) ion release, but rather measured Ag(I) ion concentration at a single time point. While monitoring of kinetic release was not a mandatory criterion for inclusion in our systematic review, it is an important aspect to consider given the wide variability of Ag(I) ion release than can occur and challenges associated with capturing kinetics of Ag(I) ion release (*vide supra*).

2.4.2 Support for Ion-Only, Particle-Only, and Combined Ion-Particle Contributions to AgNP Antimicrobial Activity

As stated earlier, the three possible contributions of the ion and particle to antimicrobial activity are supported by the literature and influenced by the physicochemical properties of the AgNP. **Table 2.1** summarizes the influence of particle parameters (i.e., size, shape, and surface chemistry) on the ion and particle contributions outlined in each of the three possibilities.

Table 2.1. Summary of ion-only, particle-only, and combined ion-particle hypotheses for AgNP antimicrobial activity as influenced by NP parameters.

Particle parameter	Ion-only mechanism	Particle-only mechanism	Combined ion-particle mechanism
Surface chemistry	Ligand density and ligand chemistry influences ion release into bulk solution 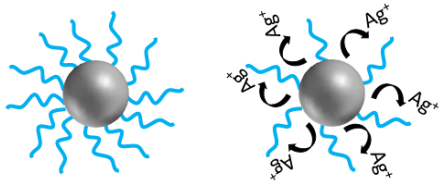	Charge influences attraction and repulsion to bacteria cell, further influencing contact with cell and damage through a physical mechanism 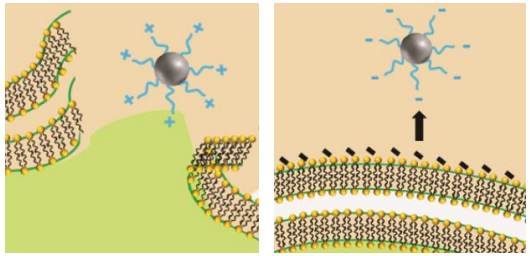	Charge influences attraction and repulsion to bacteria cell, further influencing localized ion release 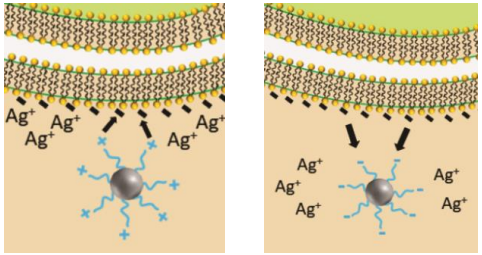
Size	Surface reactivity due to size influences ion release into bulk solution 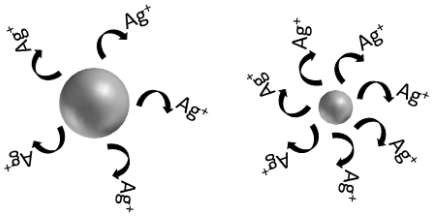	Size influences passive uptake and subsequently contact with cell and damage through a physical mechanism 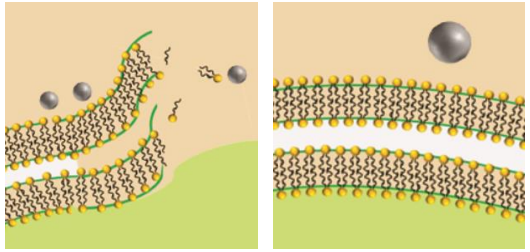	Size influences passive uptake and subsequently intracellular ion release 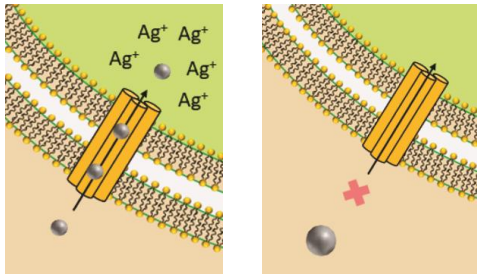

Table 2.1 (continued)

Shape	Surface reactivity due to shape influences ion release into bulk solution 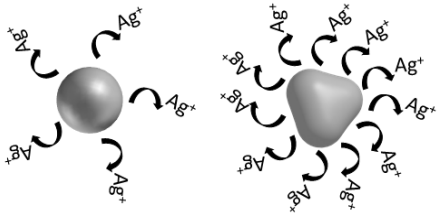	Shape influences contact with cell and damage through physical mechanism 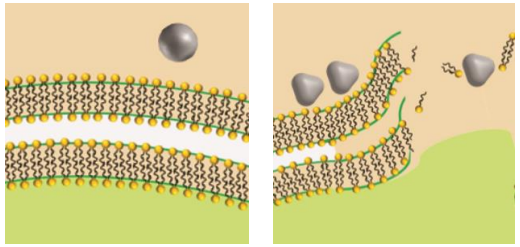	Shape influences localized and/or intracellular ion release 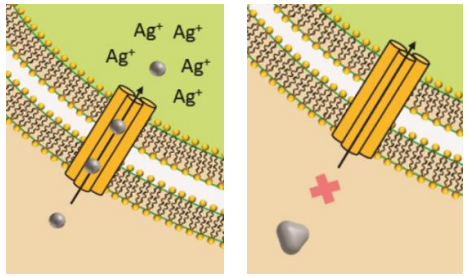

Isolating those studies that include a scaled ion control in their comparison of ion-only, particle-only, and combined ion-particle contributions to antimicrobial activity was intended to eliminate potentially confounding conclusions and to focus on those studies that offer robust discriminating conclusions. Of the 30 studies, 39% concluded that the observed antimicrobial activity results from an ion-only mechanism while 16% and 45% of studies concluded a particle-only and combined ion-particle mechanism, respectively (**Figure 2.3**).

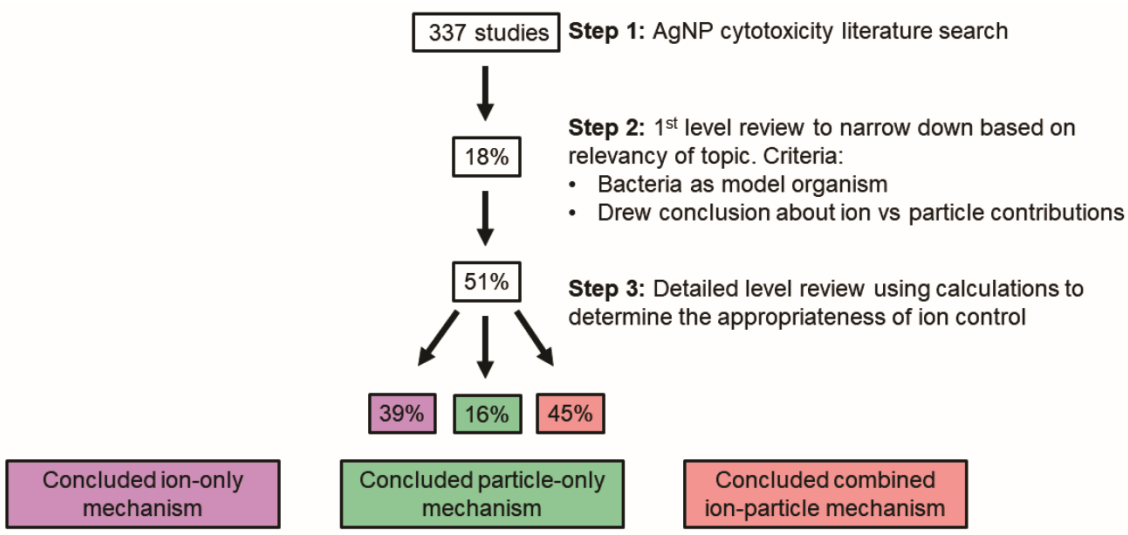

Figure 2.3. Scheme of the literature review process. The percent in the box is equal to the percent of studies fulfilling the requirement for that particular step. Only 30 studies (51%) included a scaled ion control. Of those studies, 39% concluded an ion-only mechanism (stating that the particle does not play a role) while 16% and 45% concluded a particle-only or combined ion-particle mechanism (stating that the particle plays a role).

These results indicate that the impact of the particle cannot be ignored and that there remains an opportunity to elucidate both underlying ion-independent antimicrobial mechanisms and mechanisms that act in concert with the Ag(I) ions as well as whether particle-specific parameters can be manipulated to influence these mechanisms. While the contribution of Ag(I)

ions to AgNP antimicrobial activity is largely indisputable, empirical support for ion-independent, particle-only effects suggests an opportunity to leverage particle property manipulation to further tune the mechanism and magnitude of impact. The precise mechanisms through which the particle induces antimicrobial activity are not resolved, yet particle size and surface chemistry are two critical factors that have been suggested and are further supported by the studies reviewed herein.[38, 39, 48, 57, 65, 75, 119, 165-167] The identified subset of literature included only one study[40] investigating the effect of particle shape, limiting our ability to draw any meaningful conclusions about the influence of shape.

2.4.2.1 Size-Dependent Mechanisms of AgNP Antimicrobial Activity

A size-dependent mechanism has been suggested to govern the antimicrobial activity of AgNPs with diameters ≤ 10 nm.[36, 38, 39, 48, 52, 75, 79, 119, 165] Of the studies that included AgNPs ≤ 10 nm, regardless of other sizes included, 71% concluded that particle-only or combined ion-particle effects dominate the antimicrobial activity (**Figure 2.4B**). (Note: This trend is not reflected in the '1-10 nm' size category of the main figure because studies including AgNPs ≤ 10 nm are split between the '1-10 nm' and 'range of sizes' categories.) The increased antimicrobial effect is suggested to result from more efficient contact with the bacteria[38, 165] and the increase of intracellular Ag(I) ions (determined by normalizing the EC_{50} values of the AgNPs to that of empirically determined intracellular Ag(I) ions[38, 165]). The mechanism through which intracellular silver is enhanced for particle diameters ≤ 10 nm remains unresolved, but is intriguing given that 10 nm has been identified as a threshold particle diameter below which theoretical ion release is increased due to enhanced surface reactivity (Ostwald-Freundlich equation),[76, 155, 156] meriting further research to resolve. One hypothesis is that at this length scale, particles are able to enter the cell,26[19, 64, 67, 72, 144, 146, 176]either through passive uptake (i.e., through

porins in the cell wall) or as a result of altered membrane permeability. Yet, the reported size of bacterial porins are between 30-50 kDa, which correspond to 1-3 nm, making internalization via these pathways unlikely for some particle sizes.[36, 64] The combined ion-particle mechanism proposes that enhanced localized dissolution at the NP-cell interface or intracellular dissolution through a Trojan-horse-type mechanism is enabled through increased interaction between the NP and bacteria.[38, 79] Finally, as the particle diameter decreases to below 5 nm, different atom packing densities and arrangements may become dominant,[81, 175] influencing the shape and potentially enhancing the antimicrobial activity observed at this size range. Given that only 3 studies included particles < 5 nm,[35, 69, 177] this is a topic deserving further study.[155]

Ion-only and combined ion-particle mechanisms emerge as nearly equivalent contributions to antimicrobial activity for particle diameters greater than 10 nm with negligible particle-only contributions. Interestingly, 67% of the studies that conclude ion-only mechanisms of antimicrobial activity do not include ≤ 10 nm AgNPs (**Figure 2.4B**).[40, 46, 47, 50, 51, 61, 64, 70] Those studies that included a wide range of particle sizes (including AgNPs from two or more of the size categories included in **Figure 2.4A**) overwhelmingly (79%) concluded particle-only or combined ion-particle effects[38, 39, 65, 75, 81, 119, 165-167, 169]as opposed to studies that looked at a single size or narrow size range, of which 28% concluded particle-only or combined ion-particle effects.[19, 36, 52, 57, 66, 68, 79, 178] These results suggest that size is a factor inducing particle-specific effects that emerges only when multiple AgNPs are studied simultaneously. Including a range of sizes in a study will thus establish the relationship (e.g., monotonic, monotonic and linear, non-monotonic) between mechanism of antimicrobial activity and size as well as whether the relationship is preserved across the full particle size spectrum. Adherence to or deviation from these relationships can provide support for either an ion-driven or,

in this case, particle-specific or combined ion-particle mechanisms that would otherwise not be realized by studying a single particle size or narrow size range in isolation.

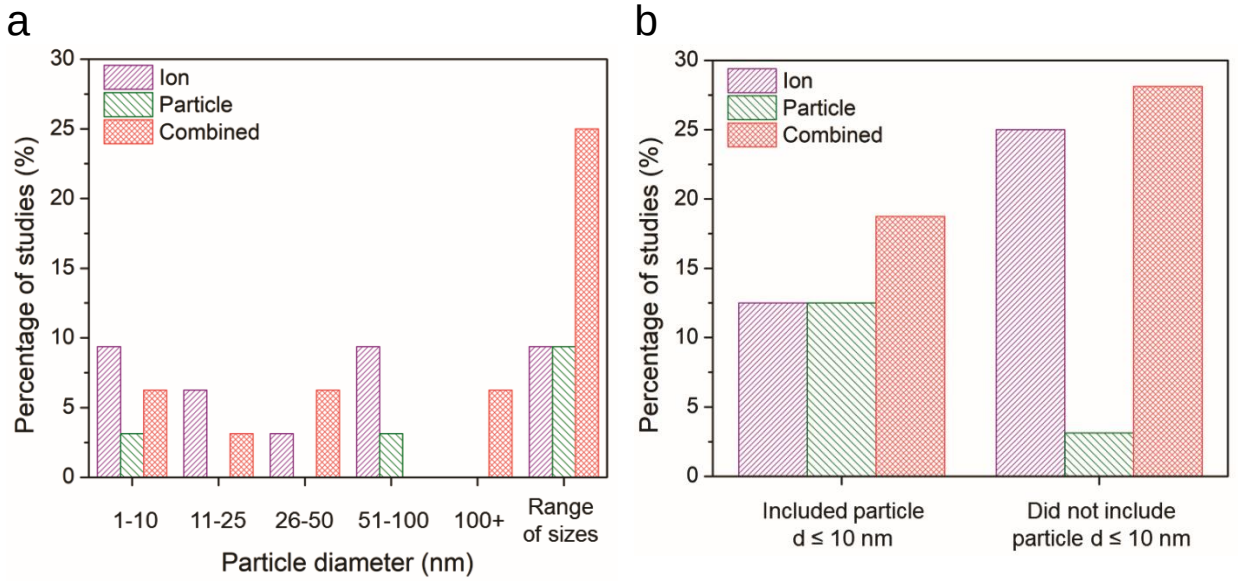

Figure 2.4. Ion-only, particle-only, and combined ion-particle conclusions drawn from studies that include AgNPs only within certain size ranges. a) Conclusions from studies including sizes from 1-10 nm,[36, 52, 56, 67, 69, 79] 11-25 nm,[46, 50, 66] 26-50 nm,[64, 68] 51-100 nm,[40, 47, 57, 70]greater than 100 nm,[19, 178] and AgNPs from more than one size range.[35, 38, 39, 48, 51, 61, 65, 75, 119, 165-167, 169] b) Ion-only, particle-only, and combined ion-particle conclusions drawn from studies that include[35, 36, 38, 39, 48, 52, 56, 67, 69, 75, 79, 119, 165] and exclude[19, 40, 46, 47, 50, 51, 57, 61, 64-66, 68, 70, 166, 167, 169, 178] AgNPs with d ≤ 10 nm. Size is an influencing factor inducing particle-specific effects, in which the role of the particle emerges only when multiple particle sizes from different size categories are included. The role of the particle also emerges when particle sizes ≤ 10 nm are included in the study. Note: This trend is not reflected in the '1-10 nm' size category of the main figure because studies including AgNPs ≤ 10 nm are split between the '1-10 nm' and 'range of sizes' categories.

2.4.2.2 Surface Chemistry-Dependent Mechanisms of Antimicrobial Activity

Typically, AgNPs are decorated with capping ligands, which are molecules that provide stability to the NPs, either through charge or steric repulsion. Ligands that contain functional groups such as amines ($–NH_2$) or thiols (–SH) typically have one chemical bond to the NP core, while other ligands such as trisodium citrate or poly(vinylpyrrolidone) have multiple interaction points. Ligands that have one bond to the NP surface have three key regions: the binding moiety (such as those mentioned above), the intramolecular region, and the solvent-facing moiety.[80] The solvent-facing moiety and the region of the capping ligand between the binding and solvent-facing moieties – the intramolecular region – can be used to introduce chemistries tailored for a given application (e.g., drug delivery, medical imaging, catalysis).[179-183] Each of these three regions, in isolation and/or in combination, may influence capping ligand density (number of capping ligands per unit surface area), interaction with the NP surface, and consequently Ag(I) ion release.[80] As a result, it is not surprising that the capping ligand is known to influence AgNP antimicrobial activity through ion release.[35, 67, 79] In addition to influencing chemical behavior (e.g., dissolution, passivation), surface chemistry has also been shown to impact physical behavior (e.g., aggregation, affinity for the bacterial cell).[76] Capping ligands specifically prevent aggregation by altering the electrostatic (Coulombic attraction between electric charges) and/or steric (spatial interference causing hindrance) repulsion between NPs in dispersion.[81] The aggregation state of the NPs and their affinity for the bacterial cell have been shown to further influence AgNP antimicrobial activity.[38, 39, 65, 75, 166]

Due to the ability for surface charge to influence the aggregation state of AgNPs and the affinity for the bacterial cell, the subset of studies was organized around surface charge to determine potential influences on the conclusions drawn. The results reveal shifts in conclusions

surrounding ion-only, particle-only, and combined ion-particle contributions to antimicrobial activity (**Figure 2.5**). We used zeta potential as the indicator of surface charge, which was included in 53% (16/30) of the studies in our identified subset. A large portion of studies (43%) that do not specify the ligand bound to the particle and do not include characterization of surface charge conclude the antimicrobial activity of AgNPs is governed by Ag(I) ions.[47, 51, 56, 61, 67, 69] Studies that used negatively charged capping ligands supported, in almost equal proportion, mechanisms that are governed by the released ions alone[35, 40, 46, 50, 64, 70] as well as synergistic effects of the ion and particle,[64-66, 68, 79, 165, 167]while only one study concluded a particle-only mechanism of activity.[57] Some of those studies supporting ion-only mechanisms, however, simultaneously varied capping ligand and particle size, which precludes isolation of a definitive conclusion surrounding the effect of the capping ligand. These studies also noted that surface chemistry-dependent antimicrobial activity did not always correlate with ionization, suggesting an additional factor (particle-driven) may be at play.[35, 50] Depending on interactions with media components, Ag-Cl and Ag-S could have formed a passivation layer on the AgNP surface that influences ion release.[76, 77, 150, 151, 160] Only when both cationic NPs and anionic NPs are included in a study do particle-only or combined ion-particle mechanisms truly emerge. Studies including multiple particle types (cationic NPs and anionic NPs) overwhelmingly (75%) supported a particle-only mechanism.[38, 39, 75] These results suggest that surface chemistry may be an influencing factor in inducing particle-specific effects, which is strongly supported when multiple ligand charges are compared. Since the particle is necessary to serve as the host for the capping ligand, the role of the particle is critical for introducing charge- (magnitude and type) and surface chemistry-induced antimicrobial activity.

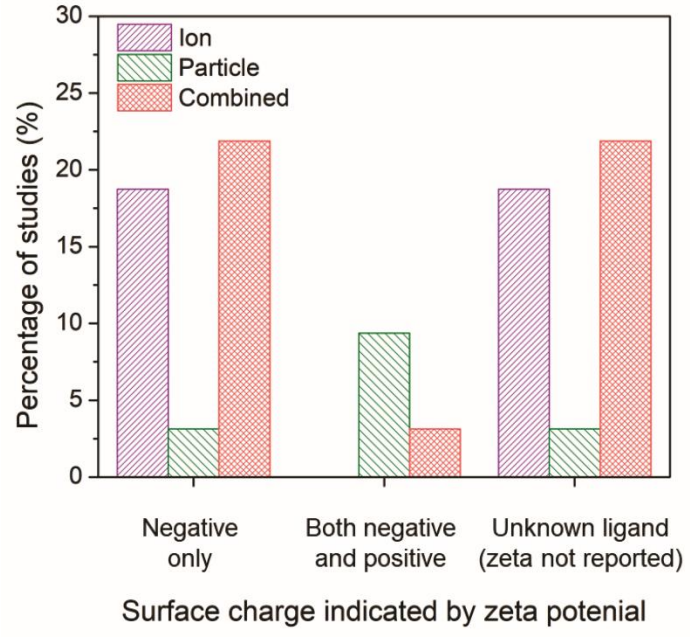

Figure 2.5. Ion-only, particle-only, and combined ion-particle conclusions drawn from studies that include AgNPs with certain surface chemistries. A single capping ligand type inducing a negative surface charge,[35, 40, 46, 50, 57, 64-66, 68, 70, 79, 165, 167] two capping ligand types to compare a negative and positive terminal group,[38, 39, 75] and unknown capping ligands.[19, 36, 47, 48, 51, 52, 56, 61, 67, 69, 119, 166, 169, 178] Surface chemistry is an influencing factor in inducing particle-specific effects, in which the role of the particle emerges only when both negatively-charged and positively-charged particles are compared. Note: No studies included a positively-charged or neutral capping ligand only.

Similar to NP size, the exact role of positively-charged capping ligands remains unresolved but it is speculated to govern a combination of indirect ROS formation, cell membrane disruption, and/or bioavailable intracellular silver. AgNPs with positive charges due to positively-charged capping ligands (hereafter referred to as cationic AgNPs) demonstrate enhanced antimicrobial activity compared to their neutral and negative counterparts, which is attributed to their electrostatic attraction and subsequent adherence to the negatively-charged bacterial cell

surface.[38, 39, 75] These observed effects are not attributed to the Ag(I) ion, since less bulk dissolution occurred with the cationic AgNPs studied than for other particle types (e.g., AgNPs with negative charges) and is present in smaller amounts than the silver salt control.[38, 39] However, the affinity of the cationic AgNP for the negatively-charged cell allows for enhanced localized release of Ag(I) ions, internalization of the particle and/or ions, and ROS production at the cell membrane.[38] Furthermore, cationic AgNPs induce physical damage to the cell membrane (i.e., pitting observed by TEM)[75] that disrupts ion efflux systems, which in turn hinders the pumping efficiency of Ag(I) ions out of the cell, thus increasing intracellular ROS generation compared to exposure to the same amount of Ag(I) ions from the equivalent silver salt control or other particle types.[169] Additionally, cationic AgNPs increase the amount of intracellular Ag(I) ions that deactivate antioxidative enzymes, potentially allowing for the buildup of ROS to occur.[1] The pathway through which the cell mitigates stress caused by cell membrane-associated ROS from cationic AgNPs was found to be similar to the pathway demonstrated by cationic polystyrene NPs, suggesting a particle-type specific response is elicited for cationic particles independent of the particle core composition.[38]

In addition to the pH-dependent charge of the terminal moiety of the ligand, the molecular weight, ligand density (number of capping ligands per unit surface area), and chemical composition of the capping ligand may also influence antimicrobial activity and the mechanism through which it occurs. While one study in the identified subset[79] supports the influence of all three regions of the capping ligand on bulk and intracellular dissolution and found antimicrobial activity to increase with this dissolution, the remaining studies lacked critical information (e.g., the absence of comprehensive capping ligand characterization, particularly those corresponding to polymer- and protein-based capping ligands) to be able to organize in a pivot table around binding

moiety, intramolecular region, and terminal group. Still, the following discussion includes potential influences of the multiple capping ligand components.

First, the NP-binding moiety influences dissolution; atoms with weaker binding affinities (e.g., oxygen versus sulfur) enable adsorption exchange with ambient oxygen and allow increased Ag(I) ion release to occur.[79] Second, the molecular weight of the intramolecular region influences the bulk density of organic matter surrounding the AgNP core, which can "shield" particle and ion effects (e.g., influence the release of Ag(I) ions to the bulk solution).[79, 184] Third, terminal groups of the capping ligands have different affinities to interact with Ag(I) ions, so the amount of Ag(I) ions remaining on the particle surface and being leached into solution can be different.[79] For example, it may be possible that the positively-charged Ag(I) ions electrostatically interact with capping ligands having negatively-charged terminal groups, limiting the amount of bioavailable Ag(I) ions. Finally, ligand density influences the interaction between the NP surface and surrounding environment (e.g., dissolved O_2), and consequently, should influence Ag(I) ion release.[80] Ion release is hypothesized to scale inversely with initial ligand density (i.e., more ion release occurs with a lower initial ligand density because more of the AgNP surface is exposed for oxidation). No studies have directly measured how the initial ligand density affects ion release, but a recent study measured *changes* in ligand density after AgNPs were incubated in bacteria growth media, where the hypothesis was that AgNPs with a larger decrease in ligand density would also have greater Ag(I) ion release. However, no correlation was found between the change in ligand density and the degree of Ag(I) ion release.[66] This complex relationship between ligand density and ion release illustrates a need for further research aimed at establishing ion release profiles of multiple ligand chemistries and densities and resolving the contribution of surface chemistry to antimicrobial activity. In doing so, opportunities to tune ion-

driven antimicrobial activity through controlled manipulation of the AgNP surface will be revealed.

2.4.2.3 Effect of Aggregation on Ion-Only, Particle-Only, and Combined Ion-Particle Contributions to Antimicrobial Activity

Aggregation of AgNPs can occur in aqueous environments due to an assortment of factors influencing surface reactivity (e.g., particle size, shape, surface coating, crystallinity, and exposure media),[81] and can suppress mechanisms activated by unique nanoscale properties of a given nanomaterial. Despite the prominence of aggregation phenomena, many studies do not characterize or else do not explicitly report aggregation behavior. Additionally, a poorly recognized critical factor in managing AgNP aggregation is the method of AgNP addition to the exposure media. For example, diluting AgNPs in water before introducing them to growth media can help retain the size and stability of the particle.[51]

In the identified subset of literature, some studies consider aggregation early in the experimental design as demonstrated through the choice of low ionic strength growth media or in the ligand selection to enhance particle stability,[19, 67, 178] but may not actually monitor aggregation under experimental conditions. Interestingly, the inclusion or absence as well as the method used to monitor aggregation impacts the conclusions drawn in these studies (**Figure 2.6**).

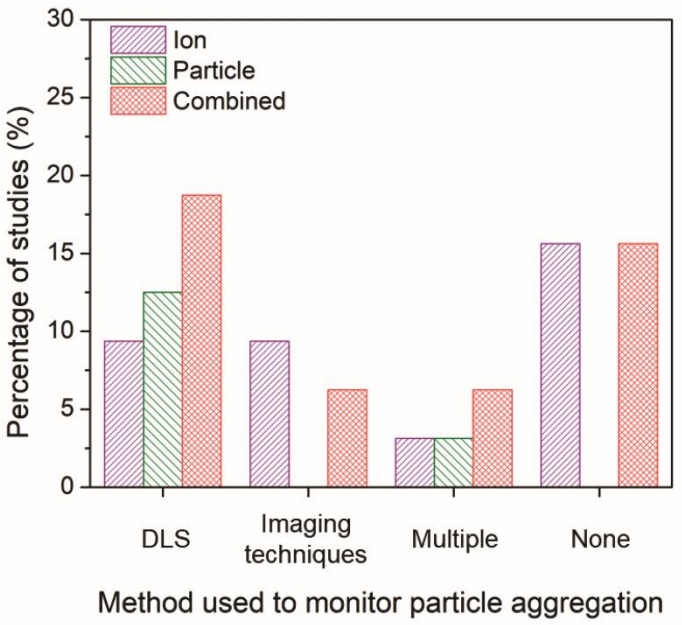

Figure 2.6. Ion-only, particle-only, and combined ion-particle conclusions drawn from studies that monitor particle aggregation. Using hydrodynamic diameter and/or zeta potential from dynamic light scattering (DLS),[38, 39, 46, 51, 57, 65, 68, 70, 75, 79, 165, 167] size and morphology from imaging techniques (e.g., TEM, SEM),[36, 61, 67, 69, 169]more than one technique (e.g., DLS, TEM, and UV-vis),[50, 52, 66, 119]or none at all.[19, 35, 40, 47, 48, 56, 64, 165, 178] Aggregation is an important factor influencing the contributions, and as such, the role of the particle emerges when aggregation is monitored with DLS.

When aggregation is not characterized, no conclusion regarding the mechanisms of antimicrobial activity can be discerned.[19, 35, 40, 47, 48, 56, 64, 166, 178] The majority of these studies noticeably did not specify the ligand bound to the particle and did not include characterization of surface charge, providing no indication about the stability of the AgNPs, thus increasing the potential for elimination of particle-specific effects. Of those studies that characterize aggregation, dynamic light scattering (DLS) is the most common method used to monitor the change in hydrodynamic diameter and/or zeta potential of the AgNP suspension. The majority of studies (77%) employing DLS conclude particle-only or combined ion-particle

effects,[38, 39, 57, 65, 68, 75, 79, 165, 167] and whether aggregation was monitored throughout the duration of the experiment or pre- and post-experiment had no effect on the conclusion being drawn. When imaging techniques (e.g., TEM, scanning electron microscopy (SEM)) were employed, there was a slight predominance of ion-only conclusions. N. B. There are inherent challenges to characterizing particle aggregation state via electron microscopy, because samples are prepared and subsequently imaged outside of their native solution, and the removal and subsequent sample preparation (most notably, sample drying) influences particle-particle interactions and may not reflect the native dispersed state. Finally, when multiple methods are employed and considered together to determine the influence of aggregation on the antimicrobial activity of AgNPs, the majority of studies conclude particle-only or combined ion-particle effects. Taken together, the analysis suggests that aggregation is an important factor influencing ion-only, particle-only, and combined ion-particle contributions to antimicrobial activity, and as such, is critically important to monitor and consider when drawing conclusions within a given experimental system.

2.4.3 Experimental Methods Used to Distinguish Ion-Only, Particle-Only, and Combined Ion-Particle Mechanisms Influences the Conclusions Drawn

While the scaling of the ion control is one experimental factor we used to isolate the subset of literature and eliminate confounding effects, we identified the method used to decouple ion and particle contributions as an additional factor influencing the conclusions with respect to those contributions. Other experimental factors that were considered and found to have a less significant independent influence on conclusions drawn (i.e., resulted in a nearly equal number of studies concluding ion-only, particle-only, and combined ion-particle) include the AgNP dose,

purification and washing procedure, method of dissolution monitoring, time of dissolution monitoring, and the Gram stain of the organism used (**Appendix Figures A.3 – A.7**).There are numerous methods available to study interactions and the impact of ENMs on bacteria, which vary based on the type and resolution of information obtained. Within the subset of literature reviewed herein, the methods used to distinguish ion and particle contributions are grouped into the following categories: (i) Ag(I) ion release is quantified (either in the bulk solution or intracellularly) and compared to AgNP exposure scenarios,[36, 38, 40, 46, 52, 56, 65, 69, 165, 167, 169] (ii) the experimental system is designed to create a particle-only exposure (e.g., anaerobic environments eliminate oxidation of Ag(0) to Ag(I)),[35, 50, 64, 67, 79] and (iii) molecular or fluorescent indicators are used to resolve specific mechanisms of interaction.[19, 36, 38, 46-48, 50, 52, 67-70, 75, 79, 119, 169, 178] **Figure 2.7A** shows the breakdown of conclusions drawn using these three general methods, each discussed in detail below.

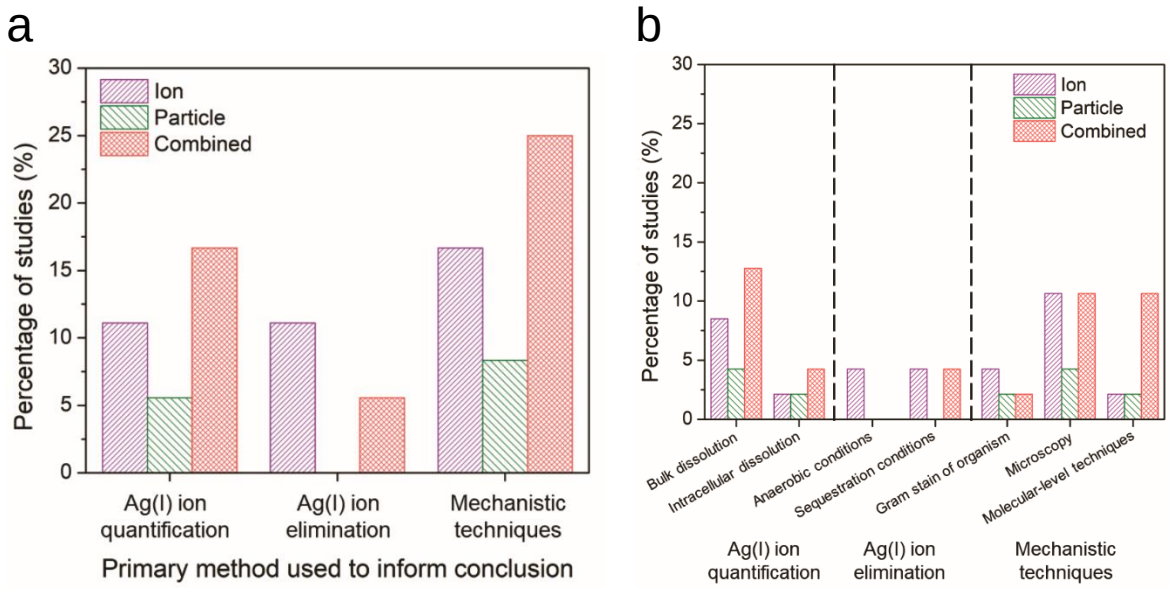

Figure 2.7. Ion-only, particle-only, and combined ion-particle conclusions drawn from studies that used three main methods. a) Ag(I) ion quantification techniques,[36, 38, 40, 46, 52, 56, 65, 69, 165, 167, 169] Ag(I) ion elimination techniques,[35, 50, 64, 67, 79] or mechanistic techniques.[19, 36, 38, 46-48, 50, 52, 67-70, 75, 79, 119, 169, 178] b) Further break down of these primary methods into specific methods is presented. Note: some studies used multiple methods to aid in their conclusion drawn. Quantifying Ag(I) ion release and using molecular-level techniques provide support for particle-only and combined ion-particle mechanisms of antimicrobial activity while aerobic and sequestration conditions provide support for an ion-only mechanism.

2.4.3.1 Quantifying Ag(I) Ion Released in AgNP Exposure Conditions Provide Support for Particle-Only and Combined Ion-Particle Contributions to Antimicrobial Activity

One approach to elucidating particle contributions of AgNP antimicrobial activity is to account for or subtract the effect of the ion from the effect of the combined ion-particle system. This approach requires isolation and quantification of Ag(I) ion from complex aqueous systems. The two prominent methods to quantify the concentration of silver released from the AgNP as Ag(I) ion include (i) using a Ag(I) ion-selective electrode or UV-vis, or (ii) isolating dissolved Ag(I) ion followed by quantification typically by ICP-MS or AES or GF-AAS. In the identified

literature subset, average bulk ion release ranges from < 1% to 16% of the AgNP. The majority of studies across varying reported percentages of bulk ionization occurring in the AgNP system conclude particle-only or combined ion-particle effects, suggesting that the mechanism of antimicrobial activity is not due to the particle releasing more Ag(I) ions into the bulk solution (**Figure 2.8**). For example, when < 2% or between 2-4% ion release occurs, particle-specific effects dominate, which is expected when the ion fraction is low.[58] However, particle-specific effects continue to dominate at higher ion fractions (8-10%).

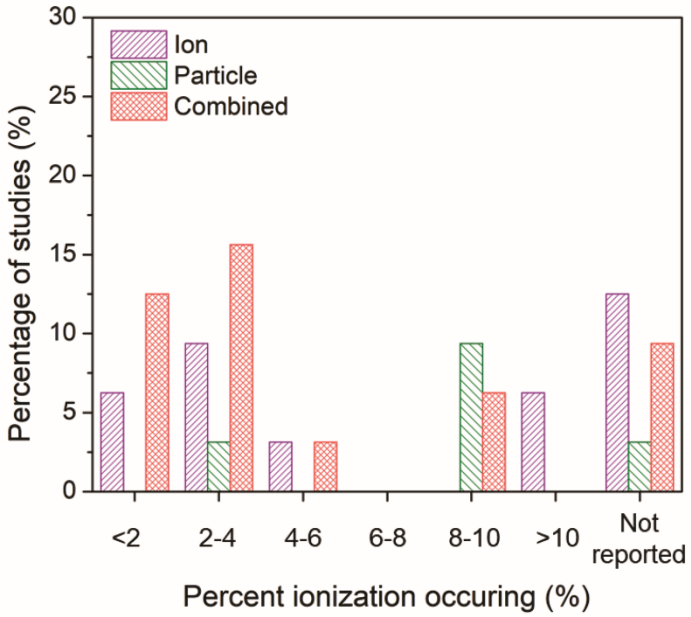

Figure 2.8. Ion-only, particle-only, and combined ion-particle conclusions drawn from studies that measured ionization. < 2%,[19, 50, 56, 65, 79, 166] 2-4%,[40, 52, 64, 66, 69, 165, 167, 169] 4-6%,[35, 68] 6-8%, 8-10%,[38, 39, 47, 50, 66, 75, 119, 167, 169] > 10%[46, 51] or did not measure[36, 47, 48, 57, 61, 67, 70, 178] average ionization taking place in the AgNP system. The majority of studies across varying percentages of ionization occurring in the AgNP system concluded particle-only or combined ion-particle effects, suggesting that the mechanism of antimicrobial activity is not due to the particle releasing more Ag(I) ions.

With the bulk dissolved Ag(I) ion concentration quantified, a specific approach to isolating ion-only, particle-only, and combined ion-particle contributions is to normalize the measured endpoints (e.g., the minimum inhibitory concentration (MIC) or the concentration that affects 50% of the test population (EC_{50})) or dose-response curves obtained under AgNP exposure conditions to the quantified concentration of Ag(I) ion to then compare the normalized impact with the corresponding silver salt control.[36, 38, 40, 46, 52, 56, 65, 69, 165, 167, 169] The results are interpreted as particle-specific or combined ion-particle effects when the magnitude of impact of the AgNP exposure condition is greater than that of the equivalent released Ag(I) ion concentration dosed in as a silver salt. When the measured endpoints or growth curves are similar or when the equivalent released Ag(I) ion imparts greater impact on the bacteria growth curve, the results are interpreted as being governed by the ion. Studies using this normalization approach predominantly (67%) conclude particle-specific or combined ion-particle effects govern the observed impact of AgNPs (**Figure 2.7B**).[36, 38, 52, 65, 165, 167, 169]

Still, definitively isolating different forms of silver in these complex systems remains an ongoing challenge in the field. The described current best-practice techniques capture free Ag(I) ions present in solution; they do not measure intracellular silver content or resolve the fraction of Ag bound to the surrounding environment (i.e., ligands, media constituents, and components of the bacteria cell), as some Ag-complexes will partition/be captured in the supernatant and others will be pelleted, depending on the size of the complex and the separation technique being used. Additionally, studies that measure ionization at a single time point (oftentimes at the culmination of the experiment) exclude the kinetics of ion release. As mentioned above, oxidation of the AgNP surface is a dynamic process and is highly dependent on the surrounding aqueous chemistry, the specifics of which are not comprehensively resolved. As a result of our inability to capture the

complexity of the system, we are currently unable to mimic the kinetics of ion release from AgNPs in ion-only exposures, limiting our ability to further distinguish ion-only, particle-only, and combined ion-particle mechanisms of antimicrobial activity.

In an effort to circumvent these limitations, an alternative method is employed in which intracellular silver is measured using a genetically engineered Ag(I)-biosensor bacteria, *E. coli* MC1061 (pSLcueR/pDNPcopAlux).[38, 40, 165] This recombinant bacterial strain harbors two plasmids from the copper resistance system essential for sensor function: (i) pSLcueR, which contains genes for the regulatory protein cueR, and (ii) pDNPcopAlux, which contains the *lux*-cassette (a group of bioluminescence encoding genes) fused to the promoter *pCopA*.[185] The protein cueR resides in the cytosol and tightly binds both cytoplasmic copper ions (Cu(I)) and Ag(I) ions due to their similar binding affinities, ionic radii, and charge densities.[19] Upon binding, *cueR* activates expression of *copA*, a Cu(I)/Ag(I)-translocating P-type ATPase involved in copper and silver efflux, and the *lux*-cassette required for the production of bioluminescence.[19, 185] This method measures strictly intracellular Ag(I) ions because it is the Ag(I) ion binding to the cysteine residues on *cueR* that is essential to induce bioluminescence. The more binding events, the stronger the bioluminescent signal (in relative light units), thus serving as an indicator of intracellular Ag(I) ion concentration.[165] Conclusions from studies employing this methodological approach predominantly (67%) support particle-only or combined ion-particle effects.[38, 165]

2.4.3.2 Methodological Approaches that Create Particle-Only Exposures Support an Ion-Only Mechanism of AgNP Antimicrobial Activity

Subtracting the effects of the released Ag(I) ion is a time and resource intensive endeavor, and quantifying intracellular silver captures only a portion of silver that impact the bacteria (albeit,

the portion having a predominant adverse impact). An alternative approach involves establishing an exposure environment that eliminates free Ag(I) ions, allowing for deduction of particle-only effects. The two leading approaches to establish this ‘particle-only’ exposure condition involve (i) anaerobic environments, or (ii) the addition of a compound that sequesters free Ag(I) ions.

2.4.3.2.1 Anaerobic Conditions

Formation of Ag(I) ions from the AgNP surface is an oxidation process. In anaerobic environments, oxygen is removed from the system, thus eliminating oxidative Ag(I) ion release. To eliminate the potential for microbial differences to confound results acquired in anaerobic studies, it is important to use a bacterial strain that grows under both aerobic and anaerobic conditions and exhibits equal susceptibility to Ag(I) ions in both conditions.[35, 64] The AgNP concentrations that elicit complete inhibition vary among anaerobic studies, ranging from above 195 mg/L[35] to 5 mg/L[59, 64] AgNP (compared to 75 mg/L[35] to 1 mg/L[59, 64] AgNP under aerobic conditions). While this approach is aimed at eliminating the Ag(I) ions and marginal concentrations are observed after multiple days (e.g., less than 1 μg/L Ag(I)[35]), other studies report detectable Ag(I) ions under anaerobic conditions, reaching the same level as in the comparative aerobic conditions.[59] Evidence for Ag(I) ion release in anaerobic conditions is one potential explanation for the significant discrepancy in AgNP concentrations eliciting complete inhibition in the above-mentioned studies. Additionally, Ag(I) ion release can occur through non-oxidative means. AgNPs can release chemisorbed Ag(I) ions, which result from the partially oxidized AgNP surface even in the absence of an oxidizer.[54, 59, 76] The presence of chemisorbed and “free” Ag(I) ions will vary between studies based on (i) the exposure conditions (i.e., in the presence of bacteria whose metabolic state can change the pH to influence dissolution and extracellular polymeric substances released from bacteria that can sequester Ag(I) ions),[35] and (ii) the AgNP synthesis and purification process.[59, 75, 76, 149] For example, when mild reducing agents (e.g., sodium citrate) are used during the synthesis, some of the silver salt may not undergo reduction and thus remain as free ions in solution or bound to the AgNP surface.[76] As such, the absence of free Ag(I) ions in solution does not preclude the presence of chemisorbed

Ag(I) ions, which could be transported to the cell by the AgNP. Additionally, if particle internalization occurs and the cytosolic pH is lower than that of the growth medium, intracellular release may occur in anaerobic bacteria. Since nitrate compounds are used as electron acceptors in anaerobic bacteria, reactive nitrogen species (e.g., nitrogen dioxide, nitrous oxide) may also form intracellularly,[186] acting as an oxidizing agent to induce Ag(I) ion release. To test this combined ion-particle hypothesis, intracellular silver could be measured using an anaerobic Ag-biosensor.

Nonetheless, when designed to avoid these potential confounding experimental factors, anaerobic exposure environments are good model systems to probe ion and particle contributions independently. Current anaerobic studies (2 reviewed herein) provide convincing support for Ag(I) ion-only mechanisms but do not conclusively rule out particle-only contributions since particle parameters (e.g., varying size and surface chemistry) have not been comprehensively varied under anaerobic conditions. An inability to demonstrate particle-only effects does not prove an ion-only mechanism. Studying a comprehensive AgNP suite that systemically varies shape, size, and surface chemistry under anaerobic conditions is necessary to rule out particle-only effects. Finally, these studies have considered a single bacterial strain and so multiple bacterial strains, having different defense systems for ions and particles, should be evaluated under anaerobic conditions.

2.4.3.2.2 Sequestering Ag(I) Ions

Another approach to eliminate the effect of Ag(I) ions without precluding their formation is to introduce a compound that sequesters free Ag(I) ions to the system. This approach reduces the bioavailability of the Ag(I) ion, thereby minimizing interaction with the bacteria. Commonly used sequestering compounds include cysteine, chloride, sulfide, thiosulfate, phosphate, and glutathione reductase,[50, 64, 67, 79] which demonstrate efficient binding with Ag(I) ion in both AgNP and silver salt exposure conditions. While half of the studies employing this approach conclude an ion-only mechanism of antimicrobial activity (**Figure 2.7B**),[50, 67] there is also evidence supporting the combined ion-particle possibility and specifically, particle-mediated intracellular ionization.[64, 79] One limitation of this approach is that the sequestration compounds also have a strong affinity for the AgNP and upon binding, could influence the NP surface chemistry and hinder the particle-only and combined ion-particle effects.[143] Furthermore, the complexed silver may still exhibit bioavailability and induce antimicrobial activity that may be different than the effect of free Ag(I) ions.[187] Despite the fact that this approach successfully establishes an ion-free system to aid in decoupling ion and particle contributions, it alters the system in a way that does not allow for a direct comparison.

2.4.3.3 Methods Used to Elucidate Specific Mechanisms of AgNP-Bacteria Interactions Support Ion-Only, Particle-Only, and Combined Ion-Particle Contributions to Antimicrobial Activity

While linking biological endpoints to the presence of Ag(I) ions and the AgNP aids in determining ion-only, particle-only, and combined ion-particle contributions, there are also techniques that adopt the same systematic approach while simultaneously providing information on specific pathways of inactivation. The identified methodologies include using multiple bacterial

strains with distinguishing phenotypes, employing microscopy techniques, and using molecular-level techniques (e.g., gene expression and gene-deletion strains).

A suite of gram-negative and gram-positive bacteria can be used to study how differences in the cell wall – the first point of contact in the AgNP-bacteria interaction – influence the response to Ag(I) ions and AgNPs. Gram-negative bacteria have a thin peptidoglycan cell wall and an outer cell membrane, while gram-positive bacteria have a thicker peptidoglycan layer and no outer cell membrane.[68] These differences in architecture introduce different susceptibilities and defense systems to AgNPs and Ag(I) ions in a way that reveals different mechanisms (**Figure 2.7B**). It is critical, however, that both bacteria strains are able to grow in the same exposure media to eliminate confounding effects associated with differences in interactions with the surrounding media. Thirteen percent (4/30) of the studies reviewed herein include both gram-negative and gram-positive bacteria,[52, 67, 68, 70] half of which showed that Ag(I) ions and AgNPs induced different magnitudes of antimicrobial activity suggesting different modes of action of the two forms of silver.[52, 68] One study shows AgNPs having greater antimicrobial activity in gram-positive bacteria compared to gram-negative bacteria while the Ag(I) ions induced approximately equivalent antimicrobial activity in both.[68] On the contrary, the thick peptidoglycan wall of the gram-positive bacteria is proposed to obstruct ions,[52, 70] rendering the action of Ag(I) ions alone less effective in gram-positive bacteria and suggesting that particle attachment to the cell surface contributes to the antimicrobial activity in a particle-only or combined ion-particle manner. However, different AgNP surface coatings can prevent this attachment, which explains why an earlier study reported AgNPs as having less antimicrobial activity in gram-positive bacteria.[52] Using multiple bacterial strains and particle types can differentially affect the antimicrobial activity of Ag(I) ions and AgNPs. This outcome underscores the importance of implementing well-

defined and well-controlled materials and biological systems to comprehensively study that differential impact and isolate the contributions of the ion and particle. Using gram-positive and gram-negative bacteria in combination with the anaerobic and/or sequestration approaches would further resolve in the influence of the bacterial cell wall on the susceptibility and dominant mechanisms of antimicrobial impact.

Capturing visual evidence of Ag(I) ion and AgNP interactions with bacterial cells as well as the resulting morphological changes can aid in determining the contributions of each to the observed antimicrobial activity. Common microscopy techniques used include transmission TEM, SEM, atomic force microscopy (AFM), and phase contrast microscopy.[19, 38, 46-48, 50, 67-69, 75, 79] In the studies reviewed, nearly 40% relied on a microscopy technique to image bacteria-NP interactions and cell morphology,[19, 38, 46-48, 50, 67-69, 75, 79] of which 42% concluded an ion-only mechanism,[46, 47, 50, 67, 69] 17% concluded particle-only effects,[38, 75] and 42% concluded a combined ion-particle mechanism[19, 38, 48, 68, 79] (**Figure 2.7B**). Direct AgNP contact with and fusion to the membrane, shrinkage of cell size to reduce its surface area available for interaction, particle entry into the cytosol, resulting membrane damage (e.g., pitting, rupture), and subsequent leakage of intracellular components occurs in AgNP exposures exclusively, suggesting that these physical effects are the result of the AgNP itself and are not dependent on Ag(I) ions.[38, 48, 68, 75] Ag(I) ions, on the other hand, have also been visualized in cells as large deposits of reduced Ag(I) (silver nanoparticles) that destroy the cell[67, 70] but may also induce another bacterial response, often culminating in the clumping of DNA in the cell center.[44] While internalization and morphological changes may be visualized and used to isolate physical contributions of the particle from the chemical contributions of the Ag(I) ions, the mechanism by which each enters the cell remains unknown. The observed presence of ‘particles’ inside the cell

could instead be Ag(I) ion agglomerates or formed by metabolite reduction intracellularly.[67, 76] Finally, TEM imaging on its own is not a convincing technique for visualization of particle uptake by cells due to the potential for a variety of misleading artifacts.[19]

Using molecular-level techniques (e.g., transcriptomics, gene deletion strains) to distinguish ion-only, particle-only, and combined ion-particle contributions are valuable due to the ability to concurrently elucidate the underlying mechanism(s) of antimicrobial activity. Given that these molecular approaches target specific mechanisms, the results of a given study might be limited in scope due to the focus on isolating a particular ion or particle interaction or impact. Still, the resulting conclusions from the 20% (6/30) of studies using molecular-level techniques are overwhelmingly (86%) in support of particle-only or combined ion-particle effects (**Figure 2.7B**).[19, 36, 38, 48, 178] The compiled findings from the 6 studies provides valuable mechanistic insight. For example, genome-wide approaches show differential gene regulation under AgNP and Ag(I) ion exposures and are used to highlight particle-only[36, 38, 48] and particle-type specific mechanisms (e.g., cationic AgNPs).[38] Specifically, particles induce antimicrobial activity by affecting cell surface activity through disruption of outer membrane liposaccharide formation.[38, 178] These particle-only effects differ from the action caused by Ag(I) ions alone, which include disruption of copper homeostasis, inducement of additional redox stress responses, and regulation of outer membrane porin proteins.[36, 178] However, the interpretation of genetic responses can lead to different conclusions about ion and particle contributions. For example, McQuillan and Shaw credit the differential genetic response between AgNPs and Ag(I) ions to the delivery mode of Ag(I) ions to the cell that affects the magnitude, location, and kinetics of Ag(I) ion release rather than to particle-only effects, so this combination is considered a combined ion-particle mechanism.[178] Despite the challenges associated with interpretation, molecular-level

techniques provide resolution of the mechanism of antimicrobial activity and can highlight particle-specific stress responses that occur at small time scales,[19, 178] with longer time scales deserving attention to study how resistance can build up over time and through multiple generations.[107]

2.5 Conclusions and Future Outlook

Results from the systematic review on the AgNP antimicrobial activity literature provide supporting evidence for particle-specific effects that act both in concert with as well as independently from the Ag(I) ion. The discriminating pivot table analysis suggests the potential to create more effective, Ag-enabled antimicrobials using critical particle properties – size, shape, and surface chemistry. The following are suggestions for ongoing research to this end.

Further research is necessary to elucidate the contributions of each NP property (both their independent and combined effects) and would be most productively pursued by using experimental conditions that have successfully demonstrated the ability to distinguish ion and particle contributions (e.g., anaerobic environments). Given that NP morphology is known to influence surface reactivity and physical interactions with the bacteria membrane, particle shape is a topic deserving investigation that could provide insightful contributions to resolving the particle-ion mechanisms. Additional resolution of the influence of environmental constituents on surface chemistry of AgNPs is needed since Ag(I) ion release and bacterial interactions are both surface phenomena and these constituents can influence ligand chemistry as well as promote or inhibit oxidation of the NP surface. As a result, more comprehensive characterization of surface chemistry will be necessary for future studies, including monitoring of changes in surface chemistry that

result from exposure to the experimental system. Finally, complete resolution of the ion versus particle debate requires development of a robust approach to isolating and quantifying released Ag(I) ions in AgNP exposure conditions, specifically Ag(I) ions bound to media constituents or bacterial components. This development will allow for an accurate representation of the AgNP to be modeled with Ag(I) ion-only exposures by delivering a series of doses that mimic the total rate of AgNP dissolution – the preferred and suggested best practice for an ion control. These recommendations for minimal characterization and reporting guidelines in future studies are summarized in **Table 2.2**.

Table 2.2. Critical characterization parameters for future studies aiming to distinguish ion and particle contributions.

Criteria to Report	Possible Methods	Rationale
General NP characterization		
Initial NP concentration	ICP-MS or AES, UV-vis, or GF-AAS.	Critical for calculating theoretical ion release.
NP size	TEM in exposure media, pre- and post-exposure.	Necessary to quantify size effects and estimate surface area for calculating theoretical ion release.
NP shape	TEM in exposure media, pre- and post-exposure.	Necessary to estimate surface area for calculating theoretical ion release.
NP surface chemistry (e.g., ligand identities, sign and magnitude of charge, ligand density)	Zeta potential for sign and magnitude of charge in the experimental media pre- and post-exposure. NMR, TGA, IR-based methods (among others) for ligand density, pre- and post-exposure.	Changes in surface chemistry can result from exposure to the experimental system, which will influence ion release.
Method of NP synthesis and purification	Several, unique to NP.	Elucidate possible synthesis or purification artefacts causing different surface morphology and ion release.
NP aggregation	Monitor hydrodynamic diameter and zeta potential over duration of experiment and in experimental media using DLS. Monitor optical density over duration of experiment.	Confounds ion and particle contributions leading to differing conclusions drawn in studies (since aggregation can lead to non-nano sized particles).
*Scaled ion control considerations**		

Table 2.2 (continued)

Bulk ion concentration	Quantify bulk ion concentration in broth and presence of organism over duration of experiment (e.g. using ion-selective electrodes, UV-vis spectroscopy, centrifugation and then quantification of ions in the filtrate using elemental analysis techniques (e.g., ICP-MS or OES or GF-AAS).	Completes the mass balance of silver in the system to inform delivery of a scaled ion dose and enable attribution of observed endpoints to the true exposed ion concentration.
Intracellular ion concentration	E.g., Monitor intracellular ion concentration using a bioluminescent analogue of the model organism over the duration of the experiment.	
Media-complexed and cell-bound ion concentration	Method needed. An ideal method would be a standard assay that can isolate and quantify ions bound to media constituents or extracellular bacteria components.	
Ion concentration associated with laboratory materials used in experiments	Digest lab materials and measure ion content with ICP-MS/OES or GF-AAS.	

*There is a need to develop methodology for quantifying the distribution of silver in all components of the experimental system.

Abbreviations: DLS – dynamic light scattering; GF-AAS – graphite furnace atomic absorption spectroscopy; HDD – hydrodynamic diameter; ICP-MS or OES – inductively coupled plasma mass spectrometry or optical emission spectroscopy; NMR – nuclear magnetic resonance; SEM – scanning electron microscopy; TEM – transmission electron microscopy; UV-vis – ultraviolet-visible spectroscopy; XPS – x-ray photoelectron spectroscopy; XRD – x-ray diffraction

While this systematic review is limited to bacteria, the importance of elucidating the mechanism of action and contribution of the ion and particle is ubiquitous across/traverses other types of organisms (e.g., algae, fungi, viruses, mammalian cells). In fact, it is critical from a human

and environmental health standpoint that AgNPs used as antimicrobial agents be designed to maximize efficacy while minimizing harm to organisms higher up on the trophic level. Elucidating the mechanism of action and contribution of ion and particle across trophic levels is important and is likely to shift due to organism-specific responses. For example, endocytosis mechanisms of eukaryotic cells support potential particle-driven and combined ion-particle mechanisms of action. Our conclusions are not directly transferrable across different model organisms due to such phenotypic differences, yet the abovementioned best practices of AgNP characterization and use of scaled ion controls do translate across trophic levels and are critical to decoupling ion and particle contributions to the mechanism and magnitude of impact.

In addition to resolving the independent and synergistic contributions of the ion and, such research activities will inform the tuning of particle design specific to the intended application. Given the rising demand for effective antimicrobials, particularly in the wake of the global antimicrobial resistance crisis, there is a need to inform the use of AgNPs as antimicrobials. More generally, the mechanistic knowledge gained can be used to inform design of other effective nano- and non-nano alternatives, particularly the delivery of multiple mechanisms of inactivation.

3.0 Role of Bacterial Motility in Differential Resistance Mechanisms of Silver Nanoparticles and Silver Ions

This chapter has been published as:

Stabryla, L.M.; Johnston, K.A.; Diemler, N.A.; Cooper, V.S.; Millstone, J.E.; Haig, S-J.; Gilbertson, L.M. Role of bacterial motility in differential resistance mechanisms of silver nanoparticles and silver ions. *Nature Nanotechnology*, **2021**. DOI: 10.1038/s41565-021- 00929-w. **(reprinted with permission from Springer Nature)**

Unlike conventional antimicrobials, the study of bacterial resistance to silver nanoparticles (AgNPs) remains in its infancy and the mechanism(s) through which it evolves are limited and inconclusive. The central question remains of whether bacterial resistance is driven by the AgNPs, released Ag(I) ions, or a combination of these and other factors. Here, we show a specific resistance in a *E. coli* K-12 MG1655 strain to sub-inhibitory concentrations of AgNPs, and not Ag(I) ions, as indicated by a statistically significant greater-than-two-fold increase in the minimum inhibitory concentration occurring after eight repeated passages that was maintained after the AgNPs were removed and re-introduced. Whole-population genome sequencing identified a *cusS* mutation as causative of the heritable resistance that likely increased silver ion efflux. Finally, we rule out the effect of particle aggregation on resistance and suggest, for the first time, that the mechanism of resistance may be enhanced or mediated by flagellum-based motility.

3.1 Introduction

Nano-enabled antimicrobials comprise a multi-billion dollar industry, and silver-based formulations are by far the most widely used.[1, 28, 29] Silver nanoparticles (AgNPs) are promising alternatives to conventional antimicrobials (e.g., antibiotics, disinfectants) due to their efficacy against a wide spectrum of bacteria.[25-27] A major challenge associated with use of any antimicrobial is decreased efficacy over time due to the development of resistance in the target microbe. However, unlike conventional antimicrobials, the study of AgNP resistance in bacteria and the mechanism(s) through which it occurs is limited and inconclusive. Resistance to Ag(I) ions has been well established, whereas the evolution of AgNP resistance in bacteria has only recently been recognized.[100, 107-111, 188]

There are many, well-established reports of bacterial resistance to ionic Ag that identify elimination of Ag(I) ions via efflux pumps or reduction to the less toxic Ag(0) oxidation state as resistance mechanisms.[87-89, 91, 100] Further, Ag-resistant mutants of *Escherichia coli* (*E. coli*) have cell membranes that are deficient in outer membrane porins, decreasing Ag uptake.[89] On a genetic level, Ag(I) ion resistance is specifically associated with the *sil* operon in gram-negative bacteria, which encodes two efflux pumps – a P-type ATPase (*SilP*) and antiporter (*SilCBA*) – and two periplasmic silver-binding chaperone proteins (SilE and SilF) that work synergistically to drive Ag(I) ions out of the bacteria.[87, 91]

Over the past ten years, there have been few studies on bacterial responses to repeated, chronic exposure of sub-inhibitory concentrations of AgNPs. Some studies demonstrate AgNP resistance,[100, 107, 109-111, 188] while other studies postulate that AgNPs pose low risk of bacterial resistance development because they concurrently affect so many aspects of bacterial physiology.[189, 190] AgNP resistance is also shown to be microorganism dependent, with

different bacterial taxa exhibiting differential resistance profiles and some not developing any resistance at all.[100, 110, 111] Furthermore, comparing resistance evolution in response to Ag(I) ions versus AgNPs reveals another inconsistency with some studies reporting a differential resistance response[111] and others observing similar resistance responses between AgNPs and Ag(I) ions.[100, 107, 188] Despite these conflicting outcomes, the majority of the scientific community attribute AgNP resistance to the premise that AgNPs serve as reservoirs for Ag(I) ions and elimination of Ag(I) ions occurs via the mechanisms discussed above.[100, 107, 109, 110, 188] The central question remains: is observed bacterial resistance driven by the AgNPs, Ag(I) ions, or a combination of these and other factors? Other factors include (i) AgNP aggregation, which was recently proposed as a resistance mechanism induced by the bacterial flagellin protein[111] and (ii) strain-specific behavior related to flagellum-mediated motility as a key fitness trait versus simply a protein binding function. Answering this question is necessary to ensure that AgNPs will aid in combatting, rather than contribute to, the global antimicrobial resistance crisis and inform the potential to evade resistance through design of the AgNPs.

This study examines the experimental evolution and genetic stability of *E. coli* resistance in response to repeated, long-term exposure to sub-inhibitory concentrations of Ag(I) ions vs. AgNPs over multiple passages in one population as well as the genetic stability of the imparted resistant phenotype when the pressure is removed. The adopted approach includes a non-selected cell-only control population and antibiotic serial passaging controls, with robust statistical analysis to confirm the resistant phenotypes. Our results further underscore the important role of bacterial motility, a key fitness trait for many bacteria, and other possible strain-specific traits in *E. coli* AgNP resistance by comparing resistance responses of a hyper-motile *E. coli* K-12 MG1655

(+IS*1*) strain and a non-motile *E. coli* K-12 JW1881 strain *(ΔflhD::kan*) (bacteria strain information in **Table B.1**).

3.2 Methods

3.2.1 Chemicals

Silver nitrate ($AgNO_3$, 99.9999%), tannic acid (purissimum grade), sodium citrate tribasic dehydrate (citrate, ≥99%), ampicillin sodium salt, 2,3,5-triphenyltetrazolium chloride (TTC, ≥98%), nitric acid (HNO_3, >99.999%, trace metal basis), and isopropyl alcohol (IPA, 99.90%) were purchased from Sigma-Aldrich (St. Louis, MO). Hydrochloric acid (HCl, >99.999%, trace metal basis), acetonitrile (ACN, 99.8%), sodium chloride (NaCl, 99.6%), potassium phosphate monobasic (KH_2PO_4), Luria-Bertani broth (LB, Miller), BD Bacto dehydrated agar, tryptone, and glycerol were purchased from Fisher Scientific (Waltham, MA). Poly(ethylene glycol) methyl ether thiol (PEGSH, average molecular weight 1,000 g mol^{-1}) was obtained from Laysan Bio, Inc. (Arab, AL). Deuterium oxide (D_2O, 99.9%) was obtained from Cambridge Isotope Laboratories (Tewksbury, MA). All reagents were used as received unless otherwise indicated. All chemicals were dissolved in deionized (DI) water obtained from a Milli-Q ultrapure water purification system. NANOpure (Thermo Scientific, >18.2 MΩ cm) water was used in the preparation of all solutions associated with AgNP synthesis. Before use, all glassware and Teflon-coated stir bars were washed with *aqua regia* (3:1 ratio of concentrated HCl and HNO_3 by volume) and rinsed thoroughly with water. Caution: *aqua regia* is highly toxic and corrosive and requires proper personal protective equipment. *Aqua regia* should be handled in a fume hood only.

3.2.2 Bacterial Strains and Cultivation

The bacterial strains used in this work were the wild-type *E. coli* K-12 MG1655(Seq) strain (CGSC #7740) and the *E. coli* K-12 JW1881 *ΔflhD::kan* from the Keio Collection (CGSC #11772), both obtained from the Coli Genetic Stock Center at Yale University (**Appendix Table B.1**). Since *E. coli* MG1655 has IS*1* elements in the *flhDC* promoter and a putative diguanylate cyclase *dgcJ*, it is hyper-motile with hyper-*flhDC* expression[191, 192] and will be referred to as the hyper-motile *E. coli* (+IS*1*) strain. *E. coli* JW1881 Δ*flhD::kan* has a deletion in the regulatory region of *flhD*. This deletion inactivates the entire *flhDC* operon with no *flhDC* expression,[191, 192] and thus the strain will be referred to as the non-motile *E. coli* (Δ*flhD::kan*) strain. Microorganism stock solutions were prepared in LB broth supplemented with 25% glycerol and stored at -80°C. Microorganisms were cultured overnight in LB broth at 37°C and 150 rpm. Overnight cultures were re-inoculated in fresh medium, grown to exponential phase, and diluted 1000-fold in LB to obtain approximately 10^6 colony-forming units (CFU)/mL.

3.2.3 Synthesis and Ligand Exchange of AgNPs

Citrate-capped AgNPs (diameter, d = 27.2 ± 4.8 nm) were synthesized according to a previously reported procedure.[66, 193, 194] Briefly, a 100 mL aqueous solution of citrate (5.00 mM) and tannic acid (0.40 mM) was brought to reflux in a 250 mL, three-neck round-bottom flask while stirring at a rate of 340 rpm. The molar ratio of tannic acid to citrate was 0.08:1 to achieve ~ 25 nm AgNPs[22]. Once 100 °C was reached and a rapid drip rate was achieved (drip rate ~one/s), 1.00 mL of $AgNO_3$ (25.00 mM) was quickly injected. The reaction mixture changed from a transparent, pale yellow color (due to the tannic acid) to a dark, golden brown within one minute. The resulting AgNP

solution was allowed to reflux for 5 min before it was removed from heat and cooled to room temperature by sitting on the benchtop. The citrate-capped AgNPs were concentrated and washed to remove excess citrate and tannic acid by centrifuging 1.50 mL aliquots in 1.50 mL centrifuge tubes at ~20,000 rcf for 6 min (Eppendorf 5424 centrifuge). The supernatants were removed and the pellet was re-suspended in another 1.50 mL aliquot of AgNP solution from the round bottom flask and centrifuged again. After the second removal of the supernatants, the particles were re-suspended in 1.00 mL of H_2O. The prepared citrate-capped AgNPs, as 1.00 mL H_2O suspensions, were functionalized with PEGSH (average molecular weight 1,000 g mol-1) using mass action ligand exchange (Scheme S1 in Ref [66]). Here, 12.90 mM PEGSH was added to each tube containing the particles in 1.00 mL H_2O. These mixtures were vortexed and then placed on a temperature-controlled mixer (Eppendorf R Thermomixer) in the dark at 400 rpm and 25 °C for 24 h. Immediately after mixing, the PEGSH-coated AgNPs in each tube were centrifuged and re-suspended in 1.00 mL of H_2O and transferred to a clean glass media bottle wrapped in aluminum foil for refrigerated storage (~4 °C). This synthesis and ligand exchange process was repeated to obtain ~10 batches of AgNPs over the span of 3 days and pooled into the same glass media bottle for storage. This was completed at the start of the bacterial resistance experiments (see below).

At the time of each bacterial passage (*vide infra*), the AgNPs were further concentrated and purified with a series of washing steps to remove excess PEGSH and displaced citrate. 1.50 mL aliquots (eight total tubes) were centrifuged and their supernatants removed. Two of the pellets were combined with 1.00 mL of H_2O so that four total tubes remained. This process of combining pellets after centrifuging was repeated two additional times, keeping the same 1.00 mL total volume, until one concentrated tube remained. The particles were then washed by centrifuging once more, the supernatant was removed, and the particles were re-suspended in 850 µL of H_2O to provide sufficient volume of concentrated AgNPs for the experiments. 10.0 µL of this solution was diluted in 500 µL of H_2O to (i) obtain a concentration that would fall under the upper limit of quantification to reliably

measure the initial AgNP concentration by UV-vis-NIR and (ii) provide good resolution for characterizing particle size by TEM. The remaining solution was used in the bacterial resistance experiments and diluted to obtain 400 µg/mL AgNPs.

For initial ligand density quantification, the same purification process was repeated on four additional tubes of 1.50 mL aliquots until one tube remained. After the last wash cycle, the supernatant was removed to yield the concentrated pellet of PEGSH-AgNPs which was saved for NMR spectroscopy, TEM, and ICP-MS analyses.

3.2.4 AgNP Characterization

AgNP solutions at each bacterial passage were characterized by UV-vis-NIR absorption spectroscopy using a Cary 5000 spectrophotometer (Agilent, Inc.). The spectrum baseline was corrected with respect to the H_2O spectrum, or in the case of the aggregation experiments, to the spectrum of LB broth. To evaluate the stability of the refrigerated AgNP stock solution over time, NP size distributions were determined by transmission electron microscopy (TEM). An aliquot was obtained weekly and diluted with H_2O prior to being drop cast onto a Formvar-coated copper TEM grid (Ted Pella, Inc.). Samples were allowed to slowly air dry and then were dried under vacuum overnight before characterization with a Hitachi H-9500 environmental TEM at 300 kV (NanoScale Fabrication and Characterization Facility, Petersen Institute of NanoScience and Engineering, Pittsburgh, PA). NP size distributions were determined from measuring at least 300 NPs (ImageJ 1.52a, National Institutes of Health, USA) in multiple images collected from various areas of the grid. For the aggregation experiments, AgNP solutions were placed in a disposable plastic cuvette (Fisherbrand™). Dynamic light scattering (DLS) was used to measure the hydrodynamic diameter of AgNPs (Anton Paar Litesizer 500). Spectra were averaged over 20 scans. All NMR measurements were performed on a Bruker 400 Ultrashield magnet with AVANCE III 400 Console (Bruker Bio-

spin, Billerica, MA) at 298 K (Figures S4-S5 in Ref [66]). ICP-MS analysis was performed using an argon flow with a NexION spectrometer (Perkin Elmer, Inc.) (Figure S3 in Ref [66]).

3.2.5 Quantifying Resistance in Response to Ag(I) Ions and AgNPs

Initial antimicrobial activity of Ag(I) ions (as $AgNO_3$) and AgNPs, as well as ampicillin as a positive control, were evaluated using standard planktonic MIC measurements. These experiments were carried out in 96-well flat bottom microplates (Corning® Costar®) and done in triplicate. A dispersion of AgNPs or a solution of $AgNO_3$ were serially diluted in H_2O and inoculated with 50 µL of *E. coli* ($5x10^5$ CFU/mL) so that the total volume of each well was 100 µL. The final tested silver concentrations were 200, 100, 50, 25, 12.5, 6.3, 3.1, 1.6, 0.8, and 0.4 µg/mL for AgNPs and 100, 50, 25, 12.5, 6.3, 3.1, 1.6, 0.8, 0.4, and 0.2 µg/mL for $AgNO_3$. The final tested ampicillin concentrations were 25, 12.5, 6.3, 3.1, 1.6, 0.8, 0.4, 0.2, 0.1, and 0.05 µg/mL. Controls, including broth (50 µL) and water (50 µL) alone, broth (50 µL) and water with the antimicrobial agent (50 µL), and water (50 µL) and untreated bacteria (50 µL), were run simultaneously. Cells were incubated at 37 °C for 24 h with medium linear shaking (~500 cpm) in a Microplate Reader (Synergy HTX Multi-Mode, BioTek). Cell growth was monitored by measuring absorbance at 600 nm every 30 min. The mean absorbance and standard deviation for at least three biological replicates is reported.

To evaluate evolution of resistance, bacteria were repeatedly exposed to sub-inhibitory concentrations of Ag(I) ions and AgNPs, as well as ampicillin, in 20 successive passages (Note: the experiment for the non-motile strain was interrupted by COVID-19 related lab shut down, so only 13 passages were completed). We prepared a parent culture that was used to inoculate a serially diluted series of AgNPs ranging from 0.4 – 200 µg/mL AgNPs (*vide supra*). The culture was incubated and after 24 hours the MIC concentration was determined to be the lowest concentration of antimicrobial agent that inhibited visible growth of the tested microorganisms. Sub-MIC cultures with surviving

bacteria (100 µL taken from each of the first three wells below the MIC) were mixed and then sub-cultured on LB agar at 37 °C for 16-18 h. A single colony was used for inoculum preparation at a density of 10^6 CFU/mL in the next passage where they were exposed to the second serially diluted series of AgNPs and incubated overnight. The entire procedure described above, from the initial inoculation to the preparation of the new inoculum, was considered to constitute one passage for the development of bacterial resistance. The next day the MIC (which remained the same or increased) was determined and the sub-MIC cultures from the latest passage were used to inoculate a new series of diluted AgNPs. The process continued for up to 20 passages, a standard timeframe for observing resistance development in evolutionary experiments,[83, 111, 113-115] and over time bacteria began surviving at higher concentrations. Dispersions of AgNPs and solutions of ampicillin having higher concentrations (e.g., 400-800 µg/mL) were used when the MIC increased past the initial concentration range (i.e., when resistance evolved). Non-selected control populations, i.e., untreated bacteria successively cultured in the absence of any antimicrobial agents and exposed to the antimicrobial agent for the first time at each passage, were also included. In all cases where resistance developed, the stability of the resistant phenotype was investigated by removing the selective pressure (i.e., AgNPs or ampicillin) and re-introducing it after a few passages of nonselective bacteria growth in broth (i.e., without the antimicrobial agent) to see if the MIC remained elevated (i.e., displayed a stable resistant phenotype) or decreased back to pre-exposure levels (i.e., returned to its susceptible phenotype).

Fold increase in the MIC was calculated by dividing the average MIC for the passage of interest 'X' by the average MIC of the initially susceptible bacteria:

$$Fold\ change_{experimental} = \frac{MIC_{experimental}\ passage\ X}{MIC_{initial}} \qquad \textbf{Eq. 3-1}$$

$$Fold\ change_{control} = \frac{MIC_{control}\ passage\ X}{MIC_{initial}} \qquad \textbf{Eq. 3-2}$$

where ‘experimental’ denotes that each passage had an antimicrobial exposure (e.g., passage 10 = 10 passages of antimicrobial exposure), whereas ‘control’ is the non-selected repeated passaging control. At each new passage, the non-selected bacteria population was exposed to the antimicrobial for the first time (e.g., passage 10 = 9 passages untreated, 1 passage of antimicrobial exposure on the 10th passage). The ‘initial’ MICs corresponding to the experimental and control were always set equal. Those values were obtained from the first passage, except for two of the conditions (i.e., AgNPs and Ag(I) ions in the case of the hyper-motile strain) where those values were obtained as the average of the first five passages because of the high variability in the initial MIC data. Additionally, multiple skip wells (i.e., wells having no bacteria growth in between wells at a higher and lower antimicrobial concentration having bacteria growth[195, 196]) appeared several times throughout the MIC assays following AgNP exposure and not in the Ag(I) ions or ampicillin treatments. The observation of skip wells in the case of AgNPs is likely due to the nature of the colloidal solution and aggregation behavior when bacteria and growth media are added. It is possible that differential aggregation occurs between wells, particularly at higher AgNP concentrations.[197] However, an alternative explanation for the presence of skip wells could be attributed to hetero-resistance, which is the formation of resistant subpopulations, where subpopulations exhibit a range of susceptibilities to antimicrobial agents.[195, 196] Replicates that contained more than one skip well were excluded from the data analysis as they are considered uninterpretable.[196, 198, 199] Replicates containing just one skip well were included by considering the well above the skip well (i.e., the well at the higher antimicrobial concentration) as the lowest dilution having no bacteria growth and therefore the MIC.[196, 198, 199]

3.2.6 Genomic Analysis

Whole-population genome sequencing (WPGS) was performed to identify genomic variants associated with the resistance observed in the AgNP treatment populations compared to the ancestor and non-selected control population. DNA was extracted from the ancestral *E. coli* K-12 MG1655 stock and both control and treatment populations at multiple time points, using samples preserved following each MIC assay. These included: (i) passage 8, which represents the earliest observation of the resistant phenotype in the treated populations, (ii) passage 20, which represents the end of the repeated exposure and persistent resistant phenotype in the treated populations, (iii) passage 24, which represents the absence of AgNP pressure, and (iv) passage 25, which represents the re-introduction of AgNP pressure in the treated populations. Genomic DNA was extracted from overnight cultures using a Qiagen DNeasy Tissue Kit according to manufacturer's instructions (Qiagen, Germantown, MD). Illumina library construction and sequencing were conducted using the Illumina Nextera DNA Sample Prep Kit with 150 bp paired-end reads, and libraries were sequenced on the NextSeq 550 sequencing platform (Illumina, San Diego, CA). WPGS was performed at the Microbial Genome Sequencing Centre (Pittsburgh, PA). Variant calling and the identification of mutations (e.g., single nucleotide polymorphisms, insertion-deletion polymorphisms) was achieved by aligning AgNP variant sequences to the reference E. *coli* K-12 MG1655 genome[200] using the breseq 0.35.4 pipeline.[201]

3.2.7 Monitoring AgNP Aggregation

AgNPs at three different concentrations (6.3, 12.5, and 25 µg/mL) were incubated in LB broth and in the presence of both *E. coli* strains at 37 °C for 14 and 21 h in 96-well microplates. Twelve wells were pooled together to comprise one sample, which was analyzed by DLS and UV-vis-NIR

spectroscopy. The samples were then filtered using a 33 mm Millex-HV Durapore syringe filter with a 0.45 µm pore size and hydrophilic polyvinylidene fluoride (PVDF) membrane (Millipore-Sigma). The filtrate was then analyzed by DLS and UV-vis-NIR spectroscopy. This experiment was carried out in triplicate was also repeated in the presence of AgNP-resistant bacteria.

3.2.8 Statistics

All statistical analyses were carried out in R (Ver. 4.0.0 (Arbor Day) Released 2020, University of Auckland, New Zealand). A two-way ANOVA was used to analyze the difference in fold-increases in the MIC between treatment group and passage number under different exposure conditions and bacteria strains to determine if either treatment group or passage number impact the fold-increase in the MIC. Experimental and passage control data were pooled together to increase the power of the statistical analyses. The level of this significance was then probed for individual groups using a paired Wilcoxon test with at least a sample size of n = 8. Specifically, the fold-increase in the MIC at the end of the experiment between treatment groups and versus the initial fold-increase in the MIC was compared. Similar analyses were carried out for maximum specific growth rate and duration of the lag phase. A backwards power analysis revealed that with our sample size we could determine statistical significance with an alpha = 0.05 and a power of 80%. This translates to being able to detect significant differences in MIC for the hyper-motile strain and passage control of at least 0.55 (i.e., n = 52, SD = 1.39) and 0.63 (i.e., n = 40, SD = 1.39), respectively. When comparing only the last five passages (i.e., n = 10, SD = 1.68), we can detect significance at a difference of size 1.7. Alternatively, using the same power and significance for the non-motile data set requires at least a difference of 0.96 to be present before a significant difference can be detected.

3.3 Results and Discussion

3.3.1 *E. coli* Develops Resistance to AgNPs but Not to Ag(I) Ions

Pseudospherical citrate-capped AgNPs were synthesized according to a previously reported procedure[66, 193, 194] and functionalized with poly(ethylene glycol) methyl ether thiol (PEGSH, average molecular weight 1,000 g mol^{-1}) using mass action ligand exchange (Scheme S1 in Ref [66]). PEGSH is a widely used, biocompatible, and charge neutral ligand[66, 202] which mitigates electrostatic attractive forces with negatively charged bacteria. After ligand exchange and subsequent purification, the particle size was determined to be 27.2 ± 4.8 nm (**Appendix Figure B.1**) by transmission electron microscopy (TEM). PEGSH ligand density of this particle size was determined to be approximately 1.0 PEGSH nm^{-2} using a combination of proton-nuclear magnetic resonance spectroscopy (^{1}H NMR), TEM, and inductively coupled plasma mass spectrometry (ICP-MS) (Figures S3-S5 in Ref [66]). Ultraviolet-visible-near infrared (UV-vis-NIR) spectra of the AgNPs revealed a characteristic localized surface plasmon resonance (LSPR) peak at $\lambda_{max} \approx 420$ nm over the duration of the bacterial resistance experiments (i.e., five weeks), indicating the presence of stable, well-dispersed colloidal AgNPs (**Appendix Figure B.2A**). Additionally, AgNP size (determined by TEM) did not change significantly over time (**Appendix Figure B.2B**). Combined, these evaluations of long-term stability support the conclusion that any fold-increase in the minimum inhibitory concentration (MIC) (i.e., the lowest concentration of antimicrobial agent that inhibits visible growth of the tested microorganisms) after repeated passaging (*vide infra*) is not attributable to differences in AgNP morphology and instability over time.

An experimental evolution approach was adopted to study responses to prolonged AgNP and Ag(I) ion exposure, in which the populations were sub-cultured every 24 h onto LB agar and then into 50 mL fresh LB followed by dosing of fresh AgNPs and Ag(I) ions. This ensures insignificant

carryover of Ag species (in the forms of AgNPs or Ag(I) ions) from the previous culture into the subsequent culture and comparable AgNP and Ag(I) ion concentrations at each stage of the prolonged exposure. The incorporation of sub-culturing periods without Ag exposure in between the prolonged exposure periods also mimics (i) clinical in vivo conditions where bacteria might encounter Ag intermittently through pulse dosing (which would create prolonged dose-free periods allowing Ag exposure levels to diminish until the next dose) and (ii) incidental release of Ag into the environmental which may also create similar intermittent or cyclic exposure conditions. Using this approach, we observed an average greater-than-two-fold increase (p = 0.0009) in the hyper-motile *E. coli* (+IS*1*) MIC after eight passages with AgNPs (**Figure 3.1A, Appendix Figure B.3** includes the raw MIC data), which was maintained throughout additional passages. An additional replicate lineage was carried out for the AgNPs and nearly all other treatment conditions to confirm the biological response (**Appendix Figure B.4**). For each treatment condition, only phenotypic and genotypic data corresponding to the evolution and genetic stability of one of the lineages is reported and discussed below. A non-selected control population (i.e., serial passaging of untreated bacteria) was included and maintained to account for potential background effects of repeated passaging on the phenotypic and genetic resistance responses. An aliquot of the non-selected control population was exposed to AgNPs every passage (i.e., for the first time) to compare the MIC in sensitive, repeatedly-passaged cells against repeatedly-treated cells. Thus, we interpret the observed significant fold-increase to result from the AgNP selection that was intentionally imposed rather than the bacterial response to repeated passaging in the non-selected control population, as indicated by the significant impact of the treatment group ($p < 0.001$) in an ANOVA analysis and the non-significant change in MIC (i.e., less than a two-fold MIC increase) in the non-selected control population ($p = 1$). Detailed comparisons and statistical analyses are summarized in **Table 3.1** and **Table Appendix B.2**. Shifts in microbial growth kinetics, including the duration of the lag phase and maximum specific growth rate, also occurred at passage 8

and aligns with the increase in MIC as an additional metric indicating evolution of resistance (**Appendix Discussion B.1, Appendix Figures B.5 – B.6, Appendix Tables B.3 – B.5**).

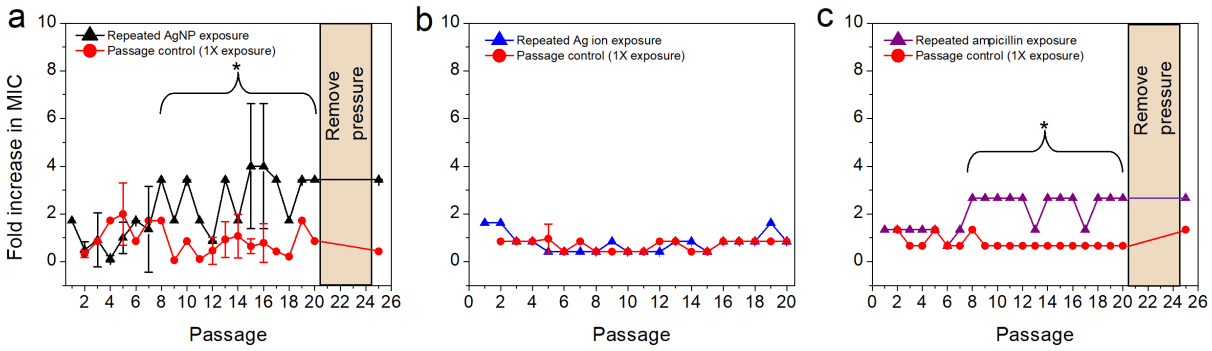

Figure 3.1. Resistance profiles of hyper-motile (+IS*1*) *E. coli*.In response to a) AgNPs (black triangles), b) Ag(I) ions (blue triangles), and c) ampicillin (positive control) (purple triangles) plotted as fold-increase in MIC vs passage number. The non-selected passage control for each condition is included as red circles and pertains to serial passaging of untreated bacteria, with an aliquot being exposed to the antimicrobial of interest each passage (i.e., for the first time). The tan box represents the absence of the antimicrobial pressure. Average ± SD of n=2-3 replicates. The asterisk signifies a greater-than-two-fold average increase in the MIC (passages 8-20) that is statistically significant at p < 0.001. The hyper-motile *E. coli* (+IS1) strain developed resistance to AgNPs at a comparable rate to the onset of resistance to ampicillin, but not in the case of Ag(I) ions.

Table 3.1. Statistical analysis of initial and final minimum inhibitory concentrations (MIC, µg/mL). Corresponding to repeated antimicrobial exposure (i.e., experimental group), and after the antimicrobial pressure is removed and reintroduced. Data corresponding to the non-selected passage control is in parentheses.

E. coli strain	Average initial MIC ± SD (µg/mL) ‡	Average final MIC ± SD (µg/mL)[+,a]	Statistical difference between initial and final fold-increase in MIC (expt. group)*	Statistical difference of final fold-increase in MIC between expt. group and passage control	Average MIC ± SD (µg/mL) after pressure removed and re-introduced[◊]
Ag(I) ions as $AgNO_3$					
MG1655 (+IS1) hyper-motile	2.1 ± 1.0 (1.7 ± 0.5)	1.9 ± 0.6 (1.6 ± 0.0)	$p = 0.382$	$p = 0.346$	N/A
AgNPs					
MG1655 (+IS1) hyper-motile	48.6 ± 40.8 (76.4 ± 56.7)	191.7 ± 79.3 (48.8 ± 37.9)	**$p = 0.006$**	**$p = 0.006$**	200.0 ± 0.0 (25.0 ± 0.0)
JW1881 (Δ*flhD*) non-motile	20.3 ± 27.8 (53.1 ± 33.2)	47.8 ± 56.7 (36.9 ± 55.6)	$p = 0.307$	$p = 0.122$	N/A
Ampicillin					
MG1655 (+IS1) hyper-motile	6.3 ± 0.0 (4.7 ± 1.7)	11.5 ± 2.3 (3.1 ± 0.0)	**$p = 0.001$**	**$p < 0.001$**	12.5 ± 0.0 (6.3 ± 0.0)
JW1881 (Δ*flhD*) non-motile	6.3 ± 0.0 (6.3 ± 0.0)	6.3 ± 0.0 (5.5 ± 1.4)	$p = 1.000$	$p = 0.149$	N/A

‡average of the first 5 passages, +average of the last 5 passages, n ≥10
[a]For E. coli JW1881 (ΔflhD::kan), the MIC is determined after 13 passages due to an interruption in the experiment caused by COVID-19 laboratory closures.
*No significant changes (p > 0.05) were found for the passage control when comparing initial and final fold-increase in MIC.
◊ No significant changes (p = 1) were found when comparing to the pre-pressure removal MIC (i.e., final fold-increase in MIC) although there remained a significant difference (p = 0) when comparing the experimental group to the passage control.

The greater-than-two-fold MIC increase occurring throughout passages 8-20 suggests resistance evolved to AgNPs[112, 203] and aligns with other AgNP resistance studies that cover a wide range of sizes and surface chemistries.[100, 107, 109-111, 188] For example, multiple strains of *E. coli* and *Pseudomonas aeruginosa* (*P. aeruginosa*) experienced a four-fold MIC increase upon exposure to AgNPs within 6-13 passages,[111] while *Bacillus subtilis* adapted to concentrations of AgNPs and Ag_2O-NPs that were at a 1.5-fold MIC increase after 13 passages.[109] The fold-increase observed in

our study indicates that *E. coli* K-12 resistance to AgNPs develops more slowly compared to conventional antibiotics reported in the literature (e.g., gentamicin, ampicillin, tetracycline, chloramphenicol), which impart a higher fold-increase in the MIC in a shorter time period.[113, 204-206] For example, *E. coli* (ATCC 11775) demonstrates resistance to gentamicin after just one passage and a 10-fold MIC increase after 10 passages.[206] The slower evolution of resistance to AgNPs may indicate that the cell-AgNP interaction leading to adaptation is more complex than the simple, direct interaction of antibiotics with the cell and is likely due to the range of AgNP modes of action on cellular processes, whereas antibiotics target a single, specific target.[206] Alternatively, the intermittent periods of sub-culturing on agar may have diminished the effective population size, power of natural selection, and mutation supply, rendering the development of AgNP resistance to be a slower process.

Ampicillin is an antibiotic known to induce resistance in several bacterial species, including *E. coli*[113, 204, 207] and was evaluated as a positive control treatment in our study. Here, we saw a greater-than-two-fold statistically significant increase in the MIC (**Figure 3.1C**) after 8-20 passages with ampicillin ($p < 0.001$), yet no change in MIC was observed in the non-selected control population ($p = 1$). ANOVA analysis further revealed a significant impact between treatment group (ampicillin exposure vs. non-selected passage control, $p < 0.001$) (**Table 3.1**, **Appendix Table B.2**). Therefore, the observed evolution of ampicillin resistance, using fold-change in the MIC as an indicator, upon prolonged exposure to ampicillin validates our methodology and confirms that the increase in fold-change after repeated passaging with AgNPs was also due to evolution of resistance. The magnitude of ampicillin resistance observed in this study is however significantly less than has been reported in other ampicillin and antibiotics studies,[113, 204] possibly due to the different strains of *E. coli* K-12 used between studies, fitness epistasis (i.e., genetic variation within populations), and the experimental evolution approach applied.

No significant change in the MIC (i.e., less than a two-fold increase) was observed over 20 passages with Ag(I) ions in the hyper-motile *E. coli* (+IS*1*) ($p = 1$), or in the non-selected control

population (p = 1), indicating that no resistance evolved to Ag(I) ions (**Figure 3.1B, Table 3.1**). The absence of bacterial resistance to Ag(I) ions was also observed by Panacek et al.,[111] yet is contrary to other studies that observe resistance to Ag(I) ions,[88, 89, 100, 107, 188] albeit some of the resistance to Ag(I) ions was found to evolve slower than for AgNPs.[188] These differences could be attributed to the use of different bacterial taxa, different methods used to select for resistance, and different bacteria growth media containing various halide ion concentrations.[88, 89, 188, 208] For example, Haefeli et al. and Li et al. found that when there was no sodium chloride present in the system, the MIC of Ag decreased significantly for *E. coli* and *Pseudomonas stutzeri*.[88, 89] Additionally, the mixed observations of resistance to Ag(I) ions within the literature could be due to fitness epistasis, i.e., genetic variation within populations, coupled with differences in the external environment, both of which can dictate specific evolutionary paths and mutation effects in evolution experiments.[209, 210] In our study, the decreased susceptibility of the hyper-motile *E. coli* (+IS*1*) to AgNPs as compared to Ag(I) ions (controlling for total Ag and Ag(I) content, see **Appendix Discussion B.2**) suggests a nanoparticle-specific bacterial response, similar to the findings of Panacek et al..[111] Bacteria likely employ different resistance mechanisms in response to the challenges imposed by different forms of Ag in order to adapt and mitigate their antimicrobial activity, which we expect given the demonstrated unique antimicrobial mechanisms of AgNPs versus Ag(I) ions.[71]

3.3.2 AgNP Resistance in Hyper-motile *E. coli* is Permanent and Conferred by *CusS* Mutation

The heritability and stability of the resistant phenotype was investigated to classify the observed AgNP resistance as reversible or permanent and thus provide some insight into the mechanism conferring resistance. After the AgNP pressure was removed and re-introduced following a few passages of nonselective bacteria growth in broth (**Figure 3.1A**), the strain maintained resistance,

suggesting the change was heritable. Thus, the type of resistance conferred can be characterized as permanent and non-reversible,[83, 211] which is corroborated by other studies that found Ag-resistance genes to be constitutively expressed (i.e., always turned on) even in the absence of Ag and regardless of form (nano-particulate or ionic Ag).[90, 100, 109, 188, 208] This is contrary to the proposal that expression of Ag-resistance genes or a Ag-resistant phenotype should be lost in the absence of Ag due to fitness costs.[86, 133, 189] Other studies investigating AgNP and Ag(I) ion adaptations have shown bacterial resistance but have not demonstrated a stable resistant phenotype in the absence of Ag,[85, 110] which could be attributed to the use of different bacteria species and different resistance selection methods, particularly duration and concentration of exposure, of which phenotypic stability is highly dependent.[83, 112]

To validate our conclusion of a permanent, genetic mutation imparting the observed stable resistant phenotype, we carried out a detailed genomic analysis using whole-population genome sequencing (WPGS). WPGS of the population exposed to repeated AgNP treatment revealed several mutations which arose and remained stable after 25 passages. Specifically, a missense mutation (R292L) in the *cusS* gene arose at passage 8 and was maintained at all passages thereafter at 100% frequency (**Table 3.2**). The presence of other mutations in the ancestor and control populations are explained in the SI (see **Appendix Discussion B.3**). CusS encodes a sensory histidine kinase that is part of a two-component regulatory system with CusR, which activates expression of the *cusCFBA* periplasmic efflux pump in response to copper or silver exposure.[212, 213] At the amino acid level, this mutation changes the positively charged arginine residue (residue 292) to a non-polar hydrophobic leucine residue (**Appendix Figure B.7**). The exact functional effect of this change is unknown, and more research is needed to elucidate the structure of the cytoplasmic domain and its functional roles. We speculate that AgNP resistance is imparted through increased silver ion efflux, which may result from autophosphorylation of the CusS cytoplasmic domain caused by this mutation. Residue 292 resides within the active site of the dimerization and the histidine phosphotransfer (DHp) domain,

which works with the catalytic and ATP binding domain to catalyze the transfer of a phosphate group from ATP to the response regulator CusR.[212, 213] Since the *cusS* mutation rose to fixation over several passages in the treatment line and was absent in the non-selected control line, this genotype is a likely response to AgNP selection and could not have risen to high frequency by genetic drift over this time scale.[214]

Table 3.2. Summary of observed mutations in the ancestor, control, and treatment populations of hyper-motile *E. coli* K-12 MG1655. All mutations were called using breseq version 0.35.4.[201] Mutations that exceeded a frequency of 15% and were not present in the ancestor strain are included.

Position (base pair)	Mutation	Gene	Passage number (% frequency)	Annotation	Description
Treatment population (exposure to AgNPs)					
593,896	C→A	cusS ←	8 (100%) 20 (100%) 24 (100%) 25 (100%)	R292L (CGC→CTC)	sensory histidine kinase CusS
159,101	C→A	pcnB ←	20 (17.30%)	C9F (TGC→TTC)	poly(A) polymerase I
2,312,039	Δ8 bp	ompC ←	8 (50.80%)	coding (704-711/1104 nt)	outer membrane porin C
802,079	+TGG	ybhI →	20 (18.90%)	coding (193/1434 nt)	putative tricarboxylate transporter
3,535,192	C→A	envZ ←	25 (74.00%)	G226V (GGT→GTT)	sensory histidine kinase EnvZ
Control population					
2,086,171	G→A	plaP ←	20 (100%) 25 (100%)	L298L (CTG→TTG)	putrescine:H(+) symporter PlaP
Ancestor (also present at all of the above passages in the treatment and control populations)					
1,873,031	IS1(-) +9bp	dgcJ →	--	coding (991-999/1491 nt)	putative diguanylate cyclase DgcJ (likely confers hyper-motility)
4,296,380	+CG	gltP → / ← yjcO	--	intergenic (+586/+56)	glutamate/aspartate : H(+) symporter GltP/Sel1 repeat-containing protein YjcO

Note: In the mutation column, arrows indicate point mutations. In the gene column, arrows indicate the direction of the gene. If one gene name is shown the mutation is within that gene. If two gene names are shown separated by a slash, then the mutation falls within the intergenic region between those two genes

Although this particular *cusS* mutation has not been documented before, increased AgNP resistance has been observed and attributed to the autophosphorylation or phosphoacceptor residues of CusS, which are essential for endogenous metal resistance in *E. coli*.[212] Other work has also identified mutations in *cusS* as a resistance response to AgNPs and Ag(I) ions, albeit several of these have been located in different domains (**Appendix Figure B.8**).[107, 215, 216]

3.3.3 Evolution of AgNP Resistance May be Shaped by Bacterial Motility

The observed increase in the MIC for the hyper-motile *E. coli* (+IS*1*) strain upon repeated passaging with AgNPs and not Ag(I) ions suggests a specificity of resistance evolution to AgNPs. To isolate if resistance evolves from interaction with the particle or as a consequence of the experimental system, we pursued evaluation of (i) strain-dependent resistance by investigating a non-motile *E. coli* strain (*ΔflhD::kan*) and (ii) particle aggregation under experimental conditions. Motility, in particular, is a key fitness trait for many bacteria and confers the selective advantage of enabling cells to escape from poor conditions and search for more favorable environments (e.g., reducing exposure to an antimicrobial, increasing nutrient availability, relocating to unpopulated areas).[217, 218]

Unlike the hyper-motile strain, the average MIC fold-increase for the non-motile *E. coli* strain (*ΔflhD::kan*) was not significantly greater than a two-fold increase (p = 0.88) during repeated passaging with AgNPs (**Figure 3.2A, Appendix Figure B.3)** nor for the non-selected control population (p = 0.99), indicating no resistance had evolved. Bacterial resistance also did not evolve towards ampicillin, as there was no significant MIC fold-increase (p = 1) (i.e., less than two-fold increase) upon repeated passaging with ampicillin (**Figure 3.2B**). Detailed comparisons and statistical analyses are summarized in **Table 3.1** and **Appendix Table B.2**. Additionally, in both cases, the duration of the lag phase and maximum specific growth rate did not show any change (**Appendix Figures B.5 and B.6, Appendix Tables B.4 and B.5**). The lack of observed resistance in both

treatments is expected because AgNP resistance typically influences bacteria features and functions that are also responsive to common antibiotics (e.g., cell wall synthesis, protein synthesis, and nucleic acid synthesis)[7]. The difference in resistance response between *E. coli* strains (hyper-motile and non-motile) to AgNPs suggests that AgNP resistance is a strain-specific response and that differences in motility may have facilitated different interactions between the bacteria and AgNPs. However, the non-motile strain contains a kanamycin selection marker that was inserted in order to knock out the regulatory region of *flhD* (**Appendix Table B.1**), which inactivates the entire *flhDC* operon that encodes the master regulator of flagellum biosynthesis.[191, 192] This marker confers resistance to kanamycin and could have also shaped the differential resistance response to ampicillin and AgNPs. We also recognize that the insertion of a IS*1* element in the putative diguanylate cyclase (**Table 3.2**) in the hyper-motile strain may not only contribute to phenotypes related to flagellum-mediated motility but can be pleiotropic and affect things such as cell adhesion, biofilm formation, growth rate, and population size.[219] This would suggest the possibility that, in addition to or instead of motility, other strain-specific differences could have played a role in the evolution of resistance and would require further investigation of phenotypic traits imparting resistance. Still, this observation is in line with other studies that have noted enhanced resistance to antibiotics in organisms that swarm, surf, or have increased motility.[220-222] Other researchers have also identified plasmid-mediated mechanisms of resistance, with the plasmid being associated with motility and biofilm formation.[223] Unlike other studies which have simply used a motility and/or flagellin inhibitor such as pomegranate rind extract to demonstrate resistance suppression,[111, 224] our study is unique in that we used a knockout *E. coli* K-12 strain displaying a non-motile phenotype to demonstrate lack of resistance onset.

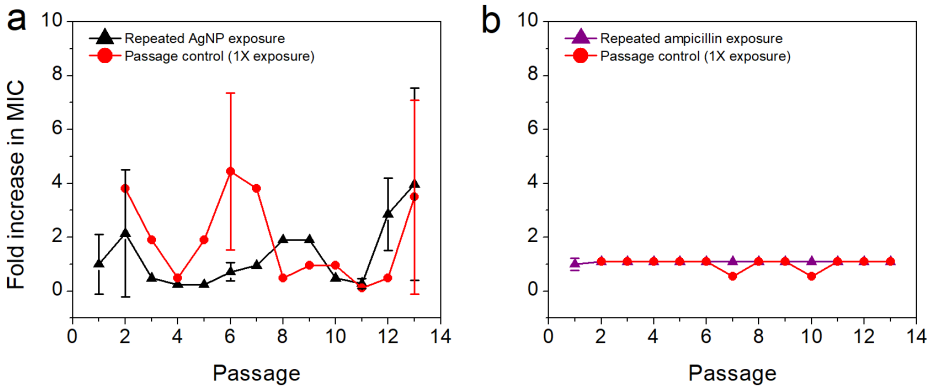

Figure 3.2. Resistance profiles of non-motile (Δ*flhD::kan*) *E. coli*. In response to a) AgNPs (black triangles) and b) ampicillin (positive control) (purple triangles) plotted as fold-increase in MIC vs passage number. The passage control is included as red circles and the tan box represents the absence of the antimicrobial pressure. Average ± SD of n=2-3 replicates. The non-motile *E. coli* (Δ*flhD::kan*) strain did not develop resistance to AgNPs nor to ampicillin. (N.B. these experiments were halted after passage 13 due to COVID-19 lab closures. Resistance evolved in the hyper-motile strain, Figure 1, around passage 8.)

Particle aggregation will influence particle-bacteria interactions and has been shown to result from experimental media[71] and proteins produced by the bacteria (e.g., flagellin).[111] Therefore, we evaluated particle aggregation as a function of bacteria strain and susceptibility, total AgNP concentration, and time in the experimental media. To provide insight into their potential influence on resistance evolution, UV-vis-NIR and dynamic light scattering (DLS) data of AgNPs were collected after incubation in (1) growth media alone and (2) growth media with each *E. coli* strain (i.e., hyper- and non-motile), including both susceptible (20 untreated passages) and resistant (20 treated passages) bacteria of the hyper-motile strain. Samples were taken at two time points over the duration of one MIC assay (i.e., a mid-point and end-point at 14 and 21 h, respectively) and three AgNP concentrations (6.3, 12.5, and 25 µg/mL AgNP) to see if time and concentration elicited differential aggregation. Generally, an increase in particle size will shift the LSPR peak obtained with UV-vis-NIR towards longer wavelengths (red-shift), result in peak broadening, and decrease the intensity of the peak.[225] These spectroscopic effects are mimicked when smaller particles aggregate. Additionally, changes in

hydrodynamic diameter (D_h) observed with DLS can indicate changes in the colloid size and suggest particle aggregation.[164, 226] Raw aliquots of each post-incubation condition were studied, as well as samples that were filtered with a 0.45 μm PVDF membrane filter to isolate the AgNPs (i.e., remove bacteria cells and eliminate their potential influence on changes in D_h). The filtrate was then analyzed by DLS and UV-vis-NIR spectroscopy, with the presence of the LSPR peak suggesting that AgNPs remained in the filtrate (**Figure 3.3**). However, any aggregates greater than 450 nm, if formed, would also have been removed (N.B. AgNP loss reported in **Appendix Figure B.9**). Both samples before and after filtration are included in **Table 3.3** to show the change in particle size by DLS upon removal of the bacteria. Only data corresponding to the 21-h time point and AgNP concentration of 12.5 μg/mL are reported and discussed below (**Figure 3.3, Table 3.3**) as the other conditions showed similar aggregation behavior.

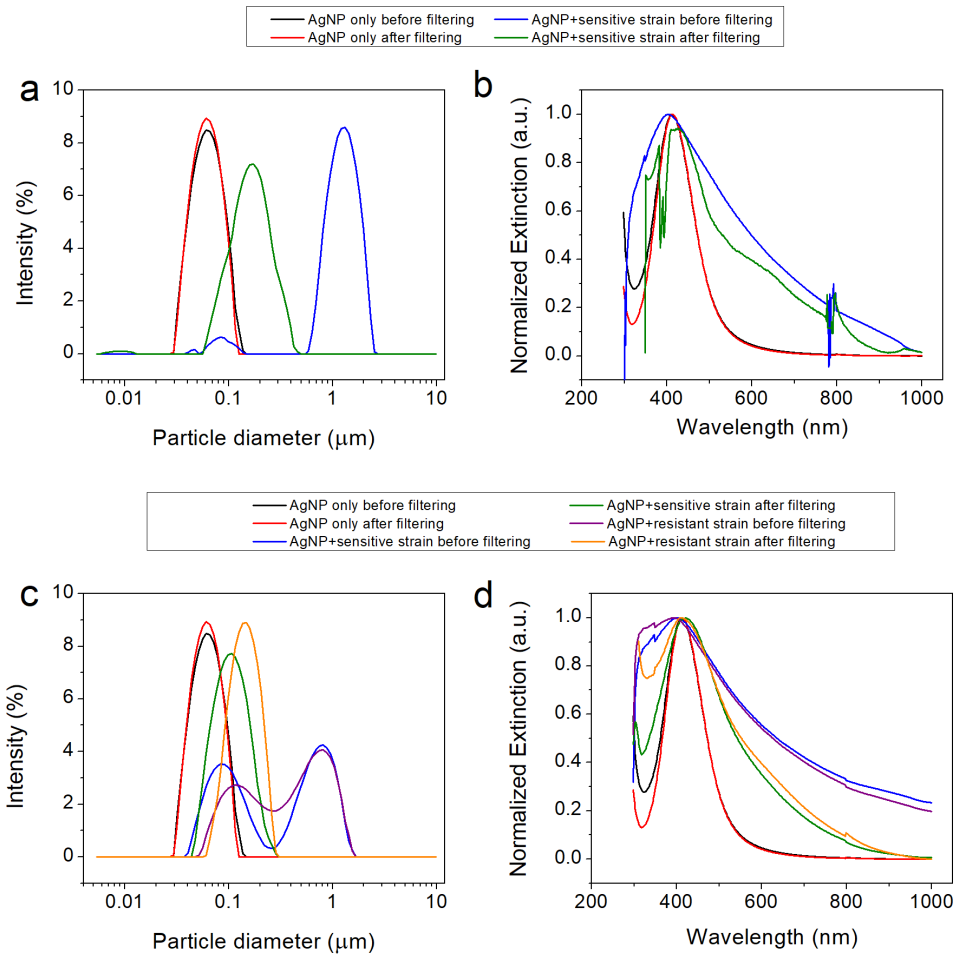

Figure 3.3. AgNP aggregation by UV-vis and DLS.Aggregation of AgNPs (12.5 µg/mL [AgNP]) after 21 hours of incubation in broth and in the presence of *E. coli* before and after filtering with a 0.45 µm PVDF membrane filter to remove bacteria cells. a) and c) show the increase in particle size (hydrodynamic diameter) by dynamic light scattering (DLS) after incubation with *E. coli*. b) and d) show the UV-vis-NIR absorption spectra of the AgNPs which reveals broadening of the characteristic LSPR at λmax ≈ 420 nm after incubation with *E. coli* to indicate that aggregation is occurring. a) and b) correspond to AgNPs in the presence of non-motile *E. coli* (AgNP-sensitive only) and c) and d) correspond to AgNPs in the presence of AgNP-sensitive and AgNP-resistant strains (after passage 20) of hyper-motile *E. coli*, which all exhibit similar aggregation behavior. Plots show the average of three replicates (for DLS, 20 scans per replicate) for bacteria-containing samples or two replicates for AgNP-only controls (in broth). Note: Aggregation of AgNPs at 14 h (and at 6.3 µg/mL and 25 µg/mL [AgNP]) was similar to the data presented here and thus was not included.

Table 3.3. Aggregation as measured through changes in hydrodynamic diameter (Dh) and full width at half maximum, (FWHM). Peaks were obtained through the intensity-weighted size distribution in dynamic light scattering (DLS) and UV-vis-NIR spectroscopy of 12.5 µg/mL AgNPs after 21 h of incubation in broth and in the presence of bacteria. Average (± SD) of n=3 replicates for all conditions except n=2 replicates for AgNPs in broth only.

Condition	Sample type	D_h ✢ (± SD), nm	FWHM of DLS peak△ (± SD), nm	Wavelength at LSPR peak height (λ_{max}) (nm)	FWHM of normalized LSPR peak△ (± SD), nm	Intensity of raw LSPR peak (optical density, OD)
AgNPs + broth only	Unfiltered	63.30 (± 3.62)	65.30 (± 9.08)	411.11 (± 0.0)	110.64 (± 1.99)	1.46 (± 0.10)
	Filtered	60.74 (± 0.00)	60.28 (± 0.56)	412.78 (± 0.78)	106.07 (± 0.20)	0.94 (± 0.10)
Susceptible non-motile *E. coli* + AgNPs	Unfiltered*	72.04 (± 22.21) and 1,284.44 (± 59.23)	1,237.63 (± 81.53) and 25.85 (± 29.79)	403.33 (± 1.12)	289.57 (± 8.96)	0.64^ (± 0.04)
	Filtered*	163.70 (± 39.49)	177.45 (± 34.85)	418.15 (± 18.10) and 646.66 (± 0)	166.96 (± 43.27) and 315.78 (± 70.08)	0.04 (± 0.03) and 0.01 (± 0.01)
Susceptible hyper-motile *E. coli* + AgNPs	Unfiltered*	86.34 (± 4.09) and 812.87 (± 65.78)	102.61 (± 10.48) and 799.84 (± 111.60)	401.48 (± 0.64)	340.84 (± 33.14)	0.54^ (± 0.02)
	Filtered	107.31 (± 8.68)	123.02 (± 28.13)	420. 74 (± 5.13)	213.91 (± 17.09)	0.30 (± 0.04)
Resistant hyper-motile *E. coli* + AgNPs	Unfiltered*	119.37 (± 5.66) and 791.83 (± 75.94)	225.93 (± 59.60) and 890.68 (± 85.06)	392.97 (± 4.49)	330.03 (± 16.80)	0.62^ (± 0.08)
	Filtered	144.20 (± 6.65)	140.26 (± 12.24)	410.37 (± 2.56)	274.12 (± 26.59)	0.26 (± 0.06)

*Presence of bimodal peaks, ✢determined from the peak location, △ range at 50% of the maximum peak intensity, ^diluted five-fold

After incubation in growth media alone, the AgNPs had a D_h of approximately 60 nm (**Table 3.3**), which is larger than the inorganic core size determined by TEM (d = 27.2 ± 4.8 nm) and is expected given that the PEGSH ligand and the solvent layer surrounding the particle also contribute to the measured D_h.[155] As a control, the AgNPs were filtered from growth media alone to ensure that the process of filtering did not alter the size distribution of the AgNPs. The D_h and full width at half maximum (FWHM) of the DLS and LSPR peaks remained consistent before and after filtering, indicating no change in particle size due to the filtering process (**Table 3.3, Figure 3.3**).

Comparing the size of AgNPs in broth alone to AgNPs in the presence of *E. coli* after filtration indicates that particle aggregation occurred to a similar extent under all exposure conditions, including for both the hyper-motile and non-motile strains as well as in the case of both susceptible and resistant phenotypes (**Table 3.3**). *E. coli* were also filtered from growth media alone to ensure that the 0.45 μm pore size was sufficient to remove all bacteria (length of 1-2 μm, diameter of 0.25 μm) (**Appendix Figure B.10**). Particle D_h increased from 60 nm to a range of 110-160 nm for filtered samples (**Table 3.3, Figure 3.3A and C)**, which is corroborated by the LSPR peak broadening (increase in FWHM) and red-shifting, indicating a shift to larger particle diameters (**Table 3.3, Figure 3.3B and D**). Since all strains induce similar aggregation behavior (i.e., aggregation is independent of strain susceptibility and bacterial motility) aggregation alone cannot be responsible for the differences in resistance emerging in the hyper- and non-motile *E. coli*. Currently unrealized, alternative mechanisms of interaction around bacterial motility (e.g., physical distancing or relocating away from the AgNPs to reduce exposure or increase nutrient availability) may be at play to induce these differential AgNP resistance profiles. Further, the non-motile strain has the regulatory region of *flhD* knocked out, which inactivates the entire *flhDC* operon that encodes the master regulator of flagellum biosynthesis,[191, 192] meaning there should be no flagellin produced (i.e., the major protein hypothesized as being responsible for AgNP aggregation[111]). Since aggregation occurs in the absence of flagellin (i.e., in the non-motile strain experimental conditions), there may be other proteins (e.g., pili, outer membrane

proteins, ribosomal proteins and enzymes involved in cellular metabolism released upon cell death[111]) present in bacteria that cause aggregation.

3.4 Conclusions

Findings from this study present different resistance responses for hyper-motile and non-motile *E. coli* strains after repeated exposure to sub-inhibitory concentrations of Ag(I) ions and AgNPs. AgNP resistance (i.e., a statistically significant greater-than-two-fold increase in the MIC) was found in hyper-motile *E. coli* and remained stable, with no reversion back to AgNP sensitivity, while non-motile *E. coli* demonstrated no resistance. A permanent mutation in *cusS* was found in the hyper-motile *E.coli* strain and suggests a direct mechanism of resistance through increased silver ion efflux that may be co-mediated or enhanced by a motile phenotype. These findings provide critical insight into bacterial development of resistance to AgNPs, underscoring for the first time the potential role of bacterial motility. Identifying that bacteria motility may play an independent role from particle aggregation is an exciting result because it directs future research to uncover detailed mechanism(s) of resistance. In addition, the findings from this study are promising for reducing the burden of pathogenic diseases and infection because there are many non-motile, clinically relevant, drug-resistant bacterial strains that are potential targets for AgNP treatments. The Center for Disease Control and Prevention lists *Clostridioides difficile, P. aeruginosa, Staphylococcus aureus,* and various types of *Acinetobacter and Streptococci* as urgent and serious threats[227], all of which are non-motile, or in the case of *P. aeruginosa,* may emerge as non-motile during late and chronic infections.[228] Our data suggest that AgNPs could be effective and remain effective in non-motile strains, with no resistance or potentially, delayed resistance emerging.

However, it should be noted that even in the absence of observed resistance, it is possible that resistance could evolve at longer time scales (e.g., more than 20 passages) or when multiple independent replicate populations are used. Uncovering these possibilities will require additional investigation. We recognize that the stochastic nature of evolutionary adaptation may not impart the same phenotype or involve the same genes, and thus may present multiple mechanisms and levels of resistance, such that replication and understanding the impact of different mutations arising in different populations is important. Possible additional mechanisms of resistance may be uncovered in future work that incorporates several replicate populations. Additionally, predicting how frequent the *cusS* mutation or other mutations occur to impart resistance can also be achieved by studying multiple replicate populations. Different exposure concentrations, periods of exposure, and the presence of other stressors will also influence evolution of resistance. Further, our study examined one type of AgNP (i.e., one size, shape, and surface ligand) within one growth media; additional research is needed to establish global conclusions that account for the wide variability of nanoparticle-dependent biological interactions and underlying genetic responses, as well as media components and concentrations that influence particle behavior in suspension. The observed absence of bacterial resistance to ionic silver in motile strains and the evolution of resistance upon exposure to AgNPs indicate a mechanism specific to nano-particulate silver and provide an opportunity to evade resistance through particle design. The particle parameters – size, shape, and surface chemistry – can be used to differentially modulate the identified AgNP properties that govern their efficacy and minimal resistance in different bacteria. Additionally, and particularly for motile strains, the focus of future work could be on designing the particle to maximize efficacy (e.g., high, sustained ion release) under given use conditions or designing for a high biological fitness cost.

Finally, our findings caution the ubiquitous use of AgNPs in consumer products (e.g., washing machines, textiles, paints) that result in potentially high human and environmental exposures. To limit and not contribute to the growing, global resistance challenge, AgNP use should be reserved for those

applications necessitating antimicrobial function, such as in the health care sector and for medical devices where resistant bacteria cause life threatening situations.

4.0 The Influence of Nanoparticle Shape on *E. coli* Antimicrobial Activity

This chapter is currently in preparation for publication:

Stabryla, L.M.; Moncure, P.; Johnston, K.A.; Diemler, N.A.; Millstone, J.E.; Gilbertson, L.M. The influence of nanoparticle shape on *E. coli* antimicrobial activity. In Preparation.

4.1 Introduction

Within the class of ionizing engineered nanomaterials (ENMs) being used as next-generation antimicrobial agents, there is a growing demand for the development of design criteria to maximize their functional performance. Current research is aimed at understanding the role that nanoparticle parameters (i.e., size, shape, and surface chemistry) play in the magnitude and mechanisms of antimicrobial activity to better guide *a priori* design and advance the application potential of ENMs, with a recent spotlight on resolving particle-specific mechanisms independent from and synergistic with ionization. In a recent review, silver nanoparticle (AgNP) size (< 10 nm) and surface chemistry (positive-charge) were revealed as parameters that could elicit particle-specific effects independently from and synergistically with Ag(I) ions.[71] The link between particle-specific antimicrobial activity and the third tunable design handle, nanoparticle shape, is not as well established, with contributions of shape on underlying mechanisms of AgNP antimicrobial activity remaining unresolved. With the potential to enhance the physical and chemical mechanisms of antimicrobial activity, manipulations of AgNP shape can be utilized as a route toward rational nanomaterial design. Resolving mechanistically the role of nanoparticle

morphology will allow us to select nanoparticle morphologies for the intended application, i.e., ones that maximize antimicrobial activity and avoid the risk of bacterial resistance to ENMs.

While nanoparticle shape has been studied, its antimicrobial effects and mechanisms of action are not well understood. Many shape-related AgNP and Ag_2O studies conclude the presence of differential antimicrobial activity arising from nanoparticle morphology distinctions,[73, 74, 116, 118-122, 124-130] although some conclude the absence of shape-based effects, i.e., shape does not influence bacterial response.[40, 55, 123] Even still, one of these studies mention that smaller particles could have shape-specific effects.[40] Additionally, there is no relative measure of antimicrobial activity by shape; triangular nanoplates and nanoprisms,[74, 116, 120, 121, 124, 126, 128-130] cubes, spheres, and hexagons[73, 118, 119, 122, 124, 125, 128] have all been identified as imparting high antimicrobial activity.

Underlying this differential antimicrobial activity related to nanoparticle morphology is the potential for different contributions from the released Ag(I) ions and the particles themselves. With AgNPs generally, there are three overarching possibilities for mechanisms of antimicrobial activity regarding particle and ion contributions, which can also be applied to understanding shape effects: (i) the observed antimicrobial activity arises from the release of Ag(I) ions via oxidation and dissolution of the surface Ag atoms and is termed as 'ion-driven' effects; (ii) antimicrobial activity is a result of the particle itself, independent from Ag(I) ion release, and is termed as 'particle-specific' effects (e.g., physical disruption or alteration of the phospholipid cell membrane, production of ROS at the cell surface); (iii) antimicrobial activity occurs from a combination of the first two mechanisms and/or some degree of synergistic effects between the released Ag(I) ions and the particle action, termed as 'combined ion-particle' effects.[71] For a more comprehensive discussion on the distinctions of these mechanisms, please refer to Stabryla et al.[71] The studies

that investigate nanoparticle morphology do not reach consensus on whether ion-driven or particle-specific effects exist to induce differential effects. Some studies propose that the relationship between biological response and nanoparticle morphology arises from ion-driven effects.[40, 116] For example, nanoparticle shape has been shown to influence ion release through differential reactivity of the exposed surface facets with oxygen as well as differing surface areas influencing the amount of dissolution taking place.[1, 73, 74, 116] Others suggest that the particles themselves induce the differential shape effects,[72, 118-122] which has also been found for other ion-producing ENMs such as Cu_2O.[229, 230]

While some of the existing mechanistic ambiguity is due to the complexity of the nanoparticle systems themselves (e.g., nanoparticle shape can increase binding to the bacterial cell membrane and cell wall constituents, and also enhance the dissolution rate of silver atoms from the nanoparticle surface via oxidation), a non-trivial component arises from inconsistences in experimental designs across studies.[71, 231] Critical components of the experimental design include control of the AgNP morphology itself (i.e. size, shape, surface chemistry, surface area) as well as experimental aspects such as the model organism and growth medium used, the choice of assay and measured toxicity endpoint,[231] particle stability and aggregation in aqueous environments based on an assortment of factors including shape, and the treatment of the Ag (I) ion control to distinguish between particle-specific and ion-driven effects.[71] Shape is not studied robustly on its own since other nanoparticle parameters such as size and surface chemistry are often not held constant, and the available surface area for interaction with the organism of interest varies. Differential particle aggregation can also occur from shape changes and is often not monitored even though it can suppress mechanisms activated by the unique nanoscale properties of a given shape and therefore influence the resulting bacterial response. Little is also known about

the influence of particle morphology on dissolution kinetics as the majority of shape-related studies have not monitored ion release,[116] and further, only one shape study has evaluated antimicrobial activity with scaled ion controls that mimic the release of ions in the associated nanoparticle system.[40]

Additional intrinsic material properties related to morphology such as crystal facets[72, 74, 119-122, 128] and surface area or effective cell contact area[73, 116, 119, 125, 127-129] have also been identified as being crucial to inducing the observed differential antimicrobial activity arising from nanoparticle shape. Crystal facets in particular impart different arrangements of atoms on the surface and influence atoms packing (atom density) and bonding with each other. These differences at the atomic level translate to unique surface energies and reactivities that can influence both ion release as well as the binding affinity and localization of the particle to the cell (e.g., cell wall, phospholipid membrane) and thus the amount of physical contact and interaction that occurs to impart downstream chemical (e.g., increased amounts of ROS) and physical (e.g., enhanced or additional membrane disruption) mechanisms of antimicrobial activity.[122] The amount of surface area of a given shape also relates directly to the number of points of interaction with the cell as well as the dissolution of Ag(I) ions into the cell. Different exposed surface facets also have different interactions with oxygen,[72, 74, 157-159] highlighting the effect of parameters such as particle shape and facet on the oxidation and dissolution process. Shapes that have uneven or rough surfaces and possess corners or edges are suggested to be more biologically and chemically reactive,[74, 177] since atoms at these locations have a lower bonding coordination than bulk atoms and therefore affect their reactivity and interaction with bacteria. Faceted AgNPs, in particular, are shown to have enhanced inhibitory effects on bacteria growth via additional membrane disruption mechanisms.[74] On the other hand, shapes with soft edges such as spheres

may enable enhanced membrane association.[117] Nanoprisms are typically rich in {111} facets[72-74, 120, 121, 128] while nanospheres and nanocubes are rich in {100} facets,[119, 122] and so which facet, and therefore shape, is more active and reactive in terms of facilitating faster dissolution and cell interaction, particularly from a surface energy perspective, is a current topic of discussion in the literature. While these material properties have been identified, they warrant a closer investigation to shed light on the exact processes responsible for their activity. Thus, there remains an opportunity to (i) provide clarity around their influence through a comprehensive investigation of crystal facet and surface area related to shape-induced antimicrobial activity and (ii) unravel the underlying downstream chemical and physical particle-specific mechanisms of action on the cellular components imposed by these properties.

Contributions of shape on underlying mechanisms of AgNP antimicrobial activity remain unexplored. Only one study investigated shape-based mechanisms and suggested membrane damage via penetration as a physical mechanism for the increased AgNP antimicrobial activity of certain shapes,[119] which is in line with studies of other ENMs such as Cu_2O that have also identified shape-specific membrane damage.[229] Chemical mechanisms of shape-dependent antimicrobial activity are also a possibility and likely involve the production of ROS, whether extracellularly generated (at the surface through particle-cell contact or in the bulk media) to oxidize lipids of the cell membrane or intracellularly generated by ions or particles to interact with DNA and proteins.

While current studies offer valuable insight into shape-dependent AgNP antimicrobial activity, there remains an opportunity to (i) identify the intrinsic shape-driven material properties that govern the observed behavior, (ii) the role that the AgNP material (versus the Ag(I) ion) plays in shape-dependent inactivation, and (iii) identify the exact underlying physical and chemical

mechanisms imparted by those components upon interaction with the cell. In this work, we prepare and comprehensively characterize a suite of AgNPs with controlled physicochemical properties, including size, surface charge, surface area (all held constant), and shape (which is systemically varied), and evaluate their antimicrobial activity. We report the influence of AgNP shape on *E. coli* antimicrobial activity, determine the effect of surface area on this shape-dependent antimicrobial activity, and postulate a mechanism underlying this shape-dependent inactivation. We hypothesize that different AgNP shapes of the same surface area will yield different magnitudes of antimicrobial activity. In other words, shapes having similar surface area may impart differential antimicrobial activity due to the presence of varying particle-specific effects involving increased contact with the cell. We also expect crystal facets to play an important particle-specific role in the influence of shape, and so comparing across shapes that have similar surface area yet still possess unique facet structures, such that different effective surface areas in terms of active facets enable interaction with the cell, allows us to probe and isolate the effects of shape and crystal facet alone. Finally, we propose that ROS and membrane damage both contribute to these particle-specific shape-effects.

4.2 Materials and Methods

4.2.1 Chemicals

Silver nitrate ($AgNO_3$, 99.9999%), tannic acid (purissimum grade), sodium citrate tribasic dehydrate (citrate, ≥99%), sodium hydrosulfide (NaHS), poly(vinylpyrrolidone) (PVP, average MW= 29,000 Da and 55,000 Da), sodium borohydride (NaBH4, ≥99%), hydrogen peroxide (H_2O_2, 30 wt%), ethylene glycol (EG), and nitric acid (HNO_3, >99.999%, trace metal basis) were purchased from Sigma-Aldrich (St. Louis, MO). Hydrochloric acid (HCl, >99.999%, trace metal basis), sodium chloride (NaCl, 99.6%), Luria-Bertani broth (LB, Miller), BD Bacto dehydrated agar, and glycerol were purchased from Fisher Scientific (Waltham, MA). All reagents were used as received unless otherwise indicated. All chemicals were dissolved in deionized (DI) water obtained from a Milli-Q ultrapure water purification system. NANOpure (Thermo Scientific, >18.2 MΩ cm) water was used in the preparation of all solutions associated with AgNP synthesis. Before use, all glassware and Teflon-coated stir bars were washed with *aqua regia* (3:1 ratio of concentrated HCl and HNO_3 by volume) and rinsed thoroughly with water. Caution: *aqua regia* is highly toxic and corrosive and requires proper personal protective equipment. *Aqua regia* should be handled in a fume hood only.

4.2.2 Synthesis and Ligand Exchange to PVP-Capped Pseudospherical-AgNPs

Citrate-capped pseudospherical-AgNPs (diameter, d = 27.2 ± 4.8 nm) were synthesized and functionalized with PVP (average MW = 55,000 Da) according to a previously reported procedure.[193] It is important to note that particles having a diameter of d = 45 nm were targeted

using increased concentrations of tannic acid and silver nitrate. Briefly, a 100 mL aqueous solution of citrate (5.00 mM) and tannic acid (5 mM) was brought to reflux in a 250 mL, three-neck round-bottom flask while stirring at a rate of 340 rpm. The molar ratio of tannic acid to citrate was 1:1 to achieve ~ 45 nm AgNPs.[193] Once 100 °C was reached and a rapid drip rate was achieved (drip rate ~one/s), 1.00 mL of $AgNO_3$ (330 mM) was quickly injected. The reaction mixture changed from a transparent, pale yellow color (due to the tannic acid) to a dark, golden brown within one minute. The resulting AgNP solution was allowed to reflux for 5 min before it was removed from heat and cooled to room temperature by sitting on the benchtop. The citrate-capped AgNPs were concentrated and washed to remove excess citrate and tannic acid by centrifuging 1.50 mL aliquots in 1.50 mL centrifuge tubes at ~20,000 rcf for 6 min (Eppendorf 5424 centrifuge). The supernatants were removed and the pellet was re-suspended in another 1.50 mL aliquot of AgNP solution from the round bottom flask and centrifuged again. After the second removal of the supernatants, the particles were re-suspended in 1.00 mL of H_2O. The prepared citrate-capped AgNPs, as 1.00 mL H_2O suspensions, were functionalized with PVP (average MW = 55,000 Da) using mass action ligand exchange (Scheme S1 in Ref 20). Here, 5 mM PVP was added to each tube containing the particles in 1.00 mL H_2O. These mixtures were vortexed and then placed on a temperature-controlled mixer (Eppendorf R Thermomixer) in the dark at 600 rpm and 25 °C for 24 h. Immediately after mixing, the PVP-capped AgNPs were further concentrated and purified with a series of washing steps to remove excess PVP and displaced citrate. Here, 1.00 mL aliquots were centrifuged, and their supernatants were removed. Two of the pellets were combined with 1.00 mL of H_2O so that half of the number of total tubes remained. This process of combining pellets after centrifuging was repeated several times, keeping the same 1.00 mL total volume, until one concentrated tube remained. The particles were then washed by centrifuging once more, the supernatant was removed, and the particles were re-suspended in 1.00 mL of H_2O to provide sufficient volume of concentrated AgNPs for the experiments. 10.0 µL of this solution was diluted in 1.00 mL of H_2O to (i) obtain a concentration that would fall under the upper limit of quantification to reliably

measure the initial AgNP concentration by UV-vis-NIR and (ii) provide good resolution for characterizing particle size by TEM. The remaining solution was used in the antimicrobial activity assays.

4.2.3 Synthesis of PVP-Capped Cube-AgNPs

PVP-capped cube-AgNPs were synthesized according to a previously reported procedure.[232] Briefly, 6.00 mL of ethylene glycol (EG) was heated in an oil bath to 155°C for one hour with stirring at 300 rpm, with care to maintain the temperature at 155°C to obtain high quality, monodispersed cubes as the etching process is very temperature-sensitive and can lead to the presence of other shapes. After one hour, a trace amount of sodium hydrosulfide (80 µL, 3mM in EG) was injected, followed by PVP (average MW = 55,000 Da, 1.5 mL, 20 mg/mL in EG) and $AgNO_3$ (0.5 mL, 48 mg/mL in EG). The molar ratio of PVP to $AgNO_3$ was 1.9:1, which is also important in producing uniform cubes since PVP binds to 100 surfaces and directs the final faceted-shape.[232] The solution was left to react for roughly eight minutes, during which the color changed from clear to transparent yellow-orange almost instantaneously, followed by additional changes to an opaque, opalescent ruddy green or whitish-brown. The cube-AgNPs were then purified in 0.5 mL aliquots by adding 0.5 mL acetone and centrifuging at ~20,000 rcf for 10 min to remove excess PVP and EG. The supernatants were discarded, and the pellet was re-suspended in 1.00 mL of H_2O and centrifuged again. After the second removal of the supernatants, the particles were re-suspended in 1.00 mL of H_2O. A series of slow-spin washes (i.e., 3-4) proceeded, where the particles were centrifuged at 5,000 rpm for 1.5 min. Here, the supernatants were kept and transferred to a new tube. This was done to remove any larger, irregular-shaped particles (i.e., wires) that were present and pelleted at the bottom. The cube-AgNPs were then further concentrated with the same series of washing and combining steps mentioned above for the pseudospherical-AgNPs until one concentrated tube remained. The particles were again re-

suspended in 1.00 mL of H_2O for sample characterization by UV-vis-NIR and TEM and use in the antimicrobial activity assays.

4.2.4 Synthesis of PVP-Capped Disc-AgNPs

PVP-capped disc-AgNPs were synthesized according to a previously reported procedure.[233] Briefly, a 24.75 mL aqueous solution containing $AgNO_3$ (0.05 M, 50 μL), trisodium citrate (75 mM, 0.5 mL), PVP (MW = 29,000 Da, 17.5 mM, 100 μL) and H_2O_2 (30 wt %, 60 μL) was vigorously stirred at room temperature. Sodium borohydride (100 mM, 250 μL) was then rapidly injected. Within one hour, the clear solution transitioned into a deep yellow, followed by changes to a magenta and finally a deep royal blue or purple color. The disc-AgNPs were then purified in 1.00 mL aliquots by centrifuging at ~20,000 rcf for 6 min. The supernatants were kept, transferred to a new tube, and subjected to the same series of washing and concentrating steps mentioned above for the other shapes until one concentrated tube remained. The particles were again re-suspended in 1.00 mL of H_2O for sample characterization by UV-vis-NIR and TEM and use in the antimicrobial activity assays.

4.2.5 AgNP Characterization

The three AgNP shapes were confirmed by UV-vis-NIR absorption spectroscopy using a Cary 5000 spectrophotometer (Agilent, Inc.). The spectrum baseline was corrected with respect to the H_2O spectrum. To evaluate the size of the AgNPs, NP size distributions were determined by transmission electron microscopy (TEM). An aliquot was obtained from the stock solution and diluted with H_2O prior to being drop cast onto a Formvar-coated copper TEM grid (Ted Pella,

Inc.). Samples were allowed to slowly air dry and then were dried under vacuum overnight before characterization with a Hitachi H-9500 environmental TEM at 300 kV (NanoScale Fabrication and Characterization Facility, Petersen Institute of NanoScience and Engineering, Pittsburgh, PA). NP size distributions were determined from measuring at least 300 NPs (ImageJ 1.52a, National Institutes of Health, USA) in multiple images collected from various areas of the grid. Inductively coupled plasma mass spectrometry (ICP-MS) analysis of the AgNP stock solutions and ion release experiments was performed using an argon flow with a NexION spectrometer (Perkin Elmer, Inc.) (Figure S3 in Ref [66]).

4.2.6 Bacterial Strains and Cultivation

The bacterial strain used in this work was the wild-type *E. coli* K-12 MG1655(Seq) strain (CGSC #7740) obtained from the Coli Genetic Stock Center at Yale University). Microorganism stock solutions were prepared in LB broth supplemented with 25% glycerol and stored at -80°C. Microorganisms were cultured overnight in LB broth at 37°C and 150 rpm. Overnight cultures were re-inoculated in fresh medium and grown to exponential phase (optical density, OD=1; 10^9 CFU/mL), after which they were washed three times with 0.9% saline at 13,000g for 1 minute, and diluted 100-fold in 0.9% saline to obtain approximately 10^7 colony-forming units (CFU)/mL.

4.2.7 Antimicrobial Activity of AgNPs

The antimicrobial activity of the three AgNP shapes was evaluated using standard planktonic half-maximum effective concentration (EC_{50}) measurements. These experiments were carried out in 96-well flat bottom microplates (Corning® Costar®) and done in biological and technical triplicates

(n = 9). A dispersion of AgNPs was serially diluted in H_2O and inoculated with 50 µL of *E. coli* (10^7 CFU/mL) so that the total volume of each well was 100 µL. The final tested silver concentrations were 100, 50, 25, 12.5, 6.3, 3.1, 1.6, and 0.8 µg/mL. A negative control (no AgNPs added) treatment was created by adding 50 µL of sterile DI water. Cells were incubated at 37 °C for 3 h with medium linear shaking (~500 cpm) in a Microplate Reader (Synergy HTX Multi-Mode, BioTek). After the 3 h contact time, the bacteria−AgNP suspensions were diluted (1:10) in Eppendorf tubes and vortexed, and 50 µL of each suspension was spread on a LB agar plate and incubated overnight at 37 °C for CFU enumeration. The mean plate count and standard deviation for three biological replicates (n = 9) is reported.

4.2.8 Effective Concentration Calculation

The half-maximum effective concentration (EC_{50}) was determined in OriginPro 8.5.1 software using a sigmoidal fit of the dose− response function with the equation:

$$y = A1 + \frac{A2 - A1}{1 + 10^{(log_x 0 - x)p}} \qquad \textbf{Eq. 4-1}$$

where A1 = bottom asymptote, A2 = top asymptote, $\log_x 0$ = center, and p = hill slope, and EC_{50} is given by:

$$EC_{50} = 10^{\log_x 0}. \qquad \textbf{Eq. 4-2}$$

4.3 Results and Discussion

4.3.1 Characterization of AgNP Suite

PVP-capped pseudospherical-, cube-, and disc-AgNPs were synthesized according to previously reported procedures.[193, 232, 233] PVP is a widely used, biocompatible, and slightly negatively-charged ligand[66, 202] which mitigates electrostatic attractive forces with negatively charged bacteria. After washing and purification, the particle sizes were determined to be 45.9 ± 9.8 nm, 36.2 ± 6.8 nm, and 19.1 ± 5.0 nm, for pseudospheres, cubes, and discs, respectively (**Figure 4.1**), by transmission electron microscopy (TEM). Note that the TEM image of the discs reveal some discs lying flat and some on their sides, which enabled determination of the thickness (5.5 ± 1.3 nm). Additionally, some discs were truncated triangular in shape, while most were completely rounded. Ultraviolet-visible-near infrared (UV-vis-NIR) spectra of the AgNPs revealed characteristic localized surface plasmon resonance (LSPR) peaks for each shape (**Figure 4.1**). Single resonance peaks appear at $\lambda_{max} \approx 440$ nm and 420 nm for the pseudospheres and cubes, respectively. For the discs, an in-plane dipole resonance peak appears at $\lambda_{max} \approx 600$ nm, while the 450 nm and 350 nm peaks are the out-of-plane dipole and quadrupole resonance peaks, respectively. The presence of these additional peaks clearly indicates the formation of discs, although the blue shift of the in-plane dipole resonance to 600 nm (from a resonance peak at 770 nm for a perfect triangular nanoplate) shows that the particles obtained here are truncated or rounded in shape. **Table 4.1** additionally summarizes the geometries and surface areas of the AgNP shapes, and **Table 4.2** provides a comparison of the shapes on an atom basis. Since the pseudospheres and cubes have comparable specific surface areas per particle, these two shapes enable a side-by-side comparison for antimicrobial activity when surface area is constant.

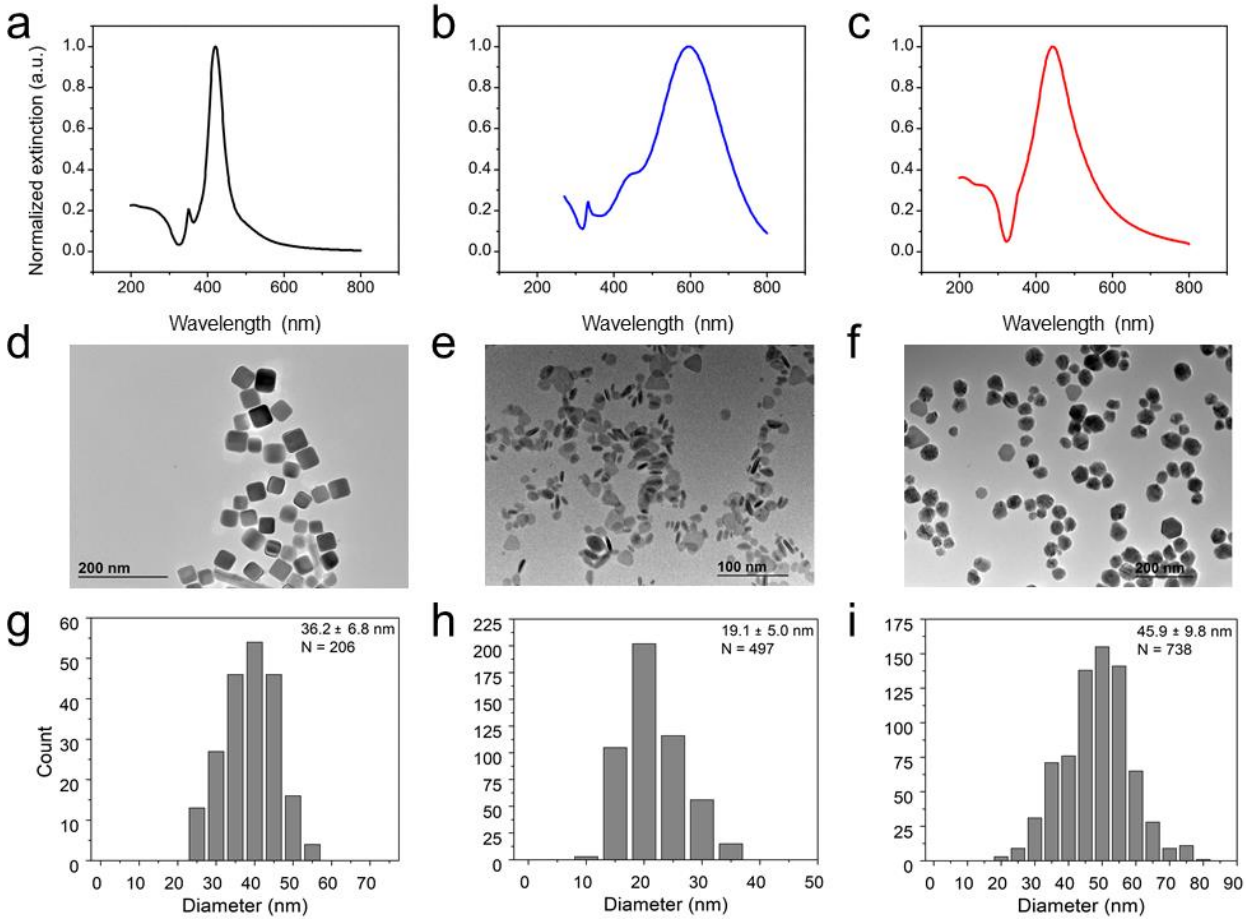

Figure 4.1. UV-vis and TEM characterization of AgNP shapes.a-c) UV-vis absorption spectra show characteristic localized surface plasmon resonance (LSPR) peaks, d-e) TEM images highlight the shape of the NPs, and g-i) particle counts show the NP size distribution for a, d, g) cubes, b, e, h) discs, and c, f, i) pseudospheres. Note that the TEM image of the discs reveal some discs lying flat and some on their sides, showing a thickness of 5.5 ± 1.3 nm. Some discs are truncated triangular in shape, while most are completely rounded.

Table 4.1. Summary of the geometries, volumes, and surface areas of the AgNP shapes. Estimated volume and specific surface area as well as mean values for particle radii, edge lengths, and thickness for the different shapes, approximated using ideal geometries and average edge lengths.

	Cubes	Discs	Pseudospheres
Radius, *r*, nm	--	--	45.9 ± 9.8 nm
Edge length, *a*, nm	36.2 ± 6.8 nm	19.1 ± 5.0 nm	--
Thickness, *t*, nm	--	5.5 ± 1.3 nm	--
Theoretical crystal facets	Anisotropic, 100% 100 facets	Anisotropic, variable% 100 and 111 facets	Amorphous, 63.4% 100 and 36.6% 111 facets
Volume equation	a^3	$\pi r^2 t$	$4/3\pi r^3$
Estimated volume per particle, nm^3	47,437.9 ± 27,202 nm^3 (25,412-79,507 nm^3)	1,575.1 ± 827 nm^3 (858 – 2,508 nm^3)	50,607.7 ± 33,150 nm^3 (24,621-90,437 nm^3)
Surface area equation	$6a^2$	$2\pi rt + 2\pi r^2$	$4\pi r^2$
Estimated specific surface area per particle, nm^2	7,862.6 ± 2,858.3 nm^2 (5,186 – 11,094 nm^2)	902.6 ± 386.9 nm^2 (555 – 1,328 nm^2)	6,615.4 ± 2,830.2 nm^2 (4,092 – 9,742 nm^2)
Surface area/volume per particle, nm^{-1}	0.17 ± 0.03 nm^{-1} (0.14 – 0.20 nm^{-1})	0.57 ± 0.06 nm^{-1} (0.53 – 0.65 nm^{-1})	0.13 ± 0.03 nm^{-1} (0.11 – 0.17 nm^{-1})

Table 4.2. Comparison of shape on an atom basis.

	Cubes	Discs	Pseudospheres
Estimated total number of atoms per particle	2,793,864 atoms	92,811 atoms	2,982,059 atoms
Estimated total number of surface atoms per particle	94,466 atoms	12,110 atoms	83,622 atoms
Estimated percent surface atoms per particle	3.38%	13.0%	2.80%

4.3.2 Antimicrobial Activity of AgNPs Related to Their Shape

The antimicrobial activities of different AgNP shapes were assessed by mixing *E. coli* with AgNP suspensions of concentrations ranging from 0 to 120 μg/mL for 3 h. A reduction of bacterial cell viability was observed at the lower concentrations, followed by a significant decrease at higher concentrations when compared to the control. All AgNP shapes inhibit 50% of the bacterial growth at different concentrations (**Figure 4.2**), determined from the sigmoidal dose–response curves using average values of three technical replicates. From the dose–response data collected, the average EC_{50} values corresponding to three biological replicates were determined to be 2.99 (±0.96) μg/mL, 2.39 (±0.26) μg/mL, and 116.33 (±6.43) μg/mL for cube-AgNPs, disc-AgNPs, and pseudospherical-AgNPs, respectively (**Figure 4.3A**). The results indicate that the antimicrobial activities of these AgNPs are in the order of disc-AgNPs > cube-AgNPs > pseudospherical-AgNPs, where the disc-AgNPs show the highest antimicrobial activity and pseudospherical-AgNPs the lowest. This is in line with several studies that found discs, also referred to as plates or prisms depending on the degree of truncation and rounding, to exhibit the greatest antimicrobial activity,[73, 74, 116, 119, 121, 122, 126-128, 130] yet contrary to studies that found spheres to be more toxic than cubes.[116, 126, 128]

The difference in antimicrobial activity can be attributed to the shape of each of the AgNPs, but the underlying mechanism(s) through which shape imparts the observed difference remains to be determined and is parsed in this work by comparing the surface areas of the various shapes (**Tables 4.1-4.3**). Surface area does not seem to play a major role, as the cube-AgNPs and pseudospherical-AgNPs have comparable specific surface areas per particle (**Table 4.1**), with drastically different observed antimicrobial activities. Furthermore, while the disc-AgNPs

exhibited the greatest antimicrobial activity, they also had the lowest specific surface area per particle available for contact with the cell.

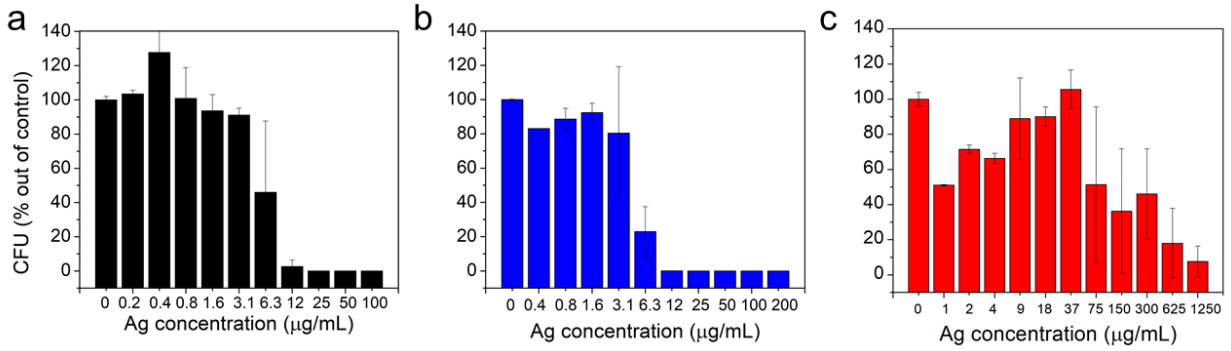

Figure 4.2. Antimicrobial activity of AgNPs to *E. coli*.Viable CFU count after 3 h of contact time between AgNPs and *E. coli* using 0−1,250 μg/mL of the particles. All experiments are compared to the negative control (no AgNPs) and has an *n* = 9. a) corresponds to cube-AgNPs, b) corresponds to disc-AgNPs, and c) corresponds to pseudospherical-AgNPs.

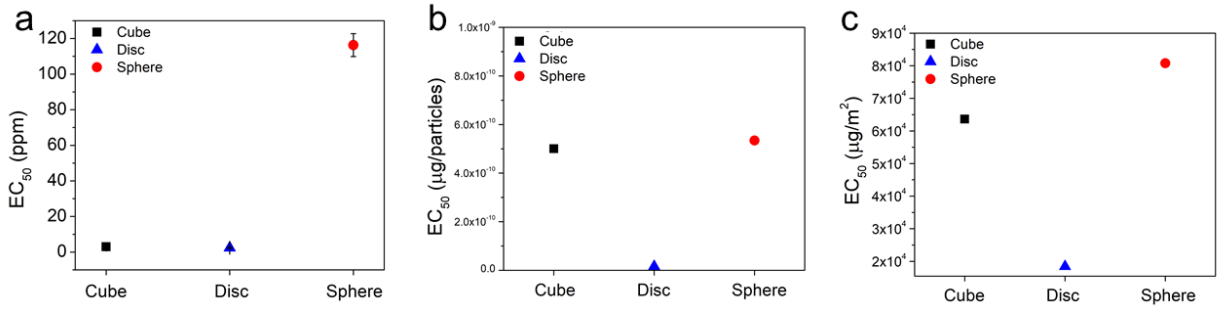

Figure 4.3. EC_{50} values of AgNPs of different shapes for *E. coli* (3 h assay). a) corresponds to the EC_{50} on a concentration basis, b) corresponds to the EC_{50} on a particle basis, and c) corresponds to the EC_{50} on a surface area basis.

When comparing surface areas based on the EC_{50} concentration, the cube-AgNPs have the lowest total surface area with the lowest number of particles/mL (**Table 4.3**) but a high number of atoms/particle (**Table 4.2**) whereas the pseudospherical-AgNPs have the highest total surface area with the highest number of particles/mL (**Table 4.3**) and highest number of atoms/particle (**Table**

4.2). The disc-AgNPs have intermediate total surface area with a high number of particles/mL **(Table 4.3)** but the lowest number of atoms/particle (**Table 4.2**). When the EC_{50} concentration is normalized to particle number and surface area (**Figure 4.3B and 4.3C, Table 4.3**), the relative trend in antimicrobial activity remains the same, although the difference between the disc-AgNPs and cube-AgNPs becomes more pronounced (i.e., disc-AgNPs >>> cube-AgNPs) and the difference between the cube-AgNPs and pseudospherical-AgNPs lessens (i.e., cube-AgNPs ~ pseudospherical-AgNPs). Taken together, this confirms that surface area likely does not play a major role in shape-based antimicrobial activity. Further, ion release relates directly to the amount of surface area available for interaction with oxygen[11, 73, 74, 116] and so this suggests that the particles themselves may induce the differential antimicrobial activity. In the case of the discs, their unique aspect ratio and/or different crystal facets present on the surface may have contributed. Shapes that have uneven or rough surfaces and possess corners or edges are suggested to be more biologically and chemically reactive,[74, 177] since atoms at these locations have a lower bonding coordination than bulk atoms and therefore affect their reactivity and interaction with bacteria. Ongoing work aims to elucidate the contributions of the ion and the particle to the observed antimicrobial activities of the different shapes, as well as the direct mechanisms of actions imposed on the cell (e.g., generation of ROS, membrane damage).

Table 4.3. Surface area comparison on a concentration basis, using the average EC_{50}.

	Cubes	Discs	Pseudospheres
EC_{50}, µg/mL	2.99 ± 0.96	2.39 ± 0.26	116.33 ± 6.43
EC_{50} normalized to particle number, µg/particles	5.01×10^{-10}	1.66×10^{-11}	5.34×10^{-10}
EC_{50} normalized to surface area, µg/m^2	6.37×10^{4}	1.84×10^{4}	8.08×10^{4}
Ag atoms/mL	$1.67 \times 10^{16} \pm 5.37 \times 10^{15}$ ($1.36 \times 10^{16} – 2.29 \times 10^{16}$)	$1.33 \times 10^{16} \pm 1.41 \times 10^{15}$ ($1.23 \times 10^{16} – 1.43 \times 10^{16}$)	$6.49 \times 10^{17} \pm 3.59 \times 10^{16}$ ($6.08 \times 10^{17} – 6.75 \times 10^{17}$)
Particles/mL	$5.97 \times 10^{9} \pm 1.92 \times 10^{9}$ ($4.85 \times 10^{9} – 8.19 \times 10^{9}$)	$1.55 \times 10^{11} \pm 1.63 \times 10^{10}$ ($1.32 \times 10^{11} – 1.55 \times 10^{11}$)	$2.18 \times 10^{11} \pm 1.17 \times 10^{10}$ ($2.04 \times 10^{11} – 2.26 \times 10^{11}$)
Surface area, m^2/mL	$4.70 \times 10^{-5} \pm 1.51 \times 10^{-5}$ ($3.82 \times 10^{-5} – 6.44 \times 10^{-5}$)	$1.30 \times 10^{-4} \pm 1.41 \times 10^{-5}$ ($1.19 \times 10^{-4} – 1.39 \times 10^{-4}$)	$1.44 \times 10^{-3} \pm 7.94 \times 10^{-5}$ ($1.35 \times 10^{-3} – 1.50 \times 10^{-3}$)

5.0 Summary and Conclusions

5.1 Major Findings

Development of new antimicrobials is imperative to protect public health as we begin to enter this post-antibiotic era. Many conventional antimicrobials are no longer effective due to the rising number of bacteria strains evolving resistance towards them as well as the increase in number of toxicity concerns to humans. Antimicrobial AgNPs are developing as a viable solution to the AMR crisis, but in order to use these responsibly in society, targeted design should be sought so that we can control antimicrobial activity and resistance outcomes. A review of the current state of the literature showed gaps in knowledge regarding: (i) ion and particle contributions to AgNP antimicrobial activity, (ii) AgNP resistance mechanisms, and (iii) mechanisms of inactivation related to differential shape-based antimicrobial activity (Chapter 1).

Support for nanoparticle-specific activity, in concert with and/or independently from Ag(I) ions, was provided in Chapter 2. Here, the literature was critically analyzed from a new lens by considering only studies that included robust comparisons between the AgNPs and Ag(I) ions in their experimental design. This ensured valid conclusions were drawn from each study, which was then used to identify trends between antimicrobial activity and particle properties. Particle size and surface chemistry were identified as key design handles imparting nanoparticle-specific effects outside of ion release. Shape was identified as not being robustly studied, with a lack of scaled Ag(I) ion controls and true shape comparisons within experimental designs precluding elucidation of the underlying mechanisms imparting shape-based antimicrobial activity.

The evolution of bacteria resistance to AgNPs was mechanistically explored in Chapter 3, where an experimental evolutionary approach was carried out. Results showed that resistance evolved to AgNPs, but not Ag(I) ions alone, suggesting that a nanoparticle-specific effect likely induced resistance. Whole-genome *E.coli* population sequencing revealed a mutation in a Ag(I) ion-efflux gene, which could suggest that AgNPs delivered the ions to the cell in a way that enabled *E.coli* to pump them out more efficiently. While this is an unfortunate outcome, at the same time, it presents an opportunity for nanoparticle design to potentially alter resistance outcomes. Furthermore, the evolution of resistance was also demonstrated to differ based on strain motility. This suggests that motility may be related to the development of resistance and could be used both as a marker to aid in prediction of resistance and also to inform targeted design towards certain microorganisms.

Finally, in Chapter 4, the influence of nanoparticle shape on *E. coli* antimicrobial activity was elucidated. Results showed that disc-shaped AgNPs imparted the greatest antimicrobial activity, followed by cube-shaped and then pseudospherical-shaped AgNPs, which remained the same trend when normalized to particle surface area. This differential shape-based antimicrobial activity is speculated to arise from differences in nanoparticle-specific activities, particularly involving the crystal facet, interaction with the cell membrane, and generation of ROS.

5.2 Implications

The mechanistic insight gained into AgNP antimicrobial activity from this research enables the promising development of a next-generation antimicrobial agent to combat the global AMR crisis. Specifically, it enables progress beyond the current disparate findings in the literature by:

1) parsing the contributions of the ion and particle on AgNP antimicrobial activity, (2) elucidating a potential mechanism of how bacteria evolves resistance to AgNPs, and (3) establishing relationships between differential shape-based antimicrobial activity and underlying mechanisms imparting inactivation that shed light on how shape can be utilized as a key design handle. Collectively, this research informs and supports the use of nanoparticle design to potentially control antimicrobial activity (maximize) and resistance (minimize) outcomes that will advance the application potential of nano-enabled antimicrobials in combatting the global AMR crisis.

5.3 Future Research

The work within this dissertation establishes many possible directions for AgNP design guidelines that aim to maximize their efficacy over the long-term and minimize their susceptibility to bacterial resistance. It also serves as the groundwork for future research opportunities that will provide additional strategies for using AgNPs in real-world applications.

5.3.1 Immediate Next Steps

Much work could be pursued on both the material and biological side. On the materials end, other shapes should be explored through synthesis of a larger shape matrix and used to correlate material properties and biological response. A detailed look at crystal facet and the ratio of crystal facet types within a shape could be explored, specifically probing crystal facet-specific membrane interaction and crystal facet-specific ion release.

On the biological end, substantial contributions to the nascent area of AgNP resistance are still needed to further evaluate the viability and longevity of AgNP-enabled antimicrobials for application in antimicrobial technologies. For one, exploring resistance over different timescales and in response to different exposure scenarios, including concentration and duration, is needed as only one duration and concentration was studied in this work. Different microbes should also be tested to see if evolution in response to AgNPs develops in the same manner. The frequency of AgNP resistance development as well as the number and identity of causative genetic mutations should also be explored as there are potentially many different routes bacteria could take to evolve resistance to AgNPs. Flagellum-mediated AgNP resistance should also be verified using multiple replicate lineages and tested in bacteria strains having varying degrees of motility (e.g., hyper-motile, normal-motile, non-motile, motor knock-outs, flagellin knock-outs, etc.) and varying degrees of flagellation (e.g., monotrichous, amphitrichous, lophotrichous, peritrichous, etc) to better understand the relationship between motility and resistance.

Finally, this work, and the methods developed herein, including experimental evolution and whole-genome population sequencing, could also be applied and translated to studying a variety of other ionizing engineered nanomaterials (ENMs), such as copper, and even carbon-based nanomaterials. Novel antimicrobial peptides and conventional antibiotics can also be added to the list. A comprehensive look at the mechanisms involved in bacteria evolving resistance to a variety of antimicrobials could enable the development of a marker, either universally or specific to a material or bacterial class, that would aid in prediction of the transition from a sensitive to resistant phenotype.

5.3.2 Probing the Mechanism(s) Underlying AgNP Shape-Dependent Antimicrobial Activity

In Chapter 4, differential shape-based antimicrobial activities were observed. The next critical step here is to probe whether nanoparticle-specific effects or ion release dominate the underlying mechanisms of inactivation. To probe this, dissolution of the AgNPs in solution should be monitored using ICP-MS and used to inform scaled ion controls, of which cell viability should be compared upon exposure to each AgNP shape, its corresponding scaled ion control, as well as the AgNP shapes in the presence of cysteine, a known Ag(I) ion quencher. These sets of experiments enable comparisons between the ions and nanoparticles to be scaled accordingly and would aid in determining whether nanoparticle-specific activity, acting independently from or in concert with solubilized Ag(I) ions, contributes to shape-dependent antimicrobial activity.

Additionally, only one study investigates shape-based direct mechanisms of action imposed on the cell and suggests membrane damage via penetration as a physical mechanism for the increased AgNP antimicrobial activity of certain shapes,[119] which is in line with studies of other ENMs such as Cu_2O that have also identified shape-specific membrane damage.[229] Chemical mechanisms may also drive shape-dependent antimicrobial activity and likely involve the production of ROS, whether extracellularly generated (at the surface through particle-cell contact or in the bulk media) to oxidize lipids of the cell membrane or intracellularly generated by ions or particles to interact with DNA and proteins. Here, it is hypothesized that increased amounts of ROS and enhanced or additional membrane disruption may both contribute to shape-dependent antimicrobial activity. Membrane disruption could be probed by monitoring changes in esterase activity following AgNP exposure using fluorescein diacetate (FDA).[234] FDA is a nonpolar ester that passes through the cell membrane and fluoresces once hydrolyzed by an esterase enzyme

only present in viable cells. Similarly, total ROS generation could be measured using the cell permeable indicator 2′,7′-dichlorodihydrofluorescein diacetate (H_2DCFDA).[234] Like FDA, cellular esterases hydrolyze the probe to the nonfluorescent 2′,7′-dichlorodihydrofluorescein (H_2DCF) under normal conditions. However, in the presence of ROS, H_2DCF is transformed to the fluorescent 2′,7′-dichlorofluorescein (DCF).

Finally, more mechanistic insight would be gained by repeating the antimicrobial assays carried out in this work in a gram-positive bacteria strain. Since membrane disruption is likely a dominant physical mechanism of antimicrobial activity, the differences in cell architecture and membrane compositions between gram-positive (thick peptidoglycan layer) and gram-negative (outer lipid membrane) organisms may shed some light on membrane disruption as a potential mechanism.

5.3.3 Designing Evolutionary Traps: Using Different Resistances That Work Against Each Other

In Chapter 3, one mechanism of resistance to AgNPs was found to arise from a mutation in an ion efflux pump that quickly works to push metal ions out of the cell. Following this, the next intriguing step to take, from an arms race point-of-view, is overcoming this mechanism of resistance through particle design or using evolution itself as a strategy. Particle shape may bode well as a design strategy as Chapter 4 demonstrated unique antimicrobial activities of various AgNP shapes and preliminary work by other groups have shown *E. coli* has a harder time evolving resistance to triangular-shaped AgNPs as opposed to spherical-shaped AgNPs.[216] As suggested in Chapter 4, different particle shapes have unique modes of interaction with the bacterial cell and

thus likely operate under different mechanisms of inactivation, such that the mechanisms of adaption are likely to be unique (and perhaps weaker or slower) compared to their spherical counterparts explored in this work. This strategy may be particularly fruitful if different shapes can employ physical modes of inactivation (i.e., outer membrane damage, extracellular ROS generation), rather than rely on intracellular ion release which may have spurred the mutation for increased efflux in the case of the spherical-shaped AgNPs, thereby bypassing this mechanism of resistance. Using different particle shapes may result in lower levels of resistance or else cause bacteria to evolve a different mechanism of resistance altogether, which would present some interesting strategies for their use as antimicrobials, i.e., coupling different AgNP shapes that elicit bacterial adaptations that counter or oppose each other (see the concept of an evolutionary trap detailed below) or else developing a periodic or alternating regimen for the AgNP shapes used in consumer products over the years.

Unless evolution is driven by NP shape, one caveat is that simply using an alternative AgNP shape will not provide a fool-proof strategy as bacteria will find a way to develop defenses against any antimicrobial. In fact, design of the next generation of antimicrobials needs to consider beyond just acute, one-time use scenarios and high bacterial inactivation, but also efficacy over repeated, long-term exposure and incorporate the evolutionary dispositions of bacteria to design for future lineages of bacteria populations that will continue to change their response after exposure to the antimicrobial.[235] Thus, we need to shift our approach from finding a single, promising antimicrobial to optimizing an engineered antimicrobial system that will shape bacterial response and natural selection to balance both the organism's goals (fitness for survival and reproduction) and the efficacy of the antimicrobial. This is where evolutionary design and the concept of designing for an evolutionary trap and/or high biological fitness costs can come into play to help

break the cycle of resistance.[235, 236] While the genetic response to an antimicrobial cannot be controlled, the adaptive landscape itself can be sculpted by harnessing fitness and the power of natural selection.[235] An evolutionary trap is a situation in which an organism adapts to an object in its environment, but in doing so, leads to negative consequences such as losing its adaptation to a different object.[236] Iron has been suggested for use as an evolutionary trap by Graves' group, as there is such a high need and stringent process in place for bacteria to acquire iron as an essential micronutrient from its environment.[236] While one evolutionary trap could arise from using a mix of AgNP shapes, other types of evolutionary traps could be explored with AgNPs and antibiotics (in hopes of rescuing them), conventional chemical antimicrobials, antimicrobial peptides, bacteriophages, or other metals. In order for this to work, the adaptations made by the cell must work in opposition to each other. For example, in line with the increased ion efflux induced by the AgNPs in Chapter 3, beta-lactams and tetracyclines diffuse through porin channels and other substrate transport systems of the outer and cytoplasmic membrane to reach their targets inside the cell [237, 238] and so employing them together with AgNPs could lead to an outcome where either i) the porin channels become blocked as a defense mechanism against the antibiotics, leaving Ag to accumulate in the cell or ii) the porin channels are left open through autophosphorylation in response to the AgNPs, leaving antibiotics to enter. This represents a similar approach to that of researchers coupling bacteriophages and antibiotics. Phages bind to specific receptors on the bacterial cell surface, and in response, bacteria adapt by modifying these surface receptors, which in turn allows them to become re-sensitized to antibiotics.[239-243] These redundant, or fail-safe, approaches may present a viable strategy for overcoming resistance and breaking the cycle, albeit practical limitations (e.g., corrosion, human and environmental toxicity) of the system to which they are employed will have to be considered upfront.

5.3.4 Designing AgNPs For Use Against Biofilms

Throughout this dissertation, the antimicrobial activity of AgNPs was probed using planktonic bacterial cells. While a lot can be gleaned from studying the interactions between AgNPs and planktonic cells, most of the applications employing AgNPs will encounter bacteria in biofilms on their surfaces, including medical devices such as catheters, showerheads and other water fixtures, and food packaging. The AgNPs will also be embedded in a polymer or cotton matrix as opposed to in aqueous suspension, and so it is critical to demonstrate the efficacy of AgNPs in environments most closely mimicking their intended applications (**Figure 5.1**). For example, the most used polymers in clinical practice include silicone, polyurethane (PU), polyethylene (PE), polyvinylchloride (PVC), PTFE, and nylon.[244] Thus, the antimicrobial efficacy of AgNPs integrated into a polyurethane film could be evaluated on several multi-drug resistant biofilms (e.g., *Pseudomonas aeruginosa*, *Klebsiella pneumoniae*, *Staphylococcus aureus*) and in synthetic bodily fluids to simulate clinically relevant conditions. Polymer-nanocomposite films (e.g., a nano silver coating on the surface of polyurethane) can be prepared using corona air plasma/discharge equipment. This is a surface modification technique that uses a low temperature corona discharge plasma to impart changes in the properties of a surface.[245] Efficacy can be assessed using biofilm viability assays (e.g., 3-(4,5-dimethylthiazol-2-yl)-2,5-diphenyl tetrazolium bromide (MTT) assay), and the evolution of adaptive resistance confirmed through the methods utilized in Chapter 3.

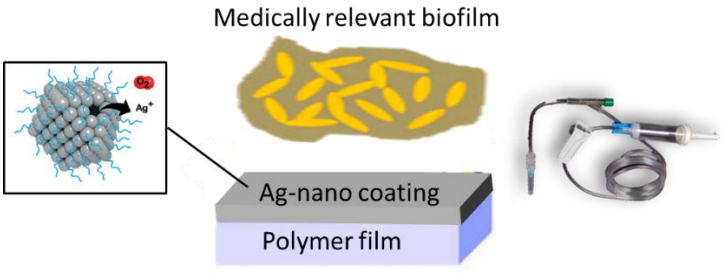

Figure 5.1. Assessing the efficacy of an antimicrobial polymer-nanocomposite film against biofilms to simulate real-world applications.

Future work should also be directed at studying and designing AgNPs for targeting biofilm architectures and determining how the identified mechanisms of inactivation in this work translate to biofilms. It is well known that biofilms are generally more resistant to antibiotics than their planktonic counterparts [246, 247] and so this is likely to be the case for AgNPs as well. Further supporting this claim are the findings from Chapter 3 where hyper-motile *E. coli* developed resistance to AgNPs, as hyper-motility and swarming behavior imparted by flagella can initiate attachment to surfaces and early stages of biofilm formation.[248] One inherent property of biofilms that could be a potential target for AgNP design is their intra-colony channels, which function as nutrient uptake systems.[249] It has been demonstrated that these channels can transport particles (e.g., one study used 200 nm microspheres)[249] and so they could potentially function as AgNP delivery systems. However, similar to porin channels and efflux pumps, these channels could work to benefit the biofilm and function as transport mechanisms to direct AgNPs out of the cell. Thus, mechanisms of inactivation and resistance to AgNPs need probed in biofilms. AgNP shape could come into play once again as a design strategy, where uptake and distribution of various shapes through the biofilm could be explored and imaged with electron and optical

microscopies. A particular size and shape could also be optimized to block these channels and preclude nutrients from entering the cell and Ag from leaving the cell.

Appendix A Chapter 2 – Supplemental Information

Appendix A.1 Discussion 1 – Total Ag atoms calculations

Ag Salt Control

Under the alternate assumption – that the reported concentration was of total Ag salt rather than Ag atom – the molecular weight would change from 107.87 g/mol (corresponding to Ag) to that of the Ag salt (e.g., 169.87 g/mol for $AgNO_3$, 166.91 g/mol for $AgC_2H_3O_2$, 311.80 g/mol for Ag_2SO_4). The molar ratio would also need to be incorporated here. For a reported concentration of 0.4 $\frac{\mu g}{mL}$ $AgNO_3$:

$$0.4\ \frac{\mu g}{mL} AgNO_3 * \frac{1\ g}{10^6\ \mu g} * \frac{1\ mol}{169.87\ g} * \frac{1\ mol\ Ag}{1\ mol\ AgNO_3} = 2.35\ x\ 10^{-9} \frac{mol\ Ag(I)}{mL}\ as\ AgNO_3,$$

which is not significantly different from $3.71x10^{-9} \frac{mol\ Ag(I)}{mL}\ as\ AgNO_3$ (assuming the reported concentration is of total Ag atom).

AgNP

The alternate assumption – that the reported concentration was of total AgNP rather than Ag atom – requires including the mass of the ligand, which depends on the number of ligands appended to the particle. Since the majority of studies do not include this information, the mass of the ligand was ignored for the purposes of this example calculation. For a 25 nm particle, the number of total Ag atoms and thus the weight of the AgNP is:

$$\frac{4.85x10^5\ atoms\ Ag}{AgNP}(for\ a\ 25\ nm\ AgNP) * \left(\frac{107.87\ g}{1\ atom\ Ag}\right)$$

$$= \left(\frac{5.19x10^7 g\ Ag}{AgNP}\right) * \left(\frac{6.02x10^{23} AgNPs}{1\ mol\ AgNPs}\right) = \frac{3.13x10^{31} g\ Ag}{1\ mol\ AgNPs}$$

For a reported concentration of 0.4 $\frac{\mu g}{mL}\ AgNPs$:

$$0.4\frac{\mu g}{mL}\ AgNPs * \left(\frac{1\ g}{10^6\ \mu g}\right) * \left(\frac{1\ mol\ AgNP}{3.13x10^{31} g\ Ag}\right) = 1.28x10^{-36}\ mol\frac{AgNPs}{mL}.$$

The associated extent of necessary AgNP oxidation is unrealistic (10^{29}%) and resulted in rejection of every study for having an overestimated ion control.

Appendix A.2 Discussion 2 – Surface Ag atoms calculations

General Considerations for Ag

Ag has face-centered cubic (FCC) lattice structure:

$$Unit\ cell = 6 * \frac{1}{2} + 8 * \frac{1}{8} = 4\ \frac{Ag\ atoms}{unit\ cell}$$

$$Unit\ cell = 4 * \frac{1}{8} + 1 * \frac{1}{2} = 1\ \frac{Ag\ atom}{surface\ unit\ cell}$$

$$Ag\ lattice\ constant\ (a_{lat}) = 0.408\ nm$$

$$Unit\ cell\ volume\ (nm^3) = {a_{lat}}^3$$

$$Bond\ length\ (BL) = 2r = \frac{\sqrt{2}a_{lat}}{2} = \frac{a_{lat}}{\sqrt{2}}$$

$$SA_{(111)} = \frac{\sqrt{3}BL^2}{2}$$

$$SA_{(110)} = BL * a_{lat}$$

$$SA_{(100)} = BL^2$$

$$Unit\ cell\ surface\ area\ (nm^2)$$

$$= (\%(111)) * \left(SA_{(111)}\right) + (\%(110)) * \left(SA_{(110)}\right) + (\%(100)) * \left(SA_{(100)}\right)$$

$$Volume\ (nm^3)\ x\ \left(\frac{1\ unit\ cell}{V\ (nm^3)}\right)\ x\ \left(\frac{4\ Ag\ atoms}{unit\ cell}\right) = total\ number\ of\ Ag\ atoms$$

$$Surface\ area\ (nm^2)\ x\ \left(\frac{1\ unit\ cell}{SA\ (nm^2)}\right)\ x\ \left(\frac{1\ Ag\ atom}{unit\ cell}\right) = number\ of\ surface\ Ag\ atoms$$

<u>*Sphere Approximated as a Cuboctahedron*</u>

$$Particle\ radius\ (r) = 25\ nm$$

$$V_{sphere} = \frac{4}{3}\pi r^3 = 65{,}450\ nm^3$$

$$SA_{sphere} = 4\pi r^2 = 7{,}854\ nm^2$$

A cuboctahedron has 8 (111) faces as equilateral triangles and 6 (100) faces as squares.[250] The relative percentage of each surface facet was determined using the edge length (E) as it defines the size of the 8 triangles and 6 squares:

$$A_{8\,triangles} = 8 * \frac{b * h}{2} = 8\frac{E * E\frac{\sqrt{3}}{2}}{2} = 2 * \sqrt{3} * E^2$$

$$A_{6\,squares} = 6E^2$$

$$A_{total} = A_{8\,triangles} + A_{6\,squares}$$

$$\%\,(111) = \frac{A_{8\,triangles}}{A_{total}} = \frac{2 * \sqrt{3} * E^2}{2 * \sqrt{3} * E^2 + 6E^2} = 0.366$$

$$\%\,(100) = \frac{A_{6\,squares}}{A_{total}} = \frac{6E^2}{2 * \sqrt{3} * E^2 + 6E^2} = 0.634$$

$$Unit\ cell\ surface\ area\ (nm^2)$$

$$= (0.366) * \left(SA_{(111)}\right) + (0) * \left(SA_{(110)}\right) + (0.634) * \left(SA_{(100)}\right) = 0.079$$

$$Total\ number\ of\ Ag\ atoms = 3,854,678\ Ag\ atoms$$

$$Number\ of\ Ag\ surface\ atoms = 99,228\ Ag\ surface\ atoms$$

$$\%\ Ag\ surface\ atoms = \%\ ionization = \frac{Ag\ surface\ atoms}{total\ Ag\ atoms}\ x\ 100 = 2.57\%$$

<u>*Nanorod/Wire Approximated as a Cylinder with Half Spheres on Each End*</u>

$$Length\ (l) = 6755\ nm$$

$$Width\ (w)/Diameter(d) = 82\ nm$$

$$V_{total} = V_{sphere} + V_{cylinder} = \frac{4}{3}\pi r^3 + \pi r^2 h = 35,528,924\ nm^3$$

$$SA_{total} = SA_{sphere} + SA_{cylinder} = 4\pi r^2 + 2\pi rh = 1,740,159\ nm^2$$

A nanorod/wire has 2 (111) faces as the half spheres while the side surface is a (100) face.[251] The relative percentage of each surface facet was determined using the edge length (E) as it defines the size of the 8 triangles and 6 squares:

$$A_{sphere} = 4\pi r^2$$

$$A_{cylinder} = 2\pi rh$$

$$A_{total} = A_{sphere} + A_{cylinder}$$

$$\%\,(111) = \frac{A_{sphere}}{A_{total}} = \frac{4\pi r^2}{4\pi r^2 + 2\pi rh} = 0.0121$$

$$\%\,(100) = \frac{A_{cylinder}}{A_{total}} = \frac{2\pi rh}{4\pi r^2 + 2\pi rh} = 0.988$$

$$Unit\ cell\ surface\ area\ (nm^2)$$

$$= (0.0121) * \left(SA_{(111)}\right) + (0) * \left(SA_{(110)}\right) + (0.988) * \left(SA_{(100)}\right) = 0.083$$

$$Total\ number\ of\ Ag\ atoms = 2,092,481,147\ Ag\ atoms$$

$$Number\ of\ Ag\ surface\ atoms = 20,941,396\ Ag\ surface\ atoms$$

$$\%\ Ag\ surface\ atoms = \%\ ionization = \frac{Ag\ surface\ atoms}{total\ Ag\ atoms}\ x\ 100 = 1.00\%$$

Appendix Table A.1. Compilation of qualitative and empirical data reported in the final subset of studies used for the pivot table analysis.

Refs	Species or organism group	Exposure medium	AgNP size (nm)[a]	AgNP shape	Surface ligand (zeta potential mV)	Ligand control present	AgNP synthesis method	Purification procedure	AgNP conc. character-ization method	Aggregation monitoring method (time)	Additional character-ization	Assay	Endpoint	Conclusion drawn
[252]	*E. coli* nonmutated Strain BW25113, biosensor *E. coli* MC1061 (pcueR/pcopAlux) and MC106 (pSLIux)	LB with 5% FBS and some antibiotics	9.1 ± 4.2	sphere	citrate (-26.3 ± 2.6)	yes – not toxic	purchased from Nanocomposix	--	GF-AAS	DLS (duration)	--	growth, biosensor, gene deletion, AFM/ TEM	IC_{50}, bioavailable Ag, gene regulation, AgNP-cell interaction	particle-only, combined ion-particle
			19.1 ± 6.0											
			43.5 ± 12											
			17.9 ± 7.0	sphere	PVP (-10.7 ± 1.8)	yes – not toxic	synthesized using $AgNO_3$ and $NaBH_4$	ultrafiltration system (Spectrum Laboratories, Inc.) equipped with a 10 kDa polyethersulfone membrane (MidiKros Hollow Fiber Module (P-X3-010E-300-02N))						
			23.3 ± 15	sphere	BPEI (+33.3 ± 1.5)	yes – not toxic	synthesized using $AgNO_3$ and UV irradiation							
[253]	*E. coli* K12 ATCC 25404	$NaHCO_3$ buffer	35.4 ± 5.1[b]	sphere	amorphous carbon (-27 ± 1.54 anaerobic, -30 ± 0.42 aerobic)	--	purchased from Novacentrix Corporation	washed 5 times with 1% HNO_3 and 5 times with deoxygenated (N_2-purged) water inside an anaerobic chamber, filtration through a cellulose membrane (MWCO 10 kDa) using an Amicon stir cell (Millipore, MA) pressurized with nitrogen	ICP-OES/MS	--	--	plate counting, dose-reponse, MLC assay	viable cell number (CFU), log reduction, MLC	ion-only, combined ion-particle
[254]	*E. coli* K12 ATCC 25404	$NaHCO_3$ minimal media	2.8 ± 0.47	sphere	PEG (-16.1 ± 1.2)	--	synthesized by reaction of tetrachloroauric acid or $AgC_2H_3O_2$ with oleylamine in refluxing toluene, hexane, or 1,2-dichloro-benzene	--	--	--	--	growth inhibition	EC_{50}, % live dead	ion-only
			4.7 ± 0.2											
			10.5 ± 0.59											
			17.5 ± 2.9	sphere	PVP (-27.5 ± 1.4)	--	commercially available from NanoAmor	--			--			
			51.4 ±18.7											
			71.5 ±20.3											

Appendix Table A.1 (continued)

[255]	*E. coli* K12 MG 1655	modified LB lacking NaCl	142 ± 20	sphere	--	--	synthesized in the vapor phase	--	--	--	SEM and XRD to characterize NP composition, BET surface area	timed release Ag toxicity, growth curve, viable plate counts, TEM, RT-PCR	viable cell number (CFU), AgNP-cell interaction, fold change	combined ion-particle
[256]	*E. coli* K12 MG 1655	modified LB lacking NaCl	142 ± 20	sphere	--	--	synthesized in the vapor phase	--	--	--	SEM/EDX for composition	plate counts, growth curve, gene expression microarray	viable cell number (CFU), fold change	combined ion-particle
[257]	*S. aureus* ATCC 6538, *E. coli* ATCC 10536	ISB, TSB, PBS Dulbecco's and HEPES, CAPS	7 ± 4	sphere	glutathione	--	mixed $AgNO_3$, sodium citrate, and $NaBH_4$.	Centrifugation and pellet precipitation	ICP-OES	UV-vis, DLS (duration)	Mie's effective refractive index for subsitution of the citrate capping layer, TGA, SEM EDS for composition, XRPD and FT-IR for capping agents	standard broth macro-dilution method, plate counting	ME, MIC	particle-only
[258]	*T. pseudonana* CCMP 1335, *Synechococcus* sp. PCC 6911	artificial seawater and freshwater	21.6	sphere	maltose (-38)	--	D-maltose monohydrate and $AgNO_3$ added to $NaBH_4$	--	--	DLS (duration)	CPS for size	dose response	% growth inhibition	combined ion-particle
			39		maltose (-49)		modified Tollens process - chemical reduction of $[Ag(NH_3)_2]+$ by sugars (mix of $AgNO_3$, NH_4OH, and NaOH - vary the latter two to control size	--						
			97.4		maltose (-48)			--						

Appendix Table A.1 (continued)

[259]	*N. europaea* ATCC 19718	AOB medium	25.2 ± 9.3	sphere	citrate (-23 ± 1.1)	yes – not toxic	$AgNO_3$ reduced with citrate	--	ICP-MS	TEM, DLS	--	micro BCA protein assay, live/dead, TEM, gene expression	% reduction in nitrite production, membrane integrity, AgNP-cell interaction, fold change	ion-only
			27 ± 6.5	sphere	GA (-21 ± 1.3)	yes – not toxic	$AgNO_3$ reduced with GA	diluted and centrifuged three times before resuspending in water						
			21 ± 17	sphere	PVP (-11.6 ± 1.8)	yes – not toxic	purchased from Nanostructured and Amorphous Materials, Inc.	--						
[260]	PolySeed (*Bacillus* sp.)	BOD5 test medium	58 ± 11	sphere	hydrogen (-22)	yes – not toxic	Ag_2O heated and then bubbled with H_2	system from Spectrum Laboratories, Inc. ultrafiltration membrane 10 kDa polyethersulfone (MidiKros Hollow Fiber Module (P-X3-010E-300-02N))	AAS	DLS	XPS, NMR, and conductivity (Orion 013010MD conductivity cell) for purity	five day oxygen consumption test; live/dead Baclight, TEM	oxygen consumption, % live bacteria, AgNP-cell interaction	particle-only
			19 ± 5		citrate (-38)	yes – not toxic	$AgNO_3$ reduced with citrate							
			12[b]		PVP (-10)	yes – not toxic	$AgNO_3$ added dropwise to an $NaBH_4$ and PVP solution							
			10 ± 4		BPEI (+40)	yes – not toxic	BPEI and $AgNO_3$ dissolved in HEPES separately, mixed together, and exposed to UV light							
[261]	*E. coli* ATCC 25922	PBS	20.3 ± 1.9	sphere	phosphate monolayer	--	bought from Nanocomposix (synthesized using aqueous reduction from Ag salts in phosphate buffer)	extensive washing	ICP-MS	TEM (duration)	DLS for HDD, UV-vis for size	plating assay	MBC	ion-only
			53.1 ± 4.1											
			112.6 ± 7.8											
[262]	*V. fischeri* DSMZ	2% NaCl	20	sphere	-11	--	purchased from PlasmaChem GmbH	--	ICP-MS	DLS	SEM, high-resolution (HR)-SEM, FTIR	standard inhibition of biolumin-escence	% lumin-escence	combined ion-particle
			200		-12.65	--								
			23		-10.85	--	synthesized by *Ocimum sanctum* plant leaf extract							
			27		-13.5	--	synthesized by *Azadirachta indica* plant leaf extract							

Appendix Table A.1 (continued)

[263]	*E. coli* AB1157 (pSLlux), *E. coli* JI130 (pSLlux), *E. coli* JI131 (pSLlux), *E. coli* AS393 (pSLlux), *E. coli* JI132 (pSLlux), *E. coli* AS391 (pSLlux), *E. coli* K12::lux, *E. coli* MC1061 (pDNlux), *E. coli* 12::soxRSsodAlux, *E. coli* MC1061 (pSLzntR/pDNPzntAlux), *E. coli* MC1061 (pSLcueR/pDNPcopAlux)	0.9% NaCl	< 100[c]	sphere	--	--	purchased from Sigma Aldrich	--	--	SEM	SEM, TEM	growth assay, luminescent bacterial test, luciferin-luciferase method	maximal growth rate, EC_{50}, EC_{99}, induction of bioluminescence, ATP content	combined ion-particle
[264]	*E. coli* K12 BW30270, *P. fluorescens* OS8	ultrapure water	11.6 ± 5.2 17.8 ± 8 47.7 ± 8 56.5 ± 9.6 94.8 ± 54	sphere	citrate (-25) citrate (-25) citrate (-24) citrate (-15) citrate (-16)	--	purchased from MK Nano (Missisauga, Canada)	--	--	DLS	single particle (SP)-ICP-MS for size, SEM-EDS for size and morphology, UV-vis	plating, ROS, and bioluminescence assays	CFU/mL, EC_{50}, ROS production, fold induction bioluminescence	combined ion-particle

Appendix Table A.1 (continued)

[265]	*E. coli* AB1157, *E. coli* K12 MC 4100, *E. coli* K12 TK 821, *E. coli* K12 MH 1471, *E. coli* K12 MH 225, E. *coli* K12 MG1655 (pKatG::*lux*), *P. aeruginosa* PAO1, *P. chlororaphis 449, S. proteamaculans 94, S. liquefaciens MG1 and MG44*	Difco nutrient broth	8.3 ± 1.9	sphere	hydrolyzed casein peptides	--	prepared Ag oxide by adding $AgNO_3$ to 20% NaOH. Reduced Ag oxide with hydrolyzed casein peptides	--	--	SEM (one time point)	--	MIC assay, MTT assay, live/dead Baclight assay, biosensor assay, mutant growth assay	MIC, biofilm formation, bioluminescence, H_2O_2 concentration, gene regulation	combined ion-particle
[266]	*E. coli, S. aureus*	LB	6	sphere	--	--	prepared by the solvated metal atom dispersion method, which involves covaporization of Ag and solvent (acetone) onto a liquid N_2 cooled surface that warms. Ligands added and then heat treated, air exposed, and KOH exposed	--	--	TEM (one time point)	SEM/XRD/EDX for morphology, BET surface area	plate counting	number of surviving bacteria colonies	ion-only
					3-mercapto-1,2-propane-diol	yes – not toxic								
					sodium 3-mercapto-1-propane-sulfonate,	yes – not toxic								
					sodium 5-mercapto-1-tetra-zoleacetate	yes – not toxic								
			1000 – 5000		Ag_2O	yes – not toxic	purchased from Aldrich							
					AgO	yes – not toxic								
[267]	*B. subtilis* UD1022, *E. coli* OP50	LB	44.9 ± 7.2	sphere [d]	citrate (-40.7)	yes – not toxic	purchased from Ted Pella Inc.	--	ICP-MS	DLS (duration)	--	growth assay, SEM	MIC/EC_{50}, growth kinetics, AgNP-cell interaction	combined ion-particle

Appendix Table A.1 (continued)

[268]	nitrifying sludge	SWW	2 – 12	sphere	starch	--	purchased from Prime Nanotechnology Co, Ltd. (chemically synthesized from $AgNO_3$ using $NaBH_4$ and starch as reducing and capping agent)	--	--	EDX	UV-vis	SEM/TEM, ammonia oxidation, FISH, CLSM, live-dead Baclight assay,	AgNP-cell interaction, physiology and morphology change, maximum ammonia oxidation rate, % inhibition ammonia oxidation, % abundance, % membrane compromised	ion-only
[269]	*E. coli* DH5alpha DSMZ 6897, *S. aureus* DSMZ 1104	Lysogeny broth medium and Roswell Park Memorial Institute medium/10% FCS medium	70 ± 20	sphere	PVP (-25)	--	reduced from $AgNO_3$ with glucose in the presence of PVP	ultracentrifugation	AAS	DLS	--	MIC/MBC assay	MIC/MBC	ion-only
[270]	*P. putida* mt-2 DSM 6125	mineral salt media with Na_2-succinate	< 10[c]	sphere [e]	Tetra-decane	yes – not toxic	commercial AgNP dispersion (736503, Silverjet DGH-55LT-25C; Sigma-Aldrich)	--	--	--	--	growth assay, surface hydro-phobicity, analysis, fatty acid composition	growth inhibition, EC_{50}, water contact angle, cis/trans ratio/ membrane adaptive response	ion-only
[119]	PI-*Lac::GFP* (propidium iodide stained *E. coli* (*lac::GFP*))	modified LB without NaCl supplemented with ampicillin	10 40 100	sphere	--	--	manufactured by Sigma Aldrich Co. LLC	--	--	UV-vis, TEM (duration)	--	dual fluorescence flow cytometric analysis, effects of divalent metal ions, plate counting	ratio of damaged to living cells, response ratio of metal ions	combined ion-particle

Appendix Table A.1 (continued)

[271]	*E. coli* MG1655	$NaHCO_3$	10.2 ± 2.3	sphere	citrate (-47.4)	--	synthesized using sodium citrate and tannic acid	ultrafiltration (10 kDa MWCO membrane; Millipore) and washed twice with deionized water	--	DLS (one time point)	X-ray binding energy analysis for surface characterization	SEM, NAD^+/NADH ratio test, intracellular ROS, malonyl-dialdehyde and 8-oxoguanine assay, Ag uptake and distribution evaluation	morphology, respiration chain disturbance, intracellular ROS production, lipid peroxidation, DNA damage, Ag uptake	combined ion-particle
			10.2 ± 2.5	sphere	MPA (-34.5)	--	ligand exchange with citrate AgNPs							
			10.2 ± 2.2	sphere	MHA (-29.1)	--								
			9.9 ± 2	sphere	MPS (-32.6)	--								
[272]	nitrifying bacteria (*Nitrosomonas* and *Nitrobacter*)	agricultural soil of Toccoa sandy loam amended with a buffered nutrient solution ($(NH_4)_3PO_4$and $(NH_4)_2SO_4$)	50	sphere [e]	--	--	purchased from Inframat Advanced Materials and Ultrasound Research Nanomaterials	--	--	--	--	batch soil-slurry nitrification method, sorption isotherm	nitrification kinetics (V_{max} nitrification potential), sorption	combined ion-particle
			15		PVP	--	purchased from Ultrasound Research Nanomaterials and Nanostructured and Amorphous Materials Inc.							
[273]	*S. oneidensis* MR-1	ferric citrate bacterial growth medium (minimized chloride content)	11 ± 3	sphere	citrate (-29 ± 3)	--	synthesized with trisodium citrate dihydrate and $NaBH_4$	centrifuged at 1500 g for 4 min using regenerated cellulose (MWCO 50 kDa) centrifugal filter units (EMD Millipore), resuspended in DI water, centrifuge/resuspension steps repeated 3X	UV-vis, ICP-MS	DLS (duration)	--	live/dead BacLight assay, TEM	live/dead ratio, morphology/ AgNP-cell interaction	ion-only

Appendix Table A.1 (continued)

[274]	*P. putida* G7	phosphate buffer	50	sphere	-49.2 ± 1.32	--	purchased from Sigma Aldrich	--	--	DLS (one time point)	BET surface area, TEM for surface characterization, CPS disk centrifugation for size	ATP production (BacTiter-Glo) assay, computer-assisted motion analysis (phase contrast microscopy), chemical-in-pond method and inverted capillary assay	% viability, motility behavior, bacterial repellent response/chemotaxis	particle-only
			100		-54.1 ± 3.4									
[275]	*N. europaea* ATCC 19718	HEPES buffer and $(NH_4)_2SO_4$ minimal growth media	20	sphere	phosphate monolayer	--	synthesized through aqueous reduction by NanoComposix, Inc	--	ICP-ES	time-resolved (TR)-DLS (duration)	--	nitrite production and inhibition reversal colorimetric assay, membrane stability, AMO- and HAO-SOUR assay	% nitrification activity, % intracellular K^+, % SOUR activity	ion-only
			80											
[276]	*E. coli*	moderately hard water	10 ± 4.6	sphere	BPEI (+28.8)	yes – not toxic	synthesized with $AgNO_3$ and HEPES and UV radiation	tangential flow filtration system equipped with 10 kD hollow fiber polysulfone membranes; buffer exchange of impurities and ions in NP suspension with nanopure water	GF-AAS	DLS (before and after experiment)	UV-vis, PALS for zeta potential	*E. coli* bioassay	% inhibition of β-galactosidase enzyme, EC_{50}	particle-only
			56 ± 14		citrate (-20.08)	yes – not toxic	synthesized with $AgNO_3$ and sodium citrate dihydrate							
			72 ± 24		PVP (-7.49)	yes – not toxic	bought from Nanostructured and Amorphous Materials Inc. and added PVP							

Appendix Table A.1 (continued)

[277]	*E. coli* MC1061 (pSLlux), *E. coli* MC1061 (pSLcueR/pDNcopAlux)	water purified with MilliQ equipment	83 ± 37	sphere	citrate (-36)	--	purchased from MKNano as aqueous suspension	--	GF-AAS	--	SEM-FIB-EDX for size and composition, DLS for HDD spheres, ELS for HDD for both shapes, UV-vis	bacterial biolumin-escence assay, bacterial viability plate assay	% inhibition of biolumin-escence, fold induction of biolumin-escence, EC_{50}	ion-only
			100 ± 40 (diameter) x 6100 ± 2700 (length)	nano-wire	-46	--	purchased from Seashell Technology as suspension in isopropanol							
[278]	Activated sludge	MLSS	5	sphere[e]	PEG	--	synthesized in another lab	--	--	--	--	SEM, community population shift, qPCR/pyrosequencing	activated sludge microstructure, % relative abundance, copy number of AMO	combined ion-particle
			35		carbon	--	purchased from Novaentrix Co.							
[279]	*E. coli* K12 TG1	distilled water, LB agar with ampicillin	52[b]	sphere	--	--	fabricated via reduction of $AgNO_3$ and hydroxylamine hydrochloride in NaOH solution	--	--	--	--	lumine-scence assay, polargraphic oxygen consumption method, AFM, cell viability serial dilution and plating assay	Biolumin-escence intensity (I), oxygen consumption rate, morphological changes, number of CFU, toxicity index (T)	ion-only
[280]	*E. coli* K12 MG 1655	LB, MH	24 ± 3.2	sphere	PEGSH (-11.2 +/- 1.5), ligand density: 1.46 ± 0.17 nm^{-2})	--	synthesized by aqueous reduction with $AgNO_3$, tannic acid, and citric acid. Ligand exchange to PEGSH	centrifuging and washing with DI water multiple times before and after ligand exchange with PEGSH	UV-vis, ICP-MS	TEM, DLS, UV-vis (duration)	NMR-TEM-ICP-MS for ligand density, XPS for AgCl formation	bacterial growth assay	OD_{600}	combined ion-particle

[a] Particle size determined by TEM/SEM
[b] DLS was used in place of TEM to determine particle size
[c] Particle size reported by manufacturer
[d] Included polygonal features (e.g., sharp corners)
[e] Assumed spherical shape

Appendix Table A.1 (continued)

Abbreviations: AFM – atomic force microscopy; AMO – ammonia monooxygenase enzyme; AOB – ammonia oxidizing bacteria; ATP – adenosine triphosphate; BET – Brunauer-Emmett-Teller; BOD – biological oxygen demand; BPEI - branched poly(ethylene imine); CAPS – N-cyclohexyl-3-aminopropanesulfonic acid; CFU – colony forming unit; CLSM – confocal laser scanning microscopy; CPS – centrifugal particle sedimentation; DI – deionized water; DLS – dynamic light scattering; DNA – deoxyribonucleic acid; EC_{50} – effective concentration that affects 50% of the test population; ELS – electrophoretic light scattering; EDS/EDX – energy-dispersive x-ray spectroscopy; FBS – fetal bovine serum; FCS – fetal calf serum; FIB – focused ion beam; FISH – fluorescence in situ hybridization; FTIR – Fourier-transform infrared spectroscopy; GA – gum arabic; GF-AAS – graphite furnace atomic absorption spectroscopy; HAO – hydroxylamine oxidoreductase enzyme; HDD – hydrodynamic diameter; HEPES – (4-(2-hydroxyethyl)-1-piperazineethanesulfonic acid); ICP-MS or OES – inductively coupled plasma mass spectrometry or optical emission spectroscopy; IC_{50}; inhibitory concentration that inhibits 50% of the test population; ISB – Iso-Sensitest broth; LB – Luria-Bertani; MBC – minimum bactericidal concentration; ME – microbiocidal effect; MH – Mueller-Hinton; MHA - mercaptohexanoic acid; MIC – minimum inhibitory concentration; MLC – minimum lethal concentration; MLSS – mixed liquor suspended solids; MPA - mercaptopropionic acid; MPS – mercaptopropionic sulfonic acid; MTT – 3-(4,5-dimethylthiazol-2-yl)-2,5-diphenyltetrazolium bromidefor; MWCO – molecular weight cut-off; NMR – nuclear magnetic resonance; OD – optical density; PALS – phase analysis light scattering; PBS – phosphate buffered saline; PEG - poly(ethylene glycol); PEGSH - poly(ethylene glycol) methyl ether thiol; PVP – poly(vinylpyrrolidone); ROS – reactive oxygen species; (RT) or (q)PCR – real-time or quantitative polymerase chain reaction; SEM – scanning electron microscopy; SOUR – specific oxygen uptake rate; SWW – synthetic wastewater; TEM – transmission electron microscopy; TGA – thermagravimetric analysis; TSB – Tryptone Soya broth; UV-vis – ultraviolet-visible spectroscopy; XPS – x-ray photoelectron spectroscopy; XRD – x-ray diffraction

Appendix Table A.2. Analysis of bulk ion release reported and theoretically calculated, determination of a scaled ion control, and the resulting conclusion from each study in the final subset.

Refs	Method used to character-ize dissolved Ag (filter and centrifug-ation settings)	Time point(s) measured (hr)	Solvent	Theoretical calculated percent Ag(I) release (%) (size (nm))	Reported = theoretically calculated dissolution? [a]	AgNP conc (mg/L)	Ag(I) ion conc (mg/L)	Form of Ag(I) ion	Assumed Ag(I) ion	mol/mL Ag as salt	mol/mL Ag as NP	Ratio of mol/mL Ag as salt:NP	Percent needing released to match ion control (%)	Scaled Ag(I) ion control present	Conclusion drawn
[252]	UV-vis	0, 24	DI water, LB	14.14 (9.1)	yes, full	1	1	$AgNO_3$	total Ag salt	5.89E-09	9.27E-09	16:25	64	no	particle-only, combined ion-particle
						100	10			5.89E-08	9.27E-07	8:125	6	yes	
				6.74 (19.1)		1	1			5.89E-09	9.27E-09	16:25	64	no	
						100	10			5.89E-08	9.27E-07	8:125	6	yes	
				2.96 (43.5)		1	1			5.89E-09	9.27E-09	16:25	63.50	no	
						100	10			5.89E-08	9.27E-07	8:125	6.35	yes	
				7.19 (17.9)		1	1			5.89E-09	9.27E-09	16:25	63.50	no	
						10	10			5.89E-08	9.27E-08	16:25	63.50	no	
				5.52 (23.3)		0.1	1			5.89E-09	9.27E-10	63:10	635.02	no	
						3	10			5.89E-08	2.78E-08	21:10	211.67	no	
				14.14 (9.1)		1.8	0.7			4.12E-09	1.67E-08	1:4	24.70	yes	
				6.74 (19.1)		8					7.42E-08	55:1000	5.56	yes	
				2.96 (43.5)		18.5					1.72E-07	3:125	2.40	yes	
				7.19 (17.9)		3.8					3.52E-08	3:25	11.70	yes	
				5.52 (23.3)		1.4					1.30E-08	8:25	31.75	yes	
[253]	ICP-OES/MS (cellulose membrane MWCO 10 kDa using a Amicon stir cell (Millipore) pressurized with nitrogen)	0.5, 240	AgNP stock solution	3.64 (35.4)	yes, partial	0.75	0.05	$AgNO_3$	total Ag atom of the Ag salt	4.64E-10	6.95E-9	7:100	6.67	yes	ion-only, combined ion-particle
						6.2	0.3						4.84	yes	

Appendix Table A.2 (continued)

[254]	ICP-MS	24, 48, 72, 96, 120	--, pH = 4	33.65 (3)	yes, partial	9	0.005	$AgNO_3$	total Ag atom of the Ag salt	4.64E-11	8.34E-08	3:5,000	0.06	yes	ion-only
						210	0.3			2.78E-09	1.95E-06	1:500	0.14	yes	
				25.74 (5)		9	0.005			4.64E-11	8.34E-08	3:5,000	0.06	yes	
						210	0.3			2.78E-09	1.95E-06	1:500	0.14	yes	
				11.70 (11)		9	0.005			4.64E-11	8.34E-08	3:5,000	0.06	yes	
						210	0.3			2.78E-09	1.95E-06	1:500	0.14	yes	
				7.15 (18)		10	0.005			4.64E-11	9.27E-08	5:10,000	0.05	yes	
						70	0.3			2.78E-09	6.49E-07	3:500	0.43	yes	
				2.52 (51)		10	0.005			4.64E-11	9.27E-08	5:10,000	0.05	yes	
						70	0.3			2.78E-09	6.49E-07	3:500	0.43	yes	
				1.79 (72)		10	0.005			4.64E-11	9.27E-08	5:10,000	0.05	yes	
						70	0.3			2.78E-09	6.49E-07	3:500	0.43	yes	
[255]	ICP-MS (centrifuged at 50,000 g for 10 min at 4C (Beckman-Coulter))	0.5, 1, 2, 4, 6, 8, 12, 24	LB lacking NaCl	0.91 (142)	yes, partial	200	0.4	$AgNO_3$	total Ag atom of the Ag salt	3.71E-09	1.85E-06	1:500	0.2	yes	combined ion-particle
						100	rate of AgNP ion release			--	9.27E-07	--	--	yes	
						500	1			9.27E-09	4.64E-06	1:500	0.2	yes	
						500	6			5.56E-08	4.64E-06	3:250	1.2	yes	
						1000	16			1.48E-07	9.27E-06	2:125	1.6	yes	
[256]	--	--	--	0.91 (142)	--	40	0.4	$AgNO_3$	total Ag atom of the Ag salt	3.71E-9	3.71E-7	1:100	1	yes	combined ion-particle
[257]	ICP-OES (Dialysis Tubing Benzoylated of nominal MWCO 2 kDa)	24	ISB	18.39 (7)	no	180	15	$AgNO_3$	total Ag salt	8.83E-08	1.67E-06	5:100	5.29	yes	particle-only
						15	10			5.89E-08	1.39E-07	2:5	42.33	no	

Appendix Table A.2 (continued)

[258]	ICP-MS (dialysis cartridge float-a-lyzer G2 (Spectra/Por, Spectrum Laboratories, USA))	24, 48, 72	artificial sea-water and fresh-water	5.96 (20)	yes, full	0.005	0.02	$AgNO_3$	total Ag atom of the Ag salt	2E-10	5E-11	4:1	400	no	combined ion-particle
						2	0.5			5E-9	2E-08	1:4	25	yes	
				3.3 (40)		0.005	0.02			2E-10	5E-11	4:1	400	no	
						2	0.5			5E-9	2E-08	1:4	25	yes	
				1.32 (100)		0.005	0.02			2E-10	5E-11	4:1	400	no	
						2	0.5			5E-9	2E-08	1:4	25	yes	
				5.96 (20)		0.36	0.01			1E-10	3.30E-09	1:33	3.03	yes	
						1	0.2			2E-9	1E-08	1:5	20	yes	
				3.3 (40)		0.36	0.01			1E-10	3.30E-09	1:33	3.03	yes	
						1	0.2			2E-9	1E-08	1:5	20	yes	
				1.32 (100)		0.36	0.01			1E-10	3.30E-09	1:33	3.03	yes	
						1	0.2			2E-9	1E-08	1:5	20	no	
[259]	ICP-MS (Amicon Ultra-4 Centrifugal Filter Unit 7,000 rpm 35 min, <3 kDa pore size)	0, 24	AOB media	5.11 (25.2)	no	0.2	0.2	$AgNO_3$	total Ag atom of the Ag salt	1.85E-09	1.85E-09	1:1	100	no	ion-only
				4.77 (27)		2	2			1.85E-08	1.85E-08	1:1	100	no	
							0.2			1.85E-09	1.85E-08	1:10	10	yes	
				6.13 (21)		20	0.2			1.85E-09	1.85E-07	1:100	1	yes	
[260]	AAS, Orion 013010MD conductivity cell, ultrafiltration membrane 10 kDa polyethersulfone (MidiKros Hollow Fiber Module (P-X3-010E-300-02N))	over 3 weeks	purified AgNP stock solution, BOD5 test media	2.22 (58)	yes, partial	0.003	0.003	$AgNO_3$	total Ag atom of the Ag salt	2.78E-11	2.78E-11	1:1	100	no	particle-only
						0.3	0.070			6.49E-10	2.78E-09	23:100	23.33	yes	
				6.77 (19)		0.3	0.003			2.78E-11	2.78E-11	1:1	100	no	
						1	0.070			6.49E-10	9.27E-09	7:100	7	yes	
				10.73 (12)		0.003	0.003			2.78E-11	2.78E-11	1:1	100	no	
						0.3	0.070			6.49E-10	2.78E-09	23:100	23.33	yes	
				12.87 (10)		0.003	0.003			2.78E-11	2.78E-11	1:1	100	no	
						0.3	0.070			6.49E-10	2.78E-09	23:100	23.33	yes	

Appendix Table A.2 (continued)

[261]	--	--	--	6.34 (20.3)	--	5	0.25	$AgNO_3$	total Ag salt	1.47E-09	4.64E-08	3:100	3.18	yes	ion-only
						50	2			1.18E-08	4.64E-07	1:40	2.54	yes	
				2.42 (53.1)		10	0.25			1.47E-09	9.27E-08	2:125	1.59	yes	
						100	2			1.18E-08	9.27E-07	3:250	1.27	yes	
				1.14 (112.6)		50	0.25			1.47E-09	4.64E-07	3:1000	0.32	yes	
						220	2			1.18E-08	2.04E-06	6:1000	0.58	yes	
[262]	ICP-MS, 40 min at 4000 g using centrifugal filter devices (Amicon ultra-4, Millipore, Ireland) with 3 kDa MWCO	0.5, 6, 24, 48, 72	2% NaCl, NBBM, Volvic water	6.44 (20)	yes, partial	0.1	0.05	$AgNO_3$	total Ag salt	2.94E-10	9.27E-10	8:25	31.75	yes	combined ion-particle
				0.64 (200)		300	7			4.12E-08	2.78E-06	15:1000	1.48	yes	
				5.60 (23)		0.05	0.05			2.94E-10	4.64E-10	63:100	63.50	no	
				4.77 (27)		100	7			4.12E-08	9.27E-07	2:45	4.45	yes	
[263][b]	biolumines cence	0.5, 2	0.9% NaCl	1.29 (100)	no	0.01	0.01	$AgNO_3$	total Ag salt	5.89E-11	9.27E-11	63:100	63.50	no	combined ion-particle
						1000	10			5.89E-08	9.27E-06	63:10,000	0.64	yes	
						0.001	0.0002			1.18E-12	9.27E-12	13:100	12.70	yes	
						3	0.2			1.18E-09	2.78E-08	21:500	4.23	yes	
[264]	Single particle (SP)-ICP-MS and GF-AAS (ultracentrifugation at 390,000 g for 30 min (Beckman-Coulter ultracentrifuge L8-55 M))	4, 24, 48, 72	Ultra-pure water, artificial fresh-water, algal media, cell culture media	11.1 (11.6)	yes, partial	0.01	0.0001	$AgNO_3$	total Ag salt	5.89E-13	9.27E-11	4:625	0.64	yes	combined ion-particle
						10	0.04			2.35E-10	9.27E-08	25:10,000	0.25	yes	
				7.23 (17.8)		0.01	0.0001			5.89E-13	9.27E-11	4:625	0.64	yes	
						10	0.04			2.35E-10	9.27E-08	25:10,000	0.25	yes	
				2.7 (47.7)		0.01	0.0001			5.89E-13	9.27E-11	4:625	0.64	yes	
						10	0.04			2.35E-10	9.27E-08	25:10,000	0.25	yes	
				2.28 (56.5)		0.01	0.0001			5.89E-13	9.27E-11	4:625	0.64	yes	
						10	0.04			2.35E-10	9.27E-08	25:10,000	0.25	yes	
				1.36 (94.8)		0.01	0.0001			5.89E-13	9.27E-11	4:625	0.64	yes	
						10	0.04			2.35E-10	9.27E-08	25:10,000	0.25	yes	
[265]	--	--	--	15.51 (8.3)	--	0.125	0.0625	$AgNO_3$	total Ag atom of the Ag salt	5.79E-10	1.16E-09	1:2	50	no	combined ion-particle
						64	2			1.85E-08	5.93E-07	3:100	3.13	yes	

Appendix Table A.2 (continued)

[266]	conductivity	--	--	21.45 (6)	--	37.5	3.75	$AgNO_3$	total Ag salt	2.21E-08	3.48E-07	3:50	6.35	yes	ion-only
						375	37.5			2.21E-07	3.48E-06	3:50	6.35	yes	
						3750	375			2.21E-06	3.48E-05	3:50	6.35	Yes	
[267]	ICP-MS, filtered through a 0.025-µm polyethersulfone membrane (Millipore, Billerica, MA, USA) and digested for 24 hrs	48-168	DI water, LB, PNS+RE	2.87 (44.9)	yes, full	0.1	0.1	$AgNO_3$	total Ag salt	5.89E-10	9.27E-10	3:5	63.50	no	combined ion-particle
						1					9.27-09	3:50	6.35	yes	
						5					4.64E-08	1:80	1.27	yes	
						0.1	1			5.89E-09	9.27E-10	635:100	635.02	no	
						1					9.27E-09	635:1000	63.50	no	
						5					4.64E-08	127:1000	12.70	yes	
[268]	AAS, ultracentrifuge machine (Optima™ MAX-XP Ultracentrifuge, Beckman Coulter, Inc., USA) and centrifuged at 165000×g, 4 °C, for 2 h using MLN-80 rotor (16 × 58 mm, Beckman Coulter, Inc., USA)	0, 30, 60	inorganic SWW, SWW with nitrifying sludge	18.39 (7)	no	1	0.05	$AgNO_3$	total Ag atom of the Ag salt	4.64E-10	9.27E-09	1:20	5	yes	ion-only
						10	0.10			9.27E-10	9.27E-08	1:100	1	yes	
						100	0.50			4.64E-09	9.27E-07	1:200	0.5	yes	
						100	5			4.64E-08	9.27E-07	1:20	5	yes	
[269]	--	--	--	1.84 (70)	--	12.5	1	Ag-$C_2H_3O_2$	total Ag atom of the Ag salt	9.27E-09	1.16E-07	1:11	8	yes	ion-only
						50	10			9.27E-08	4.64E-07	1:5	20	yes	
[270]	--	--	--	12.87 (10)	no	200	0.05	$AgNO_3$	total Ag salt	2.94E-10	1.85E-06	1:6300	0.02	Yes	ion-only
						900	0.3			1.77E-09	8.34E-06	1:4700	0.02	Yes	

Appendix Table A.2 (continued)

[119]	UV-vis/ICP-MS	--	LB lacking NaCl with ampicillin	12.87 (10)	yes, full	0.2	--	--	total Ag atom of the Ag salt	--	--	--	--	--	combined ion-particle
				3.22 (40)		0.4	0.04			3.71E-10	3.71E-09	1:10	10	yes	
				1.29 (100)		0.6	--			--	--	--	--	--	
[271]	ICP-MS, ultrafiltration with 3kDa MWCO membrane Millipore	6, 24	$NaHCO_3$	12.87 (10)	no	1	0.005	$AgNO_3$	total Ag atom of the Ag salt	4.64E-11	9.27E-09	1:200	0.5	yes	combined ion-particle
						5	0.02			1.85E-10	4.64E-08	1:250	0.4	yes	
						5	0.05			4.64E-10	4.64E-08	1:100	1	yes	
						15	0.2			1.85E-09	1.39E-07	2:150	1.33	yes	
						15	0.5			4.64E-09	1.39E-07	1:30	3.33	yes	
						15	1			9.27E-09	1.39E-07	1:15	6.67	yes	
[272]	ICP-AES; filtered by centrifugation using microfilter centrifuge tubes (washed with copper nitrate) at 3,750 g for 20 minutes	24, 48, 72, 96, 120	buffered nutrient solution	2.57 (50)	yes, partial	1	1	Ag_2SO_4	total Ag atom of the Ag salt	9.27E-09	9.27E-09	1:1	100	no	combined ion-particle
						300	10			9.27E-08	2.78E-06	1:30	3.33	yes	
						50	5			4.64E-08	4.64E-07	1:10	10	yes	
						100	10			9.27E-08	9.27E-07	1:10	10	yes	
				8.58 (15)		1	1			9.27E-09	9.27E-09	1:1	100	no	
						10	10			9.27E-08	9.27E-08	1:1	100	no	
						50	5			4.64E-08	4.64E-07	1:10	10	yes	
						100	10			9.27E-08	9.27E-07	1:10	10	yes	
[273]	Ag+ selective electrodes with ionophore-doped fluorous sensing membrane, ICP-MS, in presence and absence of bacteria	over 24	DI water	11.70 (11)	yes, full	3	0.3	--	total Ag atom of the Ag salt	3.00E-09	2.78E-08	1:9	10.79	yes	ion-only
						0.3	0.1			1.00E-09	2.78E-09	4:11	35.96	yes	
						15	1			1.00E-08	1.39E-07	7:100	7.19	yes	

Appendix Table A.2 (continued)

[274]	--	--	--	2.57 (50)	--	0.2	0.001	$AgNO_3$	total Ag salt	5.89E-12	1.85E-09	1:300	0.32	yes	particle-only
						0.2	0.01			5.89E-11	1.85E-09	1:30	3.18	yes	
						0.2	0.1			5.89E-10	1.85E-09	1:3	31.75	yes	
						0.1	0.1			5.89E-10	9.27E-10	5:8	63.50	no	
						1	1			5.89E-9	9.27E-9	5:8	63.50	no	
						100	100			5.89E-07	9.27E-07	5:8	63.50	no	
				1.29 (100)		0.2	0.001			5.89E-12	1.85E-09	1:300	0.32	yes	
						0.2	0.01			5.89E-11	1.85E-09	1:30	3.18	yes	
						0.2	0.1			5.89E-10	1.85E-09	1:3	31.75	yes	
						0.1	0.1			5.89E-10	9.27E-10	5:8	63.50	no	
						1	1			5.89E-9	9.27E-9	5:8	63.50	no	
						100	100			5.89E-07	9.27E-07	5:8	63.50	no	
[275]	ICP-ES, centrifugal ultra-filtration device with 5 kDa MWCO (Amicon Ultra-15, Millipore Co., Billericka, MA), 30 min at 5000g	3	HEPES buffer, minimal media	6.44 (20)	yes, partial	0.30	0.05	$AgNO_3$	total Ag atom of the Ag salt	4.64E-10	2.78E-09	1:6	16.67	yes	ion-only
						0.75	0.05			4.64E-10	6.95E-09	2:30	6.67	yes	
						0.75	1.25			1.16E-08	6.95E-09	83:50	166.67	no	
						10	1			9.27E-09	9.27E-08	1:10	10	yes	
				1.61 (80)		2.75	0.2			1.85E-09	2.55E-08	1:14	7.27	yes	
[276]	GF-AAS, centrifuged for 30 min at ~3150 g (4000 rpm, Thermo Electron, IEC Centra CL3 Series Centrifuge)	48	--	12.87 (10)	yes, full	0.01	0.04	$AgNO_3$	total Ag atom of the Ag salt	3.71E-10	9.27E-11	4:1	400	no	particle-only
						8.7	3.62			3.36E-08	8.07E-08	2:5	41.61	no	
				2.3 (56)		0.02	0.04			3.71E-10	1.85E-10	2:1	200	no	
						13.2	3.62			3.36E-08	1.22E-07	7:27	27.42	yes	
				1.79 (72)		0.05	0.04			3.71E-10	4.64E-10	4:5	80	no	
						41.2	3.62			3.36E-08	3.82E-07	9:100	8.79	yes	
[277]	AAS or Ag-sensor bacteria, ultracentrifuged at 390 000 g for 45 minutes	4	--	1.55 (83, sphere)	yes, partial	0.01	0.0003	$AgNO_3$	total Ag atom of the Ag salt	2.78E-12	9.27E-11	3:100	3	yes	ion-only
						30	0.5			4.64E-09	2.78E-07	2:125	1.67	yes	
				0.82 (100 X 6100, wire)		0.01	0.0003			2.78E-12	9.27E-11	3:100	3	yes	
						30	0.5			4.64E-09	2.78E-07	2:125	1.67	yes	

Appendix Table A.2 (continued)

[278]	ICP-MS, ultracentrifugation at 35,000 rpm for 4 hr	--	--	25.74 (5)	--	0.05	1	$AgNO_3$	total Ag atom of the Ag salt	9.27E-09	4.64E-10	20:1	2000	no	combined ion-particle
				3.68 (35)		40	1			9.27E-09	3.71E-07	1:40	2.5	yes	
[279]	--	--	--	2.48 (52)	--	3.4	0.005	$AgNO_3$	total Ag salt	2.94E-11	3.15E-08	9:10,000	0.09	Yes	ion-only
						34	0.1			5.89E-10	3.15E-07	19:10,000	0.19	Yes	
						8.5	0.02			1.18E-10	7.88E-08	15:10,000	0.15	Yes	
						44	11			6.48E-08	4.08E-07	8:50	15.88	Yes	
						22	0.22			1.30E-09	2.04E-07	63:10,000	0.64	Yes	
[280]	ICP-MS, centrifuged at 20000 rcf for 20 min	0, 2, 4, 6, 8, 10, 12, 14, 16, 18, 20, 24	LB, MH	5.36 (24)	yes, full	6.7	rate of AgNP ion release	$AgNO_3$	total Ag atom of the Ag salt	--	6.21E-08	--	--	yes	combined ion-particle

[a] Full = entire range of theoretical values is within the reported measured concentration range of Ag(I) ions, partial = only a portion of the range of theoretical values is within the reported measured concentration range of Ag(I) ions, no = there is no overlap in the range of theoretical values and the reported measured concentration range of Ag(I) ions (see Figure S2).

[b] Intracellular dissolution was used in place of bulk dissolution since it was the only value reported.

Abbreviations: AOB – ammonia oxidizing bacteria; BOD – biological oxygen demand; DI – deionized water; GF-AAS – graphite furnace atomic absorption spectroscopy; HEPES – (4-(2-hydroxyethyl)-1-piperazineethanesulfonic acid); ICP-MS or OES or AES – inductively coupled plasma mass spectrometry or optical or atomic emission spectroscopy; LB – Luria-Bertani; MH – Mueller-Hinton; MWCO – molecular weight cut-off; NBBM – Bold's Basal Medium enriched with nitrate; PEGSH - poly(ethylene glycol) methyl ether thiol; PNE+RE – Plant nutrient solution containing *Z. mays* root excretion; SWW – synthetic wastewater; UV-vis – ultraviolet-visible spectroscopy

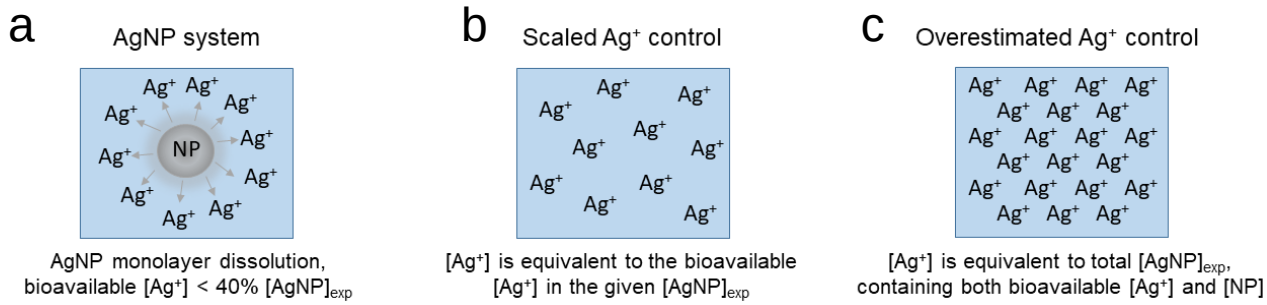

Appendix Figure A.1. Schematic demonstrating the difference between an appropriate and inappropriate ion control. a) The AgNP system contains the zero-valent NP and dissolved Ag(I) ions. b) An appropriate ion control contains dissolved silver at an equivalent concentration to the Ag(I) ions released from the AgNP. c) A concentration of dissolved silver equivalent to the total silver present in the AgNP would not serve as an appropriate ion control.

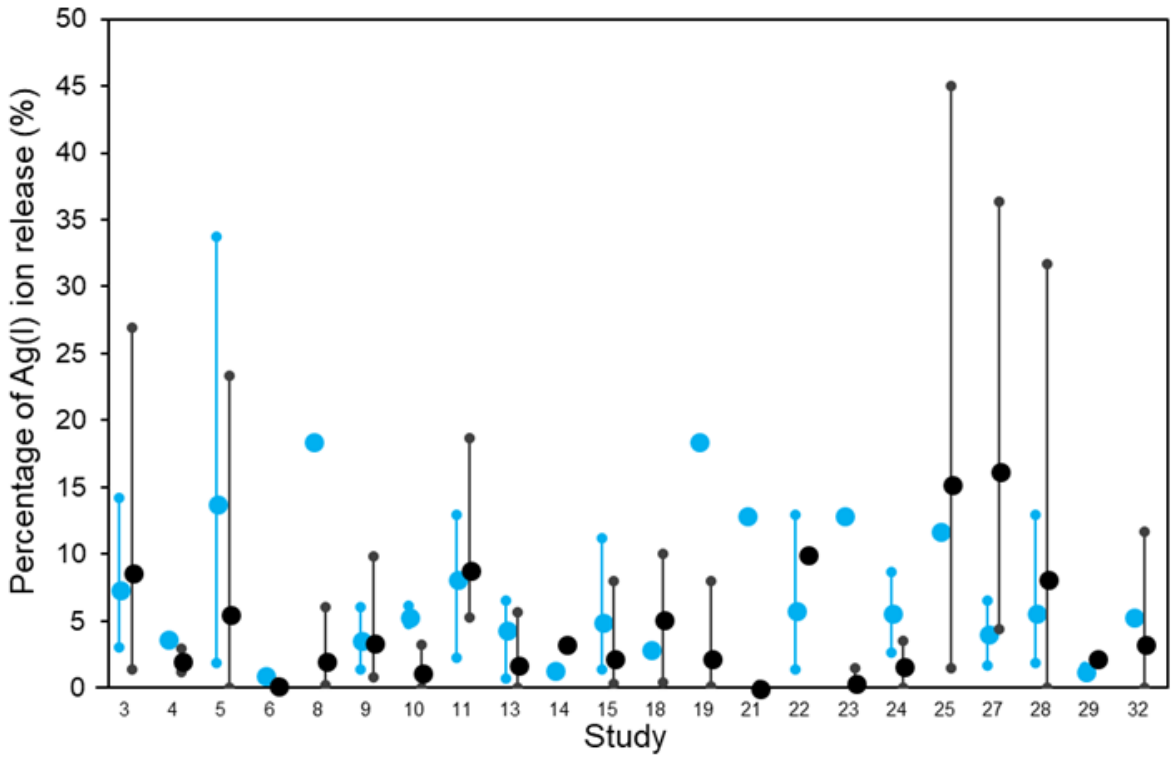

Appendix Figure A.2. Comparison of the reported dissolution values in studies that measured dissolution to our theoretical calculations of dissolution. The middle data points represent the average dissolution value with the upper and lower data points representing the maximum and minimum dissolution values, respectively. Dissolution reported by the majority of studies (73%) align fully or partially with our theoretically calculated dissolution. Thus, the agreement between theoretical dissolution values and average reported dissolution values for the majority of studies further validates our calculation approach to determining an appropriate ion control. Note: The range for the reported dissolution includes different particle sizes, concentrations of AgNPs, different techniques to measure dissolution, and different media. The range for the theoretical calculations include different particle sizes and shapes.

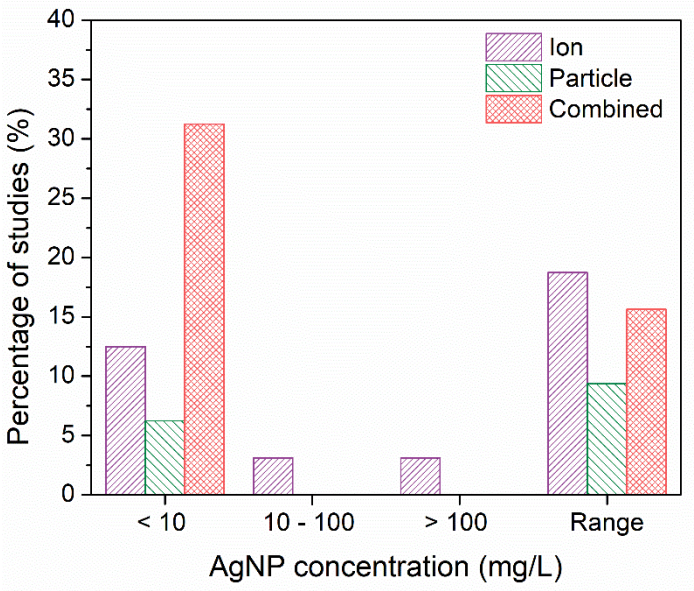

Appendix Figure A.3. Ion-only, particle-only, and combined ion-particle conclusions drawn from studies that expose bacteria to different concentrations: <10 mg/L,[119, 253, 255-258, 260, 264, 265, 267, 271, 273, 275, 279, 280] 10-100 mg/L,[269] >100 mg/L,[270] and a range[252, 254, 259, 261-263, 266, 268, 272, 274, 276-278] of AgNP concentrations. No meaningful conclusion can be discerned.

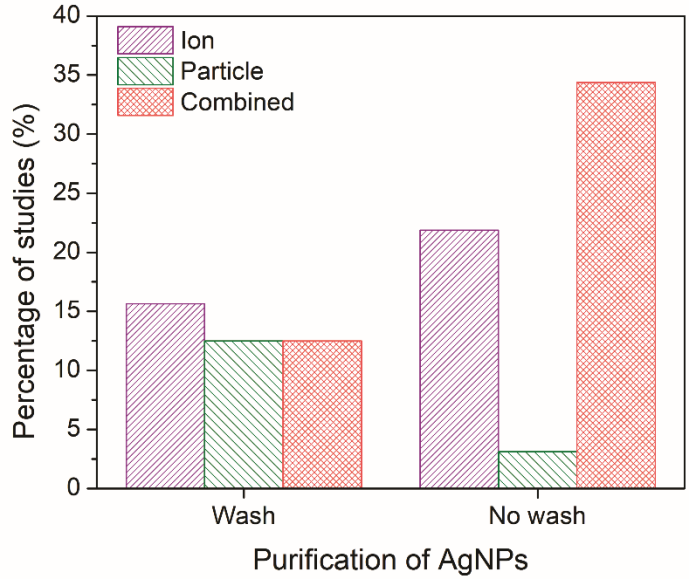

Appendix Figure A.4. Ion-only, particle-only, and combined ion-particle conclusions drawn from studies based on AgNP purification Studies did[252, 253, 257, 259-261, 269, 271, 273, 276, 280] or did not[119, 254-256, 258, 262-268, 270, 272, 274, 275, 277-279] purify AgNPs post-synthesis. No meaningful conclusion can be discerned.

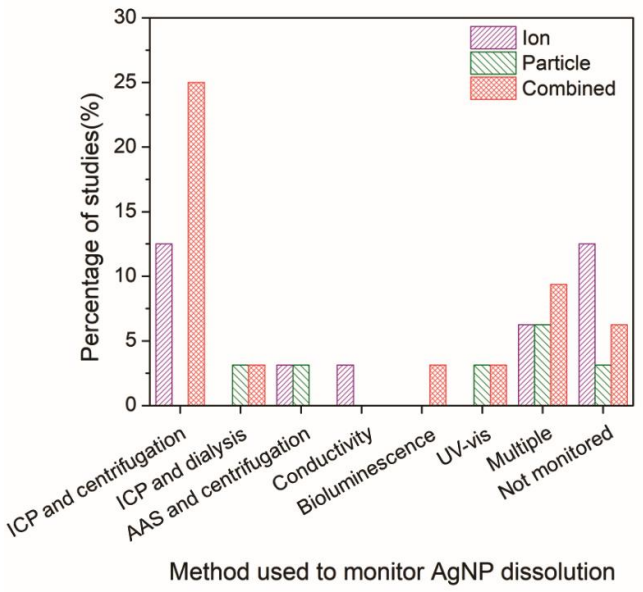

Appendix Figure A.5. Ion-only, particle-only, and combined ion-particle conclusions drawn from studies that monitor dissolutionusing ICP and centrifugation,[253-255, 259, 262, 267, 271, 272, 275, 278, 280] ICP and dialysis[257, 258] AAS and centrifugation,[268, 276] conductivity,[266] bioluminescence,[263] multiple methods,[119, 252, 260, 264, 273, 277] and no methods[256, 261, 265, 269, 270, 274, 279]. No meaningful conclusion can be discerned.

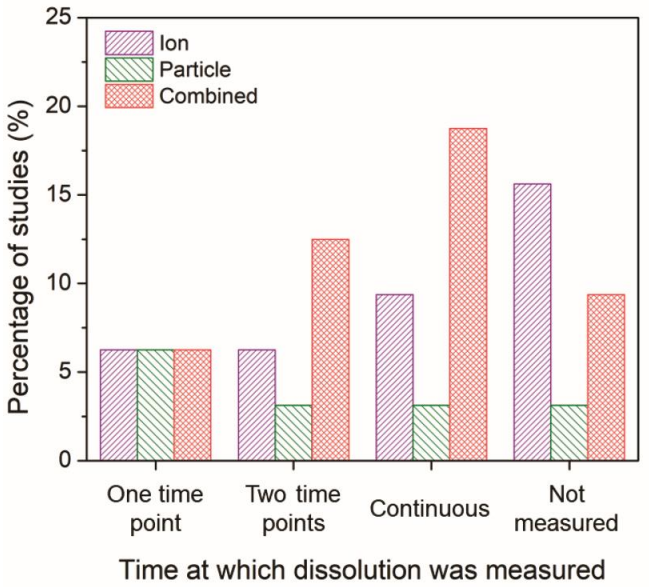

Appendix Figure A.6. Ion versus particle conclusions drawn from studies that measure ion release: at one time point,[119, 257, 262, 275-277] two time points,[252, 253, 259, 263, 271] continuously,[254, 255, 258, 260, 264, 267, 268, 272, 273, 280] or not at all[256, 261, 265, 266, 269, 270, 274, 278, 279]. Measuring dissolution is important for observing particle-only and combined ion-particle effects, especially at multiple time points.

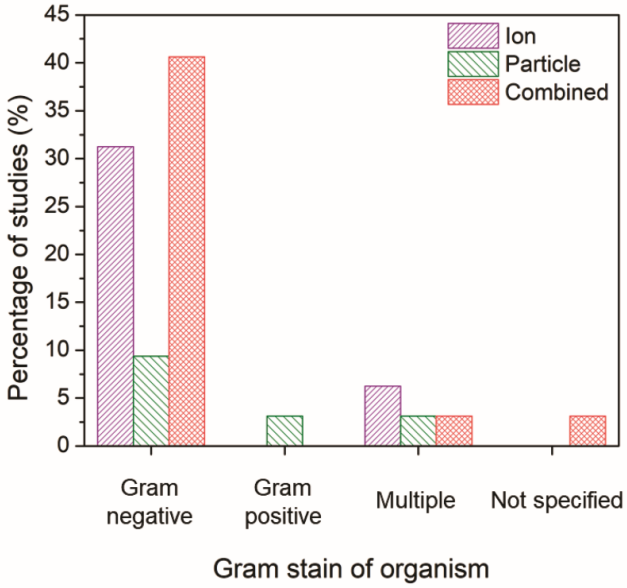

Appendix Figure A.7. Ion-only, particle-only, and combined ion-particle conclusions drawn from studies that expose AgNPs and Ag(I) ions to various bacteria: only gram-negative,[119, 252-256, 258, 259, 261-265, 268, 270-277, 279, 280] gram-positive,[260] both types,[257, 266, 267, 269] or unspecified[278] bacteria. No meaningful conclusion can be discerned.

Appendix B Chapter 3 – Supplemental Information

Appendix Table B.1. Information about bacteria strains used in the study.

Strain of *E. coli* K-12	Motility phenotype*	Genotype	*flhDC* expression	Referred to in text as:
MG1655 (CGSC #7740)	Hyper-motile	IS*1* elements in the *flhDC* promoter[1,2] and *dgcJ*	++ hyper[191, 192]	Hyper-motile *E. coli* (+IS*1*)
JW1881 (CGSC #11772)	Non-motile	Deletion in the regulatory region of *flhD*[1,2]	- - none[191, 192]	Non-motile *E. coli* (*Δ*flhD::kan)

*Note: other pleiotropic effects arising from the insertion element and the kanamycin marker in the two strains are unknown.

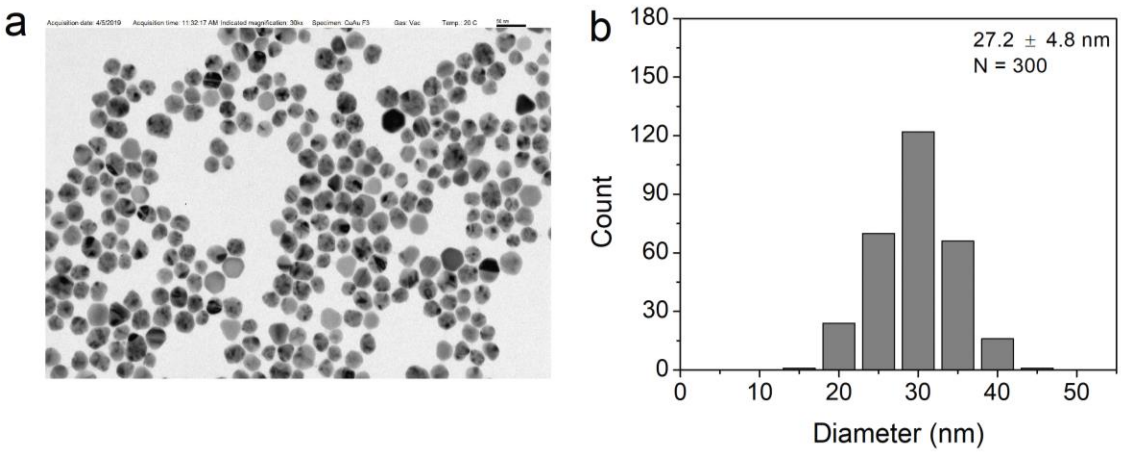

Appendix Figure B.1. Particle size of pseudospherical PEGSH-AgNPs. a) TEM image and b) nanoparticle size distribution.

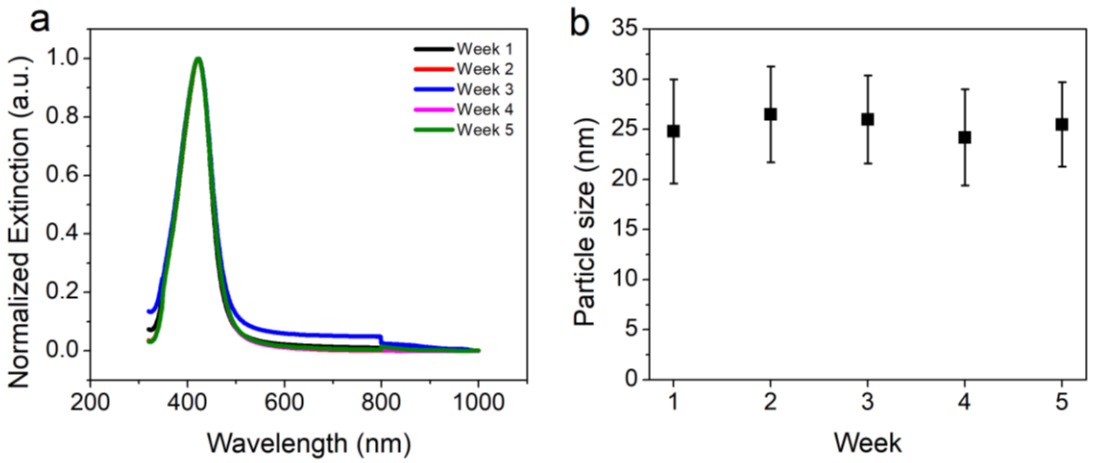

Appendix Figure B.2. Long-term stability of PEGSH-AgNPs. By both a) UV-vis-NIR and b) TEM analysis, pseudospherical PEGSH-AgNPs remain stable for the duration of the bacterial resistance experiments. a) UV-vis-NIR absorption spectra show characteristic localized surface plasmon resonance (LSPR) peaks (average λmax = 422.00 ± 0.50 nm, average FWHM = 77.97 ± 2.15 nm, average OD = 0.85 ± 0.03), indicating the presence of stable AgNPs over 5 weeks and b) average particle size as determined by TEM, as a function of weeks in storage at 4°C.

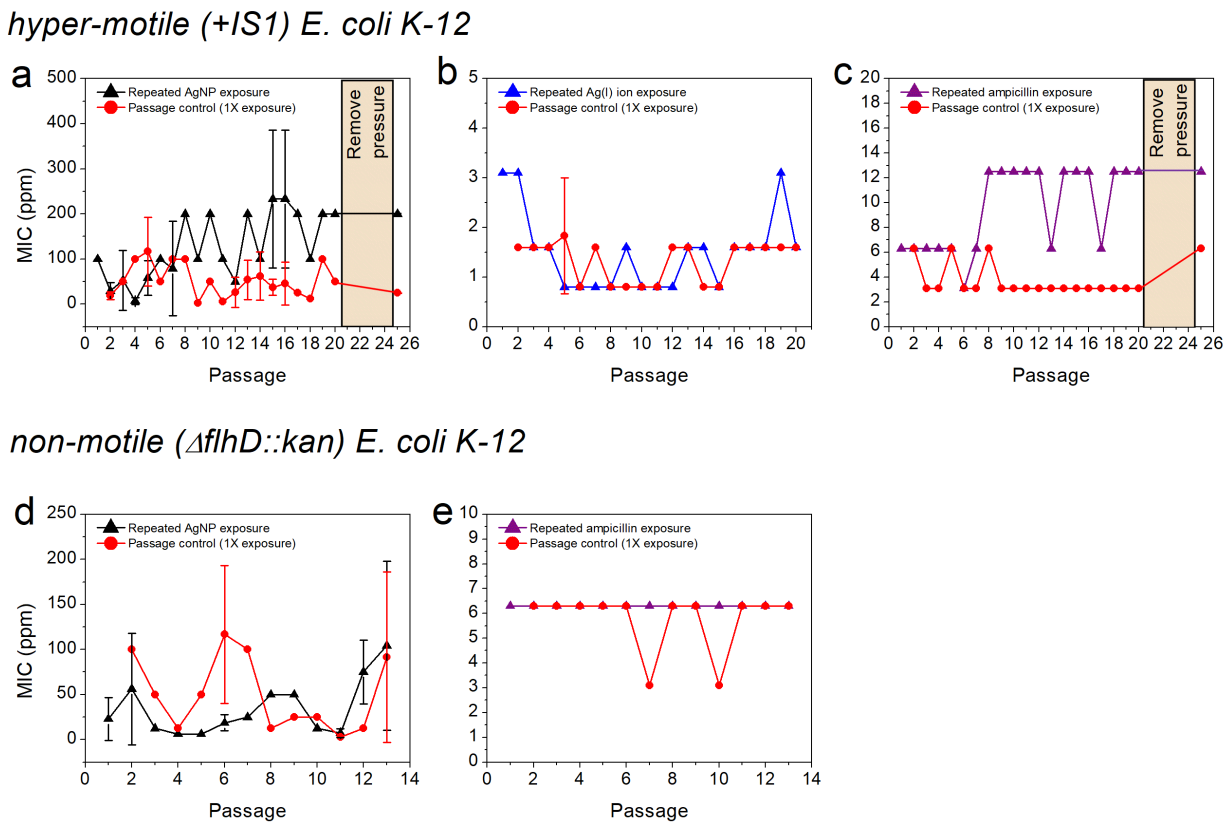

Appendix Figure B.3. Resistance profiles of raw MIC data. Resistance profile (plotted as raw MIC vs passage number) of hyper-motile (+IS*1*) *E. coli* K-12 strain in response to a) AgNPs (black triangles), b) Ag(I) ions (blue triangles), and c) ampicillin (positive control) (purple triangles), and non-motile (Δ*flhD::kan*) *E. coli* K-12 strain in response to d) AgNPs (black triangles) and e) ampicillin (positive control) (purple triangles). The non-selected passage control for each condition is included as red circles and the tan box represents the absence of the antimicrobial pressure. Average ± SD of 2-3 replicates. The hyper-motile *E. coli* (+IS*1*) strain developed resistance to AgNPs at a comparable rate to the onset of resistance to ampicillin, but not in the case of Ag(I) ions. The non-motile E. coli (Δ*flhD::kan*) strain did not develop resistance to AgNPs nor to ampicillin. (Note: experiment halted after passage 13 due to COVID-19 lab closure. Resistance evolved in other experiments ~passage 8.)

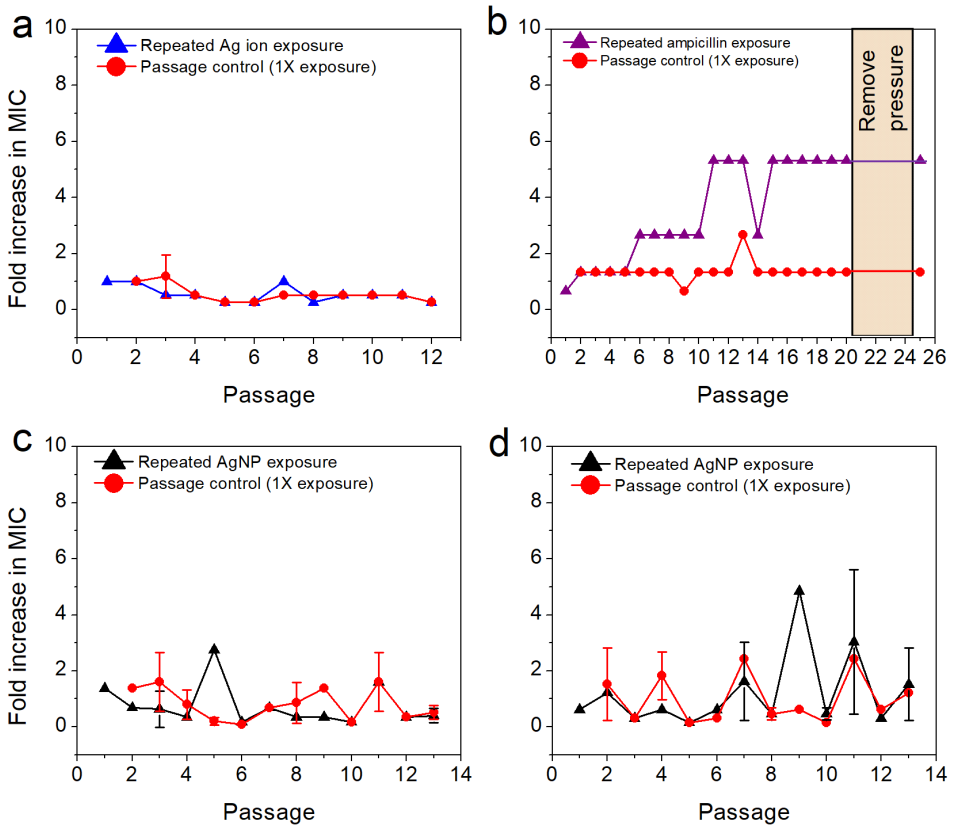

Appendix Figure B.4. Replicate lineage data. An additional replicate lineage was carried out for nearly each treatment presented in the main text, including a) Ag(I) ions, b) ampicillin, and c) AgNPs in the hyper-motile strain and d) AgNPs in the non-motile strain. The passage control for each condition is included as red circles and the tan box represents the absence of the antimicrobial pressure. Average ± SD of 2-3 replicates. We observed consistent resistance (or lack thereof) responses with those presented in the main text for all conditions except the hyper-motile strain exposed to AgNPs, where we saw a mixed (50:50) response in the hyper-motile strain (i.e., one lineage developed resistance, one did not). With this additional data, we can still conclude that resistance develops if a specific mutation event in cusS happens. Future work can look at predicting how frequent this mutation or other mutations occur to impart resistance by studying multiple replicate populations. Additionally, confirming the influence of motility on AgNP resistance using multiple independent lineages could be an area of future exploration. Note: Ampicillin resistance in this second replicate lineage was selected for by a modified method that eliminated the step of sub-culturing on agar and instead, involved transferring the surviving bacteria from sub-MIC cultures to fresh medium for the next passage.

Appendix Table B.2. Explained percentage (%) variation of MIC by treatment group, passage number, and the interaction between the two variables under varying experimental conditions (two-way ANOVA analysis, p-value in parentheses).

	AgNPs, hyper-motile	Ampicillin, hyper-motile	Ag(I) ions, hyper-motile	AgNPs, non-motile	Ampicillin, non-motile
Treatment group	22.60 (<0.001)	62.60 (<0.001)	0.04 (0.086)	4.04 (0.126)	9.13 (0.010)
Passage number	8.40 (<0.001)	4.11 (<0.001)	2.97 (0.830)	1.12 (0.417)	1.83 (0.238)
Interaction	13.95 (<0.001)	8.66 (<0.001)	0.12 (0.728)	6.13 (0.061)	2.62 (0.159)
Unexplained	55.05	24.63	96.87	88.71	86.42

Appendix B.1 Discussion 1 – Microbial Growth Kinetics Corroborate AgNP Resistance

Bacteria growth curves were fit to the Gompertz model as described by Li et al., including the following relationship from Zwietering et al.[281, 282]:

$$ln\frac{N}{N_0} = A\exp\left\{-\exp\left[\frac{\mu e}{A}(\lambda - t) + 1\right]\right\} \qquad \textbf{Eq. B-3}$$

where N is the cell number at time t, and N_0 is that at the beginning (i.e. t = 0). μ is the maximum specific growth rate (i.e. the inflection point of the growth curve, indicative of the slope of the growth curve during exponential phase). A is the maximum cell number (or maximum OD_{600} value) of a cell suspension during the experiment and λ is the duration of the lag phase (i.e., the time required to initiate bacteria growth). Bacterial growth parameters, i.e., μ and λ,[282-284] were calculated after each passage to determine how these indicators of antimicrobial activity change as bacteria transform from sensitive to resistant phenotypes. All model parameter estimates were obtained using MATLAB (Ver. R2019b, Mathworks, Inc., Natick, MA).

The Gompertz model was used as a standard sigmoid model to fit bacterial growth[282, 283, 285] and analyze microbial growth kinetics, including quantifying the lag phase and maximum specific growth rate as indicators of the impact that the antimicrobials in this study had on bacterial fitness and susceptibility.[281, 283, 284, 286] Lag phase is a key stage in bacterial development strategies to resist killing by antimicrobials (e.g., mutations for molecular defenses such as efflux pumps or oxidative stress protection). Bacterial populations can adjust parameters that determine the cell cycle, such as the duration of the lag phase, as an adaptive mechanism;[83] therefore, an in-depth understanding of how antimicrobial agents affect the lag phase is essential for reliable evaluation of bacterial resistance.[284] For this reason, we included analyses of growth kinetics, as MICs indicate the inhibition of bacterial growth but provide limited information about resistant mechanisms.[284] Typically, antimicrobial treatment promotes the development of tolerance in microbial populations as a protective response and may facilitate subsequent evolution and dissemination of resistance. Since lag phase scales with toxicity and an extended lag phase is the protective bacterial response via reduced cell growth from the onset of antimicrobial stress,[281, 283, 284, 286] a long lag phase in *E. coli* exposed to high AgNP concentrations and a short lag phase at low AgNP concentrations were expected and observed in our study (**Appendix Figure B-5**). Growth rate also scales with dose-dependent toxicity[112, 281, 283, 284] and thus growth rates of higher magnitude at lower AgNP concentrations were expected and also observed (**Appendix Figure B-6**).

Conversely, both a decrease in the duration of the lag phase and an increase in the maximum specific growth rate with increased passage indicate decreased adverse impact of an antimicrobial agent as a result of repeated exposure. This scenario was observed in several tested AgNP concentrations in the hyper-motile *E. coli* (+IS1), most notably at intermediate-to-high

AgNP concentrations (i.e., 12.5-100 µg/mL AgNPs) (**Appendix Figures B-5 and B-6, Appendix Table B-3**). In particular, at AgNP concentrations of 50 µg/mL, a notable change from a long (24 h) to short (4 h) lag phase began around passage 8, indicating a decrease in toxicity and the ability of the hyper-motile *E. coli* (+IS*1*) to acclimate to the exposure environment. The maximum specific growth rate also began to increase at passage 8 because bacteria began to grow at higher AgNP concentrations following repeated exposure and similarly indicates a decrease in toxicity. Detailed comparisons and statistical analyses for both metrics are summarized in **Appendix Table B-3** and **Appendix Tables B4-B5**. For the AgNPs treatment, the duration of the lag phase was significantly decreased on average by 15.1 times (p <0.001) when comparing the last five passages to the first five passages. Likewise, the duration of the lag phase was also significantly different from the passage control (9.2 times lower, p <0.001) and when comparing the final five passages between the treatment groups (15.5 times lower, p = 0.002). The growth rate was significantly increased on average by 0.034 times (p = 0.003) when comparing the last five passages to the first five passages. Similarly, growth rate was also significantly different from the passage control (0.023 times higher, p = <0.001) and when comparing the final five passages between the treatment groups (0.036 times higher, p = 0.002).

From passage 8 onwards, the hyper-motile *E. coli* (+IS*1*) no longer displayed evidence of fitness stress when exposed to AgNPs as they did prior to passage 8. This shift in both metrics at passage 8 aligns with the increase in MIC, indicating evolution of resistance. These findings are corroborated by Gullberg et al. who reports that resistant strains will outcompete susceptible strains by having a higher growth rate at higher antimicrobial concentrations.[112, 283, 287] This is contrary to the findings of Li et al., who were unable to detect significant differences in doubling times of bacteria populations exposed to silver salts[89] and the widely accepted postulate that

resistance mechanisms are usually accompanied by a biological fitness cost such as reduced bacterial growth rate.[83, 288] Microbial strains with a high level of resistance and/or mutations imparting resistance often have reduced growth rates compared to their susceptible counterparts because resistant mutations usually occur in genes of target molecules that carry out essential functions in the cell (e.g., transcription, protein synthesis).[83, 203, 211] In this case, with an increased or equivalent growth rate (depending on AgNP concentration) of the resistant strain compared to the non-selected passage control, it can be implied that the biological fitness cost for the *cusS* mutation conferring AgNP resistance is low, or else additional, fitness-restoring compensatory modifications were carried out by the cell to overcome these potential burdens.[83, 203, 211, 286]

After the AgNP pressure was removed and re-introduced, the duration of the lag phase remained consistent with the time observed after passage 8 (4 h), as did the maximum specific growth rate, suggesting no newly induced antimicrobial stress to which the hyper-motile *E. coli* (+IS*1*) have to acclimate. Such observations likely suggest that resistance has arisen from the permanently conferred *cusS* mutation, preventing mutational reversion to sensitivity. This finding is further substantiated by the stable elevated change in MIC observed without the selective AgNP pressure. Trends in these parameters following repeated Ag(I) ion and ampicillin exposure are shown in the SI (**Appendix Figures B-5 and B-6, Appendix Tables B-4 – B-5**), with no change in these parameters following Ag(I) ion exposure and a change similar in response to ampicillin as the AgNPs. This further supports the differential resistance response between AgNPs and Ag(I) ions. Our results are the first known application of these metrics, documenting their change to evaluate AgNP resistance as a result of repeated exposure.

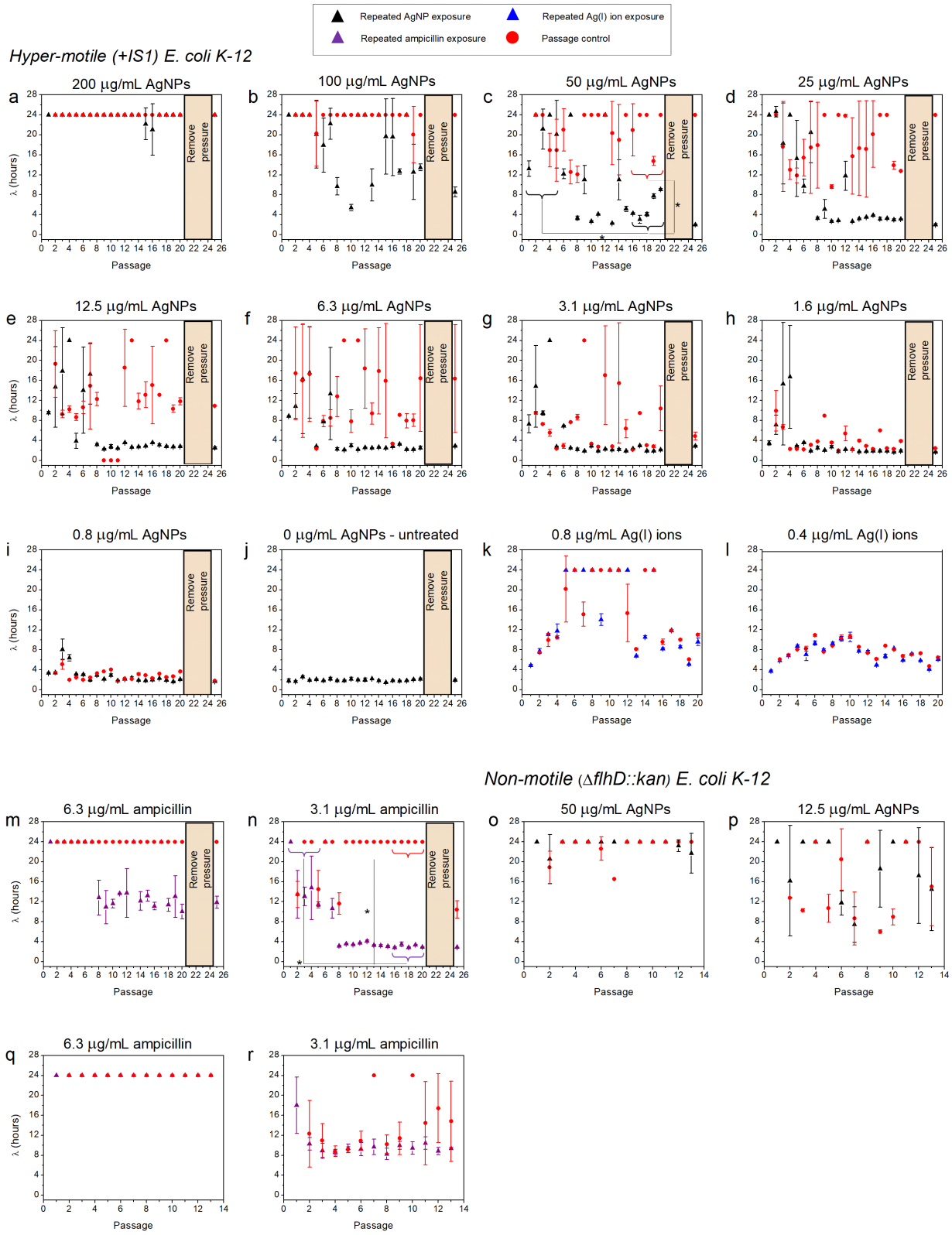
Repeated AgNP exposure
Repeated Ag(I) ion exposure
Repeated ampicillin exposure
Passage control
Hyper-motile (+IS1) E. coli K-12
a 200 µg/mL AgNPs
b 100 µg/mL AgNPs
c 50 µg/mL AgNPs
d 25 µg/mL AgNPs
e 12.5 µg/mL AgNPs
f 6.3 µg/mL AgNPs
g 3.1 µg/mL AgNPs
h 1.6 µg/mL AgNPs
i 0.8 µg/mL AgNPs
j 0 µg/mL AgNPs - untreated
k 0.8 µg/mL Ag(I) ions
l 0.4 µg/mL Ag(I) ions
Remove pressure
λ (hours)
Passage
Non-motile (ΔflhD::kan) E. coli K-12
m 6.3 µg/mL ampicillin
n 3.1 µg/mL ampicillin
o 50 µg/mL AgNPs
p 12.5 µg/mL AgNPs
q 6.3 µg/mL ampicillin
r 3.1 µg/mL ampicillin

Appendix Figure B.5. Lag phase analysis of all conditions. Duration of lag phase (λ) across passage and between experimental (black = AgNPs, blue = Ag(I) ions, purple = ampicillin) and non-selected passage control (red) samples for a-j) AgNPs in hyper-motile (+IS*1*) *E. coli*; k-l) Ag(I) ions in hyper-motile (+IS*1*) *E. coli*; m-n) ampicillin in hyper-motile (+IS*1*) *E. coli*; o-p) AgNPs in non-motile (Δ*flhD::kan*) *E. coli*; and q-r) ampicillin in non-motile (Δ*flhD::kan*) *E. coli*. The tan box represents the absence of the antimicrobial pressure. Average ± SD of 2-3 replicates. The asterisk signifies that the average of the last five passages are statistically significant (at $p < 0.001$) from the first five passages and when compared to the last five passages of the non-selected passage control.

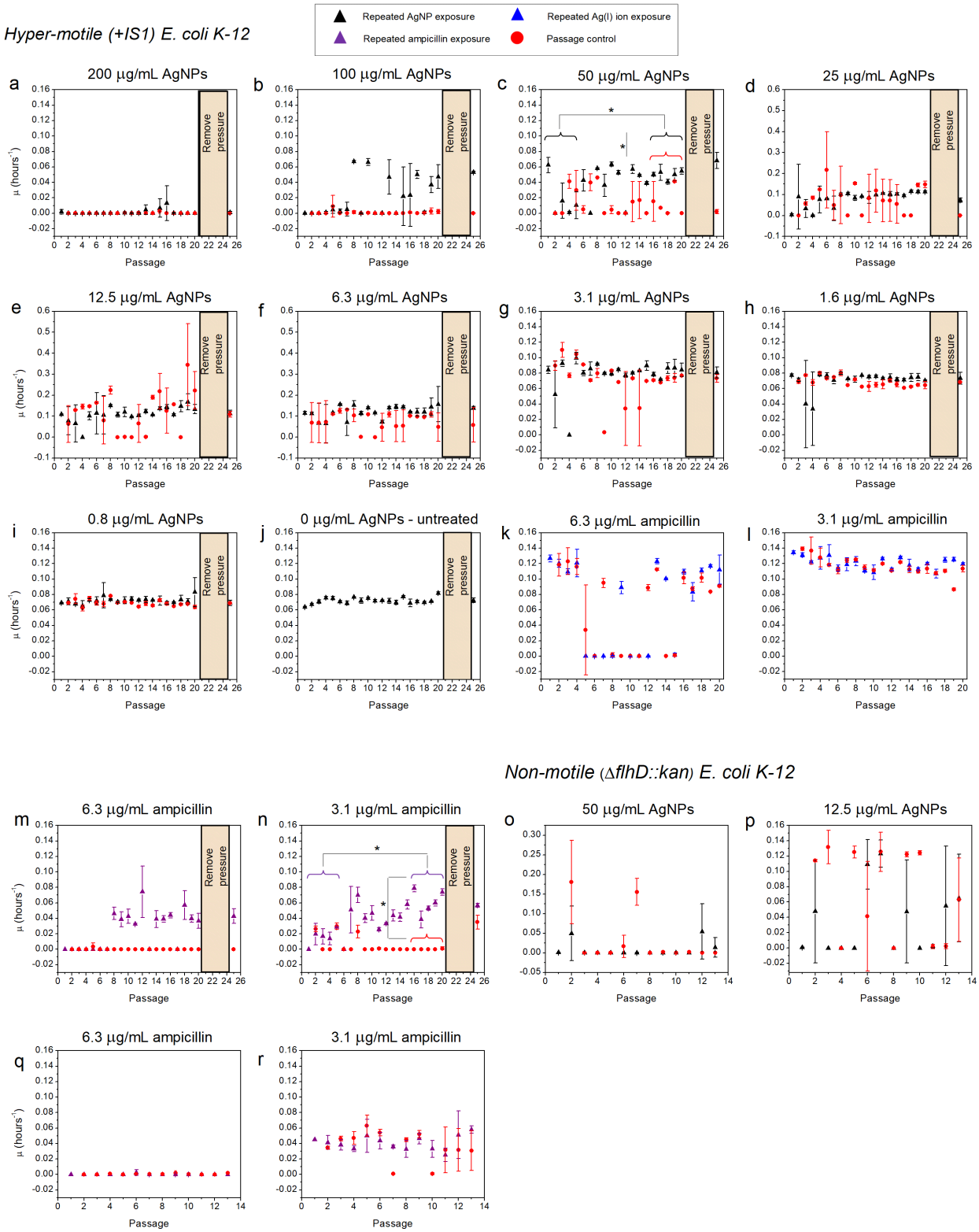

Appendix Figure B.6. Growth rate analysis of all conditions. Maximum specific growth rate (µ) across passage and between experimental (black = AgNPs, blue = Ag(I) ions, purple = ampicillin) and non-selected passage

control (red) samples for a-j) AgNPs in hyper-motile (+IS*1*) *E. coli*; k-l) Ag(I) ions in hyper-motile (+IS*1*) *E. coli*; m-n) ampicillin in hyper-motile (+IS*1*) *E. coli*; o-p) AgNPs in non-motile (Δ*flhD::kan*) *E. coli*; and q-r) ampicillin in non-motile (Δ*flhD::kan*) *E. coli*. The tan box represents the absence of the antimicrobial pressure. Average ± SD of 2-3 replicates. The asterisk signifies that the average of the last five passages are statistically significant (at p < 0.001) from the first five passages and when compared to the last five passages of the non-selected passage control.

Appendix Table B.3. Statistical analysis of initial and final duration of the lag phase (λ, h) and maximum specific growth rate (μ, h^{-1}) corresponding to repeated AgNP (50 μg/mL) exposure (i.e., experimental group) in the hyper-motile *E. coli* (+IS*1*) strain, and after the AgNP pressure is removed and reintroduced, with data corresponding to the non-selected passage control in parentheses.

Metric	Average initial metric ± SD (μg/mL)[‡]	Average final metric ± SD (μg/mL)[+]	Statistical difference between initial and final metric (expt. group)*	Statistical difference of final metric between expt. group and passage control	Average metric ± SD (μg/mL) after pressure removed and re-introduced
λ (h)	20.750 ± 5.020 (20.060 ± 5.000)	5.700 ± 2.370 (21.240 ± 4.450)	***p* < 0.001**	***p* = 0.002**	2.020 ± 0.020 (24.000 ± 0.000)
μ (h^{-1})	0.016 ± 0.020 (0.019 ± 0.020)	0.050 ± 0.007 (0.014 ± 0.020)	***p* = 0.003**	***p* = 0.002**	0.068 ± 0.010 (0.002 ± 0.003)

[‡]average of the first 5 passages, [+]average of the last 5 passages, *n ≥10*
**No significant changes (p > 0.05) were found for the passage control when comparing initial and final metrics*

Appendix Table B.4. Explained percentage (%) variation of duration of the lag phase by treatment group, passage number, and the interaction between the two variables (two-way ANOVA analysis, p-value in parentheses).

	AgNPs, hyper-motile	Ampicillin, hyper-motile	Ag(I) ions, hyper-motile	AgNPs, non-motile	Ampicillin, non-motile
Treatment group	29.86 (<0.001)	62.31 (<0.001)	5.09 (0.019)	7.77 (0.037)	12.81 (<0.001)
Passage number	9.47 (<0.001)	4.37 (<0.001)	6.72 (0.007)	0.26 (0.695)	1.60 (0.225)
Interaction	14.17 (<0.001)	7.46 (<0.001)	0.29 (0.573)	2.53 (0.226)	11.16 (0.002)
Unexplained	46.50	25.86	87.90	89.44	74.43

Appendix Table B.5. Explained percentage (%) variation of maximum specific growth rate by treatment group, passage number, and the interaction between the two variables (two-way ANOVA analysis, p-value in parentheses).

	AgNPs, hyper-motile	Ampicillin, hyper-motile	Ag(I) ions, hyper-motile	AgNPs, non-motile	Ampicillin, non-motile
Treatment group	20.39 (<0.001)	51.39 (<0.001)	3.79 (0.020)	11.06 (0.011)	1.28 (0.326)
Passage number	5.02 (0.010)	7.11 (<0.001)	24.33 (<0.001)	0.02 (0.920)	1.76 (0.249)
Interaction	10.77 (<0.001)	9.81 (<0.001)	5.80 (0.004)	5.58 (0.065)	5.64 (0.041)
Unexplained	63.82	31.69	66.08	83.34	91.32

Appendix B.2 Discussion 2 – Controlling for Total Ag and Ag(I) Content: Rationale Supporting Particle Specific Contributions to Resistance from the MIC Assay

Given the design of the minimum inhibitory concentration (MIC) assay, we are unable to directly study the Ag(I) ion concentrations released in the AgNP exposures tested, which would aid in distinguishing particle and ion contributions to the observed resistance development. Generally, the range of antimicrobial concentrations selected for testing resistance using the MIC assay depends on the organism and antimicrobial agent. For full-range MIC testing, 8-12 two-fold dilutions are tested and include both inhibitory and sub-inhibitory concentrations[289]. The dosing range of the Ag(I) ion exposure is not directly comparable to the concentration range of the Ag(I) ions released in the AgNP exposure system. Yet, we are confident that we are capturing the Ag(I) ion concentration released AgNP exposures within our current study concentration range. From our prior work, approximately 7% ion release was found to occur for similar PEGSH-AgNPs in LB broth after 24 hours.[66] The associated Ag(I) ion concentration is captured within the dosing range of the Ag(I) ions used in the current study. We also capture Ag(I) ion concentrations at

magnitudes higher and lower (e.g., assuming 40% or 0.1% of surface atoms oxidized). Since we observe no development of bacterial resistance as a result of repeated exposure to this range of Ag(I) ion concentrations alone, the combined results and concentrations tested suggest that the AgNPs themselves may elicit the observed resistance and decreased susceptibility.

Appendix B.3 Discussion 3 – Other Mutations Explained

There are a couple of differences between the ancestral sample of *E. coli* K-12 MG1655 used in our study and the reference genome that has been previously documented. Most notably, an insertion of 9 base pairs at the IS1 site appears in the *dgcJ* gene at position 1,873,031, which is involved in cell adhesion for single-species biofilm formation and negatively regulates flagellum-dependent cell motility.[219] The deletion of *dgcJ* can increase swimming motility and a *dgcJ* mutant can suppress any reduced motility function,[219] which likely confirms the hyper-motility behavior of our chosen strain. This mutation was found at a 100% frequency in all reads.

In the later passages of the control populations, a synonymous mutation in the *plaP* gene at position 2,086,171, G→A, L298L (CTG→TTG) is observed. Since *plaP* is a transporter of putrescine, an amine that forms from arginine during putrefaction,[290-292] this mutation is likely the result of (i) weakened cells from repeated culturing effects or (ii) cells under general stress, including nutrient limitation or oxidative stress, at the end of the 24-hr growth curve as they enter the decay phase.[293]

It is interesting to note that other additional mutations (e.g. a missense mutation in the *envZ* gene) occurred in the treatment populations, especially in the later passages, which may indicate that high resistance levels are possible as more mutations arise. Furthermore, the order of when

these mutations arise may be important for imparting different levels of resistance and should be explored in the future. Like CusS, EnvZ also encodes a sensory histidine kinase that regulates phosphorylation of response regulator OmpR in response to environmental signals.[294-297] OmpR activates osmoregulatory expression of the *ompF* and *ompC* genes that encode major outer membrane porin proteins in *E. coli*.[294-297] It has also been established that OmpR and FlhDC, the master regulator of flagellum biosynthesis,[191, 192] can impact expression of each other,[298] which could explain the presence of this mutation in the hyper-motile strain. *envZ* undergoes a similar change to *cusS*, i.e., a polar glycine residue (residue 226) is replaced with a hydrophobic valine residue, located adjacent to a major site for phosphorylation, and likely imparts autophosphorylation and downstream phosphotransfer to OmpR which is increased in a lipid environment.[299] Thus, we speculate that this mutation imparts AgNP resistance by modulating cellular permeability and inhibiting the penetration of Ag species into the cell. Graves et al. also identified several point mutations and indels in *ompR*, concluding that AgNP resistance likely was a production of an OmpR protein that regulated responses to Ag(I) ions.[107]

Finally, selection of resistance occurred at low levels of AgNPs, and over time the resistant cells adapted to higher, toxic levels of AgNPs. Generally, *de novo* selected mutants enriched at sub-MIC levels are expected to have relatively low fitness costs that balance resistance and growth demands.[300] Additionally, the rate at which resistance mutations arise is expected to be higher when experimental evolution is conducted at sub-MIC levels since the population continues to grow, allowing a larger population size and a continuing supply of possible resistance mutations.[300] In this study, the *cusS* mutation was selected at low concentrations and then rose to high frequency with continued passage. The mutation in *cusS* likely imparts a low fitness cost,

as made evident by the stability of the mutation in the absence of AgNPs and being swept to high frequency (100%).[300]

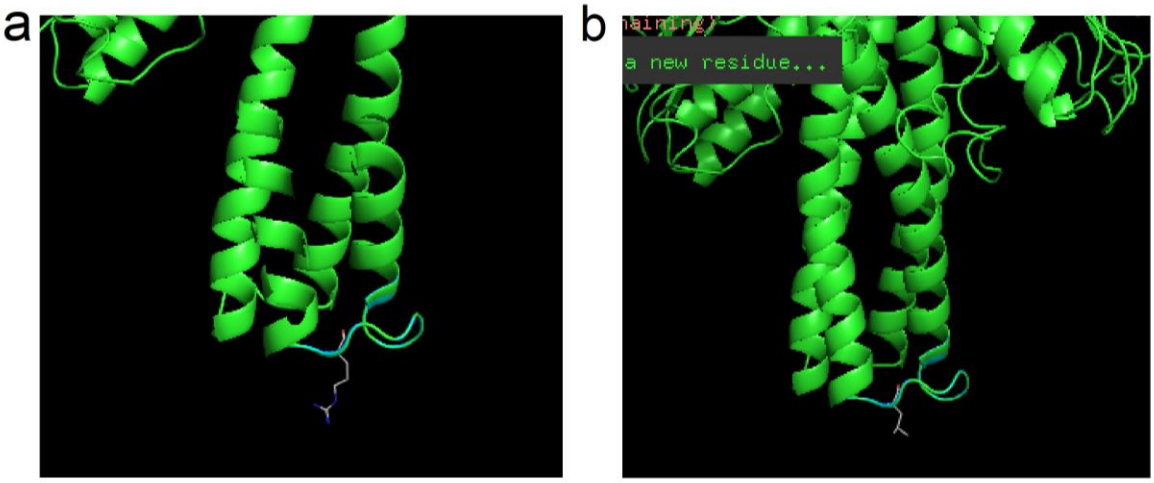

Appendix Figure B.7. 3D Structure of the CusS protein. a) the original arginine residue at position 292 and b) the mutation to leucine at position 292 upon repeated AgNP exposure. Note: The secondary and 3D structures of the CusS protein, including the cytoplasmic domains, was predicted with RaptorX [301-305] and SWISS-MODEL, respectively, and then was input into PyMOL. Position 292 is located within the coils and in terms of solvent accessibility, changes from being 80% exposed to only being 40% exposed (RaptorX [301-305]).

```
  1 mvskpfqrpf slatrltffi slatiaaffa fawimihsvk vhfaeqdind lkeisatler
 61 vlnhpdetqa rrlmtlediv sgysnvlisl adsqgktvyh spgapdiref trdaipdkda
121 qggevyllsg ptmmmpghgh ghmehsnwrm inlpvgplvd gkpiytlyia lsidfhlhyi
                                     *
181 ndlmnklimt asvisilivf ivllavhkgh apirsvsrqi qnitskdldv rldpqtvpie
                                             *               *
241 leqlvlsfnh mieriedvft rqsnfsadia heirtpitnl itqtelalsq srsqkeledv
                 *
301 lysnleeltr makmvsdmlf laqadnrqli pekkmlnlad evgkvfdffe alaedrgvel
                       *
361 rfvgdkcqva gdplmlrral snllsnalry tptgetivvr cqtvdhlvqv ivenpgtpia
                     *  *
421 pehlprlfdr fyrvdpsrqr kgegsgigla ivksivvahk gtvavtsdar gtrfvitlpa
```

TM helices
HAMP
dimerization/phosphoacceptor
ATPase
39-187-cloned sensor domain

Appendix Figure B.8. Amino acid sequence of CusS. Domains and corresponding residues highlighted. Asterisks indicate residues where mutations occurred as previously identified in the literature (D435A, R438C, Graves et al. 2015;[107] L12R, T14P, R15L, N279H, Tajkarimi et al. 2017;[216] I213S, A312E, R377H, Randall et al. 2015[215]). The boxed asterisk indicates the residue where this study's mutation occurs. Adapted from Gudipaty and McEvoy 2014 with permission.[213]

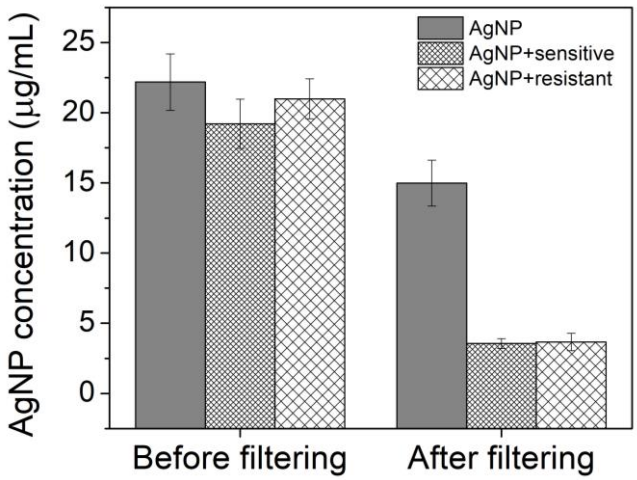

Appendix Figure B.9. Filtration causes some AgNP loss. Filtering with a 0.45 µm PVDF membrane filter to remove bacteria cells loses some AgNPs, even in just broth (AgNP only-controls) as determined by calculating the AgNP concentration after measuring with UV-vis-NIR (shown for 25 µg/mL [AgNP] after 21 h incubation). This AgNP loss after filtering is exacerbated when AgNPs are present with bacteria and could be due to either capture in the filter because of bacteria-associated aggregation of the particles and/or due to particle internalization within the bacteria cell.

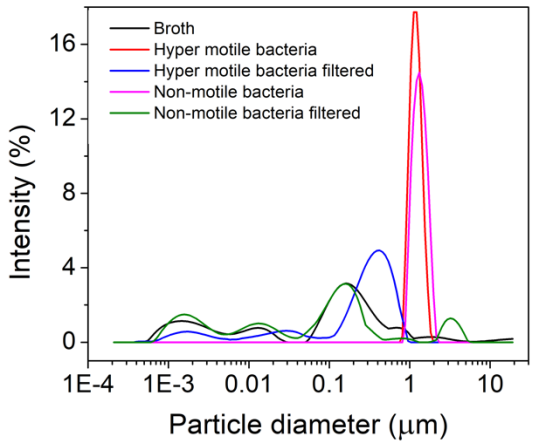

Appendix Figure B.10. Filtration removes bacteria. 0.45 µm pore size PVDF membrane filter removes bacteria as shown by DLS. The absence of bacteria in the filtrate was also confirmed by light microscopy and agar plating (data not shown).

Appendix C Additional Contributions to the Field

In addition to the work on AgNPs presented in this dissertation, contributions to the field of engineering education were made and are listed below:

1. **Stabryla, L.M.**; Clark, R.; Gilbertson, L.M. Assessment of Using Design Thinking to Foster Creativity in an Undergraduate Sustainable Engineering Course. *Advances in Engineering Education*, **2021**. Accepted.
2. Albalghiti, E.; **Stabryla, L.M.**; Gilbertson, L.M.; Zimmerman, J.B. Towards resolution of antibacterial mechanisms in metal and metal oxide nanomaterials: a meta-analysis of the influence of study design on mechanistic conclusions. *Environmental Science: Nano*, **2021**, 8: 37-66. DOI: 10.1039/D0EN00949K.
3. Clark, R.; **Stabryla, L.M.;** Gilbertson, L.M. Sustainability coursework: student perspectives and reflections on design thinking. *International Journal of Sustainability in Higher Education*, **2020**, 21(3): 593-611. DOI: 10.1108/IJSHE-09-2019-0275.
4. Johnston, K.A.; **Stabryla, L.M.**; Gilbertson, L.M.; Millstone, J.E. Emerging investigator series: connecting concepts of coinage metal stability across length scales. *Environmental Science: Nano*, **2019,** 6: 2674-2696. DOI: 10.1039/C9EN00407F.
5. Johnston, K.A.; **Stabryla, L.M.**; Smith, A.M.; Gan, X.Y.; Gilbertson, L.M.; Millstone, J.E. Impacts of broth chemistry on silver ion release, surface chemistry composition, and bacterial cytotoxicity of silver nanoparticles. *Environmental Science: Nano*, **2018**, 5: 304-312. DOI: 10.1039/C7EN00974G.

6. Clark, R.; **Stabryla, L.M.**; Gilbertson, L.M. Use of active learning and the design thinking process to drive creative sustainable engineering design solutions. *American Society for Engineering Education (ASEE) 125th Annual Conference & Exposition.* ***2018***.

Bibliography

1. Mijnendonckx, K., et al., *Antimicrobial silver: uses, toxicity and potential for resistance.* Biometals, 2013. **26**(4): p. 609-621.

2. Reidy, B., et al., *Mechanisms of silver nanoparticle release, transformation and toxicity: a critical review of current knowledge and recommendations for future studies and applications.* Materials, 2013. **6**(6): p. 2295-2350.

3. Simončič, B. and D. Klemenčič, *Preparation and performance of silver as an antimicrobial agent for textiles: A review.* Textile Research Journal, 2016. **86**(2): p. 210-223.

4. *Antimicrobial coatings markety by type (silver, copper, titanium dioxide), application (medical & healthcare, foods & beverages, building & construction, hvac system, protective clothing, transportation), & region - global forecast to 2025*. 2020.

5. *Antiseptics and Disinfectants: Global Markets to 2022*. 2017, BCC Research.

6. Sugden, R., R. Kelly, and S. Davies, *Combatting antimicrobial resistance globally.* Nature microbiology, 2016. **1**(10): p. 1-2.

7. *Bad Bugs, No Drugs*. 2004.

8. *Report to the President on Combating Antibiotic Resistance*. 2014, Executive Office of the President.

9. *WHO publishes list of bacteria for which new antibiotics are urgently needed*. 2017 [cited 2021 May 16].

10. *Antibiotic/Antimicrobial Resistance*. 2017.

11. America, I.D.S.o., *Combating antimicrobial resistance: policy recommendations to save lives.* Clinical Infectious Diseases, 2011. **52**(suppl_5): p. S397-S428.

12. G. Daniel, D.G., S. Mayer, M. McClellan, *AMR: Antibiotics Stewardship and Innovation.* Commonwealth Health Partnerships, 2014.

13. *Fluroquinolones*. 2011.

14. *Antimicrobial Resistance Global Report on Surveillance*. 2014, World Health Organization.

15. *FDA Drug Safety Communication: FDA Advises Restricting Fluoroquinolone Antibiotic Use for Certain Uncomplicated Infections; Warns about Disabling Side Effects that Can Occur Together*. 2016, U.S. FDA.

16. Ament, P.W., N. Jamshed, and J.P. Horne, *Linezolid: its role in the treatment of gram-positive, drug-resistant bacterial infections.* American family physician, 2002. **65**(4): p. 663.

17. Kaplan, S. *FDA bans antibacteria soaps containing triclosan*. 2015.

18. Lefebvre, A. *Benzethonium Chloride Replaces Triclosan as the New "Antibacterial" Agent in Cosmetics and Commerical Soap*. 2015.

19. McQuillan, J.S., et al., *Silver nanoparticle enhanced silver ion stress response in Escherichia coli K12.* Nanotoxicology, 2012. **6**(8): p. 857-866.

20. Yazdankhah, S.P., et al., *Triclosan and antimicrobial resistance in bacteria: an overview.* Microbial drug resistance, 2006. **12**(2): p. 83-90.

21. Al-Berfkani, M., A. Zubair, and H. Bayazed, *Assessment of chlorine resistant bacteria and their susceptibility to antibiotic from water distribution system in Duhok province.* Journal of Applied Biology and Biotechnology, 2014. **2**(6): p. 10-13.

22. Mir, J., J. Morato, and F. Ribas, *Resistance to chlorine of freshwater bacterial strains.* Journal of applied microbiology, 1997. **82**(1): p. 7-18.

23. Ridgway, H. and B. Olson, *Chlorine resistance patterns of bacteria from two drinking water distribution systems.* Applied and Environmental Microbiology, 1982. **44**(4): p. 972-987.

24. Sun, W., et al., *Characterization and identification of a chlorine-resistant bacterium, Sphingomonas TS001, from a model drinking water distribution system.* Science of the total environment, 2013. **458**: p. 169-175.

25. Franci, G., et al., *Silver nanoparticles as potential antibacterial agents.* Molecules, 2015. **20**(5): p. 8856-8874.

26. Panáček, A., et al., *Silver colloid nanoparticles: synthesis, characterization, and their antibacterial activity.* The Journal of Physical Chemistry B, 2006. **110**(33): p. 16248-16253.

27. Durán, N., et al., *Silver nanoparticles: A new view on mechanistic aspects on antimicrobial activity.* Nanomedicine: Nanotechnology, Biology and Medicine, 2016. **12**(3): p. 789-799.

28. *Silver nanoparticles market by application (Electronics & electrical, healthcare, food & beverages, textiles) and segment forecasts to 2022*. 2015.

29. Molling, J.W., et al., *Comparative performance of a panel of commercially available antimicrobial nanocoatings in Europe.* Nanotechnology, science and applications, 2014. **7**: p. 97-104.

30. Alexander, J.W., *History of the medical use of silver.* Surgical infections, 2009. **10**(3): p. 289-292.

31. Silver, S., L.T. Phung, and G. Silver, *Silver as biocides in burn and wound dressings and bacterial resistance to silver compounds.* Journal of Industrial Microbiology and Biotechnology, 2006. **33**(7): p. 627-634.

32. *Silver Nanoparticles Market by Synthesis Method (Wet Chemsitry, Ion Implantation, and Biological Synthesis), Shape (Spheres, Platelets, Rods, Colloidal Silver Particles, and Others), and Application (Healthcare & Life Science, Textile, Electronics & IT, Food & Beverages, Pharmaceuticals, Cosmetics, Water Treatment, and Others): Global Opportunity Analysis and Industry Forecast 2020-2027*. 2020.

33. Lazareva, A. and A.A. Keller, *Estimating potential life cycle releases of engineered nanomaterials from wastewater treatment plants.* ACS Sustainable Chemistry & Engineering, 2014. **2**(7): p. 1656-1665.

34. *Silver Nanoparticles Market Size, Share & Trends Analysis Report By Application (Electronics & Electrical, Healthcare, Food & Beverages, Textiles), By Region, and Segment Forecasts, 2015-2022*. 2015.

35. Xiu, Z.-m., et al., *Negligible particle-specific antibacterial activity of silver nanoparticles.* Nano letters, 2012. **12**(8): p. 4271-4275.

36. Radzig, M., et al., *Antibacterial effects of silver nanoparticles on gram-negative bacteria: influence on the growth and biofilms formation, mechanisms of action.* Colloids and Surfaces B: Biointerfaces, 2013. **102**: p. 300-306.

37. Shannon, R.D., *Revised effective ionic radii and systematic studies of interatomic distances in halides and chalcogenides.* Acta crystallographica section A: crystal physics, diffraction, theoretical and general crystallography, 1976. **32**(5): p. 751-767.

38. Ivask, A., et al., *Toxicity mechanisms in Escherichia coli vary for silver nanoparticles and differ from ionic silver.* ACS nano, 2014. **8**(1): p. 374-386.

39. Silva, T., et al., *Particle size, surface charge and concentration dependent ecotoxicity of three organo-coated silver nanoparticles: comparison between general linear model-predicted and observed toxicity.* Science of the total environment, 2014. **468**: p. 968-976.

40. Visnapuu, M., et al., *Dissolution of silver nanowires and nanospheres dictates their toxicity to Escherichia coli.* BioMed research international, 2013. **2013**.

41. Choi, O. and Z. Hu, *Nitrification inhibition by silver nanoparticles.* Water science and technology, 2009. **59**(9): p. 1699-1702.

42. Choi, O., et al., *Interactions of nanosilver with Escherichia coli cells in planktonic and biofilm cultures.* Water research, 2010. **44**(20): p. 6095-6103.

43. Y.J. Choi, B.-T.L., H-A. Kim, K-W. Kim, K.H. Chung, W.K. Song. *Antibacterial activity and intracellular accumulation of silver nanoparticles of Escherichia coli K-12*. in *NSTI Nanotechnology Conference and Expo*. 2012.

44. Mosselhy, D.A., et al., *Comparative synthesis and antimicrobial action of silver nanoparticles and silver nitrate.* Journal of Nanoparticle Research, 2015. **17**(12): p. 1-10.

45. Panáček, A., et al., *Antifungal activity of silver nanoparticles against Candida spp.* Biomaterials, 2009. **30**(31): p. 6333-6340.

46. Maurer-Jones, M.A., et al., *Characterization of silver ion dissolution from silver nanoparticles using fluorous-phase ion-selective electrodes and assessment of resultant toxicity to Shewanella oneidensis.* Chemical Science, 2013. **4**(6): p. 2564-2572.

47. Zarubina, A., et al., *Evaluation of toxicity of silver ions and nanoparticles using model bacteria with luminescent phenotype.* Nanotechnologies in Russia, 2015. **10**(5): p. 475-483.

48. Yang, Y., et al., *Pyrosequencing reveals higher impact of silver nanoparticles than Ag+ on the microbial community structure of activated sludge.* Water research, 2014. **48**: p. 317-325.

49. Barker, L.K., *Effects of silver ions and nanoparticles on suspended cells and biofilms of Nitrosomonas europaea.* 2014.

50. Arnaout, C.L. and C.K. Gunsch, *Impacts of silver nanoparticle coating on the nitrification potential of Nitrosomonas europaea.* Environmental science & technology, 2012. **46**(10): p. 5387-5395.

51. Radniecki, T.S., et al., *Influence of liberated silver from silver nanoparticles on nitrification inhibition of Nitrosomonas europaea.* Chemosphere, 2011. **85**(1): p. 43-49.

52. Amato, E., et al., *Synthesis, characterization and antibacterial activity against Gram positive and Gram negative bacteria of biomimetically coated silver nanoparticles.* Langmuir, 2011. **27**(15): p. 9165-9173.

53. Dams, R., et al., *Silver nanotoxicity using a light-emitting biosensor Pseudomonas putida isolated from a wastewater treatment plant.* Journal of hazardous materials, 2011. **195**: p. 68-72.

54. Lok, C.-N., et al., *Silver nanoparticles: partial oxidation and antibacterial activities.* JBIC Journal of Biological Inorganic Chemistry, 2007. **12**(4): p. 527-534.

55. Gorka, D.E., et al., *Reducing environmental toxicity of silver nanoparticles through shape control.* Environmental science & technology, 2015. **49**(16): p. 10093-10098.

56. Hachicho, N., et al., *Effect of silver nanoparticles and silver ions on growth and adaptive response mechanisms of Pseudomonas putida mt-2.* FEMS microbiology letters, 2014. **355**(1): p. 71-77.

57. Ortega-Calvo, J.J., et al., *Bacterial tactic response to silver nanoparticles.* Environmental microbiology reports, 2011. **3**(5): p. 526-534.

58. Beer, C., et al., *Toxicity of silver nanoparticles—nanoparticle or silver ion?* Toxicology letters, 2012. **208**(3): p. 286-292.

59. Chen, Z., et al., *Aerobic condition enhances bacteriostatic effects of silver nanoparticles in aquatic environment: an antimicrobial study on Pseudomonas aeruginosa.* Scientific reports, 2017. **7**(1): p. 1-8.

60. Yang, X., et al., *Mechanism of silver nanoparticle toxicity is dependent on dissolved silver and surface coating in Caenorhabditis elegans.* Environmental science & technology, 2012. **46**(2): p. 1119-1127.

61. Bowman, C.R., et al., *Effects of silver nanoparticles on zebrafish (Danio rerio) and Escherichia coli (ATCC 25922): a comparison of toxicity based on total surface area versus mass concentration of particles in a model eukaryotic and prokaryotic system.* Environmental toxicology and chemistry, 2012. **31**(8): p. 1793-1800.

62. Boenigk, J., et al., *Effects of silver nitrate and silver nanoparticles on a planktonic community: general trends after short-term exposure.* PloS one, 2014. **9**(4): p. e95340.

63. Ansari, M., H. Khan, and A. Khan, *Evaluation of antibacterial activity of silver nanoparticles against MSSA and MSRA on isolates from skin infections.* 2011.

64. Xiu, Z.-M., J. Ma, and P.J. Alvarez, *Differential effect of common ligands and molecular oxygen on antimicrobial activity of silver nanoparticles versus silver ions.* Environmental science & technology, 2011. **45**(20): p. 9003-9008.

65. Georgantzopoulou, A., et al., *Ag nanoparticles: size-and surface-dependent effects on model aquatic organisms and uptake evaluation with NanoSIMS.* Nanotoxicology, 2012. **7**(7): p. 1168-1178.

66. Johnston, K.A., et al., *Impacts of broth chemistry on silver ion release, surface chemistry composition, and bacterial cytotoxicity of silver nanoparticles.* Environmental Science: Nano, 2018. **5**(2): p. 304-312.

67. Smetana, A.B., et al., *Biocidal activity of nanocrystalline silver powders and particles.* Langmuir, 2008. **24**(14): p. 7457-7464.

68. Doody, M.A., et al., *Differential antimicrobial activity of silver nanoparticles to bacteria Bacillus subtilis and Escherichia coli, and toxicity to crop plant Zea mays and beneficial B. subtilis-inoculated Z. mays.* Journal of Nanoparticle Research, 2016. **18**(10): p. 1-19.

69. Giao, N.T., et al., *Influence of silver nanoparticles and liberated silver ions on nitrifying sludge: ammonia oxidation inhibitory kinetics and mechanism.* Environmental Science and Pollution Research, 2017. **24**(10): p. 9229-9240.

70. Greulich, C., et al., *The toxic effect of silver ions and silver nanoparticles towards bacteria and human cells occurs in the same concentration range.* RSC advances, 2012. **2**(17): p. 6981-6987.

71. Stabryla, L.M., et al., *Emerging investigator series: it's not all about the ion: support for particle-specific contributions to silver nanoparticle antimicrobial activity.* Environmental Science: Nano, 2018. **5**(9): p. 2047-2068.

72. Morones, J.R., et al., *The bactericidal effect of silver nanoparticles.* Nanotechnology, 2005. **16**(10): p. 2346.

73. Raza, M.A., et al., *Size-and shape-dependent antibacterial studies of silver nanoparticles synthesized by wet chemical routes.* Nanomaterials, 2016. **6**(4): p. 74.

74. Pal, S., Y.K. Tak, and J.M. Song, *Does the antibacterial activity of silver nanoparticles depend on the shape of the nanoparticle? A study of the gram-negative bacterium Escherichia coli.* Applied and environmental microbiology, 2007. **73**(6): p. 1712-1720.

75. El Badawy, A.M., et al., *Surface charge-dependent toxicity of silver nanoparticles.* Environmental science & technology, 2011. **45**(1): p. 283-287.

76. Le Ouay, B. and F. Stellacci, *Antibacterial activity of silver nanoparticles: a surface science insight.* Nano today, 2015. **10**(3): p. 339-354.

77. Levard, C., et al., *Sulfidation processes of PVP-coated silver nanoparticles in aqueous solution: impact on dissolution rate.* Environmental science & technology, 2011. **45**(12): p. 5260-5266.

78. Liu, C., W. Leng, and P.J. Vikesland, *Controlled evaluation of the impacts of surface coatings on silver nanoparticle dissolution rates.* Environmental science & technology, 2018. **52**(5): p. 2726-2734.

79. Long, Y.-M., et al., *Surface ligand controls silver ion release of nanosilver and its antibacterial activity against Escherichia coli.* International journal of nanomedicine, 2017. **12**: p. 3193.

80. Smith, A.M., et al., *Ligand density quantification on colloidal inorganic nanoparticles.* Analyst, 2017. **142**(1): p. 11-29.

81. Zhang, W., *Nanoparticle aggregation: principles and modeling*. Vol. 811. 2014, Dordrecht: Springer.

82. Wright, G.D., *Q&A: Antibiotic resistance: where does it come from and what can we do about it?* BMC biology, 2010. **8**(1): p. 1-6.

83. Sandoval-Motta, S. and M. Aldana, *Adaptive resistance to antibiotics in bacteria: a systems biology perspective.* Wiley Interdisciplinary Reviews: Systems Biology and Medicine, 2016. **8**(3): p. 253-267.

84. Staehlin, B.M., et al., *Evolution of a heavy metal homeostasis/resistance island reflects increasing copper stress in enterobacteria.* Genome biology and evolution, 2016. **8**(3): p. 811-826.

85. Bridges, K., et al., *Gentamicin-and silver-resistant pseudomonas in a burns unit.* Br Med J, 1979. **1**(6161): p. 446-449.

86. Chopra, I., *The increasing use of silver-based products as antimicrobial agents: a useful development or a cause for concern?* Journal of antimicrobial Chemotherapy, 2007. **59**(4): p. 587-590.

87. Gupta, A., et al., *Molecular basis for resistance to silver cations in Salmonella.* Nature medicine, 1999. **5**(2): p. 183-188.

88. Haefeli, C., C. Franklin, and K.E. Hardy, *Plasmid-determined silver resistance in Pseudomonas stutzeri isolated from a silver mine.* Journal of bacteriology, 1984. **158**(1): p. 389-392.

89. Li, X.-Z., H. Nikaido, and K.E. Williams, *Silver-resistant mutants of Escherichia coli display active efflux of Ag+ and are deficient in porins.* Journal of bacteriology, 1997. **179**(19): p. 6127-6132.

90. Lok, C.-N., et al., *Proteomic identification of the Cus system as a major determinant of constitutive Escherichia coli silver resistance of chromosomal origin.* Journal of proteome research, 2008. **7**(6): p. 2351-2356.

91. Silver, S., *Bacterial silver resistance: molecular biology and uses and misuses of silver compounds.* FEMS microbiology reviews, 2003. **27**(2-3): p. 341-353.

92. Annear, D., B. Mee, and M. Bailey, *Instability and linkage of silver resistance, lactose fermentation, and colony structure in Enterobacter cloacae from burn wounds.* Journal of clinical pathology, 1976. **29**(5): p. 441-443.

93. Carr, H.S. and H.S. Rosenkranz, *R factor in Enterobacter cloacae resistant to silver sulfadiazine.* Chemotherapy, 1975. **21**(1): p. 41-44.

94. Choudhury, P. and R. Kumar, *Multidrug-and metal-resistant strains of Klebsiella pneumoniae isolated from Penaeus monodon of the coastal waters of deltaic Sundarban.* Canadian journal of microbiology, 1998. **44**(2): p. 186-189.

95. Deshpande, L.M. and B.A. Chopade, *Plasmid mediated silver resistance in Acinetobacter baumannii.* Biometals, 1994. **7**(1): p. 49-56.

96. Grewal, J. and R. Tiwari, *Resistance to metal ions and antibiotics in Escherichia coli isolated from foodstuffs.* Journal of medical microbiology, 1990. **32**(4): p. 223-226.

97. Hendry, A. and I. Stewart, *Silver-resistant Enterobacteriaceae from hospital patients.* Canadian journal of microbiology, 1979. **25**(8): p. 915-921.

98. Klasen, H., *A historical review of the use of silver in the treatment of burns. II. Renewed interest for silver.* Burns, 2000. **26**(2): p. 131-138.

99. Percival, S.L., P. Bowler, and D. Russell, *Bacterial resistance to silver in wound care.* Journal of hospital infection, 2005. **60**(1): p. 1-7.

100. Losasso, C., et al., *Antibacterial activity of silver nanoparticles: sensitivity of different Salmonella serovars.* Frontiers in microbiology, 2014. **5**: p. 227.

101. Silver, S. and L.T. Phung, *A bacterial view of the periodic table: genes and proteins for toxic inorganic ions.* Journal of Industrial Microbiology and Biotechnology, 2005. **32**(11-12): p. 587-605.

102. Franke, S., et al., *Molecular analysis of the copper-transporting efflux system CusCFBA of Escherichia coli.* Journal of bacteriology, 2003. **185**(13): p. 3804-3812.

103. Mchugh, G.L., et al., *Salmonella typhimurium resistant to silver nitrate, chloramphenicol, and ampicillin: A new threat in burn units?* The Lancet, 1975. **305**(7901): p. 235-240.

104. June, S.G. and D.M. Dziewulski, *Copper and Silver Biocidal Mechanisms, Resistance Strategies, and Efficacy for Legionella Control.* Journal-American Water Works Association, 2018. **110**(12): p. E13-E35.

105. Torres Urquidy, O.H., *Copper Resistant Bacteria Better Tolerate Commercially Available Antimicrobial Treatments Based in Silver and Silver-Copper Ions.* 2011.

106. Torres-Urquidy, O. and K. Bright, *Efficacy of multiple metals against copper-resistant bacterial strains.* Journal of applied microbiology, 2012. **112**(4): p. 695-704.

107. Graves Jr, J.L., et al., *Rapid evolution of silver nanoparticle resistance in Escherichia coli.* Frontiers in genetics, 2015. **6**: p. 42.

108. Gunawan, C., et al., *Widespread and indiscriminate nanosilver use: genuine potential for microbial resistance.* ACS nano, 2017. **11**(4): p. 3438-3445.

109. Gunawan, C., et al., *Induced adaptation of Bacillus sp. to antimicrobial nanosilver.* Small, 2013. **9**(21): p. 3554-3560.

110. Lara, H.H., et al., *Bactericidal effect of silver nanoparticles against multidrug-resistant bacteria.* World Journal of Microbiology and Biotechnology, 2010. **26**(4): p. 615-621.

111. Panáček, A., et al., *Bacterial resistance to silver nanoparticles and how to overcome it.* Nature Nanotechnology, 2018. **13**(1): p. 65-71.

112. Gullberg, E., et al., *Selection of resistant bacteria at very low antibiotic concentrations.* PLoS Pathog, 2011. **7**(7): p. e1002158.

113. Ji, F., et al., *Tetrabromobisphenol A (TBBPA) exhibits specific antimicrobial activity against Gram-positive bacteria without detectable resistance.* Chemical Communications, 2017. **53**(25): p. 3512-3515.

114. Li, X., et al., *Functional Gold Nanoparticles as Potent Antimicrobial Agents against Multi-Drug-Resistant Bacteria.* ACS Nano, 2014. **8**(10): p. 10682-10686.

115. Narayanaswamy, V.P., et al., *In Vitro activity of novel glycopolymer against clinical isolates of multidrug-resistant Staphylococcus aureus.* PLOS ONE, 2018. **13**(1): p. e0191522.

116. Helmlinger, J., et al., *Silver nanoparticles with different size and shape: equal cytotoxicity, but different antibacterial effects.* RSC advances, 2016. **6**(22): p. 18490-18501.

117. Tree-Udom, T., et al., *Shape effect on particle-lipid bilayer membrane association, cellular uptake, and cytotoxicity.* ACS applied materials & interfaces, 2015. **7**(43): p. 23993-24000.

118. El-Zahry, M.R., et al., *Antibacterial effect of various shapes of silver nanoparticles monitored by SERS.* Talanta, 2015. **138**: p. 183-189.

119. Hong, W., et al., *Investigating the environmental factors affecting the toxicity of silver nanoparticles in Escherichia coli with dual fluorescence analysis.* Chemosphere, 2016. **155**: p. 329-335.

120. Rojas-Andrade, M., et al., *Enhanced antimicrobial activity with faceted silver nanostructures.* Journal of Materials Science, 2015. **50**(7): p. 2849-2858.

121. Van Dong, P., C.H. Ha, and J. Kasbohm, *Chemical synthesis and antibacterial activity of novel-shaped silver nanoparticles.* International Nano Letters, 2012. **2**(1): p. 1-9.

122. Wang, G., et al., *Controlled synthesis of Ag 2 O microcrystals with facet-dependent photocatalytic activities.* Journal of Materials Chemistry, 2012. **22**(39): p. 21189-21194.

123. Actis, L., et al., *Effect of silver nanoparticle geometry on methicillin susceptible and resistant Staphylococcus aureus, and osteoblast viability.* Journal of Materials Science: Materials in Medicine, 2015. **26**(7): p. 1-7.

124. Ashkarran, A.A., et al., *Controlling the geometry of silver nanostructures for biological applications.* Physics Procedia, 2013. **40**: p. 76-83.

125. Gao, M., et al., *Controlled synthesis of Ag nanoparticles with different morphologies and their antibacterial properties.* Materials Science and Engineering: C, 2013. **33**(1): p. 397-404.

126. Holmes, A.M., et al., *Varying the morphology of silver nanoparticles results in differential toxicity against micro-organisms, HaCaT keratinocytes and affects skin deposition.* Nanotoxicology, 2016. **10**(10): p. 1503-1514.

127. Nateghi, M.R. and H. Hajimirzababa, *Effect of silver nanoparticles morphologies on antimicrobial properties of cotton fabrics.* The Journal of the Textile Institute, 2014. **105**(8): p. 806-813.

128. Park, J.C., et al., *Effect of the size and shape of silver nanoparticles on bacterial growth and metabolism by monitoring optical density and fluorescence intensity.* Biotechnology and Bioprocess Engineering, 2017. **22**(2): p. 210-217.

129. Sadeghi, B., et al., *Comparison of the anti-bacterial activity on the nanosilver shapes: nanoparticles, nanorods and nanoplates.* Advanced Powder Technology, 2012. **23**(1): p. 22-26.

130. Tanvir, F., et al., *Poly-L-arginine coated silver nanoprisms and their anti-bacterial properties.* Nanomaterials, 2017. **7**(10): p. 296.

131. Chen, X. and H.J. Schluesener, *Nanosilver: a nanoproduct in medical application.* Toxicology letters, 2008. **176**(1): p. 1-12.

132. Huh, A.J. and Y.J. Kwon, *"Nanoantibiotics": a new paradigm for treating infectious diseases using nanomaterials in the antibiotics resistant era.* Journal of controlled release, 2011. **156**(2): p. 128-145.

133. Knetsch, M.L. and L.H. Koole, *New strategies in the development of antimicrobial coatings: the example of increasing usage of silver and silver nanoparticles.* Polymers, 2011. **3**(1): p. 340-366.

134. Rai, M., A. Yadav, and A. Gade, *Silver nanoparticles as a new generation of antimicrobials.* Biotechnology advances, 2009. **27**(1): p. 76-83.

135. Duncan, T.V., *Applications of nanotechnology in food packaging and food safety: barrier materials, antimicrobials and sensors.* Journal of colloid and interface science, 2011. **363**(1): p. 1-24.

136. Gruère, G.P., *Implications of nanotechnology growth in food and agriculture in OECD countries.* Food Policy, 2012. **37**(2): p. 191-198.

137. Mishra, S. and H. Singh, *Biosynthesized silver nanoparticles as a nanoweapon against phytopathogens: exploring their scope and potential in agriculture.* Applied microbiology and biotechnology, 2015. **99**(3): p. 1097-1107.

138. Li, Q., et al., *Antimicrobial nanomaterials for water disinfection and microbial control: potential applications and implications.* Water research, 2008. **42**(18): p. 4591-4602.

139. Dakal, T.C., et al., *Mechanistic basis of antimicrobial actions of silver nanoparticles.* Frontiers in microbiology, 2016. **7**: p. 1831.

140. Rai, M.K., et al., *Silver nanoparticles: the powerful nanoweapon against multidrug-resistant bacteria.* Journal of applied microbiology, 2012. **112**(5): p. 841-852.

141. Ahmed, S., et al., *A review on plants extract mediated synthesis of silver nanoparticles for antimicrobial applications: a green expertise.* Journal of advanced research, 2016. **7**(1): p. 17-28.

142. Marambio-Jones, C. and E.M. Hoek, *A review of the antibacterial effects of silver nanomaterials and potential implications for human health and the environment.* Journal of Nanoparticle Research, 2010. **12**(5): p. 1531-1551.

143. Wigginton, N.S., et al., *Binding of silver nanoparticles to bacterial proteins depends on surface modifications and inhibits enzymatic activity.* Environmental science & technology, 2010. **44**(6): p. 2163-2168.

144. Ansari, M.A., et al., *Interaction of silver nanoparticles with Escherichia coli and their cell envelope biomolecules.* Journal of basic microbiology, 2014. **54**(9): p. 905-915.

145. Hsiao, I.-L., et al., *Trojan-horse mechanism in the cellular uptake of silver nanoparticles verified by direct intra-and extracellular silver speciation analysis.* Environmental science & technology, 2015. **49**(6): p. 3813-3821.

146. Wong, K.K. and X. Liu, *Silver nanoparticles—the real "silver bullet" in clinical medicine?* MedChemComm, 2010. **1**(2): p. 125-131.

147. Kittler, S., et al., *Toxicity of silver nanoparticles increases during storage because of slow dissolution under release of silver ions.* Chemistry of materials, 2010. **22**(16): p. 4548-4554.

148. Molleman, B. and T. Hiemstra, *Surface structure of silver nanoparticles as a model for understanding the oxidative dissolution of silver ions.* Langmuir, 2015. **31**(49): p. 13361-13372.

149. Sotiriou, G.A., et al., *Quantifying the origin of released Ag+ ions from nanosilver.* Langmuir, 2012. **28**(45): p. 15929-15936.

150. Levard, C., et al., *Environmental transformations of silver nanoparticles: impact on stability and toxicity.* Environmental science & technology, 2012. **46**(13): p. 6900-6914.

151. Levard, C.m., et al., *Effect of chloride on the dissolution rate of silver nanoparticles and toxicity to E. coli.* Environmental science & technology, 2013. **47**(11): p. 5738-5745.

152. Liu, J. and R.H. Hurt, *Ion release kinetics and particle persistence in aqueous nano-silver colloids.* Environmental science & technology, 2010. **44**(6): p. 2169-2175.

153. Liu, J., et al., *Controlled release of biologically active silver from nanosilver surfaces.* ACS nano, 2010. **4**(11): p. 6903-6913.

154. Molleman, B. and T. Hiemstra, *Time, pH, and size dependency of silver nanoparticle dissolution: the road to equilibrium.* Environmental Science: Nano, 2017. **4**(6): p. 1314-1327.

155. Ma, R., et al., *Size-controlled dissolution of organic-coated silver nanoparticles.* Environmental science & technology, 2012. **46**(2): p. 752-759.

156. Sotiriou, G.A. and S.E. Pratsinis, *Antibacterial activity of nanosilver ions and particles.* Environmental science & technology, 2010. **44**(14): p. 5649-5654.

157. Gutierrez-Wing, C., et al., *Coalescence phenomena in 1D silver nanostructures.* Journal of Physics: Condensed Matter, 2009. **21**(29): p. 295301.

158. Hatchett, D.W. and H.S. White, *Electrochemistry of sulfur adlayers on the low-index faces of silver.* The Journal of Physical Chemistry, 1996. **100**(23): p. 9854-9859.

159. Wiley, B., Y. Sun, and Y. Xia, *Synthesis of silver nanostructures with controlled shapes and properties.* Accounts of chemical research, 2007. **40**(10): p. 1067-1076.

160. Sundaresan, V., J.W. Monaghan, and K.A. Willets, *Visualizing the effect of partial oxide formation on single silver nanoparticle electrodissolution.* The Journal of Physical Chemistry C, 2018. **122**(5): p. 3138-3145.

161. Rajeshkumar, S. and L. Bharath, *Mechanism of plant-mediated synthesis of silver nanoparticles–a review on biomolecules involved, characterisation and antibacterial activity.* Chemico-biological interactions, 2017. **273**: p. 219-227.

162. Li, Y., et al., *Effects of chloride ions on dissolution, ROS generation, and toxicity of silver nanoparticles under UV irradiation.* Environmental science & technology, 2017. **52**(8): p. 4842-4849.

163. Badawy, A.M.E., et al., *Impact of environmental conditions (pH, ionic strength, and electrolyte type) on the surface charge and aggregation of silver nanoparticles suspensions.* Environmental science & technology, 2010. **44**(4): p. 1260-1266.

164. Li, X., J.J. Lenhart, and H.W. Walker, *Dissolution-accompanied aggregation kinetics of silver nanoparticles.* Langmuir, 2010. **26**(22): p. 16690-16698.

165. Ivask, A., et al., *Size-dependent toxicity of silver nanoparticles to bacteria, yeast, algae, crustaceans and mammalian cells in vitro.* PloS one, 2014. **9**(7): p. e102108.

166. Masrahi, A., A.R. VandeVoort, and Y. Arai, *Effects of silver nanoparticle on soil-nitrification processes.* Archives of environmental contamination and toxicology, 2014. **66**(4): p. 504-513.

167. Burchardt, A.D., et al., *Effects of silver nanoparticles in diatom Thalassiosira pseudonana and Cyanobacterium synechococcus sp.* Environmental science & technology, 2012. **46**(20): p. 11336-11344.

168. Yi, J. and J. Cheng, *Effects of water chemistry and surface contact on the toxicity of silver nanoparticles to Bacillus subtilis.* Ecotoxicology, 2017. **26**(5): p. 639-647.

169. Ivask, A., et al., *Profiling of the reactive oxygen species-related ecotoxicity of CuO, ZnO, TiO 2, silver and fullerene nanoparticles using a set of recombinant luminescent Escherichia coli strains: differentiating the impact of particles and solubilised metals.* Analytical and bioanalytical chemistry, 2010. **398**(2): p. 701-716.

170. Grant, M.J. and A. Booth, *A typology of reviews: an analysis of 14 review types and associated methodologies.* Health information & libraries journal, 2009. **26**(2): p. 91-108.

171. Hofmeister, H., G. Tan, and M. Dubiel, *Shape and internal structure of silver nanoparticles embedded in glass.* Journal of materials research, 2005. **20**(6): p. 1551-1562.

172. Singh, A.K., *Introduction to nanoparticles and nanotoxicology.* Engineered Nanoparticles: Structure, Properties and Mechanisms of Toxicity, 2016: p. 1-18.

173. Li, Y., et al., *Surface-coating-dependent dissolution, aggregation, and reactive oxygen species (ROS) generation of silver nanoparticles under different irradiation conditions.* Environmental science & technology, 2013. **47**(18): p. 10293-10301.

174. Hartmann, M.J., et al., *Impacts of Copper Position on the Electronic Structure of [Au25-xCu x (SH) 18]− Nanoclusters.* The Journal of Physical Chemistry C, 2015. **119**(15): p. 8290-8298.

175. Negishi, Y., et al., *A critical size for emergence of nonbulk electronic and geometric structures in dodecanethiolate-protected Au clusters.* Journal of the American Chemical Society, 2015. **137**(3): p. 1206-1212.

176. Sondi, I. and B. Salopek-Sondi, *Silver nanoparticles as antimicrobial agent: a case study on E. coli as a model for Gram-negative bacteria.* Journal of colloid and interface science, 2004. **275**(1): p. 177-182.

177. Suresh, A.K., et al., *Silver nanocrystallites: biofabrication using Shewanella oneidensis, and an evaluation of their comparative toxicity on gram-negative and gram-positive bacteria.* Environmental science & technology, 2010. **44**(13): p. 5210-5215.

178. McQuillan, J.S. and A.M. Shaw, *Differential gene regulation in the Ag nanoparticle and Ag+-induced silver stress response in Escherichia coli: a full transcriptomic profile.* Nanotoxicology, 2014. **8**(sup1): p. 177-184.

179. Boles, M.A., et al., *The surface science of nanocrystals.* Nature materials, 2016. **15**(2): p. 141-153.

180. Cheng, T.-L., et al., *Analytical measurement of PEGylated molecules.* Bioconjugate chemistry, 2012. **23**(5): p. 881-899.

181. Gavia, D.J. and Y.-S. Shon, *Controlling surface ligand density and core size of alkanethiolate-capped Pd nanoparticles and their effects on catalysis.* Langmuir, 2012. **28**(40): p. 14502-14508.

182. He, G., et al., *Alkyne-functionalized palladium nanoparticles: synthesis, characterization, and electrocatalytic activity in ethylene glycol oxidation.* Electrochimica Acta, 2013. **94**: p. 98-103.

183. Jokerst, J.V., et al., *Nanoparticle PEGylation for imaging and therapy.* Nanomedicine, 2011. **6**(4): p. 715-728.

184. Love, J.C., et al., *Self-assembled monolayers of thiolates on metals as a form of nanotechnology.* Chemical reviews, 2005. **105**(4): p. 1103-1170.

185. Ivask, A., T. Rõlova, and A. Kahru, *A suite of recombinant luminescent bacterial strains for the quantification of bioavailable heavy metals and toxicity testing.* BMC biotechnology, 2009. **9**(1): p. 1-15.

186. Arai, H., et al., *Transcriptome response to nitrosative stress in Rhodobacter sphaeroides 2.4. 1.* Bioscience, biotechnology, and biochemistry, 2013: p. 120601.

187. Behra, R., et al., *Bioavailability of silver nanoparticles and ions: from a chemical and biochemical perspective.* Journal of the Royal Society Interface, 2013. **10**(87): p. 20130396.

188. Valentin, E., et al., *Heritable nanosilver resistance in priority pathogen: a unique genetic adaptation and comparison with ionic silver and antibiotics.* Nanoscale, 2020. **12**(4): p. 2384-2392.

189. Pelgrift, R.Y. and A.J. Friedman, *Nanotechnology as a therapeutic tool to combat microbial resistance.* Advanced drug delivery reviews, 2013. **65**(13-14): p. 1803-1815.

190. Wang, L., C. Hu, and L. Shao, *The antimicrobial activity of nanoparticles: present situation and prospects for the future.* International journal of nanomedicine, 2017. **12**: p. 1227.

191. Barker, C.S., B.M. Prüß, and P. Matsumura, *Increased motility of Escherichia coli by insertion sequence element integration into the regulatory region of the flhD operon.* Journal of bacteriology, 2004. **186**(22): p. 7529-7537.

192. Gauger, E.J., et al., *Role of motility and the flhDC operon in Escherichia coli MG1655 colonization of the mouse intestine.* Infection and immunity, 2007. **75**(7): p. 3315-3324.

193. Bastús, N.G., et al., *Synthesis of highly monodisperse citrate-stabilized silver nanoparticles of up to 200 nm: kinetic control and catalytic properties.* Chemistry of Materials, 2014. **26**(9): p. 2836-2846.

194. Johnston, K.A., et al., *Impact of as-synthesized ligands and low-oxygen conditions on silver nanoparticle surface functionalization.* Langmuir, 2016. **32**(16): p. 3820-3826.

195. El-Halfawy, O.M. and M.A. Valvano, *Antimicrobial Heteroresistance: an Emerging Field in Need of Clarity.* Clinical Microbiology Reviews, 2015. **28**(1): p. 191.

196. Landman, D., J. Salamera, and J. Quale, *Irreproducible and uninterpretable Polymyxin B MICs for Enterobacter cloacae and Enterobacter aerogenes.* J Clin Microbiol, 2013. **51**(12): p. 4106-11.

197. Baalousha, M., et al., *The concentration-dependent behaviour of nanoparticles.* Environmental Chemistry, 2016. **13**(1): p. 1-3.

198. Denmark, T.U.o., *Lecture 11 - Antimicrobial susceptibility testing - broth dilution*, Coursera, Editor.

199. Institute, C.a.L.S., *Methods for dilution antimicrobial susceptibility tests for bacteria that grow aerobically. Approved standard M7-A9*. 9 ed. Vol. 32. 2012, Wayne, Pa: Clinical and Laboratory Standards Institute.

200. Riley, M., et al., *Escherichia coli K-12: a cooperatively developed annotation snapshot--2005.* Nucleic Acids Res, 2006. **34**(1): p. 1-9.

201. Deatherage, D.E. and J.E. Barrick, *Identification of mutations in laboratory-evolved microbes from next-generation sequencing data using breseq*, in *Engineering and analyzing multicellular systems*. 2014, Springer. p. 165-188.

202. Ivanova, E., K. Bazaka, and R. Crawford, *Advanced synthetic polymer biomaterials derived from organic sources.* New Functional Biomaterials for Medicine and Healthcare; Ivanova, EP, Bazaka, K., Crawford, RJ, Eds, 2014: p. 71-99.

203. Olofsson, S.K. and O. Cars, *Optimizing drug exposure to minimize selection of antibiotic resistance.* Clinical Infectious Diseases, 2007. **45**(Supplement_2): p. S129-S136.

204. Adam, M., et al., *Epigenetic inheritance based evolution of antibiotic resistance in bacteria.* BMC evolutionary biology, 2008. **8**(1): p. 1-12.

205. George, A.M. and S.B. Levy, *Amplifiable resistance to tetracycline, chloramphenicol, and other antibiotics in Escherichia coli: involvement of a non-plasmid-determined efflux of tetracycline.* Journal of Bacteriology, 1983. **155**(2): p. 531-540.

206. Zhao, Y., et al., *Small molecule-capped gold nanoparticles as potent antibacterial agents that target gram-negative bacteria.* Journal of the American Chemical Society, 2010. **132**(35): p. 12349-12356.

207. Institute, C.a.L.S., *Performance standards for antimicrobial susceptibility testing: twentieth informational supplement. Approved standard M100-S20*. Vol. 30. 2010, Wayne, PA: Clnical and Laboratory Standards Institute.

208. Silver, S., *Mechanisms of plasmid-determined heavy metal resistances*, in *molecular biology, pathogenicity, and ecology of bacterial plasmids*. 1981, Springer. p. 179-189.

209. Flynn, K.M., et al., *The environment affects epistatic interactions to alter the topology of an empirical fitness landscape.* PLoS Genet, 2013. **9**(4): p. e1003426.

210. Hall, A.E., et al., *Environment changes epistasis to alter trade-offs along alternative evolutionary paths.* Evolution, 2019. **73**(10): p. 2094-2105.

211. Normark, B.H. and S. Normark, *Evolution and spread of antibiotic resistance.* Journal of internal medicine, 2002. **252**(2): p. 91-106.

212. Affandi, T. and M.M. McEvoy, *Mechanism of metal ion-induced activation of a two-component sensor kinase.* Biochemical Journal, 2019. **476**(1): p. 115-135.

213. Gudipaty, S.A. and M.M. McEvoy, *The histidine kinase CusS senses silver ions through direct binding by its sensor domain.* Biochimica et Biophysica Acta (BBA)-Proteins and Proteomics, 2014. **1844**(9): p. 1656-1661.

214. Cooper, V.S., *Experimental evolution as a high-throughput screen for genetic adaptations.* MSphere, 2018. **3**(3).

215. Randall, C.P., et al., *Silver resistance in Gram-negative bacteria: a dissection of endogenous and exogenous mechanisms.* Journal of Antimicrobial Chemotherapy, 2015. **70**(4): p. 1037-1046.

216. Tajkarimi, M., et al., *Selection for ionic-confers silver nanoparticle resistance in Escherichia coli.* JSM Nanotechnol Nanomed, 2017. **5**(1): p. 1047.

217. Koskella, B., et al., *Using experimental evolution to explore natural patterns between bacterial motility and resistance to bacteriophages.* The ISME journal, 2011. **5**(11): p. 1809-1817.

218. Samad, T., et al., *Swimming bacteria promote dispersal of non-motile staphylococcal species.* The ISME journal, 2017. **11**(8): p. 1933-1937.

219. Sanchez-Torres, V., H. Hu, and T.K. Wood, *GGDEF proteins YeaI, YedQ, and YfiN reduce early biofilm formation and swimming motility in Escherichia coli.* Applied microbiology and biotechnology, 2011. **90**(2): p. 651-658.

220. Butler, M.T., Q. Wang, and R.M. Harshey, *Cell density and mobility protect swarming bacteria against antibiotics.* Proceedings of the National Academy of Sciences, 2010. **107**(8): p. 3776-3781.

221. Lai, S., J. Tremblay, and E. Déziel, *Swarming motility: a multicellular behaviour conferring antimicrobial resistance.* Environmental microbiology, 2009. **11**(1): p. 126-136.

222. Sun, E., et al., *Broad-spectrum adaptive antibiotic resistance associated with Pseudomonas aeruginosa mucin-dependent surfing motility.* Antimicrobial agents and chemotherapy, 2018. **62**(9).

223. Zhang, H., et al., *Stress resistance, motility and biofilm formation mediated by a 25kb plasmid pLMSZ08 in Listeria monocytogenes.* Food Control, 2018. **94**: p. 345-352.

224. Asadishad, B., G. Hidalgo, and N. Tufenkji, *Pomegranate materials inhibit flagellin gene expression and flagellar-propelled motility of uropathogenic Escherichia coli strain CFT073.* FEMS microbiology letters, 2012. **334**(2): p. 87-94.

225. Paramelle, D., et al., *A rapid method to estimate the concentration of citrate capped silver nanoparticles from UV-visible light spectra.* Analyst, 2014. **139**(19): p. 4855-4861.

226. Zhang, W., et al., *Attachment efficiency of nanoparticle aggregation in aqueous dispersions: modeling and experimental validation.* Environmental science & technology, 2012. **46**(13): p. 7054-7062.

227. *Biggest Threats and Data*. 2020.

228. Demirdjian, S., et al., *Phosphatidylinositol-(3, 4, 5)-trisphosphate induces phagocytosis of nonmotile Pseudomonas aeruginosa.* Infection and immunity, 2018. **86**(8).

229. Gilbertson, L.M., et al., *Shape-dependent surface reactivity and antimicrobial activity of nano-cupric oxide.* Environmental science & technology, 2016. **50**(7): p. 3975-3984.

230. Ren, J., et al., *Crystallography facet-dependent antibacterial activity: the case of Cu2O.* Industrial & engineering chemistry research, 2011. **50**(17): p. 10366-10369.

231. Albalghiti, E., et al., *Towards resolution of antibacterial mechanisms in metal and metal oxide nanomaterials: a meta-analysis of the influence of study design on mechanistic conclusions.* Environmental Science: Nano, 2021. **8**(1): p. 37-66.

232. Siekkinen, A.R., et al., *Rapid synthesis of small silver nanocubes by mediating polyol reduction with a trace amount of sodium sulfide or sodium hydrosulfide.* Chemical physics letters, 2006. **432**(4-6): p. 491-496.

233. Zhang, Q., et al., *A systematic study of the synthesis of silver nanoplates: is citrate a "magic" reagent?* Journal of the American Chemical Society, 2011. **133**(46): p. 18931-18939.

234. Barrios, A.C., et al., *Structure–Property–Toxicity Relationships of Graphene Oxide: Role of Surface Chemistry on the Mechanisms of Interaction with Bacteria.* Environmental science & technology, 2019. **53**(24): p. 14679-14687.

235. Castle, S.D., C.S. Grierson, and T.E. Gorochowski, *Towards an engineering theory of evolution.* Nature Communications, 2021. **12**(1): p. 3326.

236. Ewunkem, A.J., et al., *Experimental evolution of magnetite nanoparticle resistance in Escherichia coli.* Nanomaterials, 2021. **11**(3): p. 790.

237. Chopra, I., *Molecular mechanisms involved in the transport of antibiotics into bacteria.* Parasitology, 1988. **96 Suppl**: p. S25-44.

238. Braun, V., et al., *Outer membrane channels and active transporters for the uptake of antibiotics.* The Journal of infectious diseases, 2001. **183**(Supplement_1): p. S12-S16.

239. Gu Liu, C., et al., *Phage-Antibiotic Synergy Is Driven by a Unique Combination of Antibacterial Mechanism of Action and Stoichiometry.* mBio, 2020. **11**(4).

240. Lin, D.M., B. Koskella, and H.C. Lin, *Phage therapy: An alternative to antibiotics in the age of multi-drug resistance.* World J Gastrointest Pharmacol Ther, 2017. **8**(3): p. 162-173.

241. Kortright, K.E., et al., *Phage Therapy: A Renewed Approach to Combat Antibiotic-Resistant Bacteria.* Cell Host Microbe, 2019. **25**(2): p. 219-232.

242. Taati Moghadam, M., et al., *How Phages Overcome the Challenges of Drug Resistant Bacteria in Clinical Infections.* Infect Drug Resist, 2020. **13**: p. 45-61.

243. Hampton, H.G., B.N.J. Watson, and P.C. Fineran, *The arms race between bacteria and their phage foes.* Nature, 2020. **577**(7790): p. 327-336.

244. *Catheter Materials*. 2015; Available from: https://www.sai-infusion.com/pages/catheter-materials.

245. Sadeghnejad, A., et al., *Antibacterial nano silver coating on the surface of polyethylene films using corona discharge.* Surface and Coatings Technology, 2014. **245**: p. 1-8.

246. Sharma, D., L. Misba, and A.U. Khan, *Antibiotics versus biofilm: an emerging battleground in microbial communities.* Antimicrobial Resistance & Infection Control, 2019. **8**(1): p. 76.

247. Mah, T.-F., *Biofilm-specific antibiotic resistance.* Future microbiology, 2012. **7**(9): p. 1061-1072.

248. Kearns, D.B., *A field guide to bacterial swarming motility.* Nature reviews. Microbiology, 2010. **8**(9): p. 634-644.

249. Rooney, L.M., et al., *Intra-colony channels in E. coli function as a nutrient uptake system.* The ISME Journal, 2020. **14**(10): p. 2461-2473.

250. Hofmeister, H. and G.L. Tan, *Shape and internal structure of silver nanoparticles embedded in glass.* Journal of Materials Research, 2005. **20**(6): p. 1551-1562.

251. Pal, S., Y.K. Tak, and J.M. Song, *Does the antibacterial activity of silver nanoparticles depend on the shape of the nanoparticle? A study of the Gram-negative bacterium Escherichia coli.* Appl Environ Microbiol, 2007. **73**(6): p. 1712-20.

252. Ivask, A., et al., *Toxicity mechanisms in Escherichia coli vary for silver nanoparticles and differ from ionic silver.* ACS Nano, 2014. **8**(1): p. 374-86.

253. Xiu, Z.M., J. Ma, and P.J. Alvarez, *Differential effect of common ligands and molecular oxygen on antimicrobial activity of silver nanoparticles versus silver ions.* Environ Sci Technol, 2011. **45**(20): p. 9003-8.

254. Xiu, Z.M., et al., *Negligible particle-specific antibacterial activity of silver nanoparticles.* Nano Lett, 2012. **12**(8): p. 4271-5.

255. McQuillan, J.S., et al., *Silver nanoparticle enhanced silver ion stress response in Escherichia coli K12.* Nanotoxicology, 2012. **6**: p. 857-66.

256. McQuillan, J.S. and A.M. Shaw, *Differential gene regulation in the Ag nanoparticle and Ag(+)-induced silver stress response in Escherichia coli: a full transcriptomic profile.* Nanotoxicology, 2014. **8 Suppl 1**: p. 177-84.

257. Amato, E., et al., *Synthesis, characterization and antibacterial activity against Gram positive and Gram negative bacteria of biomimetically coated silver nanoparticles.* Langmuir, 2011. **27**(15): p. 9165-73.

258. Burchardt, A.D., et al., *Effects of silver nanoparticles in diatom Thalassiosira pseudonana and cyanobacterium Synechococcus sp.* Environ Sci Technol, 2012. **46**(20): p. 11336-44.

259. Arnaout, C.L. and C.K. Gunsch, *Impacts of silver nanoparticle coating on the nitrification potential of Nitrosomonas europaea.* Environ Sci Technol, 2012. **46**(10): p. 5387-95.

260. El Badawy, A.M., et al., *Surface Charge-Dependent Toxicity of Silver Nanoparticles.* Environmental Science and Technology, 2011. **45**: p. 283-287.

261. Bowman, C.R., et al., *Effects of silver nanoparticles on zebrafish (Danio rerio) and Escherichia coli (ATCC 25922): a comparison of toxicity based on total surface area versus mass concentration of particles in a model eukaryotic and prokaryotic system.* Environ Toxicol Chem, 2012. **31**(8): p. 1793-800.

262. Georgantzopoulou, A., et al., *Ag nanoparticles: size- and surface-dependent effects on model aquatic organisms and uptake evaluation with NanoSIMS.* Nanotoxicology, 2013. **7**(7): p. 1168-78.

263. Ivask, A., et al., *Profiling of the reactive oxygen species-related ecotoxicity of CuO, ZnO, TiO2, silver and fullerene nanoparticles using a set of recombinant luminescent Escherichia coli strains: differentiating the impact of particles and solubilised metals.* Anal Bioanal Chem, 2010. **398**(2): p. 701-16.

264. Ivask, A., et al., *Size-dependent toxicity of silver nanoparticles to bacteria, yeast, algae, crustaceans and mammalian cells in vitro.* PLoS One, 2014. **9**(7): p. e102108.

265. Radzig, M.A., et al., *Antibacterial effects of silver nanoparticles on gram-negative bacteria: influence on the growth and biofilms formation, mechanisms of action.* Colloids Surf B Biointerfaces, 2013. **102**: p. 300-6.

266. Smetana, A.B., et al., *Biocidal activity of nanocrystalline silver powders and particles.* Langmuir, 2008. **24**(14): p. 7457-64.

267. Doody, M.A., et al., *Differential antimicrobial activity of silver nanoparticles to bacteria Bacillus subtilis and Escherichia coli, and toxicity to crop plant Zea mays and beneficial B. subtilis-inoculated Z. mays.* Journal of Nanoparticle Research, 2016. **18**: p. 290.

268. Giao, N.T., et al., *Influence of silver nanoparticles and liberated silver ions on nitrifying sludge: ammonia oxidation inhibitory kinetics and mechanism.* Environ Sci Pollut Res Int, 2017. **24**(10): p. 9229-9240.

269. Greulich, C., et al., *The toxic effect of silver ions and silver nanoparticles towards bacteria and human cells occurs in the same concentration range.* RSC Advances, 2012. **2**: p. 6981-6987.

270. Hachicho, N., et al., *Effect of silver nanoparticles and silver ions on growth and adaptive response mechanisms of Pseudomonas putida mt-2.* FEMS Microbiol Lett, 2014. **355**(1): p. 71-7.

271. Long, Y.M., et al., *Surface ligand controls silver ion release of nanosilver and its antibacterial activity against Escherichia coli.* Int J Nanomedicine, 2017. **12**: p. 3193-3206.

272. Masrahi, A., A.R. VandeVoort, and Y. Arai, *Effects of silver nanoparticle on soil-nitrification processes.* Arch Environ Contam Toxicol, 2014. **66**(4): p. 504-13.

273. Maurer-Jones, M.A., et al., *Characterization of silver ion dissolution from silver nanoparticles using fluorous-phase ion-seelctive electrodes and assessment of resultant toxicity to Shewanella oneidensis.* Chemical Science, 2013. **4**: p. 2564-2572.

274. Ortega-Calvo, J.J., et al., *Bacterial tactic response to silver nanoparticles.* Environ Microbiol Rep, 2011. **3**(5): p. 526-34.

275. Radniecki, T.S., et al., *Influence of liberated silver from silver nanoparticles on nitrification inhibition of Nitrosomonas europaea.* Chemosphere, 2011. **85**(1): p. 43-9.

276. Silva, T., et al., *Particle size, surface charge and concentration dependent ecotoxicity of three organo-coated silver nanoparticles: comparison between general linear model-predicted and observed toxicity.* Sci Total Environ, 2014. **468-469**: p. 968-76.

277. Visnapuu, M., et al., *Dissolution of silver nanowires and nanospheres dictates their toxicity to Escherichia coli.* Biomed Res Int, 2013. **2013**: p. 819252.

278. Yang, Y., et al., *Pyrosequencing reveals higher impact of silver nanoparticles than Ag+ on the microbial community structure of activated sludge.* Water Res, 2014. **48**: p. 317-25.

279. Zarubina, A.P., et al., *Evaluation of Toxicity of Silver Ions and Nanoparticles using Model Bacteria with Luminescent Phenotype.* Nanotechnologies in Russia, 2015. **10**(5-6): p. 475-483.

280. Johnston, K.A., et al., *Impacts of broth chemistry on silver ion release, surface chemistry composition, and bacterial cytotoxicity of silver nanoparticles.* Environmental Science: Nano, 2018. **5**: p. 304-312.

281. Li, B., et al., *The importance of lag time extension in determining bacterial resistance to antibiotics.* Analyst, 2016. **141**(10): p. 3059-3067.

282. Zwietering, M.H., et al., *Modeling of the bacterial growth curve.* Applied and environmental microbiology, 1990. **56**(6): p. 1875-1881.

283. Alpaslan, E., et al., *pH-Controlled Cerium Oxide Nanoparticle Inhibition of Both Gram-Positive and Gram-Negative Bacteria Growth.* Scientific Reports, 2017. **7**(1): p. 45859.

284. Theophel, K., et al., *The importance of growth kinetic analysis in determining bacterial susceptibility against antibiotics and silver nanoparticles.* Frontiers in Microbiology, 2014. **5**(544).

285. Tjørve, K.M.C. and E. Tjørve, *The use of Gompertz models in growth analyses, and new Gompertz-model approach: An addition to the Unified-Richards family.* PLoS One, 2017. **12**(6): p. e0178691.

286. Mitchell, Stephanie L., et al., *Chronic exposure to complex metal oxide nanoparticles elicits rapid resistance in Shewanella oneidensis MR-1.* Chemical Science, 2019. **10**(42): p. 9768-9781.

287. Yurtsev, E.A., et al., *Bacterial cheating drives the population dynamics of cooperative antibiotic resistance plasmids.* Mol Syst Biol, 2013. **9**: p. 683.

288. Andersson, D.I. and D. Hughes, *Antibiotic resistance and its cost: is it possible to reverse resistance?* Nat Rev Microbiol, 2010. **8**(4): p. 260-71.

289. Microbiology, E.C.f.A.S.T.o.t.E.S.o.C. and I. Diseases, *Determination of minimum inhibitory concentrations (MICs) of antibacterial agents by broth dilution.* Clinical Microbiology and Infection, 2003. **9**(8): p. ix-xv.

290. Arnold, C.N., et al., *Global analysis of Escherichia coli gene expression during the acetate-induced acid tolerance response.* Journal of bacteriology, 2001. **183**(7): p. 2178-2186.

291. Kurihara, S., et al., *A novel putrescine importer required for type 1 pili-driven surface motility induced by extracellular putrescine in Escherichia coli K-12.* Journal of Biological Chemistry, 2011. **286**(12): p. 10185-10192.

292. Schneider, B.L., V.J. Hernandez, and L. Reitzer, *Putrescine catabolism is a metabolic response to several stresses in E scherichia coli.* Molecular microbiology, 2013. **88**(3): p. 537-550.

293. Maier, R.M.P., I.L., *Bacterial Growth.* Environmental Microbiology, 2015. **Third Edition**: p. 37-56.

294. Casino, P., L. Miguel-Romero, and A. Marina, *Visualizing autophosphorylation in histidine kinases.* Nature Communications, 2014. **5**(1): p. 3258.

295. Comeau, D.E., et al., *Primary characterization of the protein products of the Escherichia coli ompB locus: structure and regulation of synthesis of the OmpR and EnvZ proteins.* Journal of Bacteriology, 1985. **164**(2): p. 578-584.

296. Ghosh, M., et al., *Lipid-Mediated Regulation of Embedded Receptor Kinases via Parallel Allosteric Relays.* Biophys J, 2017. **112**(4): p. 643-654.

297. Matsuyama, S., T. Mizuno, and S. Mizushima, *Interaction between two regulatory proteins in osmoregulatory expression of ompF and ompC genes in Escherichia coli: a novel ompR mutation suppresses pleiotropic defects caused by an envZ mutation.* Journal of Bacteriology, 1986. **168**(3): p. 1309-1314.

298. Samanta, P., et al., *OmpR and RcsB abolish temporal and spatial changes in expression of flhD in Escherichia coli biofilm.* BMC microbiology, 2013. **13**(1): p. 1-13.

299. Roberts, D.L., D. Bennett, and S. Forst, *Identification of the site of phosphorylation on the osmosensor, EnvZ, of Escherichia coli.* Journal of Biological Chemistry, 1994. **269**(12): p. 8728-8733.

300. Sandegren, L., *Selection of antibiotic resistance at very low antibiotic concentrations.* Upsala journal of medical sciences, 2014. **119**(2): p. 103-107.

301. Wang, S., et al., *RaptorX-Property: a web server for protein structure property prediction.* Nucleic acids research, 2016. **44**(W1): p. W430-W435.

302. Wang, S., J. Ma, and J. Xu, *AUCpreD: proteome-level protein disorder prediction by AUC-maximized deep convolutional neural fields.* Bioinformatics, 2016. **32**(17): p. i672-i679.

303. Wang, S., et al., *Protein secondary structure prediction using deep convolutional neural fields.* Scientific reports, 2016. **6**(1): p. 1-11.

304. Wang, S., S. Sun, and J. Xu. *AUC-maximized deep convolutional neural fields for protein sequence labeling*. in *Joint European Conference on Machine Learning and Knowledge Discovery in Databases*. 2016. Springer.

305. Yang, Y., et al., *Sixty-five years of the long march in protein secondary structure prediction: the final stretch?* Briefings in bioinformatics, 2018. **19**(3): p. 482-494.